The assessment of track deflection and rail joint performance

Maria Gallou

LB Foster Rail Technologies UK Ltd
Stamford Street
Sheffield
S9 2TX

Centre for Innovative and Collaborative Construction Engineering
Department of Civil & Building Engineering
Loughborough University
Loughborough
Leicestershire, LE11 3TU

Certificate of Originality
Thesis Access Conditions and Deposit Agreement

Students should consult the guidance notes on the electronic thesis deposit and the access conditions in the University's Code of Practice on Research Degree Programmes

Author   Maria Gallou

**Title**   The assessment of track deflection and rail joint performance

I [Maria Gallou, Loughborough University], "the Depositor",
would like to deposit [The assessment of track deflection and rail joint performance], hereafter referred to as the "Work", once it has successfully been examined in Loughborough University Institutional Repository

Status of access OPEN

Moratorium Period……………………………….years, ending……………. /…………20……………………...

Status of access approved by CAPITALS): ………………………………………………………………….

Supervisor (Signature)   M, W, Frost
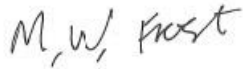
School of Architecture, Civil and Building Engineering

Author's Declaration *I confirm the following:*

CERTIFICATE OF ORIGINALITY
This is to certify that I am responsible for the work submitted in this thesis, that the original work is my own except as specified in acknowledgements or in footnotes, and that neither the thesis nor the original work therein has been submitted to this or any other institution for a degree

NON-EXCLUSIVE RIGHTS
The licence rights granted to Loughborough University Institutional Repository through this agreement are entirely non-exclusive and royalty free. I am free to publish the Work in its present version or future versions elsewhere. I agree that Loughborough University Institutional Repository administrators or any third party with whom Loughborough University Institutional Repository has an agreement to do so may, without changing content, convert the Work to any medium or format for the purpose of future preservation and accessibility.

DEPOSIT IN LOUGHBOROUGH UNIVERSITY INSTITUTIONAL REPOSITORY
I understand that open access work deposited in Loughborough University Institutional Repository will be accessible to a wide variety of people and institutions - including automated agents - via the World Wide Web. An electronic copy of my thesis may also be included in the British Library Electronic Theses On-line System (EThOS).
I understand that once the Work is deposited, a citation to the Work will always remain visible. Removal of the Work can be made after discussion with Loughborough University Institutional Repository, who shall make best efforts to ensure removal of the Work from any third party with whom Loughborough University Institutional

Repository has an agreement. Restricted or Confidential access material will not be available on the World Wide Web until the moratorium period has expired.

- That I am the author of the Work and have the authority to make this agreement and to hereby give Loughborough University Institutional Repository administrators the right to make available the Work in the way described above.
- That I have exercised reasonable care to ensure that the Work is original, and does not to the best of my knowledge break any UK law or infringe any third party's copyright or other Intellectual Property Right. I have read the University's guidance on third party copyright material in theses.
- The administrators of Loughborough University Institutional Repository do not hold any obligation to take legal action on behalf of the Depositor, or other rights holders, in the event of breach of Intellectual Property Rights, or any other right, in the material deposited.

*The statement below shall apply to **ALL** copies:*

This copy has been supplied on the understanding that it is copyright material and that no quotation from the thesis may be published without proper acknowledgement.

Restricted/confidential work: All access and any copying shall be strictly subject to written permission from the University Dean of School and any external sponsor, if any.
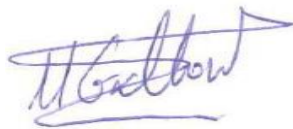
Author's Signature   Date   31/07/2018

user's declaration: for signature during any Moratorium period (Not Open work): *I undertake to uphold the above conditions:*			
Date	Name (CAPITALS)	Signature	Address

THE ASSESSMENT OF TRACK DEFLECTION AND RAIL JOINT PERFORMANCE

By

Maria Gallou

A dissertation thesis submitted in partial fulfilment of the requirements for the award of the degree Doctor of Engineering (EngD), at Loughborough University

July 2018

LB Foster Rail Technologies UK Ltd
Stamford Street
Sheffield
S9 2TX

Centre for Innovative and Collaborative Construction Engineering
Department of Civil & Building Engineering
Loughborough University
Loughborough
Leicestershire, LE11 3TU

ACKNOWLEDGEMENTS

ABSTRACT

Track stiffness is the one of the most critical parameters of the track structure. Its evaluation is important to assess track quality, component performance, localised faults and optimise maintenance periods and activities. Keeping the track stiffness within acceptable range of values is connected with keeping the railway network in a satisfactorily performing condition, allowing thereby upgrade of its capacity (speed, load, intensity). Current railway standards are changing to define loading and stiffness requirements for improved ballasted and ballastless performance under high speed train traffic. In recent years various techniques have been used to measure track deflection which have been also used to validate numerical models to assess various problems within the railway network.

Based on recent introduction of the Video Gauge for its application in the civil engineering industry this project provides the proof of effective applicability of this DIC (Digital image correlation) tool for the accurate assessment of track deflection and the calculation of track stiffness through its effective applicability in various track conditions for assessing the stiffness of various track forms including track irregularities where abrupt change in track stiffness occur such as transition zones and rail joints. Attention is given in validation of numerical modelling of the response of insulated rail joints under the passage of wheel load within the goal to improve track performance adjacent to rail joints and contribute to the sponsoring company's product offering. This project shows a means of improving the rail joint behaviour by using external structural reinforcement, and this is presented through numerical modelling validated by laboratory and field measurements. The structural response of insulated rail joints (IRJs) under the wheel vertical load passage is presented to enhance industry understanding of the effect of critical factors of IRJ response for various IRJ types that was served as a parametric FE model template for commercial studies for product optimisation.

KEY WORDS

Video Gauge, field monitoring, laboratory testing, finite element analysis, track stiffness, insulated rail joint

PREFACE

This thesis presents the research conducted from 2014 to 2018 to fulfil the requirements of an Engineering Doctorate (EngD) at the Centre for Innovative and Collaborative Engineering (CICE), Loughborough University, United Kingdom. The research programme, which aims to analyse and develop the experimental methodology of using the Video Gauge, a remote video monitoring technique, for the assessment of the vertical displacement (deflection) of the railway track structure and the validation of finite element analysis (FEA) of insulated rail joints (IRJs), was conducted within an industrial context and sponsored by LB Foster Rail technologies UK Ltd. The research programme was also funded by the Engineering and Physical Sciences Research Council (EPSRC).

The Engineering Doctorate is a four-year postgraduate doctorate programme where the core of the degree is the solution of significant and challenging engineering problems within an industrial context. The EngD provides a more vocationally oriented doctorate in engineering than the traditional PhD and is better suited to the needs of industry. The EngD constitutes a form of academic –industry collaboration that not only generates new knowledge, but also enhances the human capital development by delivering EngD research engineers with leadership, management and advanced technical skills focused on the needs of industry.

For the degree of EngD the basis of assessment shall be a discourse and a collection of at least three published papers (one being a Journal) and technical reports. In this discourse three journal papers, one conference paper and one technical report are included appended. The discourse is to be read in conjunction with the appended papers and reports that are referenced within the text, providing a background of the research with in depth technical detail and clarifications presented in the academic papers.

USED ABBREVIATIONS

AREMA	American Railway Engineering and Maintenance-of-way Association
BOEF	Beam on Elastic Foundation
BR	British Railways
BS SUS-IRJ	Suspended Insulated Rail Joint Strengthened with I-Beams
BS	British Standard
CCQ	Coloured Coded Quality
CEN	Comité Européen de Normalisation
CICE	Centre of Innovative and Collaborative Construction Engineering
CWR	Continuous Welded Rail
DAF	Dynamic Amplification Factor
DB	Deutsche Bahn, German State Railways
DIC	Digital Image correlation
EMEA	Europe, Middle East and Africa
EMGTA	Equivalent Million Gross Tons Per Annum
EngD	Engineering Doctorate
EPSRC	Engineering and Physical Sciences Research Council
Epub	Electronic publication
FE	Finite Element
FEA	Finite Element Analysis
FEM	Finite Element Modelling
fps	frames per second
FWD	Falling Weight Deeflectometer
GB	Great Britain
HS2	High Speed 2
HSTRC	High Speed Track Recording Coach
IRJ	Insulated Rail Joint
IVES	Intelligent, Versatile, Efficient, Solid
kN	kilo-Newton
LM71	Loading model 71
LVDT	Linear Variable Displacement Transducer
MDD	Multi-Depth Deflectometer

MGT	Million Gross Tons
mm	millimetre
mph	miles per hour
NM	Numerical Modelling
ORE	Office of Research and Experiments of the International Union of Railways
PIV	Particle Image Velocimetry
RJ	Rail Joint
RSMV	Rolling Stiffness Measurement Vehicle
RSSB	Rail Safety and Standards Board
RTST	Rail Trackform Stiffness Tester
RVM	Remote Video Monitoring
SD	Standard Deviation
SNCF	Société Nationale des Chemins de Fer Français: French national railways
SR SUS-IRJ	Suspended Insulated Rail Joint enhanced with Strap Rails
SUS-IRJ	Suspended Insulated Rail Joint
UK	United Kingdom
VG	Video Gauge
V-TRAS	Versatile transition module
WG46	Working Group 46

TABLE OF CONTENTS

LIST OF FIGURES

LIST OF TABLES

LIST OF PAPERS

The following papers, included in the appendices, have been produced in partial fulfilment of the award requirements of the Engineering Doctorate during the course of the research.

PAPER 1 (SEE APPENDIX A)

Gallou M., Frost M. El-Hamalawi A., Hardwick C. Applicability of Video Gauge for the assessment of track displacement. The Stephenson Conference: Research for Railways, Institution of Mechanical Engineers, London, UK, 25th-27th April 2017, pp. 141-148.

PAPER 2 (SEE APPENDIX B)

Gallou M., Temple B., Hardwick C, Frost M., El-Hamalawi A. Potential for external reinforcement of insulated rail joints. Proceedings of the Institution of Mechanical Engineers, Part F: Journal of Rail and Rapid Transit, Epub ahead of print, 22 Dec 2016.

PAPER 3 (SEE APPENDIX C)

Gallou M., Frost M., El-Hamalawi A., Hardwick C. Assessing the deflection behaviour of mechanical and insulated rail joints through finite element analysis. Proceedings of the Institution of Mechanical Engineers, Part F: Journal of Rail and Rapid Transit, Epub ahead of print, 16 April 2018

PAPER 4 (SEE APPENDIX D)

Gallou M., Frost M., El-Hamalawi A., Hardwick C. The application of track deflection measurements made by the Video Gauge. Proceedings of the Institution of Civil Engineers, Transport, 2017. Accepted on 16 May 2018. Epub ahead of print, 21 May 2018.

1   INTRODUCTION

1.1   BACKGROUND TO THE RESEARCH

Railway track system design is governed by the aim to achieve high performance with lowest whole life costs. Within the context of high speeds (360 kilometres per hour in High Speed 2 (HS2)) the mechanical behaviour and performance of track has to be enhanced to cope with higher dynamic loads, higher vibration levels of the rolling stock and superstructure that may lead to fatigue and wear, and higher stresses on the track bed and support structures. As a result, track stiffness optimisation in terms of vertical and horizontal elasticity, improvement of load transmission between track components by taking into account the bearing capacity of the support structures are the main objectives of the track design.

Track stiffness is the resistance of the entire track structure to deformation in relation to the applied force. The track stiffness is the result of the combination of the stiffness of the different constituents. The vertical track stiffness of the whole track structure is determined as applied force to the rail divided by rail vertical displacement. Therefore, the measurement of accurate rail vertical displacement (deflections) is of significant importance for track monitoring and maintenance. Rail deflection being under certain limits constitutes a European Norm (EN) requirement of track structure performance. The selection of track modulus and consequently the determination of track design are based on the desired design rail deflection. Rail deflection values in the typical UK rail ballasted network is variable. The track system shall have a certain degree of resilience for load distribution and in order to achieve this, the rail deflection shall be in certain limits. This deflection guide value corresponds to a global track stiffness guide value.

The key issue for a new track form is therefore prediction of deformation performance to match the requirements prior to construction.

1.1.1   BALLASTED TRACK

An understanding of the ballasted track system components as illustrated in Figure 1.5 is required to allow track system design optimisations. The fastening system is a vital component for track resilience and impact attenuation but they are prone to wear and tear. Poor interfaces exist between sleepers and ballast as the load distribution below sleepers is uneven. Ballast is prone to settlement and its life span is a function of the number of tamps, maintenance and renewal. Tamping restores the geometrically correct track position. Provided the lifting is

sufficient, defined sleeper supports are produced by avoiding positions which occur by slanting sleepers. On a typical ballasted plain line construction tamping, tamping after construction, 6-week follow up and annual follow up tamping shall occur. The design, construction and operation are highly dependent on the interaction between the superstructure (rail, fastening system, sleepers, ballast and substructure subballast, (subgrade). The term "formation" is used in current UK standards (Network Rail 2016), consisting of a sand blanket or other fine-grained materials over the subgrade, upon which the required depth of ballast is placed (Figure 1.2). The formation is considered permanent and shall not require replacement or maintenance. In addition, the term trackbed is used, considering the ballast and formation (Figure 1.2). Deformations may vary along the network with settlements occurring during construction and during operation due to deformation of the subsoil, embankment (earth structure) settlements or settlements due to dynamic loading (see Figure 1.3). Short and long-term movements of structures can be added due to elastic deformation and creep. Deformation varies along the route, with differential settlements from high embankments, bridges, culverts, and potential heave in cuttings.

The first phase of track settlement occurs directly after the construction of track. This comes from the vertical plastic strains of subballast and subgrade, because they have not previously been subjected to traffic (see Figure 1.4).The second phase of track settlement starts after the first has finished and can be caused firstly, due to ballast volume reduction, ballast abrasive wear, due to the motion of ballast particles under the train loading and secondly, due to the movement of sleepers under the forces of the train. This can have two effects; the movement of sleepers can either cause ballast to be pushed away, and the sleepers can sink deeper into the ballast (track has lower level) or the sleepers can be lifted by the bending rails in front or behind the wheel loading, gaps will fall into the generated gaps in the sleeper-ballast interface and after the unloading the track has a higher level. Thus, the track settlement can cause different levels of height of the track. These different track levels lead to irregularities that cause increased wheel-rail contact forces. As a result, increased track degradation can be caused due to the traffic loads as more settlement will be created due to the higher dynamic forces. To conclude, a track settlement and track degradation is a vicious cycle.

The rail is considered as a beam on continuous or discrete resilient support. The moment of inertia of the rail profile, the spacing of the support points as well as the elasticity of the whole assembly on its support have an influence in the longitudinal distribution of the vertical and

horizontal load applied on the rail. Rail is typically supported over full sleeper width with the sleeper spacing to range typically from 0.6 m to 0.75 m. Geometrical and mechanical data of each element are considered in the general system design.
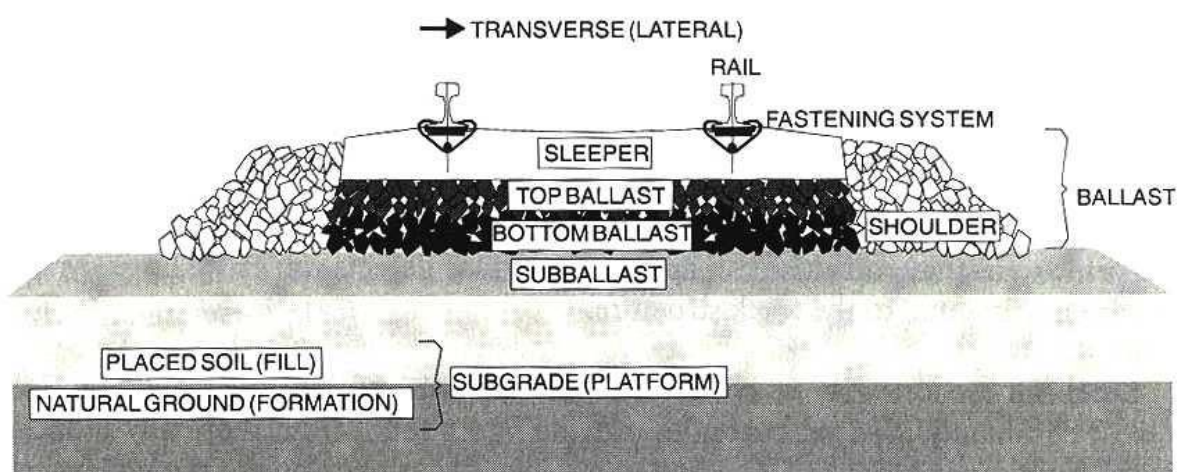
Figure 1.1 Conventional ballasted track structure from Selig and Waters (1994)
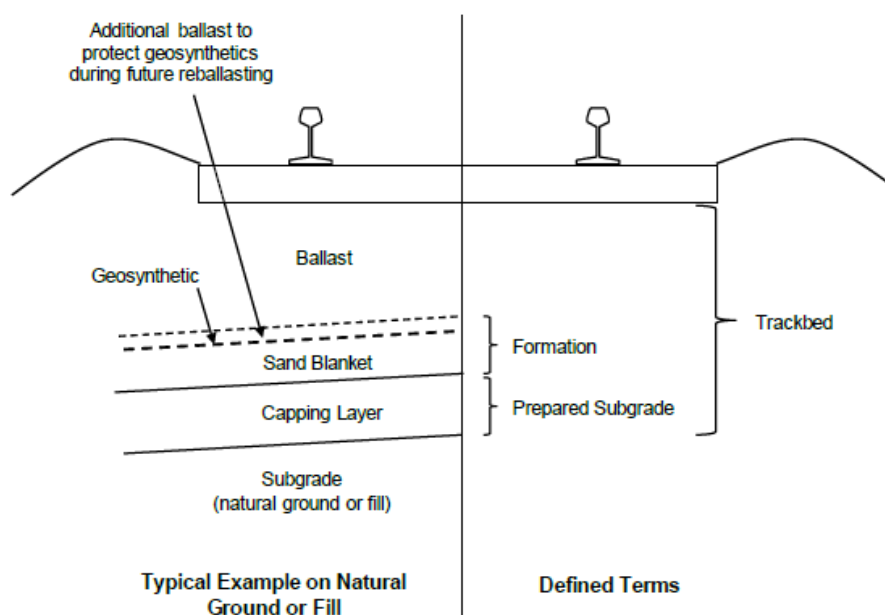
Figure 1.2 Trackbed components according to Network Rail (2016)
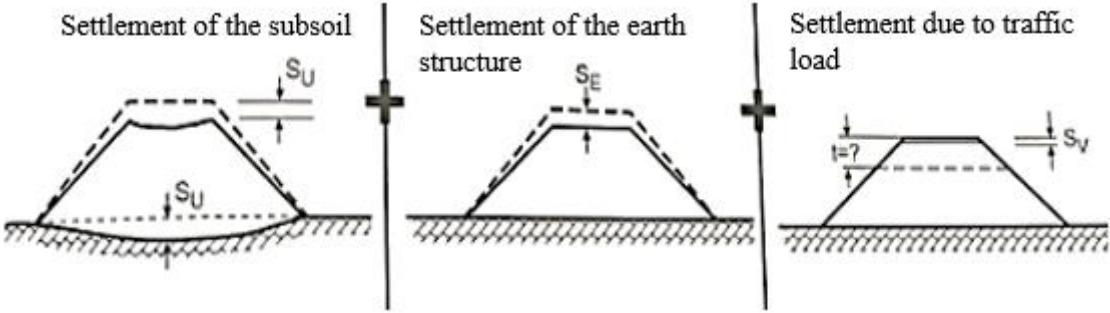
Figure 1.3 Reasons of track settlements adapted from Lichtberger (2005)
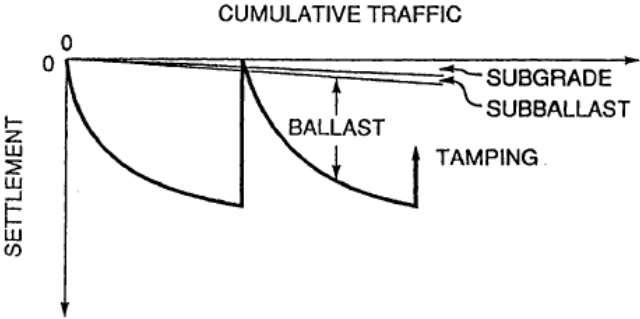
Figure 1.4 Substructure contributions to settlement from Selig and Waters (1994)

1.1.2 SLAB TRACK

On the other hand, different types of slab (non-ballasted) track systems have been developed worldwide and exist partially in the UK rail network mainly in tunnels and bridges (some longitudinal timber waybeams exist also in the UK old bridges). Slab or ballastless track is the track where the ballast layer has been replaced by a permanent structure, to which the rails are fastened. For ballastless track "the required value of track stiffness should be specified by the purchaser of the ballastless system taking into account the permissible bending tensile rail foot stress and the proposed operating conditions" (BSI 2017b). According to their main principles of construction they can be divided into pre-cast systems (Max-Boegl, PORR), wet pour systems (pre-cast elements cast in-situ into concrete) (Rheda 2000, Sateba) and other (e.g. asphalt systems) (Porrill (2015) (Figure 1.5). According to the method of design and rail support system, they can be separated among other to embedded rail, single rail supports directly fixed on the continuously reinforced concrete pavement (CRCP), sleeper panels connected to the

CRCP, sleeper panels connected to asphalt pavement (Lechner 2013). In slab track, settlement compensation is provided whether by adjustment of rail fasteners or by re-grouting.
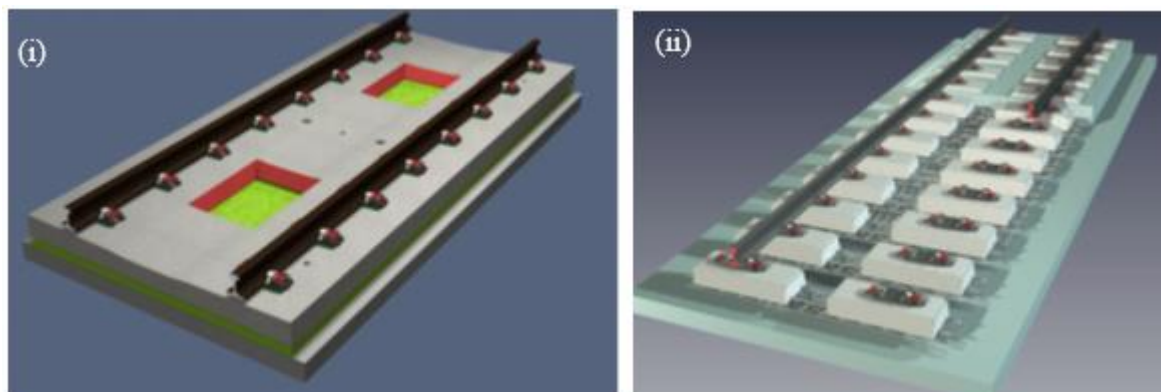
Figure 1.5 Examples of slab track (i) PORR-Austria and (ii) Rheda 2000- Germany adapted from Porrill (2015)

1.1.3 TRANSITION ZONES

A special construction is required at transition zones between ballastless track and ballasted track such as on the approach of bridges and tunnels. Witt (2008) supported that vertical stiffness changes with a factor of 2 or 4 (from 40 to 160 kN/mm) have been measured in Sweden in 2001 on a bridge transition. The different stiffness between a stiffer bridge and as softer embankment cause different deflections at the rail. These can lead to increased settlement of the ballasted track and an increased degradation risk at the ballasted track supports if softer. Therefore, the transition zone should be designed in order to limit the differential settlement to a minimum. For this reason, several measures may need to ensure that no sudden change in stiffness occurs in a transition. For example, elastic railpads, under sleeper pads, or ballast mats have been investigated, bound base layers could continue under the ballast over a certain length (such as bituminous layers), the ballast could be glued, additional rails could be installed to increase the load distribution (i.e. in expansion joints). Recently, ladder form steel, prefabricated, transition module has been developed (V-TRAS - versatile transition module by Rhomberg Sersa Rail Group 2016b); it consists of two longitudinal beams, that are fixed in the slab track end, with steel bearing plates with elastic pads at the points in contact with the sleepers to ensure that the differential settlement between the slab and ballast does cause abrupt change in level but takes the shape of a gradual ramp.

1.1.4 TRACK STIFFNESS THEORETICAL BACKGROUND

The design calculation for the ballasted and ballastless track system is primarily obtained using analytical calculations, but also using numerical calculations using finite element modelling (FEM). Validated numerical models strongly depend on the individual decisions of the designer with respect to model idealisation (boundary conditions), discretization (meshing) and convergence conditions for the solutions. The structural properties of all the individual components of the track system (rail, railpad, sleepers, ballast, subballast and subgrade) play role in the track stiffness of the entire track system. Analytically, the longitudinal distribution of the wheel loads by the rails between rail seats can be calculated using the model of the elastic beam on elastic foundation (BOEF) (Winkler/Zimmermann) (Zimmermann 1888). The influence of all elastic components is taken into account including the rail flexural rigidity. Similar to the concept of track stiffness, track modulus is also adopted by track engineers, that is defined as the supporting force per unit length of rail. The difference between track stiffness (N/m) and track modulus (N/m^2) is that track stiffness includes the rail bending whereas the track modulus refers to the support condition under the rails.

Different combinations of track components of different stiffnesses can produce the same global results. The system stiffness for one support of the rail is given by the formula:

$$c_{tot} = (\frac{1}{c_1} + \frac{1}{c_2} + \frac{1}{c_3} + \frac{1}{c_4} ... + \frac{1}{c_n})^{-1} \qquad \text{eq.1.1}$$

Where:

c_{tot} is the stiffness of the system in kN/mm

c_1 is the decisive (pad)-stiffness (kN/mm) of the fastening system specified for dynamic loading

c_2 is the stiffness of an individual elastic element (e.g. concrete sleeper)

c_3 is the stiffness of the ballast

c_4 is the stiffness of the subgrade etc.

A more detailed description of how the BOEF model can be used for the calculation of track stiffness properties for known track deflection is presented in Section 2.2.3.

1.1.5 DESIGN AND LOADING REQUIREMENTS OF RAILWAY TRACK

The current practice of track structure design in GB is based on specifying components according to NR/L2/TRK/2102 (Network Rail 2008) that is based on BS EN 1991-23 (BSI 2003) and GC/RT5112 (RSSB 2015), GC/RT5021 (RSSB 2011) and GM/TT0088 (RSSB 1993). Critical information for the design and loading requirements for the UK railway track can be found in the documents that are presented in Table 1.1.

Table 1.1 Documents related to loading and design requirements of the UK track structure.

Standards Code	Title
BS EN 1991-2 (BSI 2003)	Actions on structures. Traffic Loads on Bridges
GC/RT5021 (RSSB 2011)	Track system Requirements
GC/RT5112 (RSSB 2015)	Rail traffic Loading Requirements for the design of railway structures
BS EN 13450 (BSI 2013)	Aggregates for railway ballast
BS EN 13146-4 (BSI 2014a)	Railway applications - Track - Test methods for fastening systems - Part 4: Effect of repeated loading
BS EN 16432-1 (BSI 2017a)	Railway applications - Ballastless track systems - Part 1: General requirements
BS EN 16432-2 (BSI 2017b)	Railway applications-Ballastless track systems-Part 2: System design, subsystems and components
GM/TT0088 (RSSB 1993)	Permissible Track Forces for Railway Vehicles
NR/L2/TRK/2102 (Network Rail 2008)	Design and construction of track
NR/L2/CIV/020:10.2.6 (Network Rail 2011)	Design of bridges. Additional loads for the design of bridges structures supporting directly fastened and embedded rails
Report T1073-01 (RSSB 2016)	Loading Requirements for Track Systems

1.1.6 TRACK STIFFNESS REQUIREMENTS

Table 1.2 shows an example of how rail deflection is taken into account into the design of ballasted track (Network Rail) and the specifications of HS2. Also, the table shows the difference in the formation stiffness requirements. Here, the formation stiffness modulus (E) (in MN/m^2 =MPa), that is usually measured by the Light weight Deflectometer (LWD) on top of formation, is used as requirement that differs from the stiffness value of the conventional Falling Weight Deflectometer (FWD) (in kN/mm) (see Section 2.2.5).

The formation E modulus measured by a LWD can be calculated using the equation below (Fleming *et al.* 2007):

$$E = \frac{A*P*r*(1-v^2)}{d_0} \text{ MPa} \hspace{3cm} \text{eq.1.2}$$

where:

E = stiffness modulus (MPa)

A = plate rigidity factor, default = 2 for a flexible plate, $\pi/2$ for a rigid plate.

P = maximum contact pressure (kPa) – controlled by the operator and recorded/displayed

r = plate radius (m) – can be controlled, 50, 75 and 150mm options, UK has adopted 150mm.

v = Poisson's ratio (usually set in the range 0.3-0.45 depending on test material type)

d0 = central geophone peak deflection (mm) – recorded and presented on the readout unit

Table 1.2 Comparison of some design requirements between HS2 and Network Rail adapted from Hunt (2018)

Parameter	HS2 values	Network Rail values
Speed /tonnage	360 km/h (224mph)	300 km/h (HS1)
Tonnage	65 MGTPA (million gross tons per annum)	14 MGTPA (HS1) (million gross tons per annum)
Formation Modulus (E)	120 MN/m^2 (measured by LWD)	45-60 MN/m^2 (measured by LWD)
Wheel/rail interface	Single profile consistent axle load	Many profiles, varying axle load
Rail deflection	1.3mm (passenger)	>3mm and variable (passenger and freight)

In addition, sleeper support stiffness requirements depending on the rail line type and its speed limit are shown in

Table 1.3 (Network Rail 2016). These stiffness values (kN/mm) are measured by FWD (see also section 2.2.5) in an unclipped sleeper and are calculated based on the sleeper deflection results measured by the geophones of the FWD. These limits are currently used as the minimum to guarantee that the track quality can be maintained in an adequate standard. The use of geogrid reinforcement is also used in softer formations to improve the trackbed performance. Finally,

formation modulus requirements (E in MN/m^2 measured by LWD) for track renewals and new construction of ballasted track are given in NR/L2/TRK/2102 (see Table 1.4) (Network Rail, 2008) depending on the track category (explained in Figure 1.6). According to NR/L2/TRK/4239 (Network Rail, 2016) the formation moduli of 15, 30 and 45 MN/m^2 correspond to formation stiffness of 30, 60 and 100 kN/mm/sleeper end respectively.

Table 1.3 Dynamic sleeper support stiffness requirements from Network Rail (2016)

NR/L2/TRK/4239 (Network Rail 2016) "Trackbed Investigation, Design and Installation"			
		Required dynamic sleeper support stiffness (measured by FWD)	FWD sleeper deflection -12 tonne load
Existing lines with linespeed <50mph		30 kN/mm (per sleeper end)	2 mm
Existing lines 50<linespeed<125mph		60 kN/mm (per sleeper end)	1 mm
Greenfield sites	Up to 100 mph	60 kN/mm (per sleeper end)	1 mm
Greenfield sites	Above 100mph	100 kN/mm (per sleeper end)	0.6 mm

Table 1.4 Formation modulus (E) requirements from Network Rail (2008)

NR/L2/TRK/2102 "Design and construction of track"	
For track renewals of ballasted track where the formation is exposed by the removal of ballast and sleepers	
	Required Stiffness Modulus (E) of formation
Track category 1A, 1 & 2	45 MN/m^2 (measured by LWD)
Track category 3 to 6	30 MN/m^2 (measured by LWD)
Sidings in track category 5 & 6	15 MN/m^2 (measured by LWD)
New construction	
Required Stiffness Modulus (E) of formation	45 MN/m^2 (measured by LWD)
Required Stiffness Modulus (E) of ballasted track system	160 MN/m^2 (measured by LWD on top of ballast*)
Values for non-ballasted track systems may be different and need to be appropriate for the specific design of system selected	
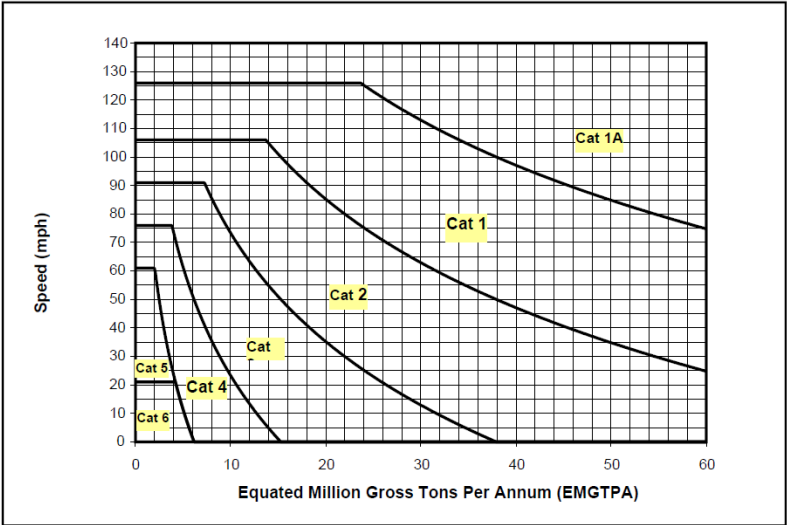
Figure 1.6 Track category matrix, adapted from Network Rail (2008)

1.1.7 RAIL JOINT: A RAIL STIFFNESS DISCONTINUITY

Another track stiffness discontinuity is the rail joint (RJ) (Figure 1.7) which constitutes a weak location in the railway network and a major component of maintenance cost. A recent study by Whitney (2015) indicated that rail breaks at rail joints constitute 16% of the total rail breaks appearing on an annual basis in the UK rail network (see Figure 1.8). Increased dynamic loading at rail joints due to the structural discontinuity causing dipped joints is the principal cause of various rail joint damage mechanisms such as cracks at bolt holes, upper and lower fillet horizontal cracks, localised batter and fishplate failure (see Figure 1.9).

Figure 1.7 (i) 6-bolt and (ii) 4-bolt rail joints in UK site 2015 (Author's personal collection)

Breaks by Type 2014-2015
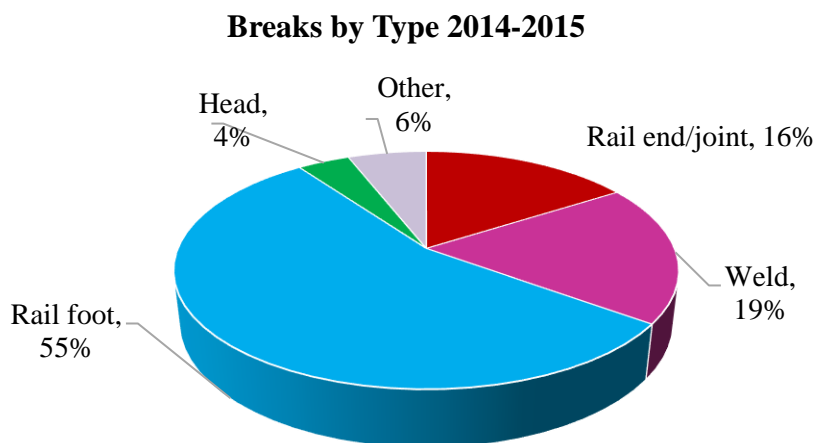
Figure 1.8 Rail breaks by type from Whitney (2015)
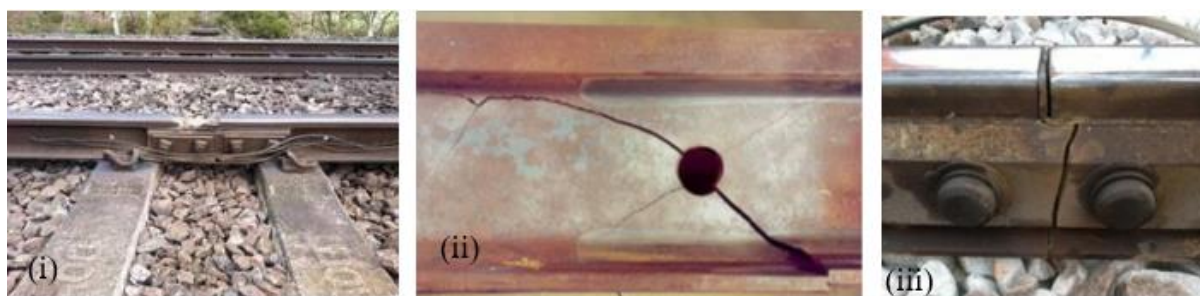
Figure 1.9 Examples of rail joint damage mechanisms from Whitney (2013) (i) broken rail head, (ii) cracks initiated from rail bolt hole and on the underside of the rail head and (iii) broken fishplate

An insulated rail joint (IRJ) is used to separate electrical circuits in rails and turnouts whilst joining two pieces of rail where continuous rail is not possible. This is achieved through the use of fishplates fastened through the web of the rail with bolts (Figure 1.10).

Figure 1.10 (i) Glued IRJ, (ii) mechanical (non-insulated) RJ and (iii) dry IRJ from LB Foster (2014).

Joints deteriorate faster than rail due to this structural discontinuity. It results in extra deflection as a consequence of dynamic loading. Over time this situation worsens as the impacts and applied stresses both damage the ballast and lead to softer support conditions under the joint leading to a vicious cycle of increased deterioration of the rail joint. This problem results from a combination of track stiffness, track irregularity, and wheel–rail contact force. The RJ's performance is further analysed in Section 2.3. This research has looked at IRJ performance and track supports and its measurement and modelling (further discussed in Sections 2.7, 2.9, 4.2.1, 4.2.2 and 4.3).

1.2   RESEARCH CONTEXT

In current standards, requirements for the performance of rail joints are determined through specifications for laboratory testing of newly manufactured RJ designs. The majority of studies have investigated rail joint failure by studying its components; these were related to RJ design optimisation through fishplate geometry optimisation, the optimisation of insulation materials, rail head material optimisation (i.e. laser cladding for increased lipping resistance). However, RJ performance realistically depends on the interaction between track stiffness and traffic load, and thus can be variable. Limited work has practically measured the vertical deformation of RJs.

This project sets out to investigate and establish a numerical model capable of being used to analyse rail joint performance under vertical wheel loads by a holistic approach of the whole track system and not by component. Ways to determine RJ deterioration are investigated. The model is to be validated by field and laboratory measurements using optical equipment provided by the sponsoring company (LB Foster). The findings will be used for industry guidance, relating rail joint design and track deflection assessment.

In parallel, this project aims to enhance industry's understanding of the overall track system's deflections through a series of field measurements made by video system technology that offers the potential to derive track stiffness characteristics.

1.3 THE INDUSTRIAL SPONSOR

LB Foster Rail Technologies UK Ltd, is a leading supplier of railway friction management solutions and rail joints to the EMEA (Europe, Middle East and Africa) rail industry. LB Foster Rail Group (UK department in conjunction with sister divisions in US and Canada) provides a great variety of products and solutions worldwide in the transportation, construction, energy and industrial automation sectors worldwide. Transportation products include rails, rail accessories, rail friction management, concrete sleepers, rail monitoring systems and passenger information systems.

All research herein has been undertaken as part of a Loughborough University EPSRC funded Engineering Doctorate (EngD) scheme at the Centre for Innovation and Collaborative Engineering (CICE).

1.4 INDUSTRIAL RELEVANCE

LB Foster UK Ltd, based in Sheffield, and Barnaby Temple (prior Head of Engineering in LB Foster Rail Technologies UK and ongoing chairman of RAE/2/-/8 Mirror Group GB of the WG46 Ballastless Track CEN Working Group) introduced, with P. Waterfall (Imetrum UK, Ltd), the use of a novel optical monitoring technique (Video Gauge) for rail applications. LB Foster UK, Ltd has a record of recent collaboration with Network Rail in areas such as lubrication and is a specialist /niche supplier of rail joints and friction management in the global rail industry. The current EngD project contains the generalised aim of investigation towards the improvement of the long-term track performance through considering the track structure as a whole rather than individual components. The EngD project aims to contribute to the understanding of the deflection performance of the track with focus on rail joints and to provide a model that will allow industry guidance (track deflections for the wider railway industry) and potential to improve performance of IRJ.

1.5 RESEARCH UNDERTAKEN

Scope

Taking into account the industrial relevance stated above, this research aspired to develop a comprehensive database of track deflection data by establishing a methodological procedure

for applying the optical technique provided by the sponsoring company. The generalised scope of the project is measuring the track performance with the aim of long-term improvement. This programme aims to develop methodologies and analysis tools to be used for the assessment of vertical track stiffness and structural integrity of track structures. It emphasises rail joints and considers the track structure as a whole rather than individual components.

1.6 AIMS AND OBJECTIVES

Aim

The overall aim of the research project is to enhance scientific understanding of the behaviour and the deformation performance of railway track structure to better understand the performance of rail joints.

Objectives

To achieve this aim the following objectives were derived:

1. Review the current practices for track design specifically relating the evaluation of vertical track stiffness and rail joint performance, and factors affecting track structures required for numerical modelling.

2. Develop the Video Gauge methodology, a remote video monitoring technique, to collect accurate vertical displacement data of track and insulated rail joints and to potentially derive track stiffness characteristics.

3. Develop a deformation model, informed from the literature, to allow analysis of rail joints. Evaluate and validate the model using the field and laboratory data measured by the Video Gauge.

4. Utilise the methods to identify achievable track structure performance improvements and as a design tool.

This will enhance understanding of the vertical stiffness of track structures and extend the knowledge of the performance of products produced by LB Foster within a holistic system design approach.

The following research activities and tasks were performed within a designed methodology: firstly a review of current standards and investigation of the track structure from an holistic point of view, investigation of current track forms, current measurement techniques of the track

deflections, current modelling techniques of rail joints; secondly, the development and optimisation of a methodology and assessment of the track deflection of various track forms with the video monitoring technique; development of a numerical model to assess the structural behaviour of rail joints; use of the model as a tool for rail joint performance optimisation. The detailed research task breakdown is presented in Section 3.3, a research map showing how the objectives, the methods and their outputs are connected is given in Section 3.4 and the methods adopted are explained in section 3.5.

1.7 THESIS STRUCTURE

The structure of the thesis is presented below, informing the reader of the content and purpose of each of the chapters. Reference to the academic papers (Appendix A to D) and internal technical reports (Appendix E and list in Table 1.5) is made through the thesis. The reader should refer to the appropriate paper in order to establish the link between the detailed work and the overall topic of the project. Tables 1.4 and 1.5 present the synopsis of the papers and reports respectively. However, the discourse should stand alone to present the principle of the work.

Chapter 1 introduces the background, aim, objectives and context of the research undertaken.

Chapter 2 imparts the findings of the literature review to acknowledge the existing research work within the research topic and explains the requirement for further research. This is conducted with reference to the corresponding published papers (see Table 1.4 below).

Chapter 3 outlines the methodology adopted for the research and maps out the interconnection between the research objectives, research activities and outcomes.

Chapter 4 presents the research undertaken with key results and discussion of the research. This is conducted through references to the published papers and technical reports by the author which are presented in Tables 1.4 and 1.5 and are included as appendices as required by the EngD. The research undertaken is presented in three parts:

I. Field deflection assessment and data analysis. Video Gauge (VG) methodology be adapted and improved for the accurate and effective measuring of track deflection and data analysis protocol, to achieve the desired scope. Description of field measurements.

II. Laboratory measurements.

III. Numerical modelling procedure.

IV.   Systematic analysis.

Chapter 5 discusses the main findings of the research and their implications for the sponsoring company, wider railway industry and academia. It also provides a critical evaluation of the research and identifies a number of recommendations for future research, in accordance with the guidance for writing an EngD.

The appendices present four academic papers (see Table 1.5) and technical reports submitted as key deliverables for the sponsoring company (see Table 1.6). Throughout this thesis direct reference is made to the relevant sections of the published research papers for further detail. Only one technical report (TR) is presented in Appendix E. The technical reports (TR) 2 to 9 are not presented in appendices due to company confidentiality and for this reason their content is only presented in Table 1.5.

Table 1.5 Published papers with a synopsis of their context

Thesis reference	Title	Publication	Synopsis
Paper 1 Appendix A	Applicability of video gauge for the assessment of track displacement	*Proceedings of the Stephenson Conference: Research for Railways, Institution of Mechanical Engineers, London, UK, 25-27 April 2017, pp. 141-148*	From the perspective of railway track dynamic deflection measurement and stiffness calculation, this paper proposes the applicability of Video Gauge as a reliable way to provide high quality data of track displacement and to calculate track stiffness through its instrumentation in ballasted track, transition zones and track irregularities (rail joints) under high speed train traffic conditions. It evaluates the use of the theoretical model of beam on elastic foundation (BOEF) recommended in relevant standards and guidelines for the deduction of track stiffness values through the VG data.
Paper 2 Appendix B	Potential for external reinforcement of insulated rail joints.	*Proceedings of the Institution of Mechanical Engineers, Part F: Journal of Rail and Rapid Transit, Epub ahead of print, 22 Dec 2016*	This paper presents a static FE model designed to simulate the mechanics of suspended IRJs under various support stiffnesses. In the beginning, previous modelling of IRJs is presented and a numerical model that can be adopted for the stiffness evaluation of IRJs is concluded. Comparison between plain track and IRJ is shown by laboratory and field measurements by using the Video Gauge (VG) and is compared with the numerical results. Product design options of reinforced IRJs by the use of strap rails and robust U -beam sections are then modelled and investigated as a way of reducing the deterioration and mechanical failure of IRJs. The effect of reinforcement for various track support conditions in IRJ deflection and dip angle is shown as a potential way to reduce ballast deterioration in an IRJ.

			Based on previous field monitoring of ballasted, IRJ deflection data and track stiffness parametric analysis for IRJs by the authors, this paper presents a 3d finite element analysis of different rail joint designs to investigate their response in a fatigue static test under a dynamically enhanced vertical load, as prescribed by industry. A detailed evaluation of previous modelling techniques of IRJs and their objectives is presented prior to the experimentation and laboratory validation of the model. The numerical modelling technique developed is then described including contact non-linearities, bolt preload and elastic support conditions. Results show the maximum deflections and the stress concentration and concludes the critical factors affecting the fatigue integrity of IRJs.
Paper 3 Appendix C	Assessing the deflection behaviour of mechanical and insulated rail joints through finite element analysis	*Proceedings of the Institution of Mechanical Engineers, Part F: Journal of Rail and Rapid Transit, Accepted, 25 Feb 2018, Epub ahead of print 8 April 2018*	
Paper 4 Appendix D	The application of track deflection measurements made by the Video Gauge.	*Proceedings of the Institution of Civil Engineers, Transport,* 2017. Epub ahead of print, 21 May 2018.	Based on the applicability of VG in consultancy projects for the UK railway industry, this paper presents the instrumentation of VG in assessing track deflection and estimating track stiffness characteristics in novel ballastless track forms and ballasted track in transition zones under various loading conditions. A comparison among the experimental techniques used and recommended in standards for measuring the track deflection and the track stiffness are presented before describing the results of the VG deployment. Support system stiffness parameters are evaluated by using the analytical model of BOEF. The derivation of deflection bowl is shown for each individual train position, through the real deflection data in absence of wheel load data, that provide indication of the track behaviour for each train position.

Table 1.6 Technical reports with a brief description of their content

Thesis reference	Title	Date	Synopsis
Report TR-1 Appendix E	Fishplate Fatigue Failure estimation	17-Jan-2018	This report proposes a methodology for fatigue assessment of fishplates based on results of FEA and theoretical fatigue criteria.
Report TR-2	Reliability and applicability of a new measurement technique for the assessment of the track movement	22-May-15 submitted to CICE as part of the EngD	A robust evaluation of the applicability of the Video Gauge for measuring track deflection. In this long report a review of the current track deflection trackside measurement techniques is presented emphasizing on the advantages of VG. The accuracy of VG for measuring rail joint deflection is validated against LVDTs in the laboratory. Then the accuracy of VG is investigated through field measurements of track deflection under various loading conditions and during various set up conditions. Investigation of deficiencies/sensitivity of the technique and recommendations for improved deployment of the VG applied to the EngD scope, thus for improved deflection data of higher accuracy

Report TR-3	Investigating the Potential for External Reinforcement of Insulated Rail Joints	May -16 Submitted to CICE as part of the EngD	Analysis of RJ design, forces acting in a RJ, behaviour and material properties of RJ components, literature review on modelling of RJs, rail bending stiffness evaluation, determination of FEM parameters and establishment of FEM of track structure, calculation of effective stiffness (I_{xx}) of IRJ. Laboratory and Field tests of IRJ and plain rail deflections. FEM parametric analysis.
Report TR-4	High Definition camera measurements of track deflections at Huntingdon Bridge 144 (ECML) –Phase 1 Prior to renewal	08-Feb-16 Confidential	LB Foster performed measurements of sleeper and rail deflections at Huntingdon Bridge 144 (ECML) after manual tamping and prior to maintenance activity of a transition zone experienced drainage problems seen as ballast attrition due to subgrade pumping. A total of 18 vehicle passes were recorded consisting of Intercity 225, Intercity 125 and Class 222 running up to the train speed of 125mph. The measurement method is explained and the results of sleeper displacements is reported.
Report TR-5	High Definition camera measurements of track deflections at Huntingdon Bridge 144 (ECML) –Phase 2- After renewal	18-Aug-17 Confidential	LB Foster performed measurements of sleeper and rail deflection at Huntingdon Bridge 144 (ECML) after the renewal of the transition zone by geocell and sand blanket trackbed reinforcement. Two train passes of Intercity 125 were recorded running up to 125mph. The measurement method is explained, the vertical displacements of sleepers and rail in several positions are reported and a comparison between the results prior and after renewal is presented.
Report TR-6	Video Gauge deflection measurements of V-TRAS at Gospel Oak site	06-Jan-17 Confidential	LB Foster performed deflection measurements of V-TRAS system on 20th of October 2016 after installation and prior to traffic operation. Two V-TRAS transition systems were measured at the Gospel Oak site in London, UK. The load was applied through a Stobart vehicle of wheel load 72.5 kN moving under controlled low speed. In the first location (V-TRAS 1) a total of 16 sleepers and the edge of PORR slab system were measured. Vertical displacements of sleepers, steel bearing plates (that support sleepers in the transition system) and rail web in several positions (above sleepers and in the midspan) were measured. The results are presented and discussed.
Report TR-7	Video Gauge deflection measurements at RIDC	09-Jan-17 Confidential	LB Foster performed measurements of four different track structures at RIDC site on 10th of October 2016. Vertical displacement of rail, sleeper, slab modules and asphalt underlayment were measured for ballasted renewed track, V-TRAS transition system, IVES ballastless system and PORR slab system under loading by a vehicle set consisting of a shunter locomotive hauling two "Sea Urchin" wagons. At least six train set passes were recorded for each track structure running at a speed range from 2 mph up to 20 mph. This report presents the maximum displacements of the wagon's wheel load for each test for each position.

Report TR-8	Network Rail Fishplate Design-FEA Design Report Rev.0	02-Nov-16 Confidential	In support of Network Rail contract No. 7655-01-6958 "The Design of Fishplates" LB Foster sought to validate designs against the load cases provided by the contract. The FE methodology, assumptions and limitations are explained. In this report the fishplate designs under the conditions stipulated in load-case 2 of the contract are assessed against the criteria for yield. Assessment against the agreed endurance limit values for fatigue is also demonstrated based on maximum von Mises stresses found in fishplates.
Report TR-9	Network Rail Fishplate Design-FEA Design Report Rev.1	20-Jun-17 Confidential	A chapter of parametric analysis for reduced bolt preload value and load case 1 is reported in addition to the initial report. Preliminary investigation of the lifted fishplates is also included. This report constitutes the complementary revision of Report 6.

2   LITERATURE REVIEW

2.1   INTRODUCTION

Firstly, in this chapter the available track deflection measurement techniques that offer potential of being adopted for the assessment of the track system's vertical stiffness for use for the assessment of rail joint's behaviour (bending resistance and vertical stiffness) are appraised. It builds upon existing information given separately in the published papers of Appendix A to D. Experimental techniques of track deflection measurements and consequent track stiffness deduction methods are covered as parts of the paper *"The application of track deflection measurements made by the Video Gauge"* (see Appendix D).

Secondly, a review of the state-of-the-art modelling of rail joints is presented as parts of the papers *"Potential for external reinforcement of insulated rail joint*s" (see Appendix B) and *"Assessing the structural behaviour of mechanical and insulated rail joints through finite element analysis"* (see Appendix C). Where appropriate the relevant sections of the papers are referred to.

2.2   TRACK DEFLECTION AND TRACK STIFFNESS ASSESSMENT BY EXPERIMENTAL MEASURING TECHNIQUES

2.2.1   RAIL LOADING FROM RAILWAY VEHICLES

The railway track is subjected to forces that are represented by three components. The total vertical wheel load Q_t equals the sum of all static, quasi-static and dynamic vertical wheel loads as described below. Their classification is presented in Figure 2.1.

$$Q_t = Q_0 + Q_w + Q_{nc} + Q_{dyn}$$
<div align="right">eq. 2.1</div>

Whereas an overview of the components of lateral and longitudinal loads exerted on the track is provided in Figure 2.2. Each force can be estimated using analytical expressions (RSSB 2016).
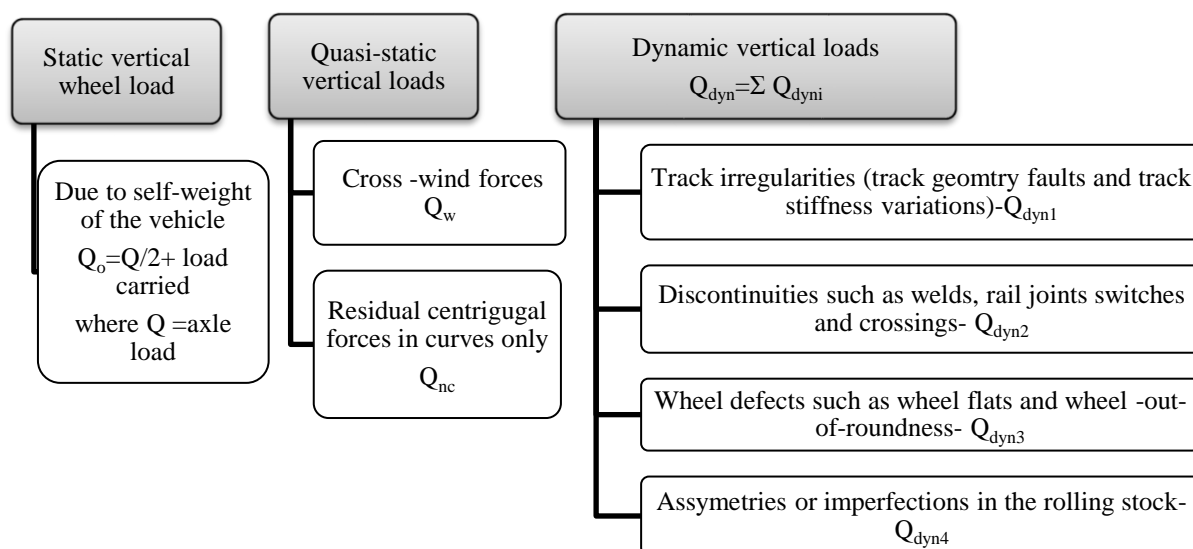
Figure 2.1 Classification of vertical loads, according to RSSB (2016)
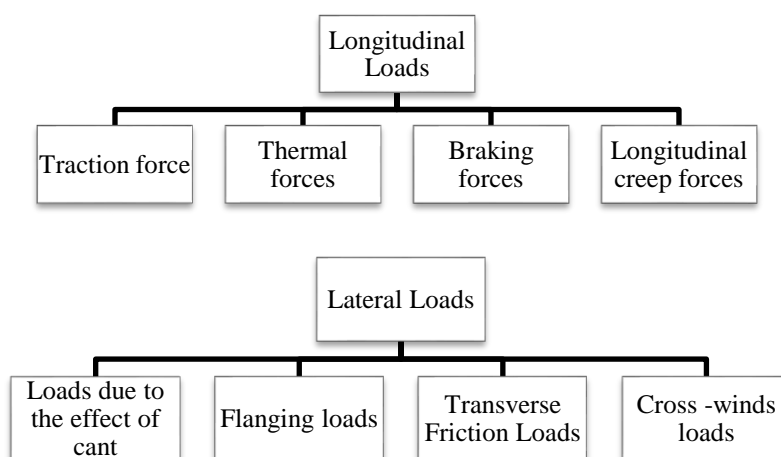
Figure 2.2 Track lateral and longitudinal loads, according to RSSB (2016)

A variety of methods (AREMA, ORE, SNCF, DB, BR, Eisenmann's) exist in literature (RSSB 2016; Van Dyk *et al*. 2013) that employ the Dynamic Amplification Factor (DAF) (or Impact Factor) approach for the determination of the design wheel load.

$$Q_{dyn} = Q_o * DAF$$ eq. 2.2

Where $DAF = 1 + \frac{D_{33} * V}{D_{wheel} * 100}$ (AREMA) eq. 2.3

Where D_{33} the diameter of a 33-inch reference wheel, V the vehicle speed in mph and D_{wheel} the wheel diameter in inches.

The dynamic factors calculated by the aforementioned methods increase with speed but each method takes into account different vehicle and track parameters such as wheel diameter, static wheel load, locomotive vehicle condition, centre of gravity of vehicle, cant deficiency in curves, sprung mass, unsprung mass, joint stiffness, joint dip angle, track stiffness and track quality.

Contrary to the quasi-static vertical loads, the dynamic vertical loads can vary measurably in practise as they depend on track-vehicle interaction, the condition of both track and rolling stock. Most of the DAF formulae have been established empirically through the investigation of wheel and track maintenance condition parameters, each of which will have improved through wheel-rail interface/rolling stock technological advancements (RSSB 2016). New calibrated values for DAF for various of the above methods, including the influence of vehicle and track maintenance parameters, joint stiffness, joint dip angle, wheel diameter, sprung and unsprung mass, track quality index and factor of probability of occurrence, are presented in recent RSSB (2016) report T1073.

Grossoni *et al*. (2014) indicates that when a wheel impacts a rail joint, there are two impact forces; the first impact, P1 force, is a high frequency peak force (500-1000 Hz) that can be five times higher than the static load and the second impact P2 force which occurs after P1 is of medium frequency (30-100 Hz) and can be three times higher than the static force. P1 depends on speed, unsprung mass, Hertzian contact stiffness (in a simple model) and dip angle whereas P2 depends additionally on the resilience of the track system and can affect its deterioration.

Standard GM/TT0088 (RSSB 1993) includes a limit only for the P2 force (see Figure 2.3) above a rail joint that can be calculated by the analytical formula:

$$P_2 = Q + (a * V_m * M * C * K)$$

eq. 2.4

where

$$M = [\frac{M_V}{M_V + M_Z}]^{0.5}$$

eq. 2.5

$$C = 1 - [\frac{\pi * C_Z}{4 * [K_Z * (M_V + M_Z)]^{0.5}}]$$

eq. 2.6

$$K = (K_Z * M_V)^{0.5}$$

eq. 2.7

Q is maximum static wheel load (N), V_m the maximum normal operating speed (m/s), M_v the effective vertical unsprung mass per wheel (kg), M_z the effective vertical mass per wheel, A_z the total angle of vertical ramp discontinuity (fixed at 0.02 rad=20 mrad), C_z the effective

vertical rail damping rate per wheel (fixed at $55.4*10^3$ N s/m and K_z the effective vertical rail stiffness per wheel (fixed at 62 MN/m).

The specifications for loading for the design of track system have been inconsistent within GB and across Europe. Part of these is defined through the standards described in Figure 2.3. An analytical review of the current practices in GB rail industry, was recently published, and is covered in the report T1073-01 (RSSB 2016).

Traffic loading on bridges BS EN 1991-2	Permissible Track Forces for Railway Vehicles GM/TT0088	Design Requirements for track systems GC/RT5021
Vertical load models LM71 and LM SW/0	Vertical Static Forces Q_{max}=125 kN per wheel	Max static axle load 250 kN
Longitudinal forces (tracking and braking forces)	Vertical Dynamic Force $P2_{max}$=322 kN per wheel on a dipped rail joint (static + dynamic increment)	A vertical dynamic force, generated by the static wheel load and the low frequency dynamic forces P2, of 350 kN per wheel and an occasional isolated vertical load of 500 kN per wheel
Lateral forces (centrifugal and nosing forces)	Longitudinal Forces	A longitudinal force of 1200 kN per rail, to allow for train acceleration and braking, and the thermal forces within the rail.
	Lateral Forces	A lateral force generated by a train of 100 kN over a length of 2m*.

Figure 2.3 Design loading for track systems, according to RSSB (2016)

2.2.2 IMPORTANCE OF TRACK STIFFNESS (PAPER 1 & PAPER 4)

Track stiffness is a vital property for the design and maintenance of railway track structures. Its evaluation is important to assess track quality, component performance, localised track faults, and to optimise maintenance periods and activities. In addition, its evaluation can help in the investigation of the performance of novel track forms, as well as the validation of numerical models. Track stiffness may be affected by many factors including track components' condition, ballast condition, by unsupported sleepers, discontinuities of rail bending stiffness (i.e. rail joints), transition zones from a ballasted track to slab systems (bridges and tunnels), as well as condition of the substructure layers. These factors can induce variations in the wheel–rail contact forces and affect the deterioration rate of track geometry and components.

2.2.3 GLOBAL VERTICAL TRACK STIFFNESS MAGNITUDE (PAPER 1 & PAPER 4)

The magnitude of global vertical track stiffness can be defined as

$$S_{system} = \frac{applied\ force\ exerted\ on\ top\ of\ rail}{rail\ vertical\ displacement} = \frac{Q(t)}{\delta(t)} \ or \ S_{system} = \frac{Q(f)}{\delta(f)} \qquad eq.2.8$$

By this definition, it is observed that S_{system} is the dynamic track stiffness that is a function of time or a function of the excitation frequency when evaluations are made in the frequency domain.

Railway system idealisation

Several rail-track structure models have been developed. Some of these are described in Figure 2.4 and Table 2.1 and show system idealisation employing masses, spring stiffness and dampers.
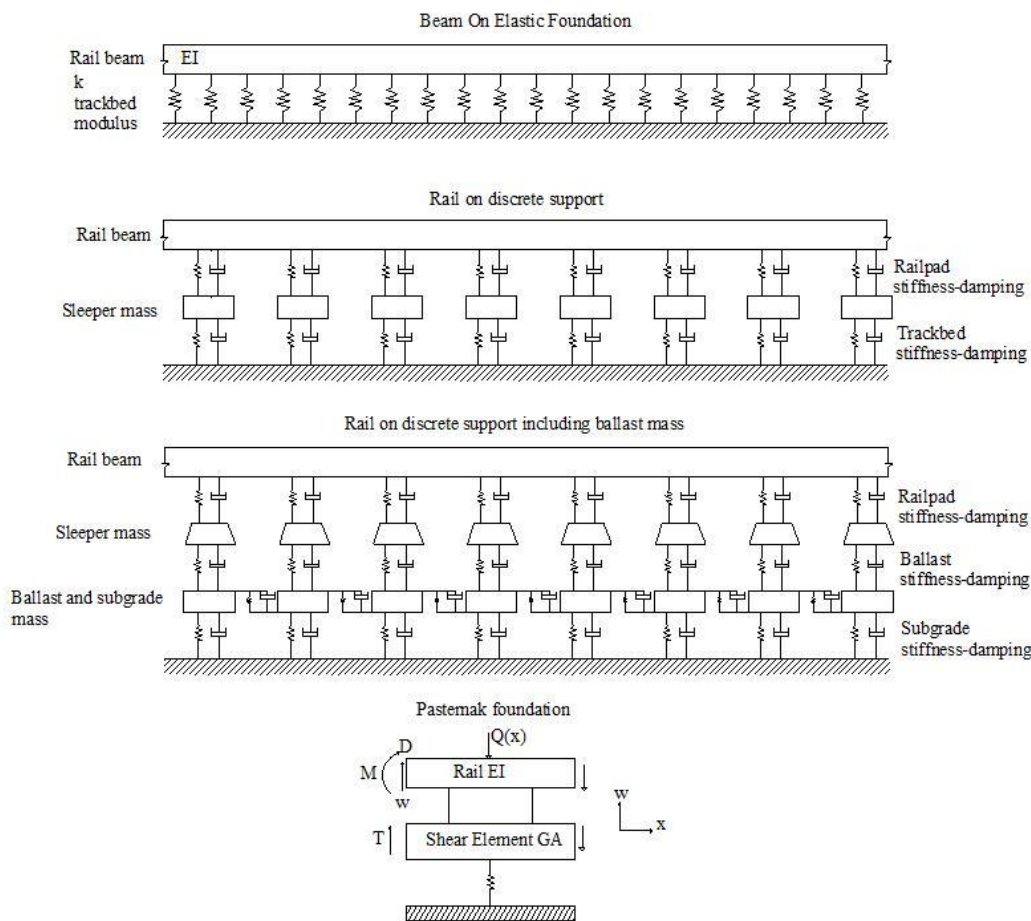
Figure 2.4 Models of rail-track system idealisation produced according to Feng (2011)

Table 2.1 Description of rail- track mathematical modelling

Mathematical model	Description
Euler-Bernoulli Beam (E-B)	Rail bending stiffness, damping is not included
Rayleigh-Timoshenko Beam (R-T)	Rotator Inertia and shear deformation is included
Beam of elastic foundation (BOEF)	Classic method, infinite E-B beam with continuous support from Winkler foundation (vertical uncoupled and elastic springs), suitable for static loading, shear deformation is not included
Beam on discrete supports	Rail beam is supported by either discrete spring-damper systems or spring-mass-spring systems modelling railpads, sleepers and trackbed
Discretely supported rail including ballast mass	Large ballast and subgrade masses with inter-connections are added allowing the investigation of ballast density on wheel-rail forces and ballast acceleration. Resonance of low frequency can be modelled.
Pasternak foundation	Shear vertical element is connected between the rail beam and Winkler foundation.

Different model techniques for static and dynamic track-soil interaction are described in detail in Section 2.8. Except the above mathematical models for railway track, various constitutive models have been developed for the simulation of soil behaviour that can be combined with a numerical approach, such as linear elastic, nonlinear elastic (variable moduli or hyperbolic), elasto-plastic (Von Mises (Soylemez and Ciloglu 2016), Mohr-Coulomb (Costa et al. 2018), Drucker-Prager (Badinier and Maïolino 2016; Biabani and Indraratna 2016)) that take into account the internal friction and interlocking mechanisms of soil particles. The majority of these models are incorporated within industrial and academic software packages of finite element modelling (e.g. ANSYS (Stark *et al*. 2015); ABAQUS (Shih *et al*. 2017) allowing the study of the plasticity, deformation and failure of trackbed layers, as well as their interaction with the track superstructure. In addition, vehicle dynamic models are also incorporated in academic and industrial software packages such as VAMPIRE, SIMPACK, VI-Rail, GENSYS (Iwnicki and Stow 1998; Spiryagin *et al.* 2014) that can be combined with track deterioration models.

The classical finite element equations for dynamic analysis are given by

$$[M]\{\ddot{u}\} + [\bar{C}]\{\dot{u}\} + [K]\{u\} = \{F(t)\}$$ eq. 2.13

Where [M], [$\bar{C}$] and [K] are the mass, damping and stiffness matrices, respectively, {u} is the vector of nodal displacements, {F(t)} is the vector of time dependent nodal forces and the overdote denotes time derivative.

Furthermore, a moving-load/track interaction model has been developed by Dahlberg (2001) that assumes discretised track settlement, taking into account a moving wheel load with a constant car body load (wheel mass and half axle mass are included, to give inertia force from unsprung mass) (see Figure 2.5). An example configuration of a quasi-static vehicle-track model is illustrated in Figure 2.6, including a simplified train model. Vehicle-track interaction models have been developed to investigate the short and long-term behaviour of track. The model developed by Ribeiro and Calçada (2017) comprises dynamic vehicle-track 2D and 3D FE analyses combined with a Matlab procedure for the application of a deformation law and the determination of permanent deformation in transition zones. The vehicle –track geometry model includes the bogie modelled as beam with mass and primary suspension with springs and dampers, the wheel as a concentrated mass with a spring with stiffness calculated using Hertz theory (Hardwick 2013; Telliskivi and Olofsson 2001) connected to the beam elements that model the rail.
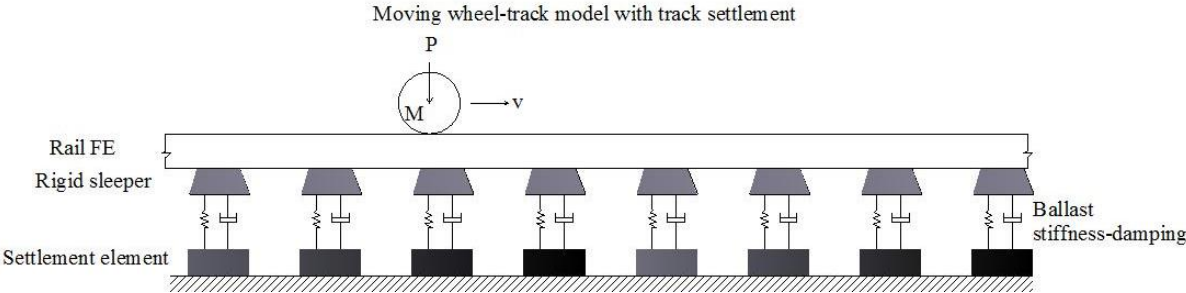
Figure 2.5 Moving wheel-track settlement model produced from Dahlberg (2001)

Quasi-static model of vehicle/track
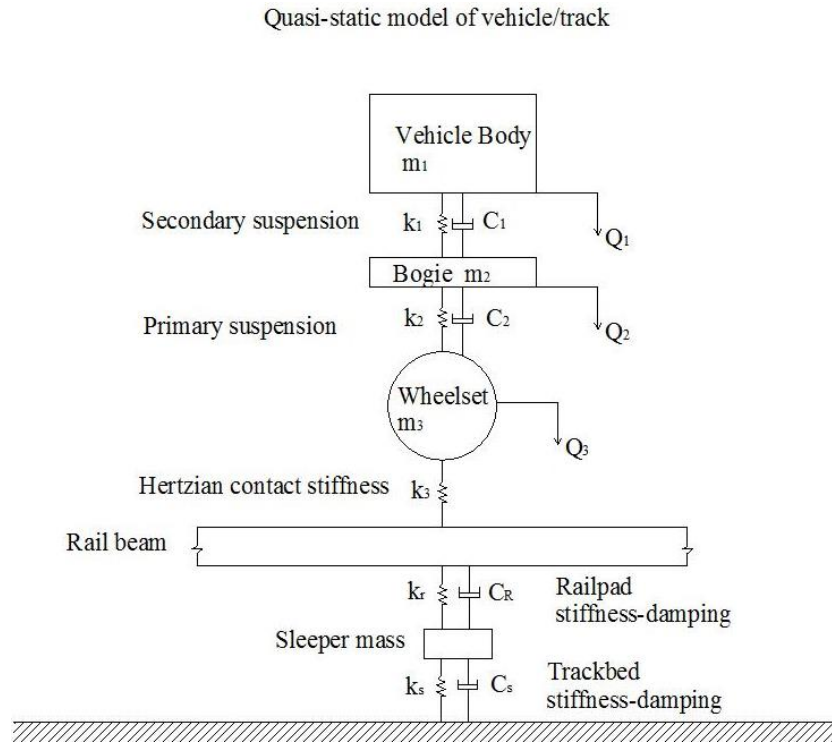
Figure 2.6 Quasi-static model of vehicle-track interaction.

Beam on Elastic Foundation (BOEF)

Conventional calculations of track stiffness are based on the static approach of beam on elastic foundation (BOEF) developed by Winkler in the 1860s assuming the rail is infinitely long and continuously supported by an elastic foundation. In this, the rail deflection can be calculated based on the wheel load, the rail bending stiffness (EI), the foundation modulus (kN/mm/mm). This theory was improved later by Zimmermann (1988) who developed a model where the rail is supported by a continuously supported sleeper; this method was later extended by Eisenmann who transferred the support areas of adjacent half sleepers into continuous support for the rail. According to these theories, the function $\delta(x)$ gives the solution for the rail deflection:

$$\delta(x) = \frac{Q}{2k_{system}L} e^{-\left(\frac{x}{L}\right)} \left(\cos\frac{x}{L} + \sin\frac{x}{L}\right) \qquad \text{eq. 2.9}$$

where x the distance from the wheel load application point to the point of interest to measure, Q the applied force exerted on top of rail and L is the characteristic length of the track, a parameter that defines the deflection bowl of the point load along the rail and is determined by

$$L = \sqrt[4]{\frac{4EI}{k_{system}}} \qquad \text{eq. 2.10}$$

and k_{system} is defined as the series support system modulus, a combination of railpad modulus ($k_{railpad}$) and trackbed modulus ($k_{trackbed}$) given by

$$\frac{1}{k_{system}} = \frac{1}{k_{railpad}} + \frac{1}{k_{trackbed}}$$
eq. 2.11

The term modulus, k, used to describe the line load required to cause a unit deflection is defined as load per unit length (MN/m) per unit displacement (δ) (measured in MN/m^2). The distributed support stiffness can be calculated from the sleeper spacing (c) and the discrete stiffness of railpad, ballast, and subgrade: $k_{trackbed}=s_{trackbed}/c$, and $k_{railpad}=s_{railpad}/c$.

For the wheel load application (x=0) and rail displacement measurement by combining eq. 2.8 and eq.2.9 the global static-stiffness is given by:

$$S_{system} \left(in\ \frac{MN}{m} \right) = \frac{Q}{\delta_{(0)}} = 2k_{system}L$$
eq. 2.12

It should be noted that in eq. 2.11, the rigid sleeper stiffness is omitted as the inertia effects and the ground acceleration have not been considered (quasi-static analysis). A quasi-static analysis does not automatically calculate loads that may arise from dynamic effects and assumes that the accelerations of the track structure and the ground are negligible (Powrie and Le Pen 2016).

In transition zones, the BOEF can be applied for the investigation of track moduli from the deflections of individual sleepers, however, the BOEF does not take into account any non-linearities and inelastic behaviours such as the existence of voids under the sleepers. For this reason, the investigation of the deflection bowl would be a better indication of the average stiffness over a short section of track such as in a transition zone. A deflection bowl can be determined through the measurement of a number of sleeper deflections under the application of the wheel load in one position (one sleeper). As a result, the whole deflection bowl is captured showing the number of sleepers deflected under the specific load. The deflection bowl can be determined for various wheel load positions giving an indication of the bearing capacity of the sleepers' support.

What is important in order to reduce track degradation and track maintenance costs, is to eliminate track stiffness variations along the track. This is predominantly affected by the ballast and subgrade condition, the existence of voids and the design stiffness limits for ballasted and slab track. However, there is not universally agreed limits for stiffness variation for transition zones.

2.2.4 TRACK STIFFNESS MEASURING TECHNIQUES (PAPER 1 & PAPER 4)

Track system stiffness can be measured in two ways: track instrumentation that mainly measures track deflection in discrete locations, and using estimated static train wheel load or measured dynamic wheel load; or by standstill or rolling vehicles that are used for local or continuous measurements of the dynamic stiffness over a longer track length (see also Section 1 of P1 (Appendix A), Section1 of P4 (Appendix D), Background and Table 1 of P4).

2.2.5 TRACK STIFFNESS MEASUREMENT BASED ON STANDSTILL AND ROLLING VEHICLES (SECTION 1 OF PAPER 4)

Dynamic stiffness is a complex parameter that can be represented by its magnitude and its phase. Its magnitude is defined by the ratio of the applied load to the direct rail deflection (kN/mm), whereas the phase is a measure of deflection delay by comparison with force. The phase has a partial relationship with damping properties and ground vibration (Innotrack 2006). Examples of such vehicles are the RSMV (Rolling Stiffness Measurement Vehicle) (Li and Berggren 2010) and the Portancemètre as described in Innotrack (2006). These methods include loading and measurement equipment. The track is dynamically excited through a suspension mass above a vibrating wheel axle. The stiffness is calculated from the measured axle box forces and through double integration of the wheel accelerations.

The FWD (Falling Weight Deflectometer) (Sharpe and Collop 1998) and the recent developed Rail Trackform Stiffness Tester (RTST) (Govan *et al*. 2015) are also used to determine dynamic sleeper support stiffness at discrete points by measuring indirectly the deflection of an unclipped sleeper under a known falling mass. Both are based on load cell and geophone recording. A known weight is dropped in the load cell which sits on an unclipped sleeper which transfer the pulse load into the trackbed. The ground wave generated is measured using three geophones at set offsets to the loading position.

2.2.6 TRACK STIFFNESS MEASUREMENT BASED ON TRACK INSTRUMENTATION (SECTION 1 OF PAPER 4)

The static track stiffness can be measured by several pieces of trackside equipment. Track instrumentation includes either measuring the track system displacement and calculating the

stiffness from the applied load (a direct approach) or measuring the velocity of a sleeper, integrating the velocity data to displacement data and evaluating trackbed stiffness per sleeper end from the applied load (an indirect approach). In both cases the calculation of track stiffness requires a calculation of the axle load and a model of track behaviour such as the beam on elastic foundation (BOEF).

The load can be estimated according to the train type (gross static load) neglecting the number of passengers and dynamic effects. Accurate determination of wheel loads can be based on shear forces by using strain gauges in the rail at the point of load application. Such devices need calibration against known applied loads which is difficult to achieve in the field. Thus, track instrumentation techniques can be separated into:

- **Direct Track deflection measuring techniques (Section 1 of Paper 1, Section 1 of Paper 4)**

Trackside technologies that include direct methods of measuring the track deflection include:

- linear variable displacement transducers (LVDTs) (Paixão *et al*. 2014; Zakeri and Abbasi 2012; Anderson and Rose 2008).

- laser deflectometers (Innotrack 2006; Paixão *et al*. 2014)

- multi-depth deflectometres (MDD) (Mishra *et al*. 2014)

- remote video monitoring using PIV (Particle Image Velocimetry), (Bowness *et al*. 2007)

- remote video monitoring using DIC (Digital Image Correlation)) (Murray 2013; Thompson *et al.* 2015; Stark *et al.* 2016)

- Video Gauge (Gallou *et al*. 2017)

- **Indirect track deflection measurement techniques (Section 1 of Paper 4, Section 1 of Paper 4)**

Track instrumentation that includes indirect methods of track deflection measurement includes:

- geophones (Innotrack 2006; Bowness *et al.* 2007; Le Pen *et al.* 2014)

- accelerometers (Lamas-Lopez *et al.* 2014; Stark *et al*. 2016)

2.2.7 COMPARISON OF TRACK STIFFNESS MEASUREMENT TECHNIQUES (TABLE 1 OF PAPER 4)

The factors affecting the choice of the deflection measurement technique and the parameters affecting the sensitivity of the derived track stiffness values are presented in Figure 2.8 Figure 2.8. Table 2.2 describes the advantages and disadvantages of each measurement technique.
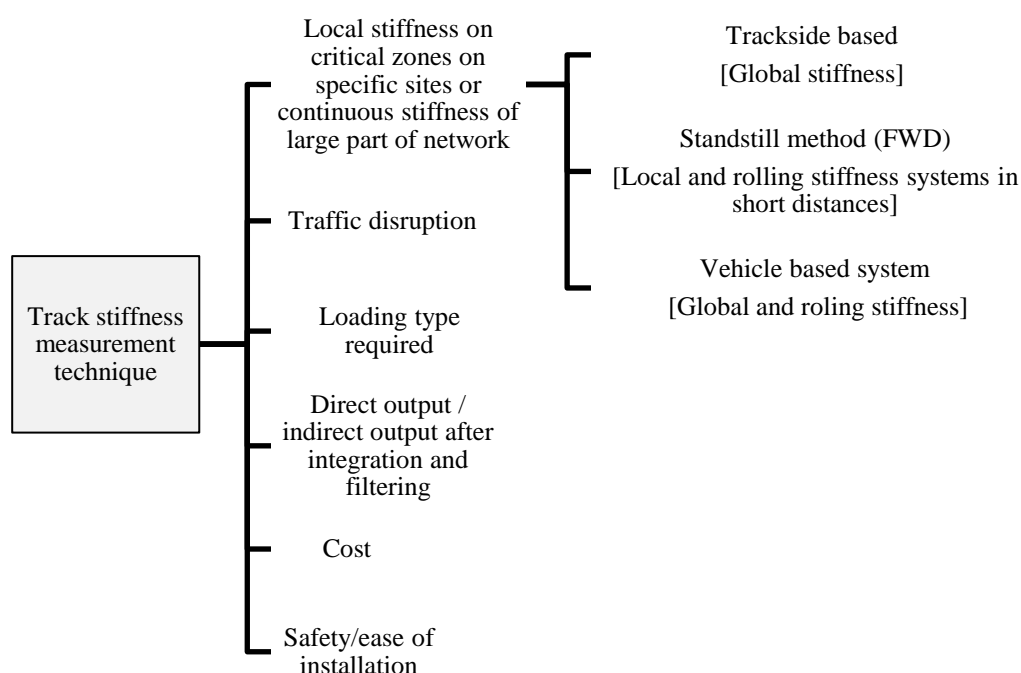
Figure 2.7 Factors affecting track stiffness measurement technique
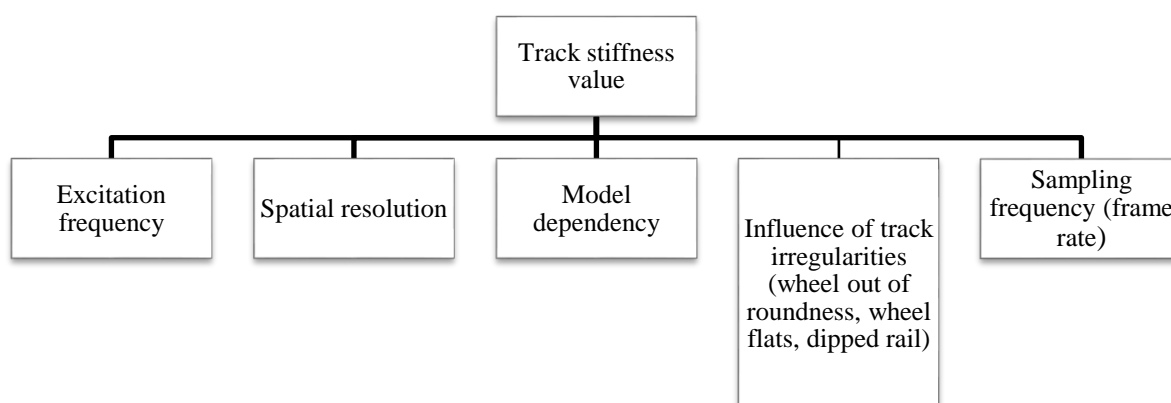
Figure 2.8 Factors affecting track stiffness sensitivity

Table 2.2 Advantages and disadvantages of track stiffness measurement techniques

Measurement technique	Advantages	Disadvantages
LVDT (Paixão *et al.* 2014)	High accuracy for high speed Direct deflection High capture rate (e.g. 500Hz)	Single axis (non- accurate results if movement in 2 axis) Needs track access Need steel rods-additional non-movable reference zero deflection frame
Laser deflectometer (Innotrack 2006; Paixão *et al*. 2014)	High resolution to 0.001mm Direct deflection	High cost Ground borne vibration of the tripod may affect the accuracy Single point measurement
Multi-depth deflectometer (Mishra *et al.* 2014)	Direct deflection Measures permanent deformation	Requires fixed datum at depth Can be problematic to install
Geophones (Innotrack 2006; Bowness *et al*. 2007, Le Pen *et al.* 2014)	Output voltage proportional to relative velocity, measures velocity of sleepers Resolution to 0.07mm	Initial noisy data need correction of signal, filtering and post processing to give accurate displacement values (need Inverse Fourier Transform and integration of velocity to absolute displacements) Train principal vehicle passing frequency must be higher than geophone natural frequency (above 0.5-1 Hz), problematic for low speed train passage. High unit cost (£380) Single point measurement where each geophone is positioned High capture rate of raw voltages (e.g.500Hz) but not of actual deflection
Accelerometers (Lamas-Lopez *et al.* 2014; Stark *et al.* 2016)	Measures acceleration Low cost	Requires double integration and filtering of the signal from acceleration to displacement Less reliable in low frequencies (typically <3 Hz) Single point measurements
Remote video monitoring (RVM) using PIV (Bowness *et al.* 2007)	Direct deflection Software comprising with multiple cameras Noise reduction Post process 2D OR 3D Remote monitoring apart from target positioning-Safe Easy set up	High resolution only when long sight e.g. 15m Small capture rate e.g. 30Hz Affected by ground borne vibration Only 1 sleeper or location can be monitored at a time

RVM using DIC (Murray 2013; Thompson *et al.* 2015) and Video Gauge (Gallou *et al.* 2017)	All advantages of RVM using PIV High capture rate (e.g. 200Hz) High resolution to 0.001mm Multiple points at a time, enables measuring structures from <0.01mm wide to >1km long. Applicable in frequencies more than 200Hz by using expensive higher frame rate cameras Deflection bowl can be measured	Sensitivity is affected by alternating lighting conditions during outdoor recording.
Vehicle systems RSMV/ Portancemètre/TLV (Innotrack 2006; Li and Berggren 2010)	Dynamic track stiffness up to 50 Hz and stiffness phase (deflection delay by comparison to force) Continuous measurements over long track length	Additional cost of transport to site and locomotive during measurements. Difficult for widespread use.
FWD (Sharpe and Collop 1998), RTST (Govan *et al.* 2015)	Based on load cell and 3 geophone recordings at set offsets to the loading position. Indirect deflection of unclipped sleeper under a known falling mass. Static support system stiffness without a live train wheel load	Assumptions of linear load distribution with depth outside the loading cone to provide deflection of nearby track, uncertainty due to model dependency. Uses as input parameters the surface deflection bowl and the layer thickness to deduct bottom of ballast and top of subgrade indicative deflections. Assumes consistency of ballast and subballast layers thicknesses. Geophones' signal processing is used (integration and filtering). The loading is not instantaneous, the signal is taken after the settle-down of the oscillation caused by 3 drops to the load cell. Neglects the uneven stress distribution below sleepers e.g. due to voiding

2.2.8 CONCLUSION AND JUSTIFICATION OF CHOICE OF THE VIDEO GAUGE (PAPER 1 & PAPER 4)

The focus of the above list was to show the advantages of the Video Gauge system, as a newly-introduced system for track investigation (Waterfall *et al.* 2015), to be used in this project to assess direct real-time overall track deflections under low and high-speed train operation shortening the cost, the time of set-up, and without the need for traffic disruption and extensive track access.

The Video Gauge (VG) is a remote video monitoring technique that is based on DIC and Video Extensometry. It offers advantages over the previous remote video monitoring techniques. DIC is based on pattern recognition principles and image pixel tracking, by comparison of original and deformed images. Frame by frame comparison allows for measurement of displacement (and strain calculations from the displacement) of pixel blocks, that should be random and unique, with a range of contrast (intensity) levels. DIC uses surface features of specimens, or applied coatings, or targets. VG enables ultra-high-resolution measurements of distance, displacement, strain, and rotation to be made. It supports the use of multiple cameras for 2D or 3D measurements. It combines resolutions of up to 0.001 mm with high capture rates (up to 300 Hz or even higher when using more expensive, higher frame rate industry cameras) enabling structures of various widths and multiples points to be measured, at once (over 100 points at time). The VG system provides data of high quality and quantity with high accuracy offering substantial time and cost saving when compared with traditional trackside instrumentation.

The development process required to improve the methodology of the proposed system in order to obtain accurate rail deflection data to meet the aim and objectives of this project is explained in section 3.5.2. The methodology development is analysed in section 4.1. The methodology used and results are presented in Appendix A (P1) and in Appendix D (P4).

2.3   INSULATED RAIL JOINT MECHANICS (PAPER 2)

The main purpose of an IRJ is to separate electrical circuits in rails and turnouts whilst joining two pieces of rail. This is achieved through the use of joint bars (fishplates), fastened through the web of the rail with bolts. Insulated rail joints (IRJs) are critical components of railway signalling infrastructure where sections of track are separated into separate blocks so track circuits can be used for train detection. While a purely mechanical bolted joint just comprises fishplates and bolts, an IRJ includes material fitted between the rail ends made of a non-conductive material (endpost) as well as an insulated lining to separate the fishplates from the rails to maintain electrical separation of the adjoining rails (see Figure 2.9). Sometimes IRJs are also glued to increase joint robustness.

Although the fishplates are designed to offer a similar shear capacity to the parent rail section they support, a bolted joint arrangement remains weaker in resistance to bending. As a consequence, rail joints deflect more than adjacent continuous rails on nominally the same

support conditions. This also means that an increased dynamic force is generated as a wheel passes over the joint and over time, a ballasted support structure will accrue more damage and the deflection at a joint is usually found to progressively increase until maintenance limits are reached or failure occurs.
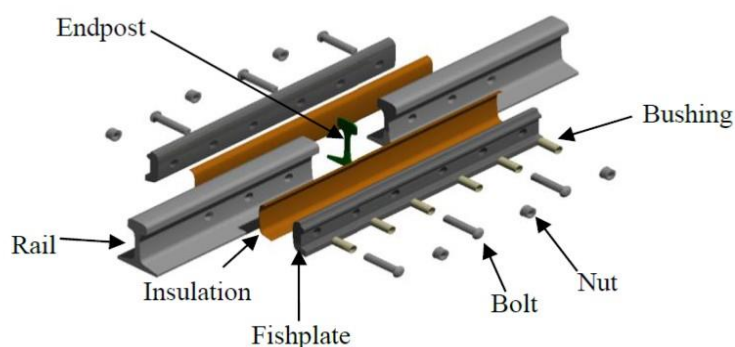
Figure 2.9 IRJ assembly (reproduced from Paper 3)

In a standard UK fishplated joint, the moment of inertia of the joint fishplates is only 29% of that of the parent rail (Beaty 2014). The load distribution is different due to the stiffness discontinuity. This can be improved by modifying the design of the joint or the support conditions; however, the weakness in bending is still present. In addition, it has been found that the dynamic impact from a wheel on a rail joint is three times larger than the static wheel load (Akhtar *et al*. 2008). The service life of rail joints varies depending on the traffic loading and frequency: Australian research has claimed that it can be only 50 MGT (million gross tons) of freight traffic (Dhanasekar and Bayissa 2009); American research has claimed 200 MGT with replacement requirements in a period of 12-18 months with costs of $10,000 per mile per year (Akhtar *et al*. 2008), which is significantly less than the service life of other rail components that withstand up to 1000 MGT (Zarembski *et al.* 2005); whereas failures of IRJ cost Network Rail (UK) ten million pounds in a two year period (Beagles *et al.* 2015). This project investigates the rail joint behaviour made by LB Foster with the aim of vertical stiffness/deflection assessment and its improvement.

2.4 FAILURE MECHANISMS OF INSULATED RAIL JOINTS (PAPER 2 & PAPER 3)

The railway system's dependability is based on rail components' structural integrity. The failure of insulated rail joints (IRJs) is a worldwide problem in railway networks and a major component of the maintenance cost. An IRJ can fail mechanically, electrically, or both. Mechanical (structural) failures occur either in the fishplates, rail, bolts, or epoxy (Charlton 2007) due to high static, dynamic, and fatigue loads that weaken or cause the total failure of rail joint components. Electrical failure is caused when the electrical isolation between the two adjoining rails is lost and can be caused either by a mechanical failure or by other factors such as lipping or contamination. Figure 2.10 shows a list of the failure modes of IRJs as they have been listed by UK national rail network owner and operator. The statistics though do not give any information on the train speeds or track configurations with respect to joint failures. The major failure modes, their causes and mitigation measures are presented in Table 2.3.

Rail Joint Failure Modes
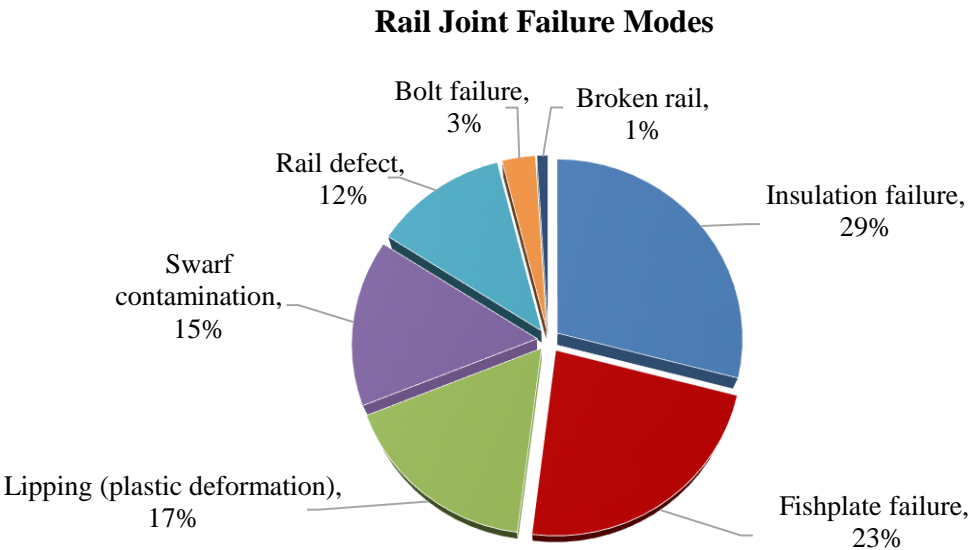
Figure 2.10 Rail Joint failure modes as listed by Network Rail study (LB Foster Rail Technologies 2010)

Table 2.3 Major failure modes and mitigation measures

Failure mode	Cause	Detection for maintenance	Mitigation measure
Joint dip angle	Inadequate support to sleepers from the underlying ballast that causes additional bending at the joint	Track geometry train reports, visual inspection	Speed restriction, lifting, packing, repair/ replacement according to dip angle level (≥30, ≥40, ≥50 mrads) (Network Rail 2015)
Broken Fishplates	Stress developed in the fishplate exceeding endurance limit based on tonnage (fatigue)	Visual indication of cracks.	Replacement of IRJ within anticipated lifespan. Periodic visual inspection.
Bond Failure / De-lamination of End Post	Vertical deflection of the rail at the joint which induces shear stress in the adhesive bond between the rail and fishplate or endpost.	Visual inspection	Reduce vertical deflection of the rail so as to reduce shear stress developed in the adhesive. Deflection reduction is achieved by IRJ's effective stiffness increase.
Loosening of Bolts	Vibration on track, more significant for non-glued IRJs (dry) where fishplates are kept in place on the rail only through bolts, it can lead to increased deflection.	Manual or inspection with tool (hammer) during visual inspection	Improved damping methods to reduce vibration on track

The mechanical failure of an IRJ can increase ballast degradation and can also impede the electrical integrity of an IRJ thereby causing train detection issues (signalling). IRJs are considered a weak point because of the discontinuity in the stiffness of rail. IRJs deflect more than regular plain track because of the lower cross section area, lower section moment of inertia of the fishplate and the elasticity of the insulation layer. This structural discontinuity interacting with the wheel impact load causes a vicious cycle of joint and track degradation. As wheel pass over the joint, joint anomalies such as bolt looseness and rail height mismatches can be caused, and with repeated wheel passes rail end wear occurs. Degraded joints cause large deflections and amplify the dynamic force induced at the joint. This leads to the acceleration of the track degradation, which in turn provokes a progressive increase of joint deflection.

2.5 METHODS OF IMPROVING THE RAIL JOINT LIFE

Methods of improving the rail joint life that have been investigated or tested in literature in the past include:

- Mounting a joint on top of a sleeper: supports the joint from underneath but involve extra complications due to the need for insulating sleeper plates and rail clips (Endura-Joint system, LB Foster 2014).

- Increasing the size of fishplates or their material (fibre glass reinforced plastics, high tensile steel, micro-alloyed steel) to make them capable of coping with higher stress values.

- Joints with thicker section in the middle in the vicinity of the rail end to increase vertical stiffness of the joint assembly (Endura-Joint system, LB Foster 2014).

- Inclined-cut joints (Vossloh 2017): improve wheel transfer and improve lipping, but no increase of fatigue life was shown.

- Increasing endpost thickness: this has been suggested as a means to reduce the rate of metal flow or lipping across the gap. However, the wider the gap between two rail ends the weaker the joint becomes, and this could increase the deterioration rate of an IRJ associated with the support structure. So, this has been controversial in the literature (Beaty *et al.* 2016). Further *in situ* field testing is required to determine the effect of endpost thickness.

- Improving endpost material (polyurethane, aramid, polyamide 12, epoxy/glass composite, ceramic) to reduce lipping (Beaty *et al.* 2016) or to reduce fishplate stresses (Soylemez and Ciloglu 2016).

- Increasing the hardness and strength of rail steel to reduce lipping or vertical deformation (R260, R350), or laser clad Stellite 6 layer on top of rail end surface that is very cost ineffective for industry (Beaty *et al.* 2016).

Most of the techniques focus on the reduction of the localised lipping effect. However, the effect of overall joint deformation needs to be considered. In addition, the vertical plastic deformation around the centre of an IRJ leads to dips in the track. Dipped joints are recorded through trains that measure track geometry. These joints act as precursors of premature failure of the joint and the surrounding track structure. They are associated with track support degradation and structural failure of the IRJ. The idealised dip angle $\alpha_1 = \alpha_2 = \alpha$ can be defined through eq. 2.1 below, where the ratio of the tangent of α can be defined through the difference between the rail deflections in the position of the dip and at a distance L/2 away of the dip, divided by L/2, where L the effective length equal to 0.25m, 0.5m, or 1m (Grossoni *et al*. 2014). Figure 2.11 shows an idealised form of a dipped angle where the dotted lines are the geometrical constructions for the calculation of the effective length (Grossoni et al. 2014). Thus, the total idealised dip angle can be calculated by the following formula:

$$2a \ (in \ rad) = 2 * atan \left(\frac{(defelction \ at \ the \ centre \ of \ the \ joint \ (x=0)) - (deflection \ at \ x=L/2)}{L/2} \right) \qquad \text{eq.2.1}$$
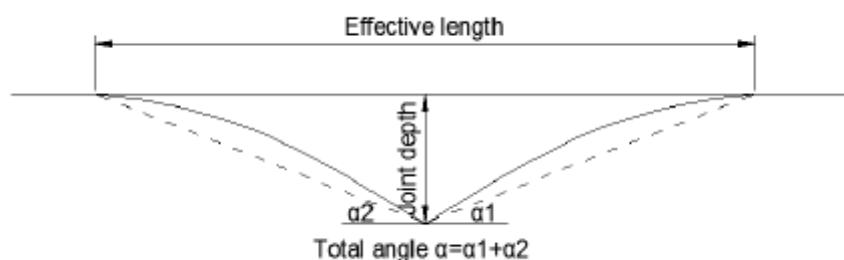
Figure 2.11 Idealised dip angle form, from Grossoni *et al.* (2014)

2.6 RAIL JOINT TYPES

2.6.1 BASED ON INSULATION (PAPER 3)

Insulated rail joints are designed to insulate track sections and are classified in the UK rail network according to the insulation type and the type of track they are used for [Network Rail 1996].

- Class A: glued joints suitable for CWR (continuous welded rail)
- Class B: dry (non-glued) encapsulated joints suitable for CWR
- Class C: dry (non-glued) joints for jointed track.

A description of the components of each assembly is given in Sections 1.1 and 3.3 of Paper 3 (Appendix C).

2.6.2 BASED ON SUPPORT TYPE AND NUMBER OF BOLTS (PAPER 3)

Support for joints is split into two types. A suspended joint that is an unsupported joint situated between two supports (sleepers) with regular spacing. A supported joint is situated on top of one support, one sleeper or a double sleeper. Rail joints can be 4-bolt or 6-bolt (see Figure 2.12). 4-bolt joints are positioned in straight track and near switches and crossings mainly due to space restrictions, whereas 6-bolt fishplates are used when the joint is needed to be as strong as possible so that the stiffness discontinuity can be reduced, they are more common in tangent track.

Figure 2.12 (i) A glued 6-bolt IRJ and (ii) a dry 4-bolt IRJ

Another type of joint is the inclined-cut, "angle-scarfed", joints whose rail ends are cut diagonally to the rail direction. A previous study by Dhanasekar and Bayissa (2011) concluded that they resulted in lower vertical strains but higher shear strains than the square-cut joint. An inclined-cut joint has been developed (Vossloh 2017) and was proposed for reduction of noise, improvement of wheel transfer, and potential reduction of lipping in the rail head; but no fatigue life improvement was demonstrated. These are not considered in this thesis.

2.7 EXPERIMENTAL MONITORING OF RAIL JOINTS (PAPER 2 & PAPER 3)

Experimental investigation of rail joints is very limited and includes only measurements of strains (vertical, shear, lateral) and impact wheel forces. The evaluation of IRJ performance in the laboratory has been assessed by strain gauges and in the field by very expensive impact load detectors. These are summarised in Table 2.4.

Table 2.4 Literature findings of experimental investigation of IRJs

Author	Experimental technique	Comments
Soylemez and Ciloglu (2016)	Strain gauges attached to the IRJs estimating the tension stresses on fishplates up to 100MPa for 160kN at 62 mph measured in the field by strain gauges and impact load detectors.	No indication of the position of these stress values in the fishplates.
Bandula-Heva, Dhanasekar and Boyd (2012)	Vertical, lateral and shear strain of railhead edge from a half-cut rail joint in the laboratory measured by PIV method and validated by strain gauges.	A wheel-rail contact assessment to be used for the lipping failure mechanism of the IRJ only. The results are indicative only for an IRJ cut in the half; the vertical stiffness of the joint may affect the results.

Askarinejad, Dhanasekar Boyd and Taylor (2012)	Wheel-rail contact impact force at an IRJ in a heavy haul rail line using the shear-strain gauge-based wheel-load detector finding that the peak force at an IRJ is 35% higher than that of the reference rail.	Very expensive method.
Askarinejad, Dhanasekar and Cole (2012)	Field measurements of wheel –rail vertical force, rail/fishplate bending strains, sleeper vertical acceleration and sleeper ballast pressure at two IRJs.	Experimental method that required pre-installation process for the detailed strain gauging of rail and fishplates. It cannot be used for routine assessment.

Looking at the above studies it is concluded that there is very limited experimental work conducted to identify the overall deflection values of IRJ both in laboratory and in field. In addition, it is concluded that IRJ stress/strain measurements depend strongly on the exact location of strain gauge installation, and may not be an accurate method to determine IRJ deterioration routinely. The literature mainly concentrates on local stress and strain issues or areas of performance of the joints.

2.8 MODELLING TECHNIQUES OF TRACK STRUCTURE

In order to evaluate the track performance under traffic loading, a realistic stress distribution between the interfaces of the track components is required. The effect of sleeper geometry, the rail pad stiffness, the sleeper spacing, the track bed stiffness, mechanical and physical soil properties should be taken into account (Dahlberg 2004). Modelling can couple vehicle-track-soil interaction according to the scope of the project.

2.8.1 MODELLING FOR STATIC LOADING

The analysis of track structure today is mostly realised in two ways:

1. Simple representation of the track structure where ballast, subgrade and sleeper bending are not sufficiently evaluated. For example, the beam on elastic foundation model where the damped Winkler foundation represents the substructure as a spring damper system (Garcia-Palacios et al. 2011).

2. Detailed finite-element model with capability of representing the interactions between the track components and taking into account the effect of traffic loading on the stresses, strains and deformations on the interfaces between the sleeper, ballast and subgrade and producing realistic pressure distributions (Dahlberg 2004).

Previous models for static loading have used multi-layer linear elastic theory to simulate the ballast and the subgrade mostly focusing on the stresses developed in these layers for varying ballast thickness and subgrade type (stiffness).

2.8.2 MODELLING FOR DYNAMIC LOADING

Two types of techniques are used for investigating train and track interactions by taking into account the vibrations and their consequences: frequency-domain techniques, and time-domain techniques. Both techniques try to capture the dynamics of the compound train and track system. The first, by investigating the track and wheel response to a "moving irregularity": the rail and a stationary wheel are excited at the wheel-rail contact patch by a prescribed displacement; Dahlberg (2004) compared this excitation with a strip of irregular thickness inserted and moved between the rail and the wheel in order the irregularity of the strip to excite the wheel and the rail; a sinusoidal wheel-rail response, can then be described through a frequency domain receptance function. The second calculates time domain deflections of the track and displacements of the vehicle by numerical time integration as the vehicle moves along the track.

The first aims to handle fully linear systems; the track responses are also assumed to be stationary and cannot handle singular events along the track (such as a rail joint, a sleeper hanging in the rail, varying stiffness) and the Fourier Transform is calculated by combination of track and wheel receptances and the wheel rail contact stiffness. Then the inverse of transform provides the time-domain response (Dahlberg 2004). A non-sinusoidal irregularity (as from wheel-rail interface) must first be transformed into the frequency domain by the Fourier Transform. The track and wheel receptances and the wheel-rail contact stiffness are combined to create the transfer function. Then the together with the Fourier transform of the irregularity the Fourier transform of the track response can be obtained and the inverse transform will provide the time domain response. This technique has been used for the investigation of the short wavelength corrugation on railhead (Dahlberg 2004). In the second, the track can be modelled by finite elements and a modal analysis of the track can be performed: this enables including elastic deformations of the wheelset without a large increase of the number of degrees of freedom of the compound train-track system. The modal analysis technique requires linear models, but non-linearities can be handled by considering extra loads on the linear track model (Dahlberg 2004). Other than the Finite Element method (FEM) other methods have been used such as coupled FEM with Boundary Element method (BEM) for

modelling the train- track –soil interaction (Auersch 2005), Discrete Element method (DEM) for the investigation of sleeper behaviour and ballast settlement (Laryea et al. 2014) or Finite Difference method (FDM) such as modelling with FLAC (Fast Lagrangian Analysis of Continua) for the investigation of soil-track interaction in geogrid-reinforced and pile-supported railway embankments (Huang, Han and Collin 2005).

A wide literature review of modelling techniques for both static and dynamic modelling of the railway track is presented in Steffens (2005) where implications in modelling the vehicle, the wheel rail contact, the track, and irregularities of the system are discussed. A summary of recent work relating to modelling of the track structure is presented below.

Table 2.5 Literature findings of methods of track structure modelling

	Authors	Research aim/description
Analytical/ mathe-matical	(Garcia-Palacios *et al*. 2011)	Linear elastic analysis of the railway track as spatially periodic structure (continuous beam of finite length of thousands of spans (2N) supported by elastic vertical springs) in MATLAB using Discrete Fourier Transform to reduce q(2N+1) linear stiffness equilibrium equations to a set of 2N+1 uncoupled systems of q equations each. The model is validated against Zimmerman-Timoshenko (for low values of N) in terms of force reactions and displacements and is considered to be 20 times more efficient in computational time than standard matrix structural analysis (e.g ANSYS script).
FEM	(Lundqvist & Dahlberg 2005)	Dynamic 3D FE train-track interaction model to investigate the influence of voided sleepers and load impact in the track. The model was built up using the preprocessor TrueGrid and explicit LS-DYNA, lasts for 20h on 1.5GHz processor and is 30 sleepers long. The wheel is modelled as a rigid body loaded by the car body weight taking into account the unsprung mass. The voids are modelled using penalty methods (master, slave surfaces) allowing the calculation of contact forces. Three sleepers are modelled as flexible deformable bodies and the rest as rigid bodies. The results showed that 1mm gap of 1 sleeper can cause 70% increase in the contact force of the adjacent sleeper/ballast and 40% deflection increase in the adjacent sleeper. Worst case is when 1 well supported sleeper is surrounded by 2 unsupported sleepers.
	(Himebaugh *et al.* 2008)	Static linear elastic FEM of supported IRJ to assess deflections and epoxy stresses (adhesive) using ABAQUS. The effect of wheel location, wooden sleeper size, length and thickness of fishplates are investigated. Elastic foundation below sleepers is used. It was shown that increasing the fishplate thickness increased significantly the stresses found in the epoxy.
	(Stark, Wilk, Thompson II, & Sussmann Jn 2015)	Effect of unsupported sleepers in open track and in transition zones on the approach of stiff bridge abutments using explicit LS-DYNA. The model is 32 sleepers long, includes primary and secondary suspension (4 wheels with 2.8m axle spacing). The increase (%) of wheel-rail forces and sleeper-ballast contact forces is investigated using master-slave penalty methods (resistance to penetration) for varying voided sleeper scenarios.
	(Burrow, Shi, Wehbi and Ghataora 2017)	Dynamic 3D modelling including train-track interaction with Hertzian contact, vertical track quality and elastic behaviour of trackbed to investigate damage on track foundation and predict additional ballast thickness requirements combining analytical approaches for plastic strain and settlement. Findings indicated the significant effect of track quality in ballast life.

DEM	(Laryea *et al.* 2014)	Use of DEM of sections of sleepers and ballast particles to simulate laboratory cyclic testing to compare the behaviour of concrete and steel sleepers and their effect in ballast settlement and ballast-subgrade interface pressure. It was shown that in the short term the steel sleepers perform better and thus they are suggested as a short-term solution.	
	(Zhang, Zhao and Zhai 2016)	A 2D DEM model coupled with vehicle-track coupled dynamic model to investigate the dynamic behaviour of ballast particles under moving high speed vehicle loads by using the Particle Flow Code (PFC). Contact forces, vibration response, stress and vibration attenuation of ballast particles at various speeds are investigated. Clump model is used to simulate the interlocking of ballast particle with real irregular shape though coupling PFC with digital image and bubble pack algorithms. Sleepers are also modelled as a clump, railpad as a disk element and rail as a series of bonded disk elements. Contact forces in ballast follow linear Coulomb law. The dominant frequencies of particle displacement and velocity were found to be lower than 1000Hz whereas the acceleration contained even higher frequencies of 150-300Hz.	
FEM with multibody dynamics and 3D wheel-rail formulation	(Recuero, Escalona, & Shabana 2011)	Effect of unsupported sleepers using a nonlinear 3D multi-body system formulation (primary and secondary suspension) that takes into account the rail, sleeper and ballast flexibility on the creepage, creep forces and wheel rail contact locations. 6.5m flexible track with rail and sleepers as beams, ballast as continuous springs and 73.5m of rigid track. Modal superposition is used for the flexible track deformations using the floating frame of reference formulation to investigate deflections, wheelset coordinates (lateral creepage).	
FDM (FLAC)	(Huang, Han and Collin 2005).	The use of numerical analysis using 3D-FLAC of geogrid-reinforced and pile-supported railway embankment to investigate maximum deflections, forces and stresses on geogrid and piles. Use of linear elastic-perfectly plastic constitutive law for soft soil, use of pile elements and shell elements for modelling geogrid.	

2.9   MODELLING OF RAIL JOINTS (PAPER 2 & PAPER 3)

A description of previous work conducted around rail joint modelling is presented in Paper 2 (Appendix B) and in Paper 3 (Appendix C). There are limitations in computer modelling compared to real life situations. The scope of most FEA analyses of IRJs is lipping (localised plastic deformation in the rail head edges) and the majority of them have focused on the wheel-rail contact considering the joint as a bonded assembly. There is no current literature that shows the effect of structural enhancement of the performance of rail joints by using numerical modelling of joints compared to plain track validated with accurately assessed field displacements. Furthermore, no modelling was found describing the structural performance of various types of less stiff, four bolted IRJs under a critical dynamic load case taking into account the following factors: (a) frictional contact in rail/fishplate/insulating layer interfaces (b) the bolt preload (c) the effect of support conditions, within the aim of assessing their resistance to bending, their vertical stiffness/deflection, and critical areas of stress concentration in the fishplates that can be used for fatigue assessment. This research focus on *in situ* field testing

and validation of the numerical modelling with parametric analyses of joint and track factors to determine the consequences of potential design changes.

2.10 SUMMARY – CONCLUSION AND RESEARCH REQUIREMENTS

A brief insight into the theory and practice behind the research topic has been given. Although literature highlights many studies for monitoring track deflection (Section 2.2), remote monitoring is identified as advantageous with VG being promising for rail application (Section 2.2.8). However, robust evidence of the effective applicability of the VG in assessing accurately the deflection of various track components under various loading and speed conditions has not been yet developed.

Rail joints fail at a greater rate compared to standard track (Section 2.3). Literature shows that limited work has been conducted experimentally, either in laboratory or in field, to measure the deflection of rail joints and to compare the deflection between IRJ and reference plain rail (Sections 2.5, 2.7 and 2.9). No report of numerical modelling results of deflection having been validated by in situ field data has been found. Field and laboratory testing of RJs until now have only been made by using strain measurements and impact force calculations by using difficult to install strain gauges and very expensive wheel impact detectors (Section 2.7). For this reason, the VG measurement technique for track deflection will be investigated to identify IRJ deflection and as method of effective routine assessment.

Some design solutions for increasing the service life of IRJs have been proposed in the past (Section 2.5). Increasing the stiffness through thicker fishplate dimensions or by using stiffer material have been investigated while most of the numerical modelling reported aims to investigate the plastic strain accumulation in the vicinity of the wheel contact in a RJ (Section 2.9). Limited attention has been given to the effect of track support conditions on the vertical bending stiffness and deflection of an IRJ.

Fishplate failure is the second most frequent failure mechanism of IRJs. A dipped joint (connected with track support conditions) is a common precursor of IRJ failure (Section 2.4). Thus, joint life can be improved if dip angle and vertical deflection can be reduced. There is a lack of studies investigating the resistance to bending and fishplate fatigue failure of joints. Most previous FEA studies of rail joints consider a joint as a bonded assembly. The deflection behaviour and fishplate failure of less-stiff 4-bolt IRJs (that are commonly used in UK rail network) have not been investigated (Sections 2.6 and 2.9) under critical dynamic load cases,

taking into account the bolt preload, the frictional contact in rail/fishplate/insulating layer interfaces, and the support conditions.

FEM will be used to model the track structure and IRJs to analyse deformation performance (deflections and stresses) (Sections 2.8 and 2.9). FEM will allow the simulation of the interaction between track components by taking into account the effect of track loading on deflections, stresses, and strains. FEA is suitable for system approach and search for a solution for the entire structure comprising nodes, connections between elements and boundary conditions. Static FEA is suitable for the evaluation of deflection performance of track and of IRJs for various locations of the wheel load, various wheel load magnitude cases that correspond to various dynamic forces and various support stiffness conditions (Sections 2.8, 2.9). The dynamic phenomenon with be taken into account with the static force increased by a dynamic amplification factor. Linear and non-linear structural behaviour is required to represent changes in structural stiffness if material plasticity or contact non-linearities exist. Wheel-rail contact can be modelled using Hertz theory to approximate the real contact patch shape. A time domain analysis would be more beneficial if the model would be validated by railhead stress/strain performance or a measured wheel-rail force, that is not in the herein objectives. Furthermore, a static analysis omits all the uncertainties of a dynamic analysis, such as validation of damping properties, and simulation errors due to inaccurate assumptions regarding the vehicle-track system. The P2 dynamic force should be taken into account for IRJ loading (RSSB, 1993) as stated in Section 2.2.1).

The behaviour and material properties of all IRJ critical components are required for the establishment of a FE model to address the scope of this project (see Paper 2, Appendix B).

3 THE RESEARCH METHODOLOGY

3.1 INTRODUCTION

This chapter outlines the research philosophy adopted during this project. The mapping of methodological approached to the research objectives (Section 1.6) is presented by placing the research tasks in relative context with one another and with the wider industry. Tasks are put into the context of subsequent developments, and a "research map" is presented with clear definition of how each objective has been achieved. The adopted research techniques are addressed in Section 3.5 and summary of the research tasks is presented in Table 3.2.

3.2 SCIENTIFIC APPROACH AND RESEARCH PROCESS

The theoretical approach that is used in this research project is positivism. Positivism belongs to epistemology that proposes observation and measurement can lead to factual knowledge (Gray 2014). The research approach used is quantitative that involves generation of data in quantitative form, which are subjected to quantitative analysis. This approach is sub −classified to experimental and simulation approach. The research reasoning lines that are used are both inductive and deductive during the different phases of the research procedure. "Through the inductive approach, data are accumulated and analysed to see if relationships emerge between variables whereas the deductive approach uses a theory to generate a working hypothesis. Inductive and deductive approaches are not mutually exclusive. A researcher may turn a collection of data into a set of concepts, models (inductive) which are then tested" (Gray 2014). Firstly, an inductive approach was used to define the problem within the performance of IRJs. Literature review as well as input from experienced practitioners revealed initially the problem and indicated that the research was worth doing (exploratory); then laboratory and field measurements were conducted to verify the difference in the deflection between regular track (plain, continuous rails) and RJ (descriptive and explanatory research to show "how"). Secondly, the hypothesis that an external reinforcement in the vicinity of the rail joint will improve the mechanical strength of the RJ was formed and a deductive approach was used to answer the research question. This hypothesis was tested with numerical modelling to lead to quantified and measurable results that would confirm or reject the hypothesis. An inductive process was used for collecting data (from literature review and field measurements) for the development of a model that will allow the IRJ deformation to be measured. A deductive

process was used for data collection from field measurements for the establishment of the applicability of the VG to assess track deflection under various track loading, track forms and speed conditions. A deduction approach was used to derive track stiffness characteristics from the data collection. A deductive approach was used to assess fishplates against fatigue form the parametric FE modelling.

Research methodology is a way to systematically solve the research problem. The research methods used are literature review, laboratory measurements, field measurements, numerical modelling and analysis of the results.
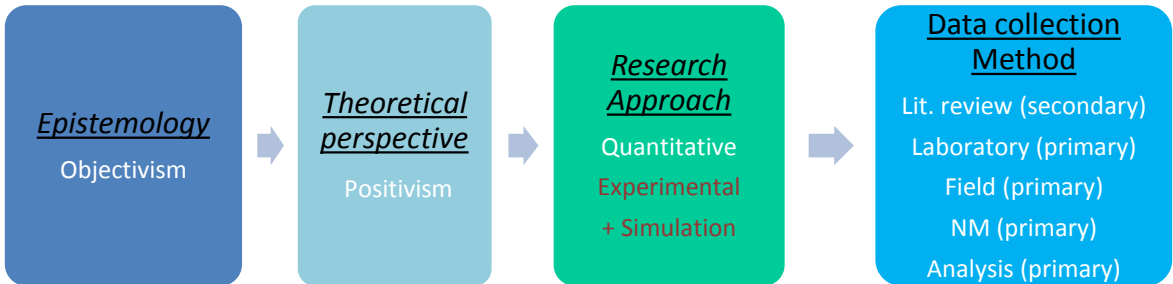
Figure 3.1 Elements of the research process

Table 3.1 Research objectives and associated methods and publications

Objective	Research Method	Outputs/Papers
Objective O1 Review the current practices for track design specifically relating the evaluation of vertical track stiffness and rail joint performance, and factors affecting track structures required for numerical modelling.	Literature review	Design criteria, hypothesis for Paper 2, Literature review sections in all papers
Objective O2 Develop the Video Gauge methodology, a remote video monitoring technique, to collect accurate vertical displacement data of track and insulated rail joints and to potentially derive track stiffness characteristics.	Lit. review, VG measurements, data analysis, system analysis	Papers 1 & 4
Objective O3 Develop a deformation model, informed from the literature, to allow analysis of rail joints. Evaluate and validate the model using the field and laboratory data measured by the Video Gauge.	Numerical modelling, Field measurements, Laboratory testing	Papers 2 & 3
Objective O4 Utilise the methods to identify achievable track structure performance improvements and as a design tool.		Papers 2, 3 & 4

3.3 RESEARCH TASKS BREAKDOWN

In order to address the research aim (Section 1.6) the first step was to undertake a comprehensive literature review so that the research project could be broken down into a series of tasks associated with the objectives presented in Section 1.6 allowing selection of appropriate research methodology. A summary of the research objectives and methods adopted is contained in Section 3.5. The table below includes a general overview mapping the project objectives and deliverables to main activities undertaken.

Table 3.2 Research tasks and associated outputs

Research task	Target	Obj.	Method	Paper/Technical Report (TR)
Review state of art UK track design philosophy, measurement and modelling techniques	Break down tasks and research segments	O1, O3	Lit. Review	Papers 1, 2, 3, 4
Evaluate the IRJ structural integrity	Identify and quantify the problem	O3	Laboratory Test	TR-2, TR-3
Validation of VG with LVDT	Validation of VG	O2	Laboratory Test	Paper 2
Understand IRJ performance under fatigue loading	Quantify the problem to be used as validation for the numerical modelling	O3	Laboratory Test	Papers 2, 3
Obtain VG primary deflection data of ballasted track under train traffic conditions	Data to be used for research, for comparison and validation of the numerical model	O2	Field Measurements	Papers 1, 4
Obtain VG primary deflection data of rail joints under train traffic conditions	Data to be used for research, for establishment and back evaluation of numerical model	O2	Field Measurements	Papers 1, 2
Commercial application of developed VG methodology	Collect data of transition zone performance prior to renewal	O2	Field Measurements	Papers 1, 4, TR-4, (Network Rail)
	Collect data of transition zone performance after renewal	O2	Field Measurements	TR-5 (Network Rail)
	Collect data of novel ballastless forms and ballasted track under RTST loading	O2	Field Measurements	AECOM
	Comparison with RTST data		Field Measurements	AECOM, LBF

	Collect data of novel ballastless forms and ballasted track under controlled train loading	O2	Field Measurements	TR-7 (Network Rail), Paper 4
	Collect data of novel V-TRAS (versatile transition system)		Field Measurements	TR-6 (Rhomberg Rail)
Develop numerical model of plain track and IRJ	Allow analysis of IRJ deflection performance	O3	Numerical modelling	Paper 2
Develop numerical model of enhanced IRJ	Investigate IRJ deflection performance improvement	O4	Numerical modelling	Paper 2
Optimising the adopted model for industrial use	Develop and provide a modelling technique that can be used for the validation of designs of multiple RJ types	O4	Numerical modelling	Paper 3
Commercial application of developed modelling techniques	Validate fishplate designs against load cases provided by the contract, assessment against yield and fatigue endurance limits. Parametric analysis	O4	Numerical modelling	TR-8 (Network Rail)
Analysis of VG data	Develop a back-calculation analysis for derivation of track stiffness parameters and deflection bowl	O2	Systematic analysis	Paper 4
Fishplate fatigue failure estimation	Aimed to evaluate the fatigue life of fishplates	Additional	Systematic analysis	LBF, TR-1

3.4 METHODOLOGY DEVELOPMENT

A research map showing the research tasks, information flow, research output and contextual developments is shown in Figure 3.2.
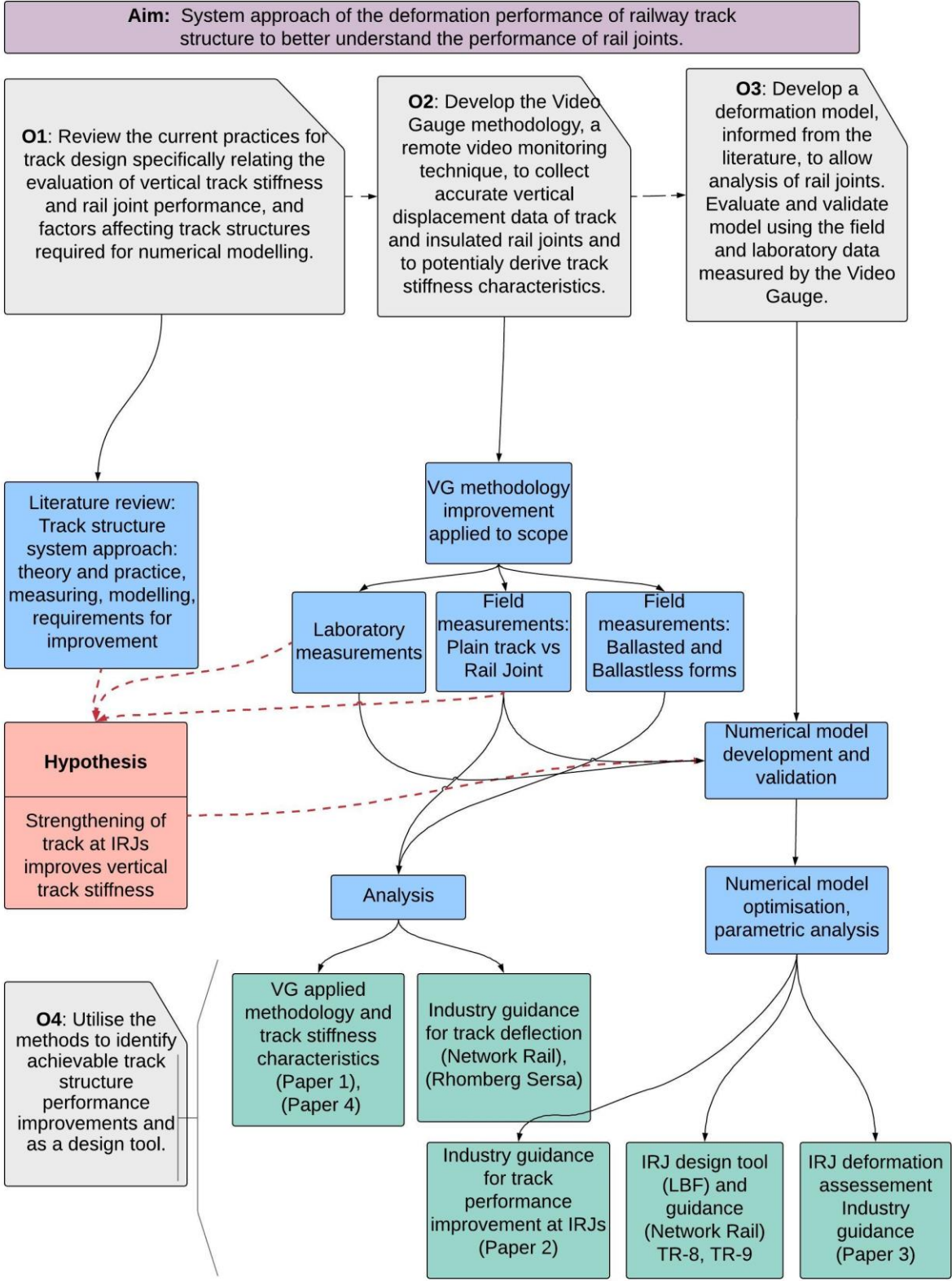
Figure 3.2 Research map showing the research development overview

3.5 ADOPTED RESEARCH METHODS AND DEVELOPMENT

This section details the processes undertaken; specific details of tests can be found in Chapter 4.

3.5.1 LITERATURE REVIEW (OBJ.1)

The literature review (Objective 1) was the first key stage of the research programme, aiming to shed light into theory behind the research topic, to reveal existing knowledge, and to establish the state of the art. Initially a comprehensive broad literature review was performed that led to the structure and design of the project methodology, focused on specific topics aimed to obtain understanding, and to prepare the ground for the research actions. This review aimed to:

- Identify the existing European and UK standards for track structure design (BS EN 1991:2 (BSI 2003)), track system requirements (GC/RT5021 (RSSB 2011)), EN 16432-1 (BSI 2017a)), rail traffic loading requirements (GC/RT5112 (RSSB 2015), track components specifications, track forces (GM/TT0088 (RSSB 1993)), design and construction of track (NR/L2/TRK/2102 (Network Rail 2008)). The findings were incorporated in the numerical modelling (NM) establishment and the hypothesis.

- Identify the failure mechanisms of IRJs and requirements for IRJ design (EN 16843 (BSI 2015), NR/SP/TRK/023 (Network Rail 1996), NR/SP/TRK/064 (Network Rail 2003)). Findings contributed to laboratory conditions set up, hypothesis establishment, NM establishment, asessment of research results. Findings are shown in Appendices B and C.

- Identify the theoretical background for track stiffness evaluation (findings reported in Appendices A and D).

- Identify the techniques for track deflection and track stiffness measurement, define their issues, identify VG advantages (findings reported in Appendices A and D).

- Identify IRJ modelling techniques to assess their performance through a holistic track system approach (findings reported in Appendices B and C).

- Evaluate track structure and IRJ modelling techniques to establish those most appropriate for this project (Appendices B and C).

3.5.2 FIELD DEFLECTION ASSESSMENT AND DATA ANALYSIS (OBJ.2 & 4)

VG methodology to be adapted

In this project the Video Gauge (VG) is used for real –time in situ high definition measurements. The function and advantages of the VG over other remote monitoring techniques is described in Chapter 2, Section 2.2.8.

In order to meet objectives 2, 3 and 4 it was required to adapt and optimise the VG methodology in order to efficiently assess the track's vertical displacement addressing the conditions required in the UK industry. This was conducted through resource planning, trials, good planning of the laboratory and in situ measurements, data post processing, and analysis.

Field measurements

The aims of the field measurements were:

1. Evaluating the rail and sleeper vertical displacement for conventional ballasted track under various train speeds and deriving track stiffness values to inform model development.

2. Evaluating the rail joint vertical displacement to inform model validation.

3. Evaluating the vertical displacement of transition zones and deducing vertical track stiffness values to further validate the applicability of VG measurement approach.

4. Evaluating the vertical displacement of ballastless track forms and deducing vertical track stiffness values to inform industry.

3.5.3 LABORATORY MEASUREMENTS (OBJ.1, OBJ.2, OBJ.3)

The review of existing studies revealed a lack of deflection data of RJs. In order to assess the vertical displacement of an IRJ and evaluate the deflection increment in comparison with plain rail a laboratory test was conducted. The results were used to validate the VG against LVDTs, understand the problem and inform NM development and validation.

As described in Appendices B and C, laboratory measurement of a 4-bolt glued Class A CEN 60 IRJ of 3 m length was tested in a 4-point bend configuration under cyclic loading at a frequency of 1 Hz. The controlled laboratory conditions allowed greater control on the accuracy of the results of the VG and the investigation of the deformation behaviour of the IRJ.

3.5.4 NUMERICAL MODELLING (OBJ. 3 & 4)

In order to meet Objectives 3 and 4 a numerical model (NM) validated by the laboratory and field data was developed and used to systematically investigate the rail joint response under vertical wheel loading. The modelling procedure was broken down into components (i.e isolate the track stiffness influence, evaluate the effect of reinforcement and identify stress concentration areas in the rail joint interfaces). The NM tool allowed analysis of RJs exposed to multiple loading scenarios with a system approach, applying modelling processes to meet the requirements for various RJ types.

3.5.5 SYSTEMATIC ANALYSIS

After the data had been collected, an analysis was carried out to examine influential factors and interpret them. Data analysis to deduce track stiffness characteristics from the track vertical displacement processed data was conducted. The theoretical model, BOEF, was used to address this requirement. Parametric analysis of the NM to assess the effect of track stiffness, the effect of RJ strengthening, the effect of insulating materials, and the effect of bolt preload and wheel position on RJs' response to bending was conducted.

3.5.6 SUMMARY

The research methods have been identified for each of the objectives in Figure 3.1 and inter-relationships identified in Figure 3.2. The research tasks for each method with their aims and outputs are presented in Table 3.2. The main research methodologies included reviewing information (objective 1), experimental research through laboratory and field measurements (objectives 2 and 4), simulation (objectives 3 and 4), and systematic analysis of the results (objective 4). The methodological approaches and tools developed by this thesis were applied, during the four-year period of this, in various consultancy projects between the sponsoring company and the wider UK railway industry providing industry guidance and recommendation for product developments.

4 THE RESEARCH UNDERTAKEN

With objective 1 being met by literature review (Chapter 2), this chapter details the research undertaken to achieve Objectives 2 to 4 set out in Section 3.2 and highlights the main findings of the project. The literature review (Chapter 2) and methodology (Chapter 3), along with Papers 1, 2, 3 and 4 are referred to throughout this section and should be read in conjunction. The chapter is divided into 4 sections as shown in Table 4.1, in line with the research map discussed in Section 3.4.

Table 4.1 Work Package Overview

	Work Package Item	Objective	Paper
Section 4.1	Review of current practices for track design and track stiffness evaluation, critical factors for numerical modelling	Objective 1	Paper 1,2,3,4
Section 4.2	Exploration of the VG method for track, rail joint deflection assessment and track stiffness evaluation	Objective 2	Paper 1,4
Section 4.2.1	Laboratory measurements and comparison to LVDT	Objective 2,3	Paper 2,3
Section 4.2.2	Field measurements of plain track and insulated rail joint	Objective 2,3	Paper 1,2
Section 4.2.3	Field measurements of ballastless forms and transition zones & derivation of track stiffness properties	Objective 2,4	Paper 1,4
Section 4.3	Numerical modelling to allow analysis of rail joints. Evaluation and validation of the model using the laboratory and field data measured by the VG.	Objective 3	Paper 2,3
Section 4.3.1	Numerical modelling to investigate the effect of track reinforcement on the deflection behavior of IRJs to allow track structure performance improvement.	Objective 3,4	Paper 2
Section 4.3.2	Expanding the models's usability as a design tool to investigate the response to bending of various rail joints under fatigue vertical wheel load.	Objective 3,4	Paper 3
Section 4.4	Summary		

This chapter discusses the development of the four objectives of the project and it has the following structure: Section 4.1 summarises the main findings of the literature review based on the current practices for track design and track stiffness evaluation indicating the critical factors affecting the performance of the track that will be used for the development of deformation models of track and IRJs. Secondly, Section 4.2 describes the development of the Video Gauge (VG) method for track and rail joint deflection data collection, aiming to provide an evaluation of track stiffness and to inform numerical modelling. This is divided into three work package items including (i) laboratory measurements of a plain rail and rail joint by the VG and

validation using LVDTs, (ii) field measurements of rail joint deflection and comparison with plain track, (iii) field measurements of deflections of ballasted, ballastless track forms and transition zones to investigate track stiffness properties. Subsequently, Section 4.3 outlines the development of a numerical model to allow analysis of the deflection behaviour of rail joints under vertical wheel load. An evaluation and validation of the model is conducted by using the aforementioned laboratory and field deflection data measured by the VG. The modelling procedure is broken down into several model configurations to explore the effect of different parameters. More specifically, Section 4.3.1 details finite element (FE) analyses for the investigation of track reinforcement adjacent to IRJs to allow track stiffness improvements; the effect of IRJ reinforcement is investigated with respect to track support stiffness. Section 4.3.2 presents FE analyses to investigate the response to bending of various rail joint types for two fatigue loading scenarios and to identify potential stress concentration areas in the rail joint interfaces; the effect of wheel position, bolt preload, and type of insulation/joint are investigated. Finally, Section 4.4 discusses how the aforementioned methodology and modelling findings can be utilised in the rail industry and the benefits of applying the VG method to evaluate track structure performance.

4.1 REVIEW OF TRACK STIFFNESS EVALUATION AND CRITICAL FACTORS FOR NUMERICAL MODELLING

This section provides a brief review of the current practices for track stiffness evaluation and rail joint performance, emphasising the critical factors required for numerical modelling of insulated rail joints (IRJs).

The literature on track stiffness evaluation identified vehicle-based systems and track instrumentation measuring either directly or indirectly, track deflections. These include LVDTs, laser deflectometers, geophones, video systems based on PIV and DIC, FWD, and RSMV (see Section 2.2.7). It was concluded that the VG system is an advantageous video remote monitoring technique based on DIC principles that, while it has been used recently in material testing and civil infrastructure applications, offers the potential for rail application. Therefore, this project aims to explore how the VG method can be applied for an accurate track deflection assessment; this is investigated in Section 4.2 (Paper 1 –Appendix A) through real-time primary data collection from various case studies.

The rail joint is a weak component of the rail network, as it constitutes a track stiffness discontinuity (Section 2.3). Its performance can be assessed by dip angle measurements and visual inspections *in-situ,* and deflection measurements using LVDTs in laboratory for the approval and testing of new IRJ types. Strain gauges and wheel/rail force detectors have been applied in-situ for research only (Section 2.7). This project seeks to investigate for first time the application of VG for RJ deflection assessment and RJ model validation.

Joints suffer from a vicious damage cycle, due to the structural discontinuity present. This weakness results in both dip angle and extra deflection as a consequence of the applied load and is exacerbated by the increased dynamic force that is induced on the joint. Over time, this situation worsens as the impact loads and applied stresses lead to damage and softening of the ballast and supporting subgrade under the joint (see Section 2.3). The existing research in RJ performance improvement was described in Section 2.5 and the objective of GB Railway Strategy (published by the Technical Strategy Leadership Group - TSLG) is to develop track design by improving longevity and minimizing long term costs. Hence, this project sought to investigate alternative ways of reducing the deterioration of track and premature failure of IRJs (Objective 4).

Thus, the main hypothesis tested here is whether the initial deflection increment seen on an IRJ can be significantly reduced, to less than or equal to that of continuous plain rail, by reinforcing the track around the joint. In this way, the damage cycle can be reduced. A numerical evaluation tests and validates this hypothesis; see Section 4.3.1 (Paper 2-Appendix B).

The majority of literature and previous research has been focused on the localised plastic strain accumulation in the rail head material of an IRJ. Herein, emphasis is placed on the second most frequent failure mode of IRJs, that is fishplate failure (see Figure 2.10) due to stress increased deflection; one of the major causes of IRJ failure (see Table 2.3). More specifically, the deflection behaviour of IRJs is directly connected with the effect of support conditions and the non-linearities in rail-fishplate interfaces, about which little exists in the literature (Carolan, Jeong and Perlman, 2014).

Therefore, firstly, the effect of external structural reinforcement on the bending behaviour of a typical suspended glued insulated RJ is investigated through FEM for various sleeper support conditions (Section 4.3.1 and Paper 2-Appendix B). An alternative way of reducing the IRJ deflection, by improving the track stiffness adjacent to IRJs, is suggested aiming to minimise the deterioration caused in the trackbed below IRJs.

Furthermore, the fatigue performance of four different suspended RJs under high magnitude vertical loads is assessed for specific sleeper support stiffness. Deflections and stress distributions in the rail-joint interfaces are examined to shed light on areas of premature mechanical failure/defects (Section 4.3.2 and Paper 3-Appendix C). This study is conducted to improve understanding of the vertical stiffness of various joints, and takes into account the support conditions, the non-linearities in the RJ assembly, and the bolt preload under a fatigue load. The method is utilised by the sponsoring company as a design tool to inform RJ design validation and assess fishplate design against fatigue when delivering projects.

Finally, in order to address the aforementioned objectives, the establishment of a preliminary plain track numerical model is required. The material properties of the critical track components required for this were determined from literature, and are presented in Table 4.2. A detailed description of the selection of track properties (rail, sleepers, spacing, track gauge, railpad) for the FE track model is presented later in Section 4.3.1.

Table 4.2 Material properties of critical track components (Soylemez and Ciloglu, 2016; Hunt, 1996)

Component	Material	Stiffness	Modulus of Elasticity	Poisson's ratio	Density
		k	E	v	ρ
Rail, Fishplate	Steel		210 GPa	0.3	7850 kg/m^3
Railpad	Elastomer	150 MN/m	38.265 MPa	0.3*	300 kg/m^3
Sleeper	Concrete		30 GPa	0.18	2300 kg/m^3
Endpost	Polyurethane		20.7 MPa	0.3*	1265 kg/m^3
Stiffness per sleeper end	5-200 MN/m (RSSB 2011; Network Rail 2016; Andersson et al., 2013; Grossoni et al., 2014) (see Section 1.1, Table 1.3)				

*The Poisson's ratio and Young's modulus of polyurethane was selected from Soylemez and Ciloglu (2016). Although Poisson's ratio of railpad may be found up to 0.46 (v=0.463 (Witt, 2008), v=0.394 (Zhang 2015)) and Poisson's ratio of elastomeric materials may be found in literature between 0.34 - 0.48, the reported values are not significantly different, the thin elastomeric components form a small part of the model and it is unlikely to affect significantly the shear modulus and consequently the results of the analysis.

4.2 EXPLORATION OF THE VIDEO GAUGE METHOD FOR TRACK AND RAIL JOINT DEFLECTION ASSESSMENT AND TRACK STIFFNESS EVALUATION

This section aims to explore the use of VG methodology, a remote video monitoring technique, to collect accurate vertical displacement data of track and IRJs and potentially to derive track stiffness properties. This was investigated through a series of laboratory measurements which were compared to LVDTs, field measurements comparing plain track and RJ deflections, and finally, field measurements of ballasted, ballastless forms and transition zones. The findings and results of all the above were analysed in order to update the numerical modelling and explore the application of VG for the evaluation of track stiffness properties.

A detailed review of the VG exploration and discussion of the findings are presented in Paper 1 (Appendix A) and in Paper 4 (Appendix D).

Before proceeding to the laboratory results, it should be mentioned that the experimental methodology to collect VG track deflection data had to be adapted and optimised through the project for the accurate measurement of operational deflection data under high speed traffic loading. The accuracy of the technique depends on the image capture rate and the amount of displacement measured. The higher the train speed, the higher the rail displacement frequency due to each axle passage. Further issues were needed to be investigated before using the VG in the field. These are presented in Appendix F.

4.2.1 LABORATORY MEASUREMENTS AND COMPARISON TO LVDT

Chapter 2 revealed a lack of literature in deflection assessment of RJs both in laboratory and operational conditions. It was decided to firstly examine the rail and RJ deflection in the laboratory by constructing repeatable full-scale models, under controlled conditions. The measurements were undertaken using the VG, in order to meet objective 2. Building laboratory models is useful to assess individual variables, as along as other variables can be controlled. The literature review was unable to find suitable deflection data of IRJs during laboratory conditions (Section 2.7). In terms of instrumentation for deflection estimation in the laboratory, traditional displacement sensors such as mechanical dial gauges and linear variable differential transducers (LVDTs) are used in contact measurements, through which static or cyclic displacement values can be obtained directly or fed into a computer for processing and displaying. The non-contact VG deflection measurements were compared to the above

traditional contact methods in four-point bending tests. The laboratory experiment was used in Paper 2 (Appendix B) and in Paper 3 (Appendix C).

Instrumentation

A CEN 56 rail section (3 m length) and a four-bolt glued Class A IRJ (consisting of two CEN 60 rail sections) were tested in a four-point bend test under cyclic loading at a frequency of 1 Hz (see Figure 4.1). The IRJ was centrally positioned between two vertical hydraulic actuators (separation distance 600 mm), and a synchronised vertical cyclic force was applied onto the rail. The endpost was of 6 mm thickness and it was in bonded contact with the rail faces. The distance between the supports was 1600mm. The two forces were applied at 300 mm from the gap at the centre of the IRJ. A digital controller was used to control the load application. The loading cases for each test are shown in Table 4.3. The loading used exceeds the maximum static UK rail wheel load (12.5 tonnes) and approximates the vertical dynamic force generated by the static wheel load and the low frequency dynamic forces (Beaty, 2014). In addition, the load limits and set-up configuration were determined according to NR/SP/TRK/023 (Network Rail, 1996) to reach mechanical failure of the rail joint. The displacement was recorded by the VG at a frequency of 66.36 Hz with a resolution of 0.0055 mm (the VG software provides in real time the sampling frequency and resolution indicators of each recording but both values can be calculated through the time series-output of the VG software). A LVDT was also positioned on the top of the endpost for comparison with the VG values in order to check the accuracy of the VG. A target array was used on the head and web of the rail and rail joint (see Figure 4.2) for the non-contact measurement so that multiple positions could be measured to allow checking of the consistency of the results.
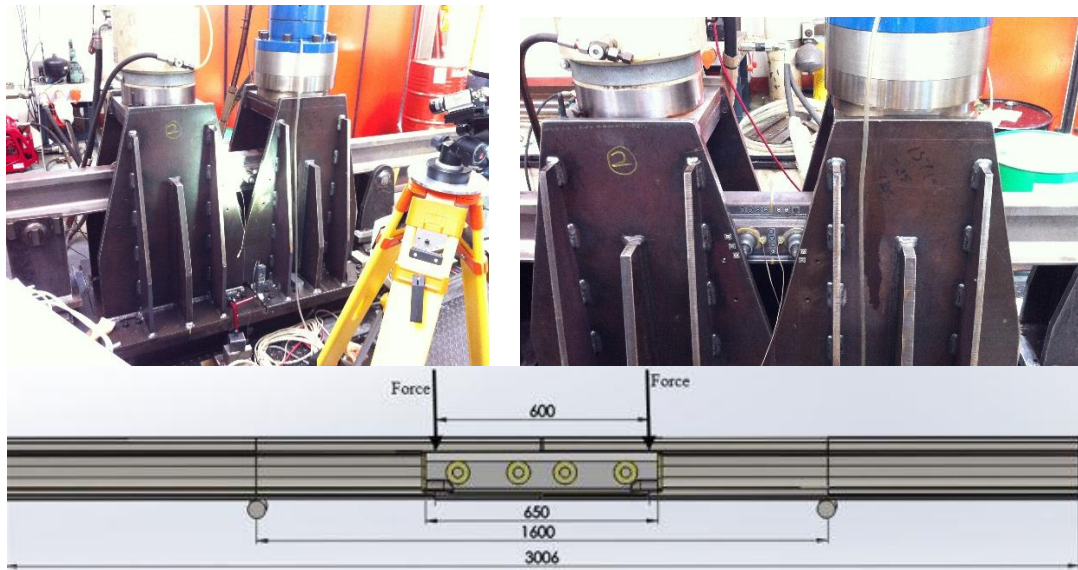
Figure 4.1 Four-point bending test configuration.
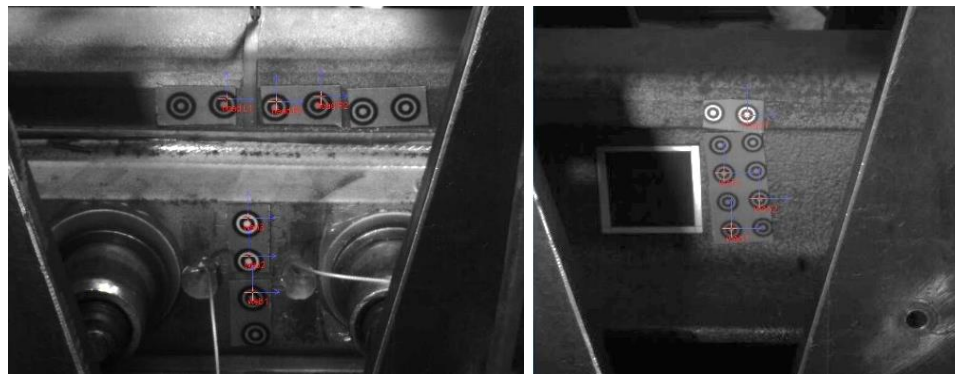
Figure 4.2 Video images showing measurement positions of (i) IRJ rail head and fishplate web and (ii) plain rail head and web during the 4-point bend test.

Analysis and validation

The results of the laboratory tests are presented here. In particular, Figure 4.3i depicts a comparison between the LVDT and the VG IRJ deflection data for the rail head position and Figure 4.3ii shows a comparison between the deflections of IRJ and plain rail for various load cases measured by the VG. Deflections of IRJ in the position of the rail head were found to be 4% larger than the deflections of the fishplate web surface, whereas a difference of 9-15% was observed between the head and web positions for the plain rail experimental test based on the measurements by the VG. The measured deflection in the centre of the IRJ head of rail (rail head ends) was found to be in a range of 2.76 mm to 7.12 mm, below the limit of 10mm

(Network Rail 2003). An excellent correlation of the VG and LVDT results indicated that the VG accurately measured the deflection histories of IRJ in the laboratory.
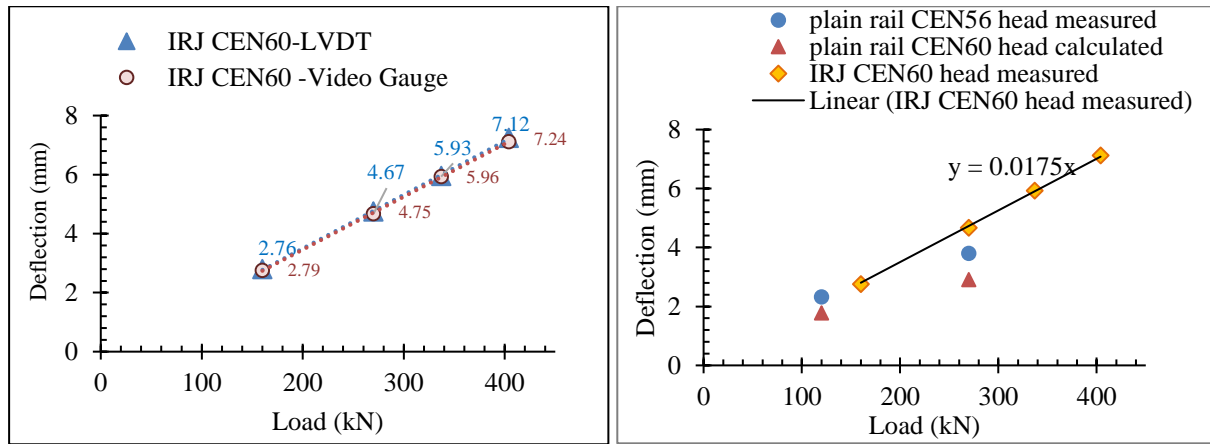
Figure 4.3 (i)Validation of VG deflection data against LVDT deflection data and (ii) Comparison between plain rail and IRJ deflection data measured by the VG.

At this point it would be useful to calculate the degree of weakening between plain rail and IRJ. This can be defined as the percentage of stiffness difference between the continuous rail and the IRJ. It can be calculated by deriving the effective/equivalent moment of inertia I_{eff} using the four-point bend beam supported at both ends formula.

$$\delta_{max} = \frac{W*a}{24*E*I} * (3l^2\text{-}4a^2)$$

eq. 4.2

$$I_{eff} = \frac{W*a}{24*E*\delta_{max}} * (3l^2\text{-}4a^2)$$

eq.4.3

Where E the rail steel modulus of elasticity (200GPa), I is the rail section moment of inertia (m^4), W the load applied, a the distance of each load from the support, l is the length of the rail between supports (see Figure 4.1) and δ_{max} the rail/IRJ deflection measured by the VG.

It should be mentioned that the elements of the rig, the rail and IRJ sections were sourced locally by LB Foster and a rig at Sheffield University was used. Due to lack of availability of same section of plain rail and IRJ, the deflection of a CEN 60 plain rail was back calculated by using the ratio between the moment of inertia of a CEN 56 and a CEN 60 rail section.

Looking at Table 4.3, from this analysis, by comparing the deflections found for plain rail CEN60 at 270kN and of glued IRJ CEN60 at same load, the IRJ was found to deflect 61% more than the plain rail for the specific support spacing/configuration at 270 kN. The ratio of the moment of inertia of two fishplates I_{2xFISH} to the moment of inertia of plain rail $I_{RAIL\ CEN60}$ is

0.23, whereas the ratio of the effective $I_{eff\ IRJ\ CEN\ 60}$ to $I_{RAIL\ CEN\ 60}$ was found to be 0.625. This means that the IRJ was found to be 37% less stiff than the plain rail.

Table 4.3 Description of tests and findings

Test	Component	Total forces (kN)	Deflection (mm)	I_{eff} (cm^4)
1	Plain rail CEN 56	120	2.32	2321
2	Plain rail CEN 56	270	3.8	2321
3	Glued IRJ CEN 60	160	2.76	1921
4	Glued IRJ CEN 60	270	4.67	1916
5	Glued IRJ CEN 60	337	5.93	1883
6	Glued IRJ CEN 60	404	7.12	1880
*	Plain Rail CEN 60	270	2.90	3038
	2 x Fishplate 6- hole			695.7

*Calculation based on Test 2

Concluding remark

Comprehensive dynamic experimental results in the laboratory tests demonstrated the deflection increment an IRJ experiences (under support conditions specified for laboratory tests) and validated the VG method as an effective means of assessing rail joint deflection, allowing its deployment in track site applications. The collection of detailed RJ deflection data, particularly under cyclic loading, meets objective 2 and is later used in the validation of the numerical modelling (Section 4.3), where the study was extended.

4.2.2 THE USE OF VIDEO GAUGE FOR FIELD MEASUREMENTS OF PLAIN TRACK AND INSULATED RAIL JOINTS

In order to meet objective 2 there was need to obtain further operational train traffic deflection data. For this purpose, the author developed a methodology using the VG in-situ. This section in conjunction with Paper 1 and Paper 2 provide details of its development for the assessment of rail and rail joint deflection in-situ.

As discussed in Sections 2.2.6 and 2.2.7, there are many published case studies with rail deflection data measured in-situ directly by using traditional trackside instrumentation through LVDTs, laser deflectometers and RVM and indirectly through geophones and accelerometers. Their main drawback is their lack of ease of routine application, lack of ability to capture multiple positions/components at a time, the level of accuracy, and their need for track access.

As mentioned in Section 4.1, limited work has been found for RJ behaviour assessment in-situ that mainly included strain gauges and wheel impact detectors. The installation and calibration of the first is highly time consuming while the latter is very expensive.

A new method was required that would record the position of a large number of measuring points during many phases of traffic loading. VG is of immense potential because of its high resolution, accuracy and versatility. It can provide fast and high precision multi-point 2D or 3D displacement data, saving time and money through minimising access and contact.

Throughout the project, the VG was utilised to obtain primary deflection data from a range of track components and track forms (objective 2). This section provides a brief overview of the application of VG for the assessment of the deflection of plain ballasted track and jointed ballasted track.

Site A-Ballasted track under low speed

To begin with, the applicability of the VG was checked in ballasted track in order to investigate the deflection of plain rail under real traffic conditions. Rail and sleeper deflections were measured simultaneously, by one camera at a sampling frequency 124 Hz (Figure 4.5), during the passage of a Class 170 train on a main line at a speed of 40 mph (Site A).

The system was able to pick up the detailed impact of individual axles. Deflections were measured from two different distances (5 m and 2 m) by using lenses of different focal length in the cameras (50 mm and 16 mm correspondingly); consistency in the data was observed. The anticipated resolution for the two set up combinations of the VG system was ($1/100^{th}$ pixel) 0.0112mm and 0.014mm. Variations in the measurement resolution on the time series of different targets within a single image are principally down to the quality of the target the software sees. Magnetic targets were used on the rail whereas brackets with mounted targets were positioned on the sleeper edges to achieve higher accuracy. The resolution obtained has been calculated as the standard deviation of the measurement points when there is no load being applied to 0.032 mm and 0.022mm for the two set up combinations. The location of the apparatus and the measurement points are depicted in Figure 4.4.

The rail deflection is depicted in Figure 4.5. From this it can be observed that the measured deflection was about 3 mm. From Figure 4.5, one can observe the number of vehicles and individual wheels of the recorded train passage, as each peak corresponds to the passage of a wheel. The location of the eight axles of the two-vehicle train is indicated with small circles in the figure. Looking at Figure 4.5, it can be also observed that the rail deflection is fully

recoverable between adjacent bogies whereas the rail does not return to its original level between adjacent wheel spacings (minor undulations). Small undulations are observed ahead or behind the wheel passage due to the uplift of the rail.

The exact train speed was calculated as 40mph though the time history and the length of the recorded train (Class 170). By using the estimated static axle load for the Class 170 (car tonnage divided by 4 axles) and the measured deflection, the corresponding global track stiffness was estimated to 19.9 MN/m. This can be characterised as the elastic track stiffness describing the elastic behaviour of the track assuming that the vertical deformation caused on vertical loading is fully recovered when the load is removed. The ratio of elastic (recoverable) to plastic (irrecoverable) deflection component is 10^5 or 10^6 and thus, the track behaviour can be considered as reversibly elastic over a single loading cycle (Powrie and Le Pen, 2016). Initial settlement (permanent deformation) occurring during tamping after renewal forms an exception to this. In general, the deflections found are in the same order of magnitude with previous literature findings (Murray, 2013; Bowness *et al.,* 2007, Powrie and Le Pen, 2016). Herein, the static train wheel loads are used as an input in the BOEF model to back-calculate track stiffness parameters. The railpad stiffness was back calculated using the BOEF to 94.7 MN/m (in perfect correlation with Powrie and Le Pen, 2016; Oregui *et al*., 2017) through the relative deflection between the rail and sleeper (see Paper 4). The BOEF assumes a quasi-static analysis and does not account for dynamic loading that may arise from vehicle dynamic effects (train speed) that could be related to increased local track deflections. Also, in the BOEF model, accelerations from the track structure and the ground are neglected (Powrie and Le Pen, 2006). Dynamic loads could be taken into consideration, for improved accuracy of the calculation of the dynamic stiffness values, if the actual loads from the train could be measured using strain gauges, wheel impact load detectors (WILDs) or by calculation of the dynamic amplification factor (see Section 2.2.1), and input of the estimated dynamic load Q_{dyn} into the stiffness formula.
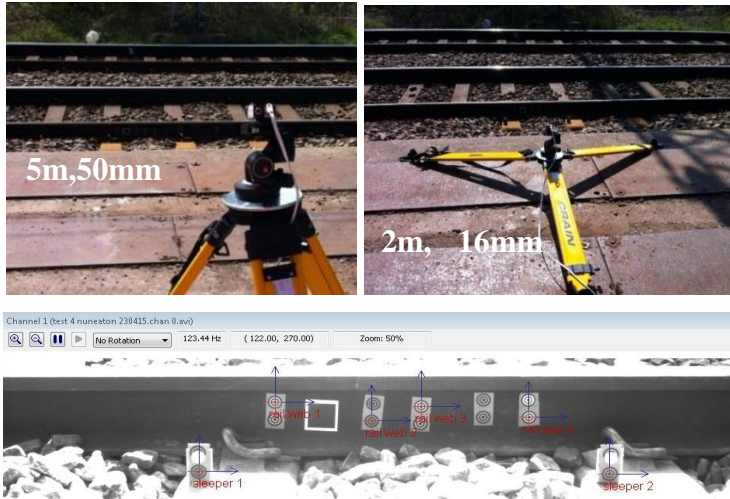
Figure 4.4 View of set-up at site A and video image of single camera showing target array in rail and sleepers.
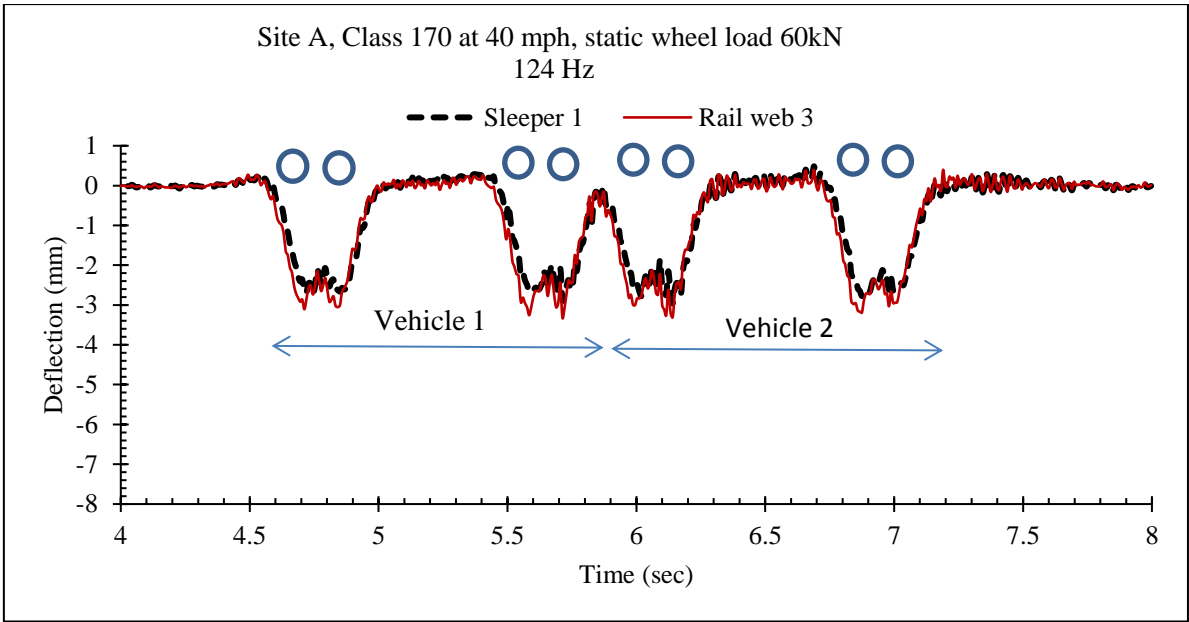
Figure 4.5 Rail and sleeper deflection at Site A under the passage of Class 170 at 40 mph.

Furthermore, in order to verify the quality of track of Site A, additional track geometry recording data was obtained from Network Rail's databases. A CCQ chart (coloured coded quality) is part of the Route Assessment process and constitutes a record of the SD (Standard Deviation or σ) values for vertical track alignment per 8th mile sections, whereas the Top 35 traces constitute a record of the change in the vertical profile along the track, filtered to remove wave lengths of longer than 35m.

Looking at Figure 4.6,it can be observed that no track renewal was conducted at Site A [WNS, 1100, 0 mile, 448 yards] until 2016. The deflection measurements were undertaken on the 23rd of April 2015. It can be observed that, for this period, Site A experienced a rate of deterioration 0.4 mm/year (calculated through the calculation of the inclination of SD values for one year), that further justifies the magnitude of the deflections measured (see Table 4.4 below).

Figure 4.6 CCQ char for Site A.

Site B-Rail joint vs plain rail at high speed

In this site, the VG is used to assess the IRJ deflection in real-time traffic conditions. At this point, a comparison between the deflections of a six –hole glued IRJ and the adjacent plain rail during the passage of five high speed trains (two Desiro Class 350 and three Pendolino Class 390), on a line with a top speed of 125 mph, was conducted. The measurements were undertaken at a sampling frequency of 75 Hz at a distance of 5.5 m from the running line. Here, it should be noted that the sampling frequency achieved on each recording depends on the camera settings (image format, camera exposure, and lighting conditions etc) as calibrated during the live recordings on site, thus different values of sampling frequency may be achieved on each recording despite the camera's maximum performance characteristics (maximum frame rate (sampling frequency)). Two cameras (using lens of focal length 50 mm and 75 mm each) were mounted in two tripods covering in total 1.23 m horizontal field of view, one recording the RJ and the second recording the adjacent plain rail 730 mm away from the centre of IRJ (see Figure 4.7). Spray paint was used as a non-movable target on the rail to ensure stationarity under the high-speed train, to achieve good accuracy.
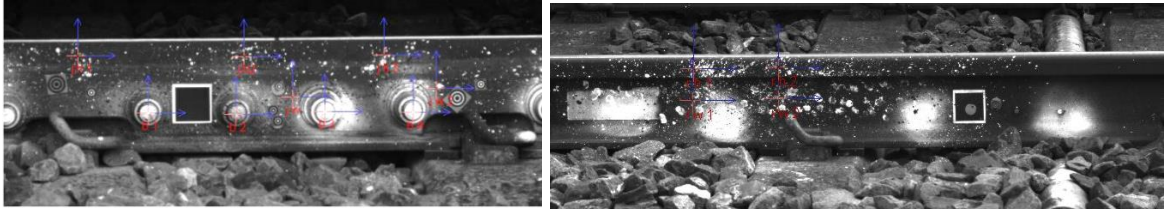
Figure 4.7 Video images of two cameras showing speckle target pattern on IRJ and adjacent plain rail in Site B.

The deflections of multiple points were measured, as the VG allows the real time and post processing of over 100 points at a time in the image recorded. Thus, multiple points of the rail and IRJ head/web, as well as IRJ bolt positions, were analysed for the aforementioned two types of trains. A comparison between the deflection time histories of the centre of IRJ and plain rail are presented in Figure 4.8-Figure 4.10. Figure 4.8 presents the passage of a Desiro 350 consisting of four wagons running at 101mph. Figure 4.9 shows the passage of a Desiro 350 consisting of three wagons running at 72 mph and Figure 4.10 shows the recording of the passage of an eleven-car Pendolino running at 125 mph. The actual train speeds were calculated through the time series based on the length of each train vehicle.
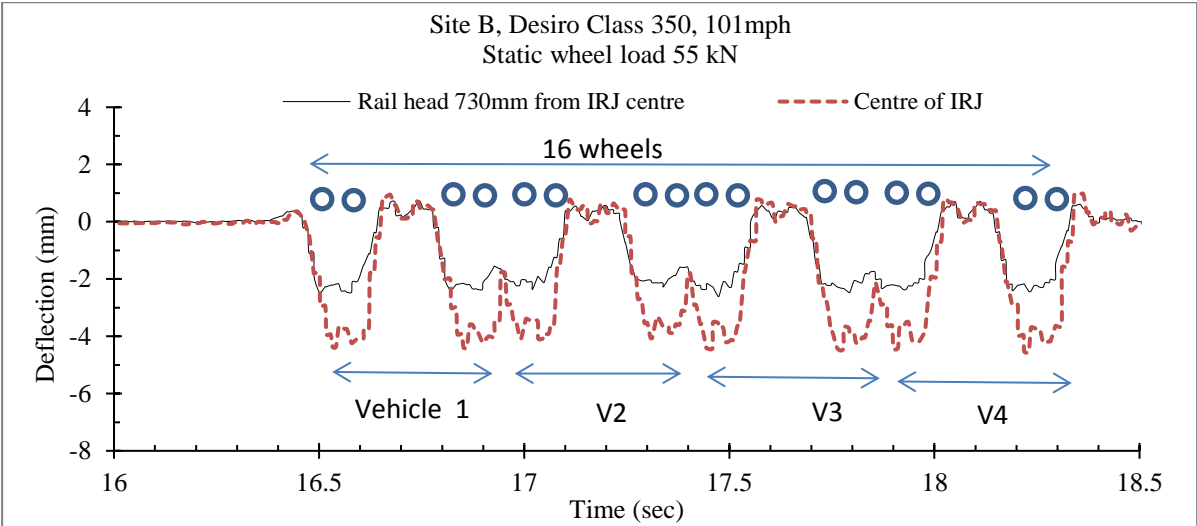
Figure 4.8 Deflection time histories under the passage of four-vehicle Desiro at 101mph.
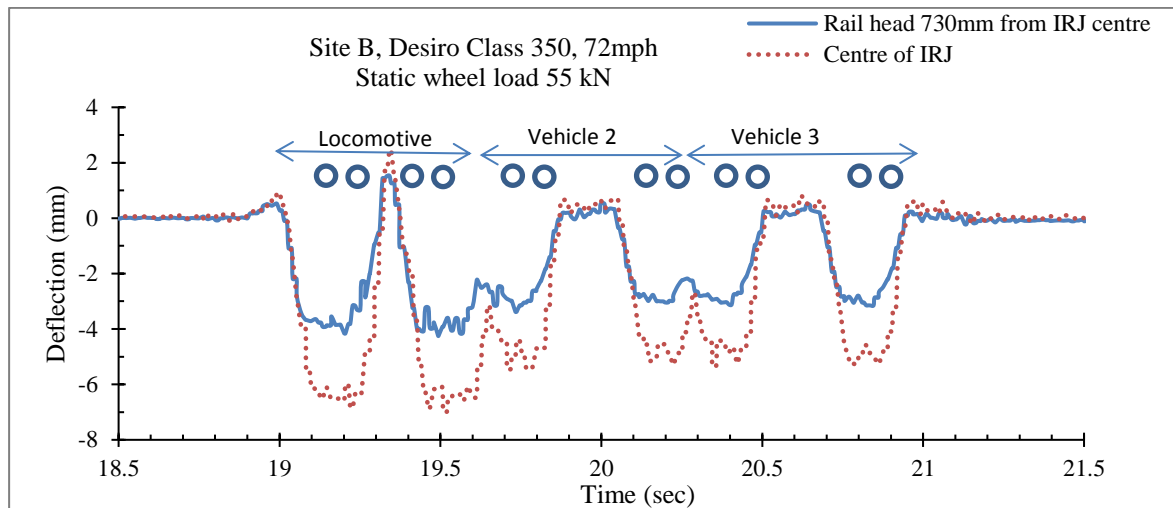
Figure 4.9 Deflection time history under the passage of three-vehicle Desiro at 72mph.
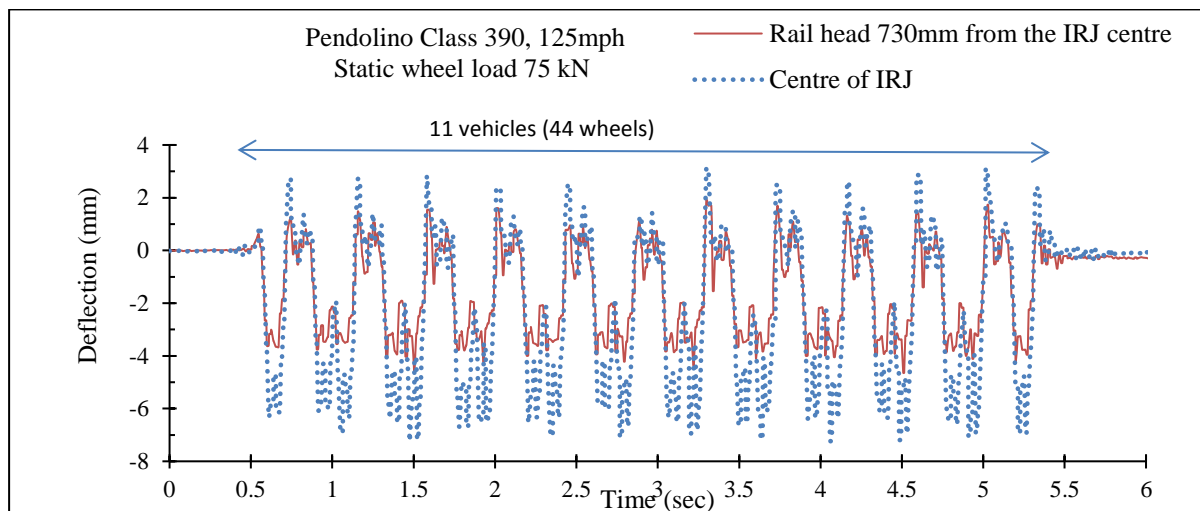
Figure 4.10 Deflection time history under the passage of 11-vehicle Pendolino at 125mph.

From the previous plots, some differences in the magnitude of the peak values of IRJ deflection for the intermediate cars were observed. This can be attributed, firstly, to variation of the actual static wheel load (due to varying passenger load among the vehicles) and secondly to increased wheel-rail dynamic contact forces (due to potential wheel defects such as wheel flats or wheel out-of-roundness). Further details on the measured data are provided in Paper 2 (Appendix B).

The effect of load variance and train speed variance on the magnitude of the measured deflection is concluded in Figure 4.11. The consistency of the magnitude of the maximum deflections found for each train passage was shown through the repeatability of peak values

over the various axles of each train. The obtained resolution was calculated in a range from 0.013 mm to 0.03 mm.
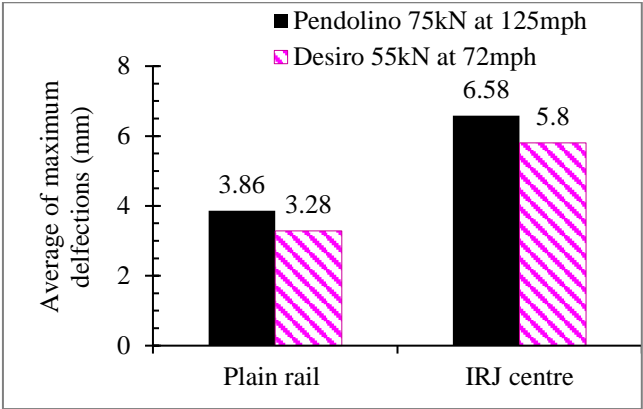
Figure 4.11 Comparison between IRJ and plain rail deflection for different trains and speeds.

In addition, the dip angle provides a level of deterioration of the IRJ, as described in Table 2.3. This can be calculated through the above measurements (Figure 4.11) for the distance of 730mm (see equation 2.1, Figure 2.11, Section 2.5). It is calculated to 7.4 mrad for Pendolino and 6.9 mrad for the Desiro, below the specified limit value (30 mrad, see Table 2.3).

Site B-Investigation of dipped joint through track geometry data

As an experimental technique had not been found in the literature to find RJ deflection data, a comparison was not possible, however, the track geometry data (determined from Network Rail databases) is provided here to show the level of deterioration that was present at Site B. The track deflection values can be combined with the track geometry data to verify the difference in vertical track alignment found in plain rail and IRJ. This method would allow the prediction of any dipped joint. The deflection measurements were undertaken on the 28th of August 2015 at Site B (location characterised as CGJ1, 1100 up fast line, 159 mile, 58 yrds).

Looking at the CCQ chart-Top 35 for Site B (Figure 4.12) the last track renewal of this section of track was conducted in 2010. The rate of deterioration of track quality in this section for the year 2014-2015 was found to be 0.5 mm /year (SD_{2014}=1 mm, SD_{2016}=2 mm). This was calculated through the inclination of the SD values in the CCQ chart. Thus, this site experienced, at the time of the measurements, a medium level of track quality deterioration (according to Table 4.4) that further justifies the magnitude of deflections found.

Table 4.4 Route evaluation (Nogy, 2016)

Route evaluation	Rate of deterioration/year
Low	0.0-0.4 mm
Medium	0.5-0.6 mm
High	0.7->> mm
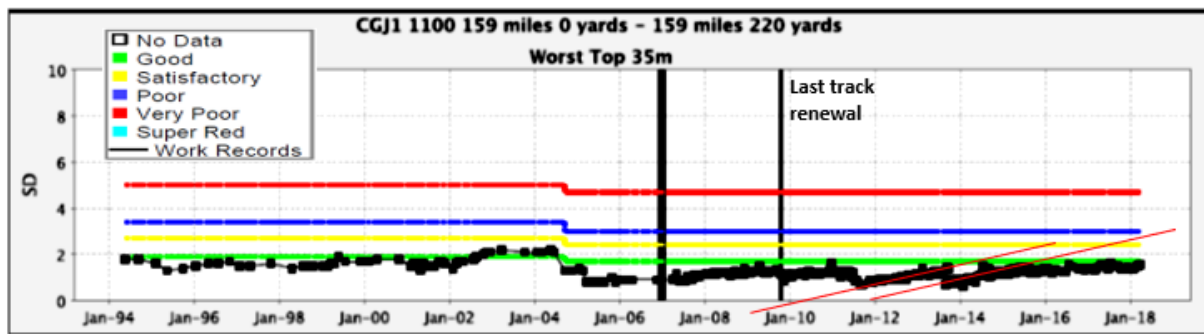
Figure 4.12 CCQ chart-SD values for vertical alignment for Site B.

In UK's rail network, the vertical profile of the track is measured by the HSTRC (High Speed Track Recording Coach). Information on dip angle for a loaded track may be computed from the HSTRC measurements. One example is shown in Figure 4.13 for two different dates for the left rail of Site B. The results have been filtered in the same wavelength band of 35 m for two different sampling distances, 1 m and 0.5 m.

A fault in the vertical profile is observed at the location of the IRJ (58yrds) as a dip. As shown in Figure 4.13, the sampling frequency has a small contribution in the appearance of the fault leading to almost equal magnitude of SD value (variance of vertical profile), between the upper and lower graph.
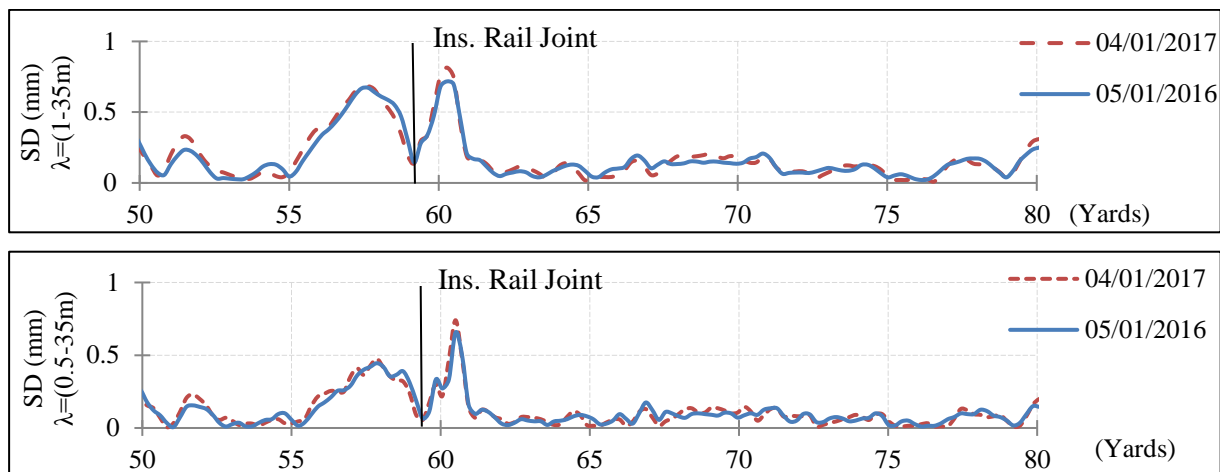
Figure 4.13 Vertical level from Site B [CGJ1], up fast [1100], 159 mile, left rail measured by HSTRC. Upper graph: wavelength band λ=[1, 35]m, lower graph: λ=[0.5, 35]m

The above analysis indicates that the track geometry data can be also used to identify locations of potential faults (e.g dipped joints-however dip angle measurements can be also recorded with the HSTRC but were not available for this site, cracked fishplates, rail end breaks). However, it would be beneficial for the railway industry to implement deflection measurements as an inspection tool that complements track geometry measurements. Further investigation is required to define deflection threshold values to inform industry about the required track improvements. For this purpose, an evaluation of a wide range of track deflection measurements under various known substructure conditions (subgrade type) under the same known axle load is recommended.

Concluding remark

This section aimed to demonstrate the use of VG in order to directly obtain deflection measurements of IRJ in real-time operational conditions. In particular, this is performed by comparing the deflections of IRJ with that of plain rail. The global track stiffness was found to be below 20 MN/m (Paper 1) for both plain rail and IRJ positions. This value corresponds to soft trackbed conditions according to NR/L2/TRK/4239 (Network Rail 2016) (see also Table 1.3, Section 1.1). Furthermore, consistency was observed between the global stiffness values observed at the two sites, although both sites provided poor stiffness conditions according to Wehbi and Musgrave (2017) (optimum rail deflections 1.5-2 mm and optimum global track stiffness 45 kN/mm for well-maintained track sites) (see also Section 1.1, Table 1.3). One of the main conclusions made here was that a small increase of rail deflection above the limit (3-

4 mm) corresponds to deteriorated stiffness conditions. This finding is important for the current UK track design engineers who design for long term track performance by taking into account a desired target rail deflection level. The deflection increment seen on the IRJ is explained by the structural discontinuity and the lower section modulus of the fishplates interacting with the wheel load. This causes a vicious cycle of gradual RJ and trackbed deterioration and increased dynamic forces induced over the RJ. The results found here meet objective 2 and are later used in the validation of the numerical modelling (Section 4.3), where the study was extended.

4.2.3 FIELD MEASUREMENTS OF BALLASTLESS FORMS AND TRANSITION ZONES & INVESTIGATION OF TRACK STIFFNESS PROPERTIES

In addition to the deflection data obtained from laboratory testing (Section 4.2.1) and field measurements (Section 4.2.2) and having shown the effective application of the VG for track deflection assessment, further field measurements were undertaken meeting objectives 2 and 4, using the VG as a tool for the assessment of track structure performance and for industry guidance. In the case studies discussed in this section, the VG was used to derive stiffness properties of various trackforms, demonstrating its use as a guidance tool for the industry. The research findings of this section are described in Paper 4 (Apendix D).

Stiffness properties were estimated through VG measurements at two sites. Firstly, at Site C, the stiffness of two novel ballastless systems was evaluated for known loads. Secondly, at Site D, the performance of a transition zone was evaluated under live train traffic; stiffness properties were deduced based on the static wheel load, from the known gross weight of the rail vehicles, and the deflection bowl was deduced in absence of vehicle load, directly from the real time recorded data.

As discussed above the global stiffness is calculated for Site D based on the static wheel loads of the trains. The calculation of the actual dynamic track stiffness would only be possible through accurate measurement of the dynamic load by either strain gauges on the rail or wheel load impact detectors (WILDs). Although these are expensive and difficult to install methods, they are recommended for further research. Previous RMSV (see Section 2.2.5) measurements that actually excite the track dynamically at frequencies between 3 and 50 Hz at speeds up to 50 km/h (31 mph) have shown that dynamic track stiffness variations of 5-20 kN/mm are common between adjacent sleepers with a variability even up to 60 kN/mm having been

detected on modern railway track due to short wave irregularities that cause high dynamic train-track interaction forces (Berggren, 2006). The use of void meters is recommended to be used in combination with the VG in further research to investigate the existence of hanging sleepers that could cause increased dynamic loads. However, the static and low frequency dynamics of the track is related mostly to the geotechnical issues, and thus, the stiffness as calculated based on the static loads can be useful for the investigation of the bearing capacity.

Site C- Evaluation of stiffness properties for known load

Deflections of two types of novel ballastless trackforms with asphalt underlayment (IVES - Intelligent versatile efficient and solid slab track (Rhomberg Sersa Rail Group 2016a)) and PORR slab, (PORR 2012)), and of conventional renewed ballasted track, were measured by the VG on a test track. The measurements were undertaken using two cameras, of focal length 16 mm mounted on surveyors' tripods 2 m from the line, measuring at a capture rate of 105 Hz and with a resolution of 0.01 mm-0.02 mm. The deflections of rail, sleeper, slab modules and the asphalt layer were measured under the passage of a Sea Urchin locomotive (16.3 ton per axle) and two wagons (13.25 ton per axle) running at 2-20 mph. Six train passes were recorded for each trackform and consistency of the maximum deflections was found.

Looking at Figure 4.14 and Figure 4.15, the rail deflections found were below 2 mm, lower than the two previous sites (A and B) as expected for a newly, constructed track, whereas limited deflection was found for the asphalt and slab modules. Further details are given in Section 3.1.2 of Paper 4 (Appendix D).
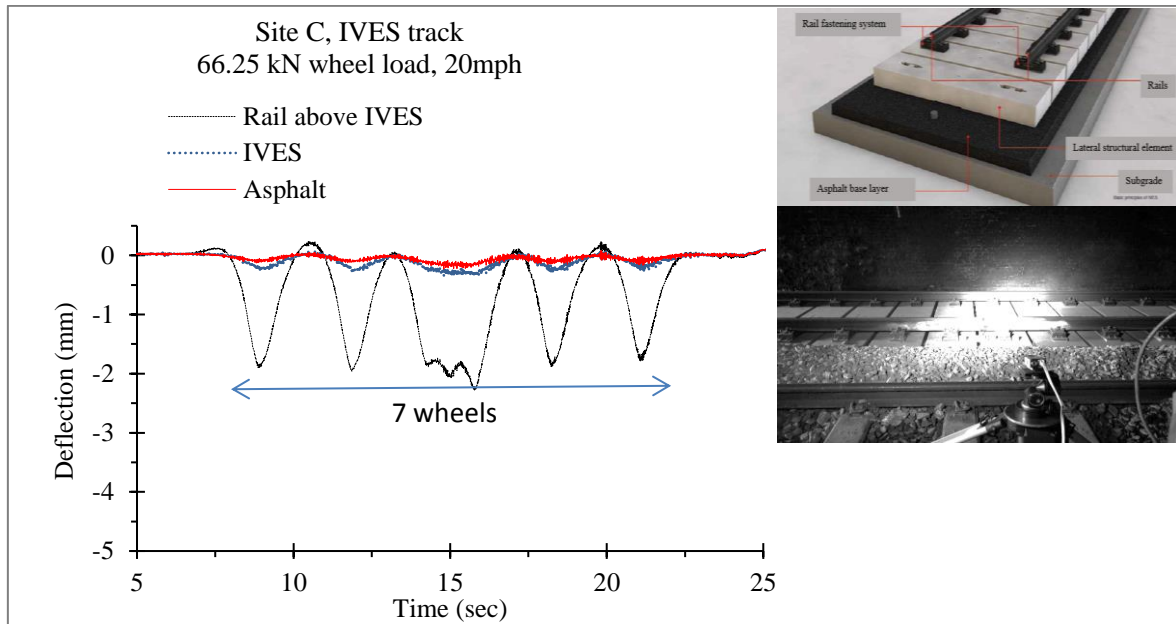
Figure 4.14 Deflections of IVES track at Site C.
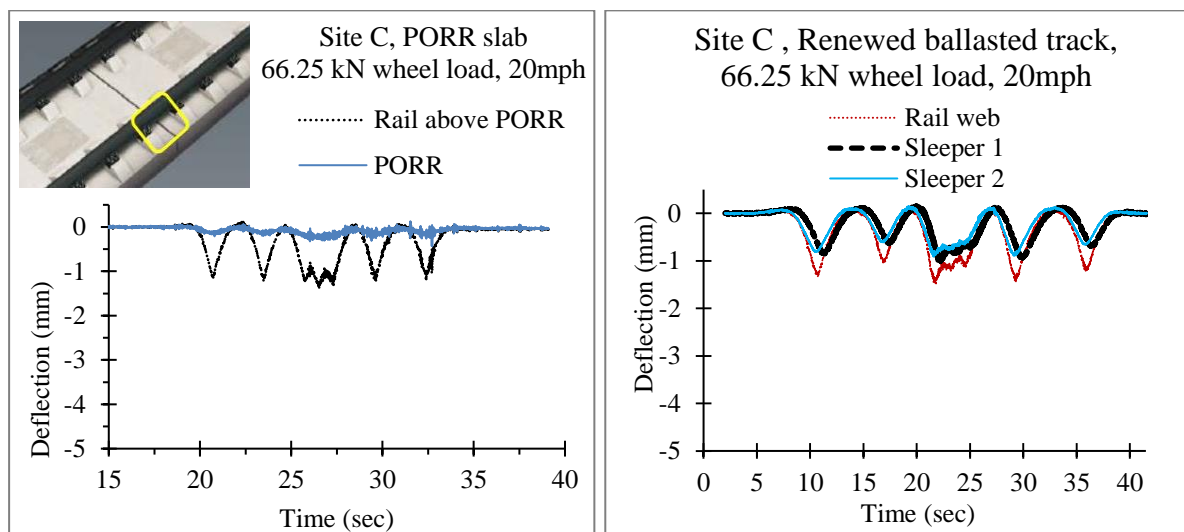
Figure 4.15 Deflections of PORR slab and renewed ballasted track at Site C.

.

The above deflection results of the ballastless modules correlate well with literature; slab deflection of 1.5 mm according to Bastin (2006); 0.8-1.5 mm according to Vossloh (2009); 1.58 mm according to Vale, Ribeiro, Calçada and Delgado (2011); 1.47 mm according to Liu and Freudenstein (2013). From the above measurements and taking into account the known static wheel load, stiffness and moduli parameters for the three trackforms were back calculated using the BOEF (described in Section 2.2.3).

More specifically, looking at Figure 4.16 similar global stiffness is found for the PORR and renewed ballasted track, whereas the IVES was found to be more elastic due to the lower stiffness of its fastening system that allowed slightly higher deflection (1.84 mm in IVES instead of 1.25 mm in PORR). The fastening system and the asphalt layer underlayment provide the elasticity that the ballast and the fastening system provide in the ballasted track.

The stiffnesses found for the fastening systems are as expected in comparison with published values; 50-650 MN/m for ballasted track (Hunt 1996; Oregui *et al*., 2017) and $\geq$ 22.5 MN/m for slab track (DFF304) (Vossloh, 2015). The global stiffness found for all track forms is between 30-60 MN/m. According to Wehbi and Musgrave (2017) the suggested optimum value is 45 MN/m. On the other hand, the support stiffness found was 51 MN/m underneath IVES and 62 MN/m underneath PORR that actually represents the stiffness of the asphalt layer that exists below the slab modules. The support (trackbed) stiffness of the ballasted track was calculated to be 24 MN/m. It is observed that this value is close to the recommended values (NR/L2/TRK/4239 (Network Rail 2016)). For a typical fastening system of stiffness 64.5 MN/m and an optimum global stiffness 45 MN/m the optimum trackbed stiffness is calculated to be 20 MN/m, very close to the value found.
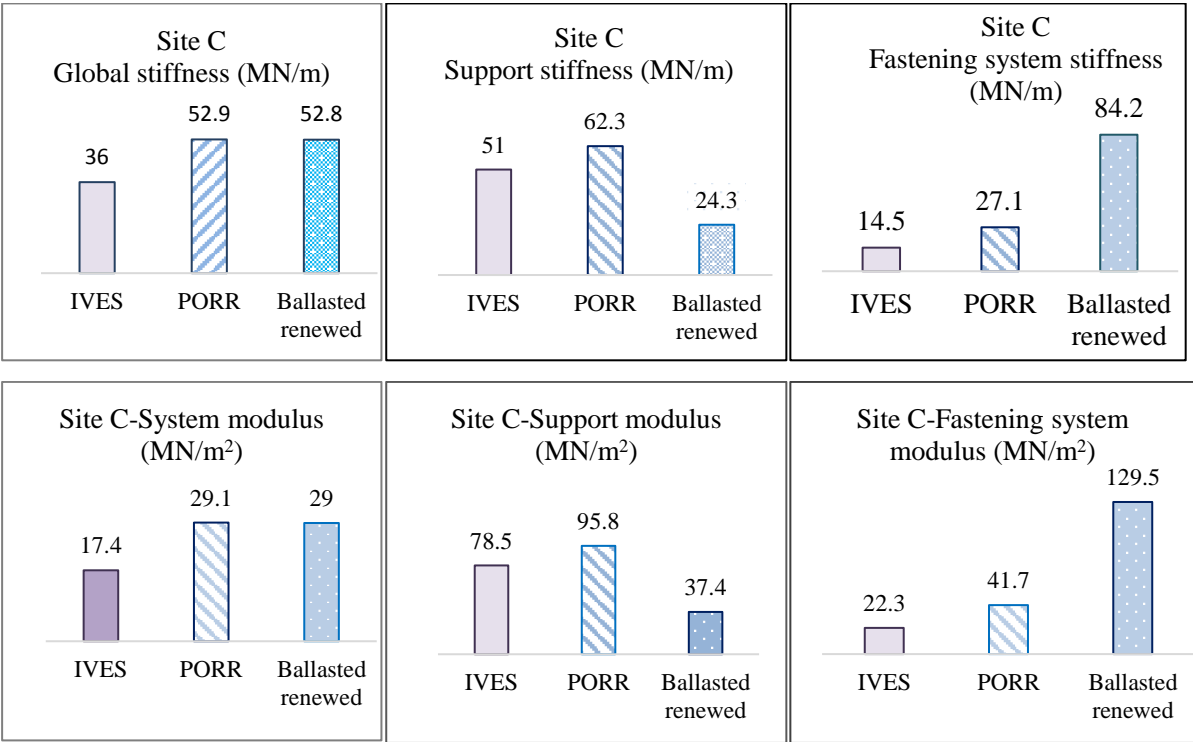
Figure 4.16 Stiffness characteristics calculated for Site C.

Site D- Evaluation of stiffness properties for assumed load

Having shown the capability of the VG for measuring ballasted track and slab deflections and assessing track stiffness properties under a known load, in this section, the stiffness properties of a transition zone on the approach to a railway bridge are evaluated through the VG data under live train passages, the loads of which are assumed based on the train type (see Section 3.2 of Paper 4 in Appendix D). Transition zones usually require high levels of maintenance due to increased differential settlement of the substructure caused by the abrupt change of track stiffness.

A fast line on a transition zone, on the approach to a railway bridge, with a line speed of 125 mph was measured using two cameras mounted on two tripods at a distance of 5 m from the line (Section 3.2.2 of Paper 4). Two lenses of 16 mm focal length recorded the deflection of 6.5 m of track covering ten sleepers. Rail and sleeper deflections were measured at the same time by each camera at a sampling frequency of 175 Hz. The resolution of the measurements was found in a range of 0.016 mm to 0.042 mm. Measurements were undertaken for two phases: I) prior to renewal, after manual tamping and II) after renewal (trackbed reinforcement). Eight Intercity 125 passages were recorded in Phase I and two in Phase II. Further details are given in Section 3.2 of Paper 4 (Appendix D).
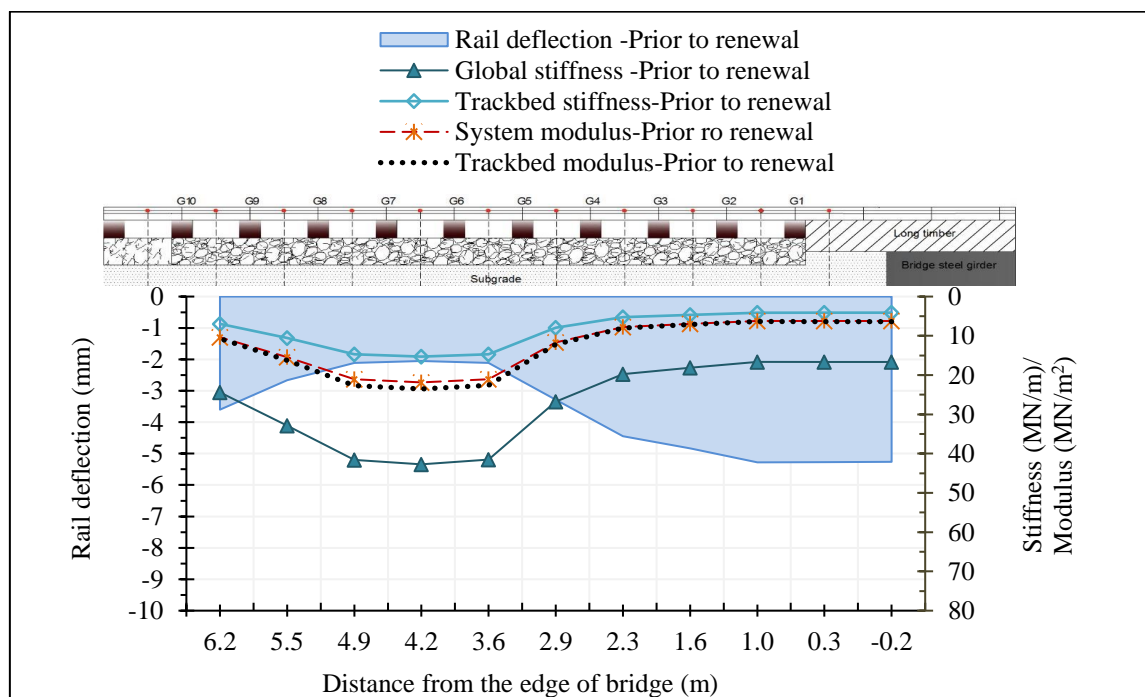
Figure 4.17 Deflection and stiffness properties along the transition zone –Phase I.
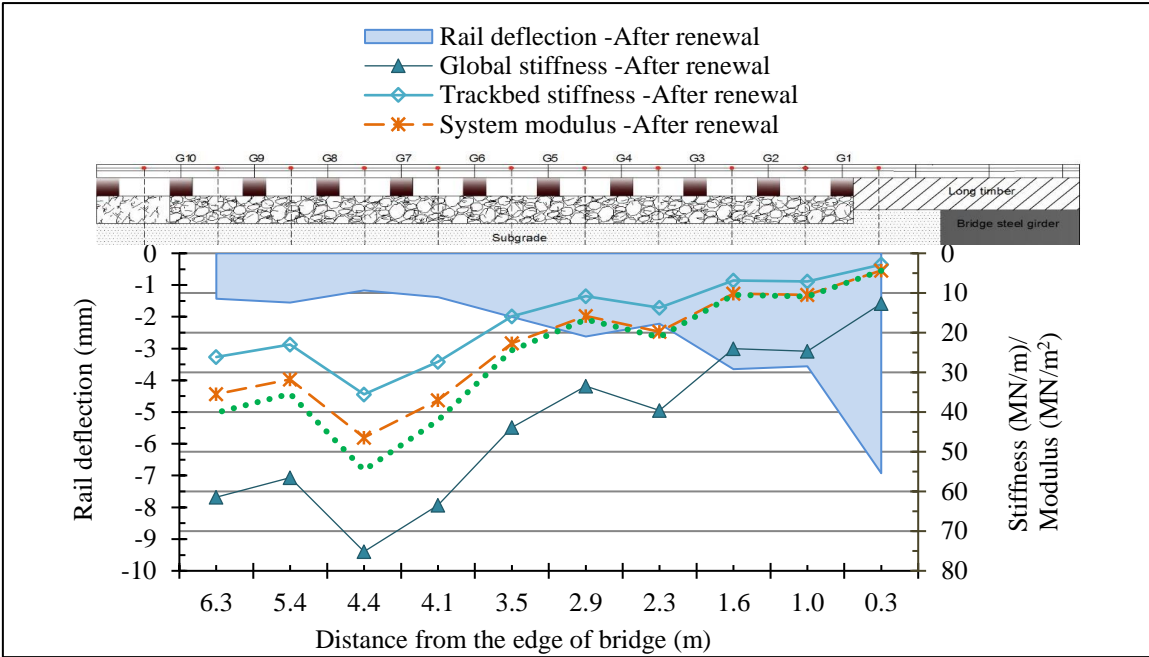
Figure 4.18 Deflection and stiffness properties along the transition zone -Phase II.

The variability of the inferred stiffness characteristics from one point to another along the length of the transition zone for the two phases was evaluated. This is presented in Figure 4.17 and in Figure 4.18 (see also Sections 3.2.3 and 3.2.4 of Paper 4 in Appendix D). The deflection for each position shown in the above graphs constitutes the maximum deflection as averaged for the total number of train passages. Phase I occurred after repacking the ballast by manual tamping, therefore the deteriorated condition of the transition zone was temporarily improved. The track deflection was found lower on the approach to the bridge (sleeper G1 to G4). Ballast abrasion was observed around G1, G2 and G3. Voided sleepers and poor drainage (subgrade pumping) was the cause of deflection and stiffness variations prior to the maintenance activity. Deflections and consequently stiffness properties were improved after the treatment.

Moreover, the back-calculation method based on BOEF enables the determination of track system moduli and trackbed moduli by taking into account the effect of railpad stiffness and rail bending stiffness (described in Section 2 of Paper 4). Initial moduli are assumed, deflections are calculated and then the moduli are adjusted in an iterative fashion to converge on the empirically measured deflections. This method is based on linear elastic assumptions without taking into account the non-linear, stress dependent, response of the railpad and trackbed (ballast and subgrade) behaviour. For this reason, the VG data of Site D were further analysed

below to allow investigation of the deflection bowl of several positions under the live moving wheel. This will provide additional information for the condition and bearing capacity of the track structure.

Site D-Evaluation of the deflection bowl in absence of wheel load data

A different way of visualising the track stiffness change over a short length of track, such as the transition zone of Site D, is looking at the deflection bowl for several positions (see also Section 3.2.5 of Paper 4 in Appendix D). Two examples of the deflection bowls due to the passage of Intercity 125 are shown in Figure 4.19 and Figure 4.20. Each line represents the deflection measured on each sleeper of the transition zone at the same time for a specific position of the wheel. A normal deflection bowl will have decreased deflection with increasing offset distance.

In particular, looking at Figure 4.19 it is observed that the deflection bowls of sleepers G6 to G10 are normal. The trackbed modulus was evaluated as around 20 MN/m for this area (see Figure 4.17), considered good for a ballasted track. In contrast, the load distribution is different when the wheel is above sleepers G4 to G1 indicating the problematic area. The improvement of the trackbed condition can be concluded when the deflection bowl is analysed for Phase II in Figure 4.20. Consistent increased deflection is observed before and after renewal for sleeper G1 that can be attributed to the flying end (extension into the ballast for a short length after the retaining abutment) of the longitudinal timber beam of the bridge track structure, the support of which may not be adequate. Further detail is provided in Paper 4 (Appendix D).
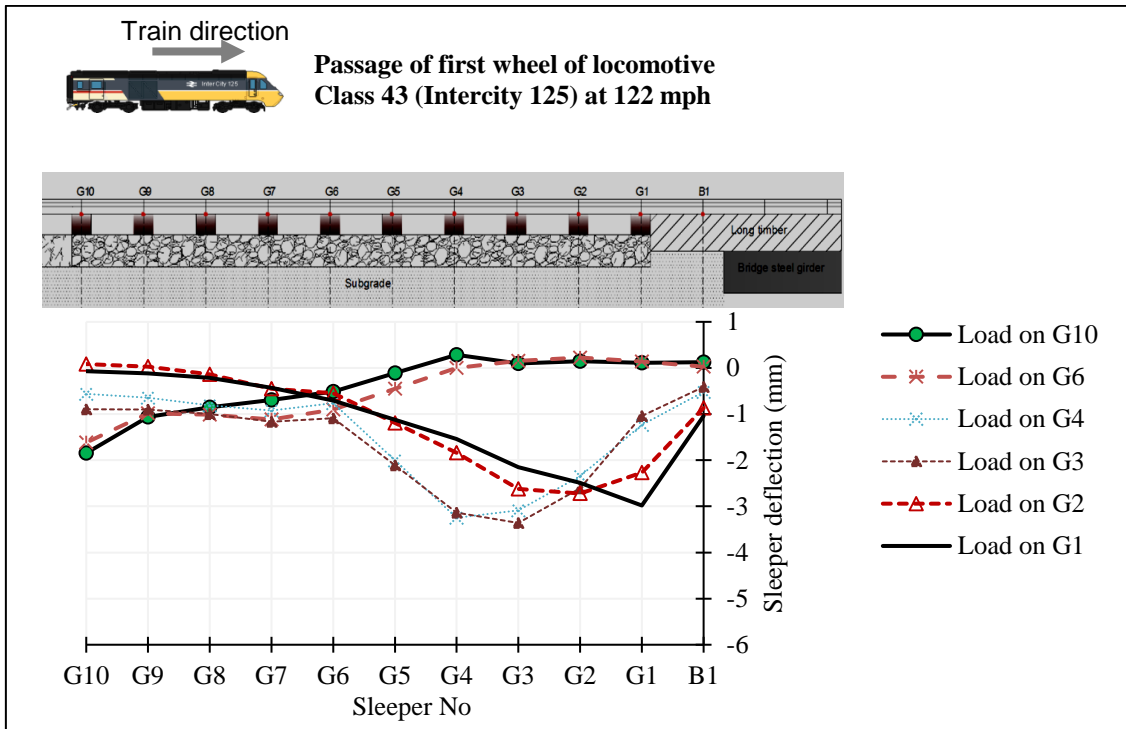
Figure 4.19 Deflection bowl-Class 43-Phase I
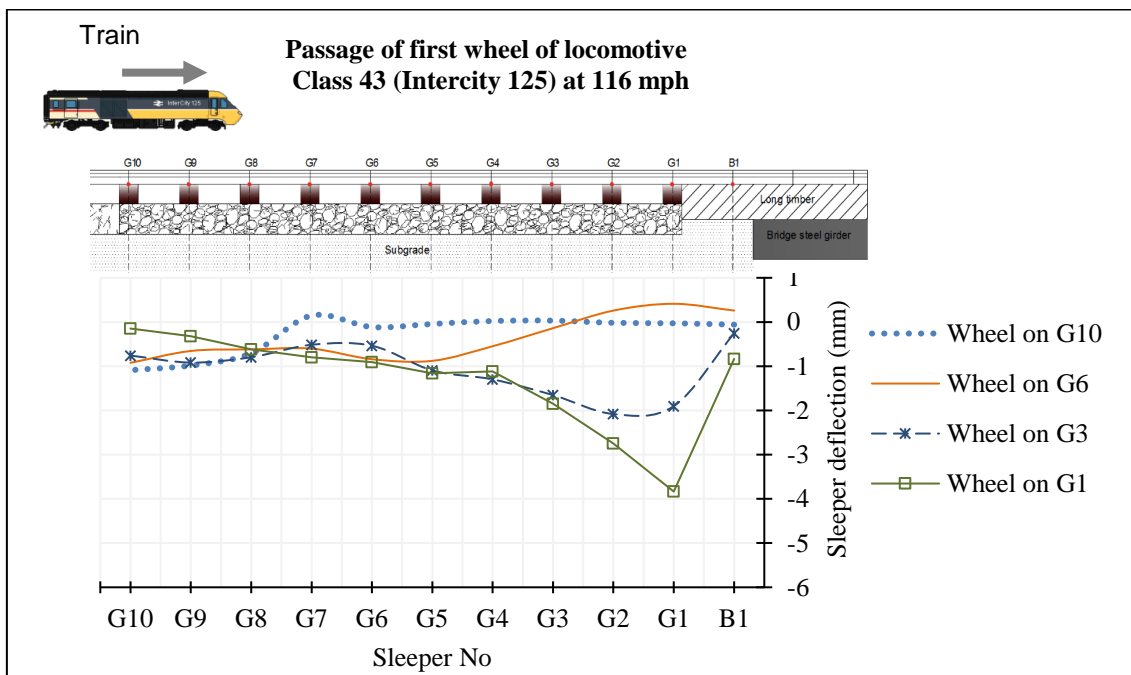
Figure 4.20 Deflection bowl-Class 43-Phase II

Concluding remarks

The collection of VG data and their application described in this section, meet objective 2 by demonstrating that the VG can be used for the assessment of track stiffness properties of a critical zone that needs to be investigated promptly, remotely without the need for track possession (see also Section 4 of Paper 4 in Appendix D). In addition, the ability of VG to measure the deflection bowl along several positions in absence of the vehicle's load data is shown. The findings of this section are used in Section 5.2.1, where the impact on the wider industry is described (objective 4).

4.3 NUMERICAL MODELLING TO ALLOW ANALYSIS OF RAIL JOINTS

The understanding of a RJ performance through field inspection is highly demanding and costly. The laboratory testing indicated the deflection increment seen on a RJ but this was not adequate to investigate structural performance improvement techniques. As described in Section 4.1, a numerical model (including multiple model configurations to accommodate the RJ's structural variables), validated with experimental deflection data, was developed to meet the objectives described in Section 4.1, to systematically investigate factors controlling the deflection behaviour of rail joints, and as a tool for IRJ design optimisation (Objectives 3 and 4).

4.3.1 INVESTIGATION OF THE EFFECT OF EXTERNAL REINFORCEMENT ON DEFLECTION BEHAVIOR OF INSULATED RAIL JOINTS

This section describes the numerical modelling established with the aim of investigating the potential for external reinforcement of IRJs. The hypothesis, described in Section 4.1, was based on the use of strap rails as a cost-effective means of structural enhancement of the track in the vicinity of a glued IRJ, aiming to reduce the deflection to less than or equal to that of plain rail. Thus, the ongoing joint wear and damage can be reduced. This was shown by a static finite element model validated using the deflection field measurements presented earlier in Section 4.2.2.

There are a number of examples of using numerical models to investigate track structure and IRJs, as discussed in Section 2.8. Following these examples, a 3D finite element (FE) model was required, capable of replicating the behaviour of conventional track structure and the behaviour of a RJ within it. This section details the development of the FE model, the main findings and its correlation to the field data. A detailed description is provided in Paper 2 (Appendix B).

Numerical model development

The numerical model was created using 3D FE modelling code, ANSYS. The type of analysis selected was based on the availability of resources and time. A static structural analysis determines the displacement, stresses, strains and forces in structures and components caused

by loads that do not induce significant inertia and damping effects. A static structural analysis can be either linear or non-linear. Here, isotropic linear elastic material models were used as the induced stresses from the static loading were not in excess of the yield limits (see section 5 of Paper 3 in Appendix C), while non-linear elastic frictional contact details were introduced between all interfaces among rail-fishplate-liners and among ferrules-fishplate hole faces (more information in given in Section 3 of Paper 3, Appendix C).

A view of the model is provided in Figure 4.21. The stiffness of CEN 56 rails, 6-hole fishplate, railpad, endpost and G44 concrete sleepers (200mm depth, 2500 mm length, 200 mm width) was defined through Young's modulus, Poisson's ratio, and density (see Table 4.2) for the mass and inertial loads calculations. In addition, rail loading, sleeper spacing (0.65 m) and type of external strengthening for a suspended glued IRJ were determined. The support stiffness was applied using spring elements on both sides of the rail seat load with stiffness in a range from 5 to 200 MN/m, matching literature and trackbed UK specifications (see Section 1.1, Table 1.3) (RSSB 2011; Network Rail 2016; Andersson *et al*. 2013; Grossoni *et al*. 2014), and the stiffnesses found in the field investigation (see Section 4.2.2). A refined mesh with maximum element size 5mm was applied in the vicinity of the rail joint (rail, fishplates and four central sleepers) and a larger element size of up to 30mm was used for the rest of the sleepers. 10-node tetrahedral quadratic elements SOLID187 were used in the model. Further description of the precise dimensions, materials, boundary conditions and of the four model configurations is given in Section 3 of Paper 2 (Appendix B).

Furthermore, the effect of uniform degraded track support underneath the IRJ was investigated. A vertical load of 125 kN that represents the maximum static load applied to UK track infrastructure was applied at the centre of each rail joint. The wheel load was applied on an area corresponding to the wheel-rail contact patch (see Paper 2). In the model, the elastic linear behaviour of the railpad partially controls the rail uplift, whereas bonded contact between rail-railpad-sleeper was set. The simulation of fastening clips for the assessment of IRJs' response to vertical bending was considered to not be critical. The bolt interface was not of direct interest for this analysis as an ideal, non-degraded, glued IRJ was modelled. The induced stresses in the fishplates were not in excess of the yield limits, thus an elastic constitutive law was used. A detailed description of the parameters, including geometry, boundary conditions, loading, mesh, constraints, and contacts, considered in the model development, as well as further visualisations of the model configurations are provided in Section 3 of Paper 2 (Appendix B).
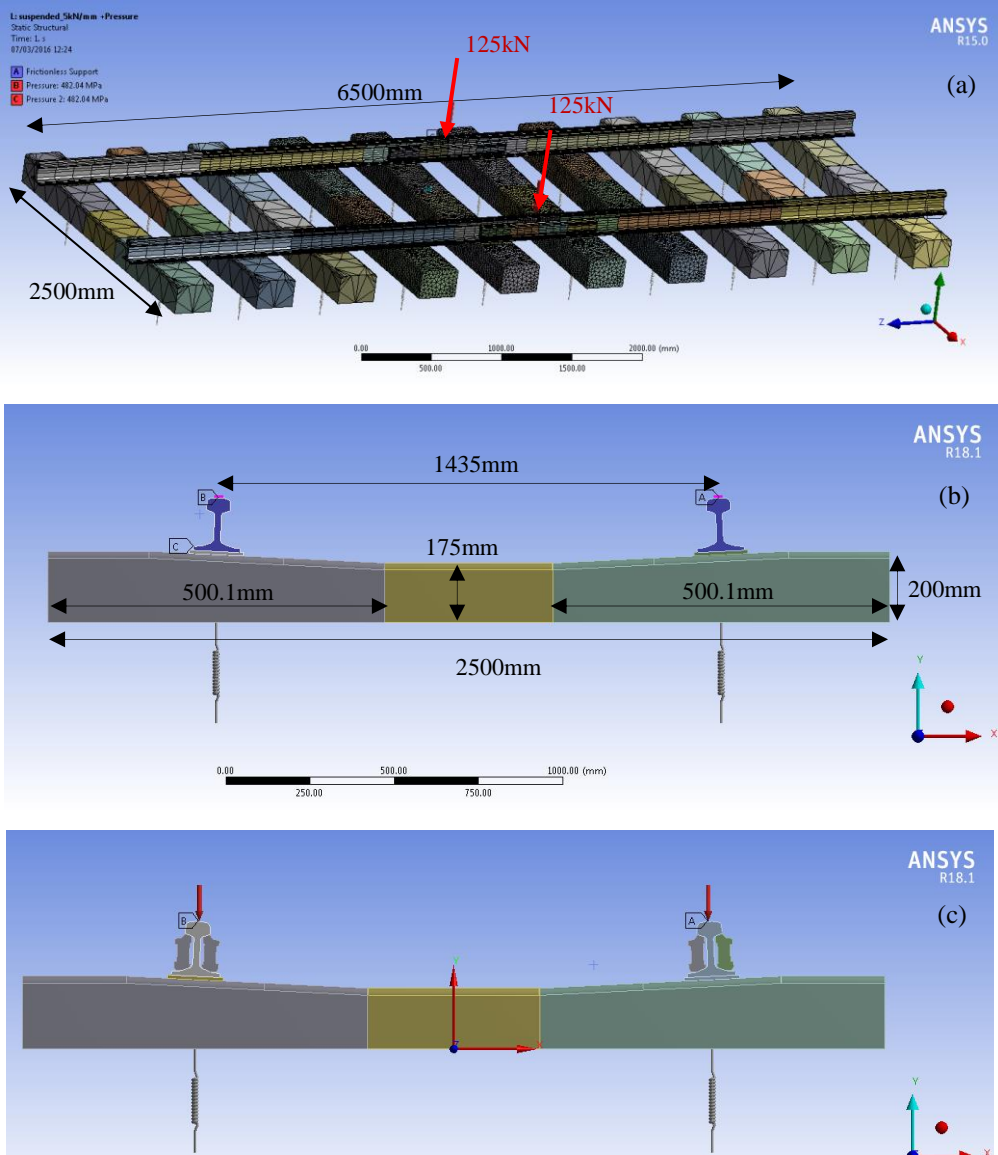
Figure 4.21 (a) Model layout and side view of (b) plain track model (c) suspended IRJ model amended from Paper 2

Four model configurations were analysed: a) plain track, b) suspended IRJ (SUS-IRJ), c) suspended IRJ enhanced with strap rails (SR SUS-IRJ) and d) suspended IRJ strengthened with I-beams (BS SUS-IRJ) (see Table 4.5) (Section 3, Paper 2). The reinforcing strap rails are rails of same section, CEN56, positioned on top of the four central sleepers surrounding the IRJ (Figure 4.22). A preliminary analysis was undertaken for the effective position, and length of the reinforcement. A strap rail of same profile as the running rail (CEN56) was decided to be investigated in the analysis as this was considered the best practice solution in terms of availability during the field installation. The effect of a steel I beam section (39% stiffer than the strap rail, see I values in Table 4.5) in a size that can fit in the track geometry was also

evaluated (see Figure 4.22c). Several sizes of beams were evaluated before the selection of the most appropriate to fit in the track geometry (with moment of inertia higher than that of the rail CEN56). As outputs, the deflection and dip angle of the IRJ were evaluated. Here, it should be noted, that the fixing of strap rails/strengthening beams to the sleepers was not realistically idealised in the model (fastening system, railpads) but bonded contact was considered in the model between the beams and the sleepers that may lead to increased stiffness of the overall model configurations. Further analysis is required to investigate the effect of the fastening system in the deflection of the reinforced IRJs.

Table 4.5 Parametric study cases from Section 3 of Paper 2

Configuration	Sleeper type	Second moment of area of enhancement	Stiffness per sleeper end (kN/mm)
Plain track	Concrete		5, 15, 30, 115, 200
Suspended IRJ (SUS-IRJ)	Concrete		5, 15, 30, 115, 200
Suspended IRJ enhanced with strap rails (SR SUS-IRJ)	Concrete	$I=2320 \text{ cm}^4$	5, 15, 30, 115, 200
Suspended IRJ strengthened with I beams (BS SUS-IRJ)	Concrete	$I=3227 \text{ cm}^4$	5, 15, 30, 115, 200
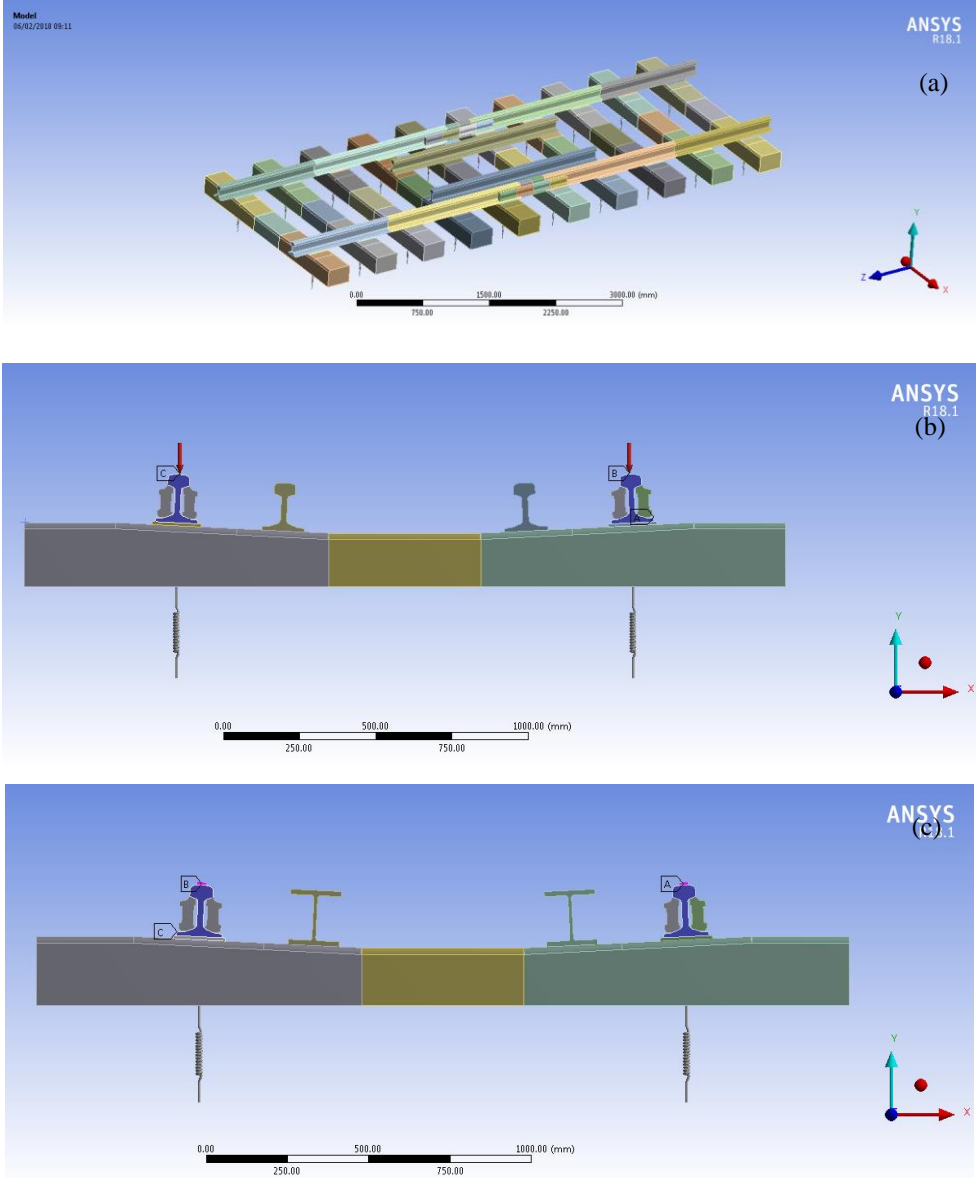
Figure 4.22 View of the Suspended IRJ model enhanced with (a, b) strap rails and (c) I-beams of same length as in (a) from Paper 2

Results of numerical model

Maximum rail deflections and dip angles were evaluated for the four FE model configurations (Table 4.6) (see also Section 4 of Paper 2).

Table 4.6 Deformation results for plain track, jointed and enhanced jointed track for varying support stiffness from Section 4 of Paper 2

Stiffness per sleeper end (kN/mm)	200	115	30	15	5
	Maximum vertical displacement (mm)				
Plain rail	0.93	1.11	2.13	3.26	6.78
SUS-IRJ	1.28	1.49	2.67	3.97	8.03
SR SUS-IRJ	1.22	1.42	2.45	3.57	7.01
BS SUS-IRJ	1.19	1.38	2.37	3.45	6.8
	Total dip angle (mrad)				
SUS-IRJ	3.57	3.72	4.31	4.79	5.88
SR SUS-IRJ	3.5	3.61	4.04	4.35	5.04
BS SUS-IRJ	3.37	3.47	3.84	4.11	4.7

The magnitude of IRJ deflections, found by FEA, is in agreement with previous FEA research (Himebaugh, 2006; Carolan et al., 2014). The analysis emphasizes the significant effect of poor support conditions on IRJ deflection; 49% increase (from 2.67mm to 3.97mm) from 30 to 15 MN/m/sleeper end and 100% increase from 15 to 5 MN/m/sleeper end (from 3.97mm to 8.03mm). The softer the support conditions, the higher the additional deflection an IRJ accumulates compared to that of a reference rail. Looking at Figure 4.23, the relationship between the deflection increase and the support stiffness decrease is not linear. The effect of strap rails is greater for the soft support conditions provoking 13% deflection decrease (from 8.03mm to 7.01mm), with the I –beams reducing it to a level lower than that of the plain rail (from 8.03mm to 6.8mm; 15% decrease for soft support conditions).

The magnitude of total dip angle found is in good agreement with previous experimental research (<14 mrad, Sun *et al.* 2009). Here, a non-degraded (new) glued IRJ is modelled. The dip angle increases 11-23% (from 4.79mrad to 5.88mrad) for degraded support conditions in a non-linear relationship with track stiffness decrease. The effect of reinforcement is more significant for the degraded support conditions leading to 11-20% dip angle decrease (from 5.88mrad to 4.7mrad). More detailed discussion is provided in Paper 2.
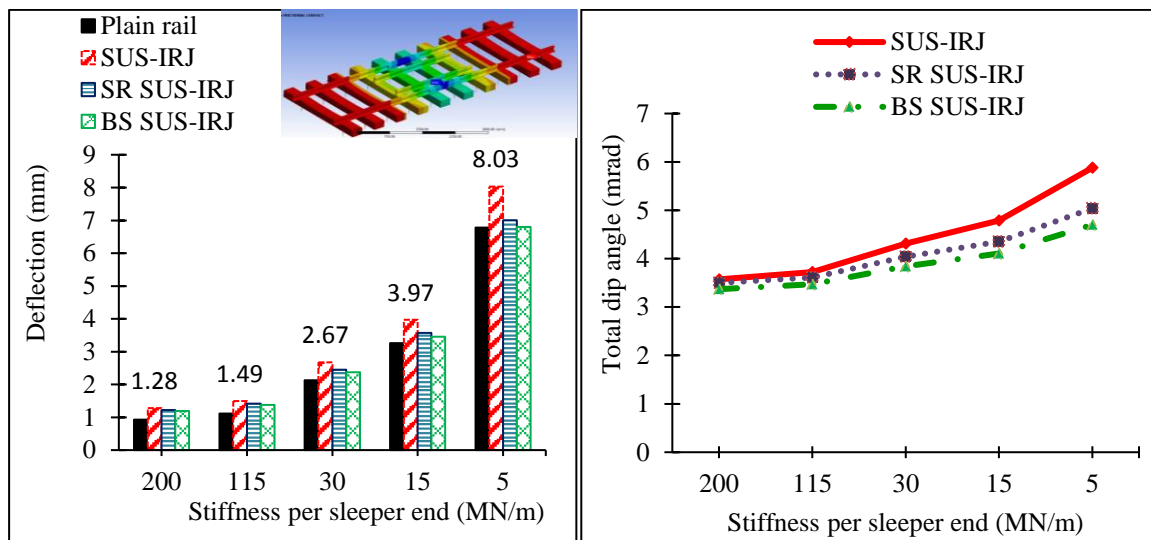
Figure 4.23 Effect of reinforcement on the deflection and dip angle of suspended IRJ for varying support stiffness from Paper 2

Correlation of the numerical model with the field data

The wide range of support stiffness values was selected in the FE model in order to capture all the likely range of support conditions seen in the field. For support conditions 5 - 30 MN/m/sleeper end, plain rail deflections were found in a range of 2.13 - 6.78 mm, comparable to the ones in field (Figure 4.24). The rail deflections in the ballasted track of Site A and B were found in a range of 2.36 – 3.86 mm (Section 4.2.2) and higher values up to 5.5 mm were found for the degraded trackbed conditions of the transition zone (Site D, Section 4.2.3, Figure 4.17). In well-maintained trackbed conditions, a maximum trackbed stiffness of 35-37 MN/m/sleeper end was assessed (Site D, Phase II, Site C) with 5 - 15 MN/m for Sites A, B, and D. These values correspond to a range of trackbed moduli 7.7 - 23 MN/m^2 that are lower than those recommended by standards (target value 30 – 45 MN/m^2 for track renewals according to NR/L2/TRK/2102 (Network Rail 2008) but agree with literature (Andersson et al., 2013; Grossoni et al., 2014). Thus, the measured track deflection values correspond to degraded track support conditions and they match with the cases 5-15-30 MN/m/sleeper end of the numerical model.

By looking at Figure 4.24, the SUS-IRJ deflections found in the numerical model (FEA) with a stiffness of 5-30 MN/m/sleeper end (2.67-8 mm) are in good agreement with the field measured data (4.23 - 6.58 mm). The results indicate the significance of soft trackbed conditions in the IRJ performance and how countermeasures can affect it.
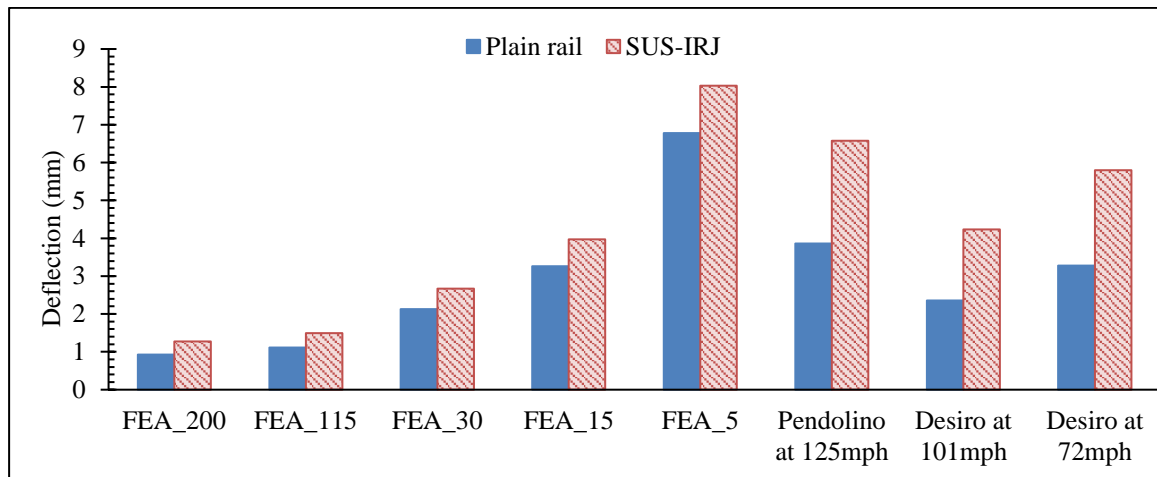
Figure 4.24 Comparison between numerical model and field deflection data for plain rail and SUS-IRJ from Paper 2

An absolute validation of the model was not possible as the exact P2 forces (see Section 2.2.1) that occurred above the IRJ due to high-speed trains was very difficult to measure in the field, although it is assumed that they can reach up to 2 -3 times the static wheel load (Wen, Jin and Zhang, 2005; Grossoni *et al*., 2014). In addition, by taking into account the vicious cycle of trackbed degradation underneath an IRJ and the consequent dynamic force increase, described in 2.3 and also discussed in 4.1, it is possible that the IRJ deflections found in Site B were a result of discrete ineffective support conditions or due to the existence of voids (hanging sleepers).

Concluding remarks

A numerical study based on FEM was conducted including four model configurations (plain track, suspended IRJ, enhanced IRJ with strap rails and enhanced IRJ with I-beams) for varying support stiffnesses. This showed that for support conditions 5-30 MN/m/sleeper end, that match the existing stiffnesses observed in the field estimated through the VG, the external reinforcement can improve the bending behaviour of IRJs and potentially increase their life expectancy. For verification of the above findings, a field trial is recommended using precast concrete sleepers with incorporated fastening system fixings (CEMEX, 2013, EG47GR2) where the strap rails are required. Using I beams is a more complex solution due to the way they will be fastened to the sleepers. A cost/life estimation of the potential product is required, to identify benefits for the rail industry. The results of this section meet objective 3, showing the development of a numerical model to allow analysis of the deflection behaviour of IRJs, and objective 4, identifying an alternative method to achieve track structure performance improvement.

4.3.2 EXPANDING THE MODEL'S USABILITY AS A DESIGN TOOL TO INVESTIGATE THE RESPONSE TO BENDING OF VARIOUS RAIL JOINTS UNDER FATIGUE VERTICAL WHEEL LOAD

Section 4.3.1 indicated the significance of the sleeper support conditions in the deflection performance of an IRJ. However, a perfectly glued IRJ was modelled as in the majority of literature (see Section 2.9). In this section, the numerical modelling method, established in Section 4.3.1, was utilized and optimised to a more advanced model for the analysis of IRJs. This was utilised to evaluate the performance of (a) different types of RJs (b) under a fatigue static test to assess their performance against fatigue limits, by including the effect of (c) the sleeper support condition, (d) the bolt preload and (e) any frictional contact among the rail/fishplates/insulating layers interfaces. The influence of the above factors on the RJ response to vertical loading has not been considered in detail by other research (Section 2.9). In this section, firstly, the optimised modelling technique is described; secondly, the main findings are discussed and finally a validation of the optimised modelling method is presented.

The analysis of this section was utilized on a project that LB Foster undertook for Network Rail. The project included the re-design of the fishplates for all types of rail joints in the UK rail network (including insulated Class A, B, and C, mechanical standard, mechanical transition joints connecting different rail sections, and lifted joints connecting new with worn rail sections with/without height mismatch). This work was described in two technical reports that the author produced for the project (TR-6 and TR-7 presented in Table 1.2, Chapter 1).

Numerical model optimisation

The FE model as described in Section 4.3.1 was optimised in order to allow routine assessment of different RJ designs. Its basic material properties remained similar (Table 4.2 as described in Section 4.1), while geometry was slightly modified (see Figure 4.25). The model included six sleepers, with 700 mm spacing and stiffness 30 MN/m/sleeper end (minimum sleeper stiffness for existing lines according to Network Rail (2016) (see Section 1.1). A wheel load of 200 kN was applied as a nodal force on the top of the centre of the railhead, as prescribed by Network Rail, that accords with the maximum static load on the UK rail infrastructure (125 kN) increased by a dynamic factor of 1.6. Two loading cases were initially studied in order to assess the joint's "sagging" and "hogging" deformation (see Figure 4.26). The first loading case

represents the wheel above the RJ whereas the second represents the joint in the middle of a wheel spacing of 1.8 m (the minimum wheel spacing as described in GM/GN2589 (RSSB 2004) and GE/RT8073 (RSSB 2009)). Precise details about the geometry, materials, mesh and boundary conditions are provided in Section 3.1 of Paper 3.
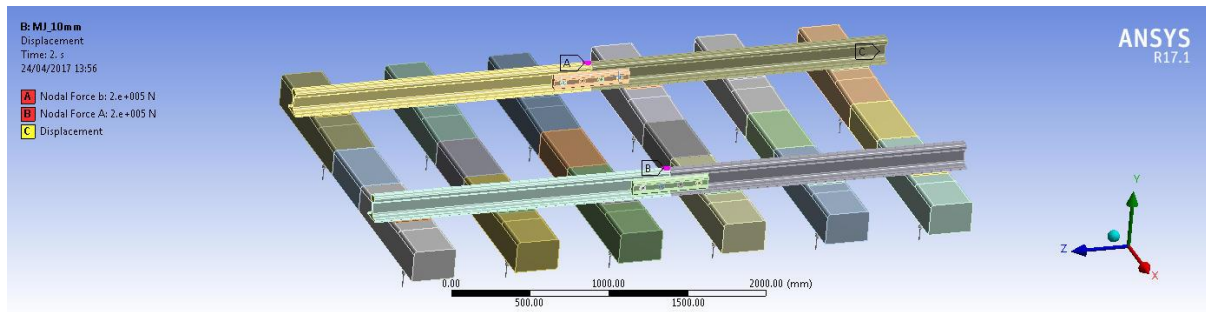
Figure 4.25 Model layout from Paper 3
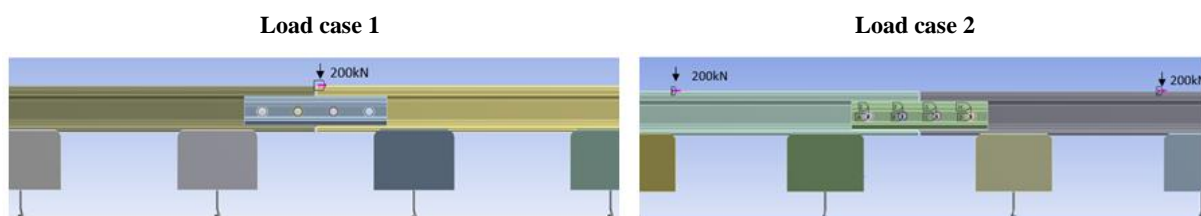
Figure 4.26 Loading cases (1) wheel load at 10mm from the rail end; RJ in sagging deformation (2) two wheel loads at 900 mm from the rail end; RJ in hogging deformation

The effects of bolt pre-tension are accounted for in the model. Beam elements were used to provide shear resistance to vertical load (ANSYS, 2015). These elements were then given a preload value (156-184 kN) equivalent to the expected preload generated from the tightening torque permissible on the bolt of the RJ (750 Nm for M24 and 995 Nm for M27, Grade 8.8). The bolt pretension is detailed in Section 3.2 of Paper 3.

Four different four-bolt RJ types were modelled: (a) glued IRJ- Class A, (b) mechanical RJ, (c) dry (encapsulated) IRJ- Class B and (d) dry (non-glued) IRJ- Class C (see Section 2.6). Among these joints there are several differences regarding their geometry, the insulation material properties and the type of contact in the interfaces within the joint assembly. A detailed description of these, as well as of the assumptions and type of contacts applied in the FE modelling, is presented in Section 3.3 of Paper 3.

This model was therefore developed to assess the response of four less stiff four–bolted rail joints under a critical fatigue vertical load by taking into account the frictional contacts in rail-

fishplate-insulating layer interfaces including bolt preload and elastic underlying sleeper support.

Discussion of the results of optimised numerical modelling (Section 5 & 6 of P3)

Results in terms of rail deflection and equivalent von Mises stresses from the models were displayed for all case studies. Although a strain demonstration at some key points of the model could indicate local weaknesses, this could not be validated against experimental data. The deflections, the stress contours, the stress concentration areas, assessment against yield and against endurance limit for the four types of RJs are presented. Later, a mesh sensitivity study is discussed, the effect of decreased bolt preload on the stress contours is investigated before a RJ fatigue life estimation approach is suggested.

Deflection at rail foot

The deflections were evaluated along the centre of the rail foot for the four RJ types with a stiffness of 30 MN/m/ sleeper end for the two load cases. However, load case 1 (load at 10 mm from the rail end) was the most critical case, for which results are presented here. Looking at Figure 4.27 deflections 3.8 mm to 5.4 mm were found that accord with the VG IRJ deflections measured in the field (4.2-6.6 mm) (see Section 4.2.2) and are within the limit criterion (10 mm) described in NR/SP/TRK/064 (Network Rail 2003). Glued IRJ deflects less than the other RJs as it is stiffer due to the increased glued contact interfaces. Frictional contact was applied to the fishing surface between the rail and fishplate in the mechanical RJ, whereas multiple frictional contacts were applied among the rail-insulating liners-fishplate for the rest of the RJs, probably affecting their vertical stiffness. Previous FEA studies provided deflection values of 1.7 -3.1 mm (Carolan *et al*., 2014; Himebaugh *et al*. 2008), however an absolute comparison is not possible as different assumptions and input variables exist among models.
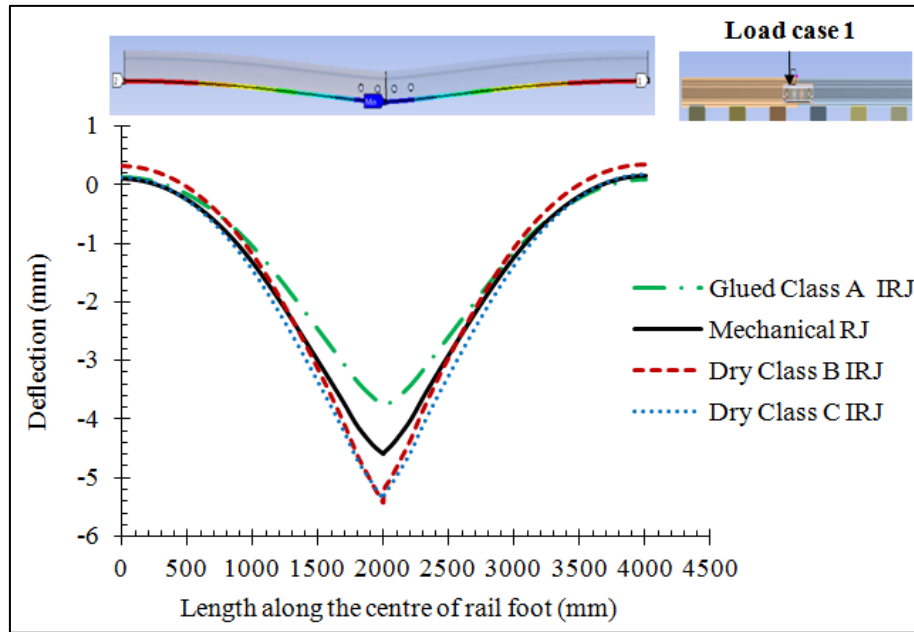
Figure 4.27 Deflection along the centre path of rail foot for four rail joint types

Von Mises stresses on top and bottom fishing surfaces

Equivalent stress allows any arbitrary three-dimensional stress rate to be represented as a single positive stress value and is related to the principal stresses by the equation (ANSYS 2016):

$$\sigma_e = \sqrt{\frac{(\sigma_1-\sigma_2)^2+(\sigma_2-\sigma_3)^2+(\sigma_3-\sigma_1)^2}{2}} \qquad \text{(eq.4.1)}$$

This stress is part of the maximum equivalent stress failure theory used to predict yielding in a ductile material such as steel. According to this theory, the maximum equivalent stress values are compared to material yield limits (σ_y=850 MPa) to generate the safety factor:

$$F_s = \frac{S_y}{\sigma_e} \qquad \text{(eq.4.2)}$$

The fishplates meet the criteria against yielding as the maximum stresses found are below the yield strength (850 MPa). The safety factor was calculated in a range of 1.92 to 2.2(>1) for the four cases. The stresses found in the web face of the fishplates are in agreement with experimental data (100 MPa, Soylemez and Ciloglu, 2016). Consistent stress plots were observed in the fishplates (up to 200 MPa) except for small stress concentration areas on the top and bottom fishing surfaces and around holes (see Figure 4.28, the stress contour of the pair of fishplates of each RJ type is provided in Paper 3). The location of maximum stress (on top and bottom fishing surfaces) was expected due to the location of the wheel load, directly above the joint (however, this singularity may be related by the mesh size, and a refined mesh could

maybe lead to a singularity in an area of smaller radius). This leads to high stresses in the rail end head/ web fillet area and to high compressive bending stress in the top fishing surface and high tensile bending stress in the bottom fishing surface (see Figure 4.29). The peak stress found in the rail end head –web fillet area (see Figure 4.30 and

Figure 4.31) is considered a singularity as it constitutes a sharp internal corner with a strong change of direction that represents stress concentration with an infinitely small radius. The peak stress singularity is greater in the Glued IRJ because it is a result of the stiffness of the entire model (bonded contacts were applied in glued IRJ whereas frictional contacts in the other three RJ types, see Paper 3). Immediately adjacent to this peak, circa 8 mm from the rail head fillet edge, the stress value is diminished to the range of 150-200 MPa. Increasing mesh refinement in that area only serves to increase the stress without limit. The singularity would be eliminated only by replacement with a larger fillet curve.
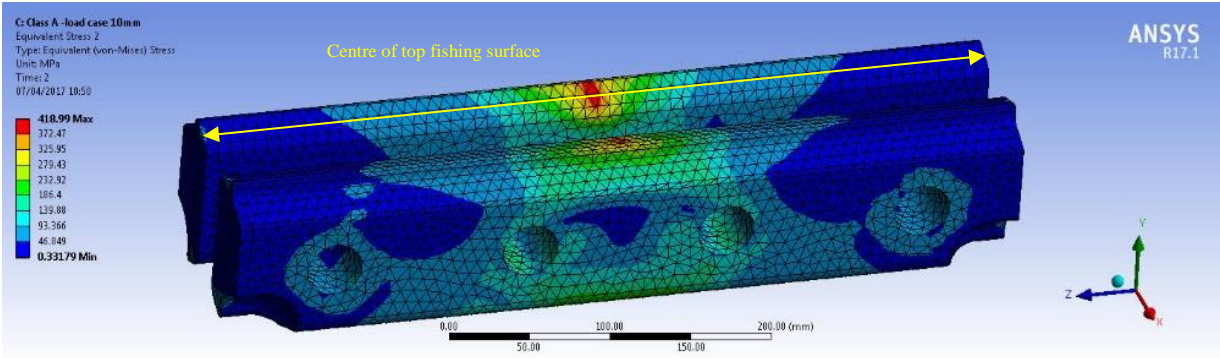
Figure 4.28 Equivalent (von Mises) stresses – Glued Class A IRJ- Load case 1
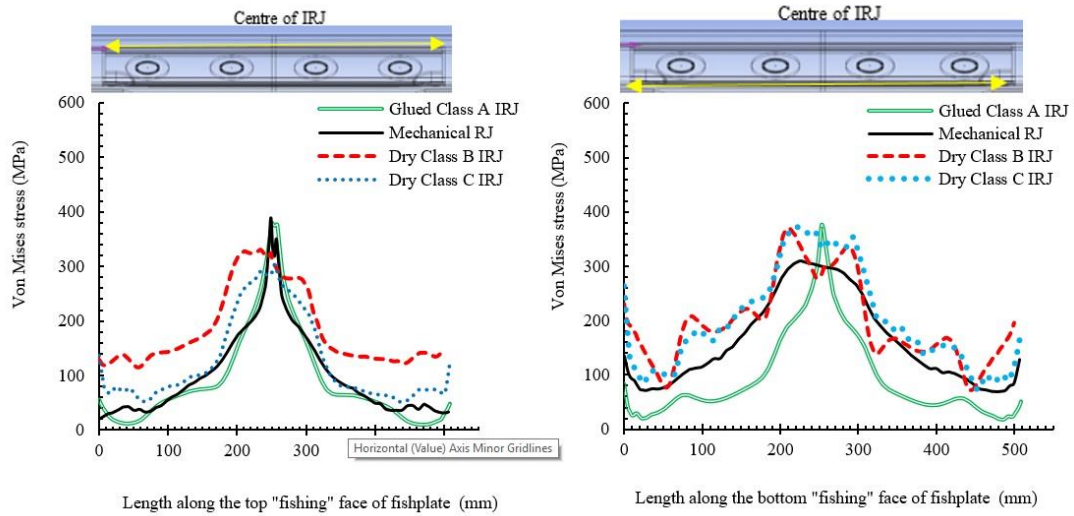
Figure 4.29 Equivalent (von Mises) stress plots of the centre of the top and bottom fishing surface of the fishplate for various RJ types.
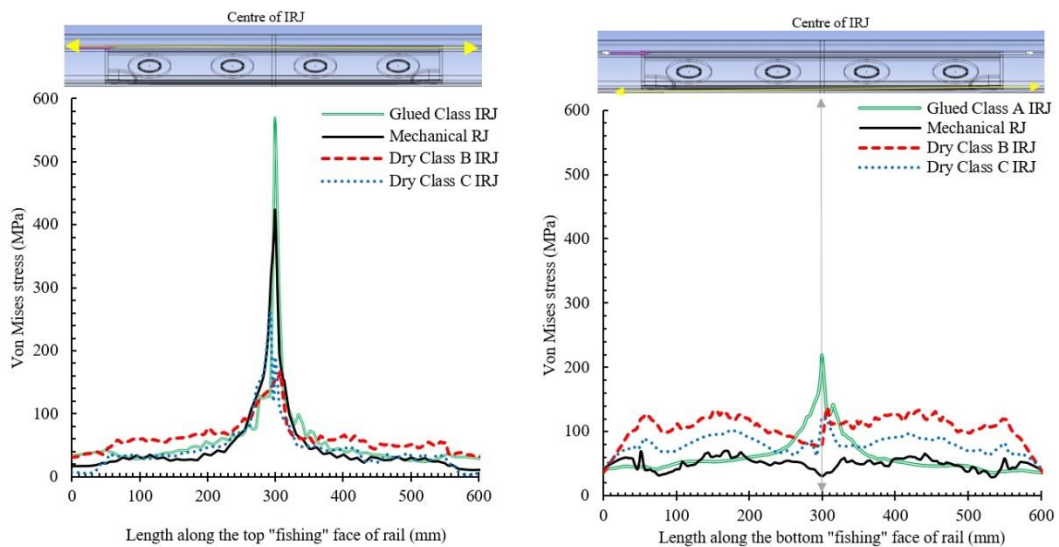
Figure 4.30 Equivalent (von Mises) stress plots of the rail head and foot fishing surfaces for various RJ types.
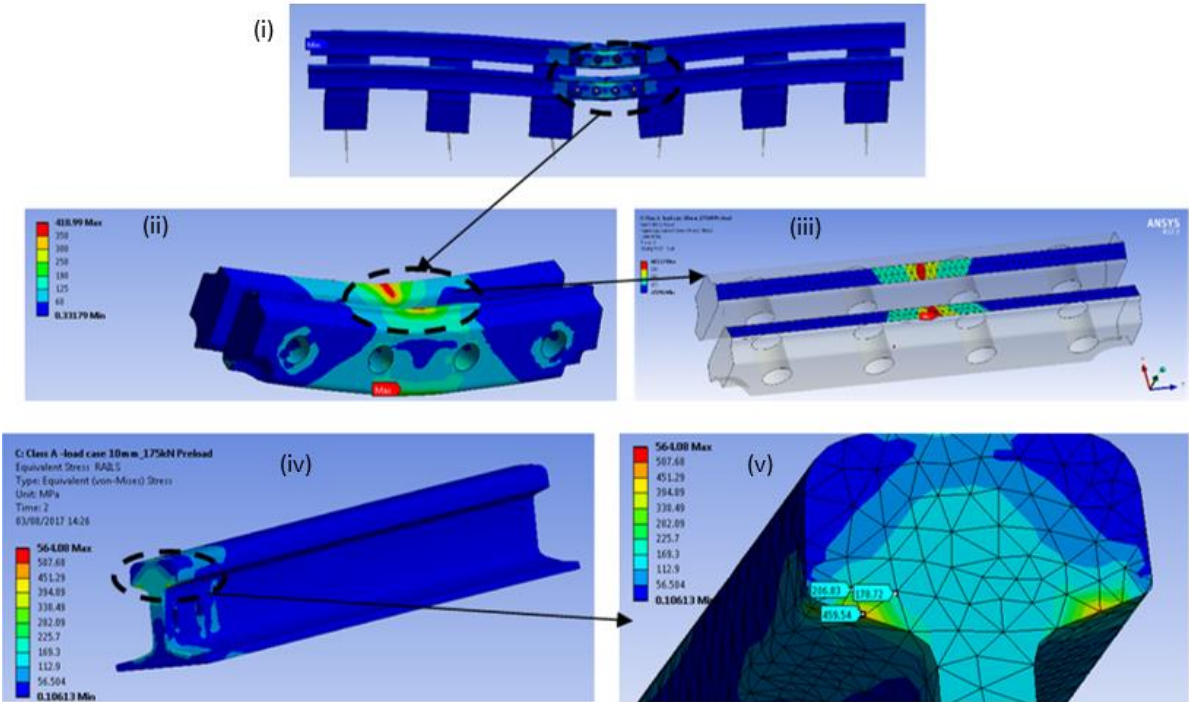
Figure 4.31 Example for glued Class A IRJ –load case 1 (i) deflection (exaggerated in scale) (ii)von-Mises stress at fishplates in average <190 MPa, (iii)von Mises stress at fishplate top fishing surfaces (iv, v) stress singularity in rail end head-web fillet area

The maximum von Mises stresses at the fishplate top and bottom fishing surfaces are presented in Figure 4.32 for four RJ configurations. The results due to the two load cases are presented in order to show the largest vertical stress fluctuation during the loading cycle provoking sagging and hogging deformation of the fishplate. The steel of fishplates was specified to be 817M40, with a minimum yield stress of 850MPa and a tensile limit in the range of 1000-1150MPa. The red dashed line shows the material endurance limit of 350MPa, which was estimated as 35% of ultimate tensile strength (1000MPa) (LB Foster, 2016). The endurance limit is a threshold below which stress amplitudes do not lead to failure while stress amplitudes above this can lead to crack initiation and crack growth to failure. It should be noted that the fishplates are subjected to multiaxial loading considering the bolt pretension and the vertical wheel load.
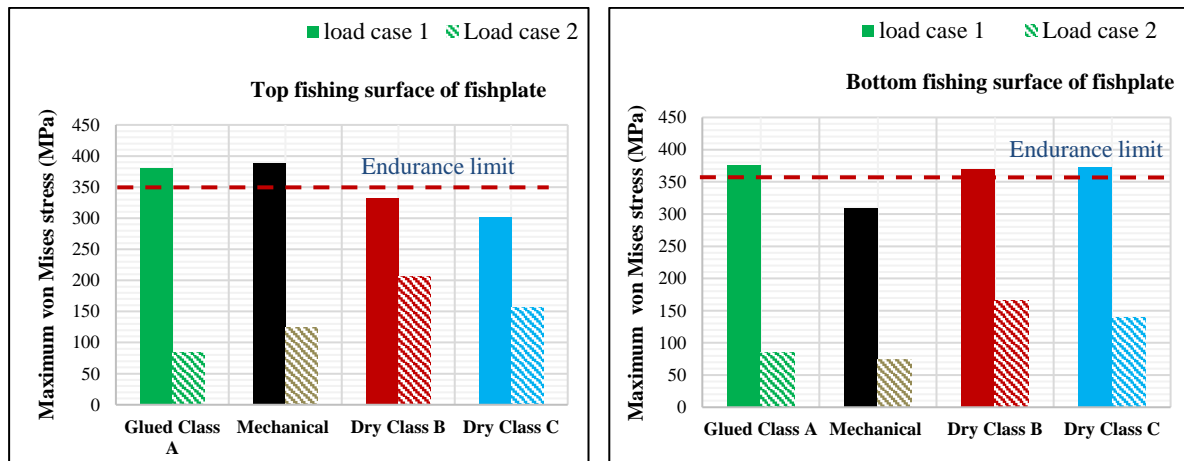
Figure 4.32 Maximum von Mises stress found in the fishing surfaces of the fishplates

Looking at Figure 4.32 it is concluded that the design of the joint significantly affects the stress concentration and consequently the fatigue failure initiation on top and bottom fishing surfaces. However, the fatigue failure of the fishplates should be investigated based on both the worst case load cases and according BS7608 (BSI 2015b) "when the resultant stress range involves stress reversals through zero, the effective stress range to be used in the fatigue assessment should be obtained by adding 60% of the range from zero stress to maximum compressive stress to that part of the range from zero stress to maximum tensile stress. A recent study (Zhu *et al.,* 2017) investigated rail joint design in terms of the contact area between the rail-end upper fillet area and the fishplate. They considered the response to vertical loading of mechanical joints for different fishplate length (6-hole and 8-hole), fishplate thickness, and rail section. The fishplates examined here have increased thickness throughout the bolt area and constitute an optimised design solution with increased fillet contact area, thus, the findings of the previous study (Zhu *et al.,* 2017) are taken into account in the optimised geometric profile of the fishplates of this thesis. A direct comparison between the two studies is not possible as in this thesis, we emphasise IRJ design as these are the most frequently used in the UK CWR (continuous welded rail) network (for signaling purposes in high traffic track); jointed track (with mechanical joints) has significantly diminished and is only used in the UK light traffic rail network.

Von Mises stresses around fishplate bolt-holes

Peak stresses were developed around holes of the fishplates in two of the four joints of load case 1 (Class B and C) and in all joints of load case 2 (see Figure 4.33). These peaks are

considered amplified due to localised discontinuities within the model. Peak stresses can occur at local discontinuities (e.g., sharp corners, notches, holes, fillets). Such points can be considered to be stress singularities (ANSYS, 2016) and can be attributed to the interaction of the linear beam elements with the fishplate body; these beams were used in place of modelling physical bolts to reduce the model size significantly. Yielding of ductile materials is important; failure occurs when yielding occurs across a complete section. In all instances, no values were recorded in excess of the material yield strength, and the peak stresses have small radii of influence, less than 4 mm.
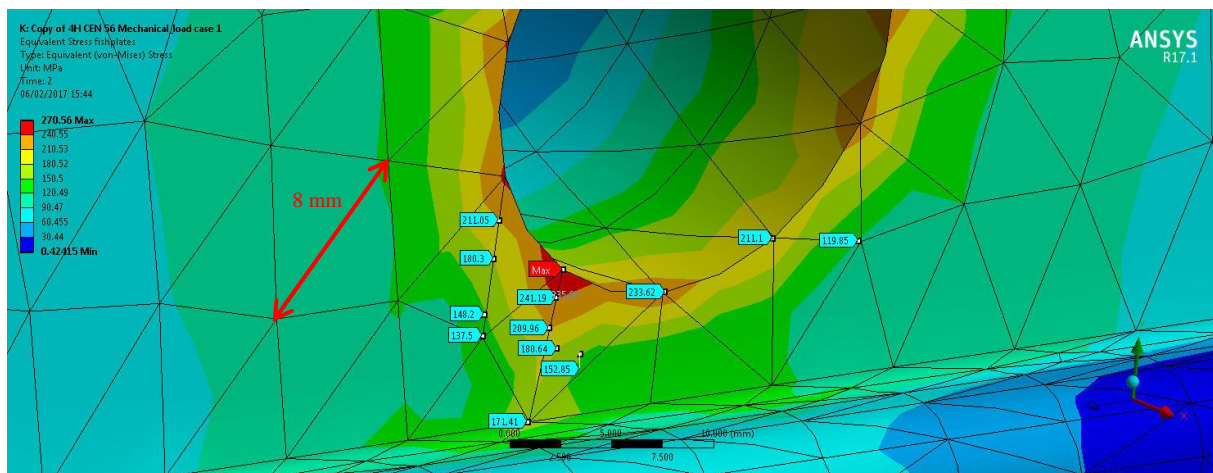
Figure 4.33 Peak von Mises stress in the fishplate hole, 270 MPa, decreased to 150 MPa in 4 mm radius - Mechanical RJ- Load case 2

A crack can typically initiate at a discontinuity in the material where the cyclic stress reach its maximum level, whereas crack growth occur along planes normal to maximum tensile stresses. Fatigue failure is due to crack formation and propagation. Bolt holes are potential areas of fatigue failure initiation; high (tensile or shear) stress around the bolt hole is caused by repeated impacts from wheel-rail loads. Neither bolt-hole nor top and bottom rail –fishplate interfaces are detectable with visual inspection in the field. Further investigation is required to determine the effect of modelling technique (beam element bolt, solid bolt, threaded bolt) on the principal tensile and shear stress distribution around the fishplate holes, on the effective cyclic stress, and on the consequent fatigue failure around bolt holes.

Mesh sensitivity study

Further refinement of the mesh size of the model was possible, however this would increase significantly the computational time. By refining the mesh size of the fishplates and of the rail

in the vicinity of the fishplates by 1mm, a 6.1% increase was found in the stress on the top fishing surface for the model of glued IRJ at the second load case whereas there was no difference in the deflection value (see Figure 4.34) and the computational time increased significantly. The computational time needed for the other three types of joints was higher than that required for the glued IRJ due to the applied frictional contacts. Thus, a 8mm minimum element size was used for all the model configurations (10-node tetrahedral quadratic elements SOLID185, see Paper 3).
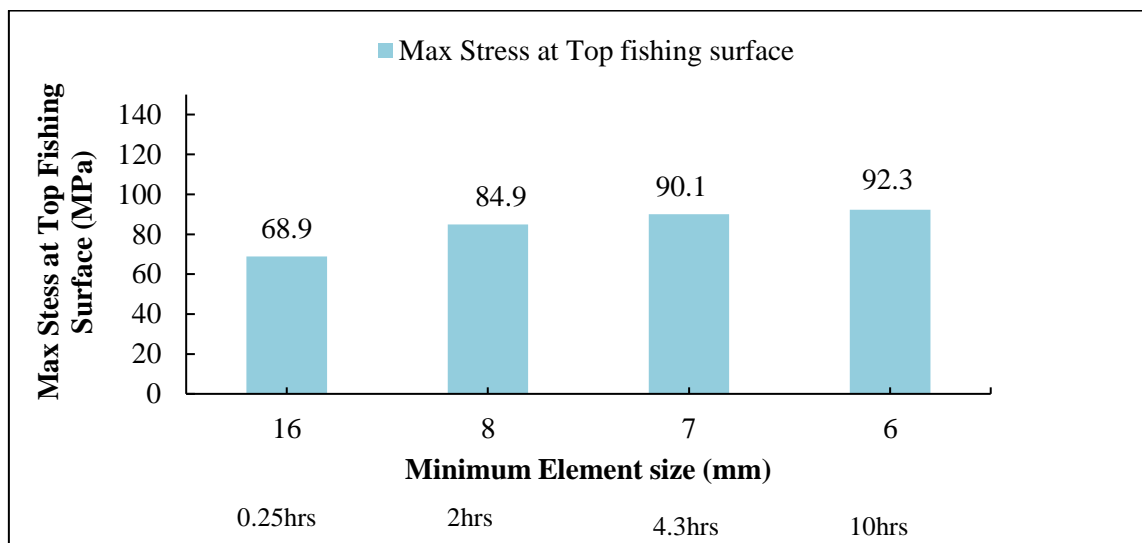
Figure 4.34 Mesh sensitivity study for Glued IRJ, Load case 2

Effect of bolt preload on stresses in fishplates

Pre-load values in previous FEA configurations assumed recommended tightening torques were to be applied. However, lower pre-load values may provide acceptable clamping force (British Steel, 2016). For this reason, a reduced bolt pre-load study was carried out to observe the effect on resulting stresses in the fishplate. Looking at Table 4.7 and Figures 4.35 - 4.38, it was observed that, when the wheel load was not above the joint (hogging deformation, load case 2), a 43% preload decrease, lead to a 37% decrease of the von Mises stresses developed in the fishplate. However, when the wheel was above the joint (sagging deformation, load case 1) the effect of vertical load was dominant in the relative magnitude of von Mises stresses that were developed.

Table 4.7 FEA results of bolt preload parametric analysis

Joint type	ID	Bolt preload	Load case	Maximum Equivalent (von Mises) stress	Safety factor	Location of σ_{emax}	Maximum Principal stress	Fatigue Factor	Location of σ_{1max}
		kN		$\sigma_{e\,max}$ (MPa)	S_y/σ_{emax}		σ_{1max} (MPa)	S_e/σ_{1max}	
Mechanical	1A	100	1	411	2	Top fishing surface	340	1.03	Bottom fishing surface
	1B	175	1	431	1.97	Top fishing surface	339	1.03	Bottom fishing surface
	1C	175	2	305	2.79	Hole	175	2.00	Hole
	1D	100	2	191	4.45	Hole	105	3.34	Hole
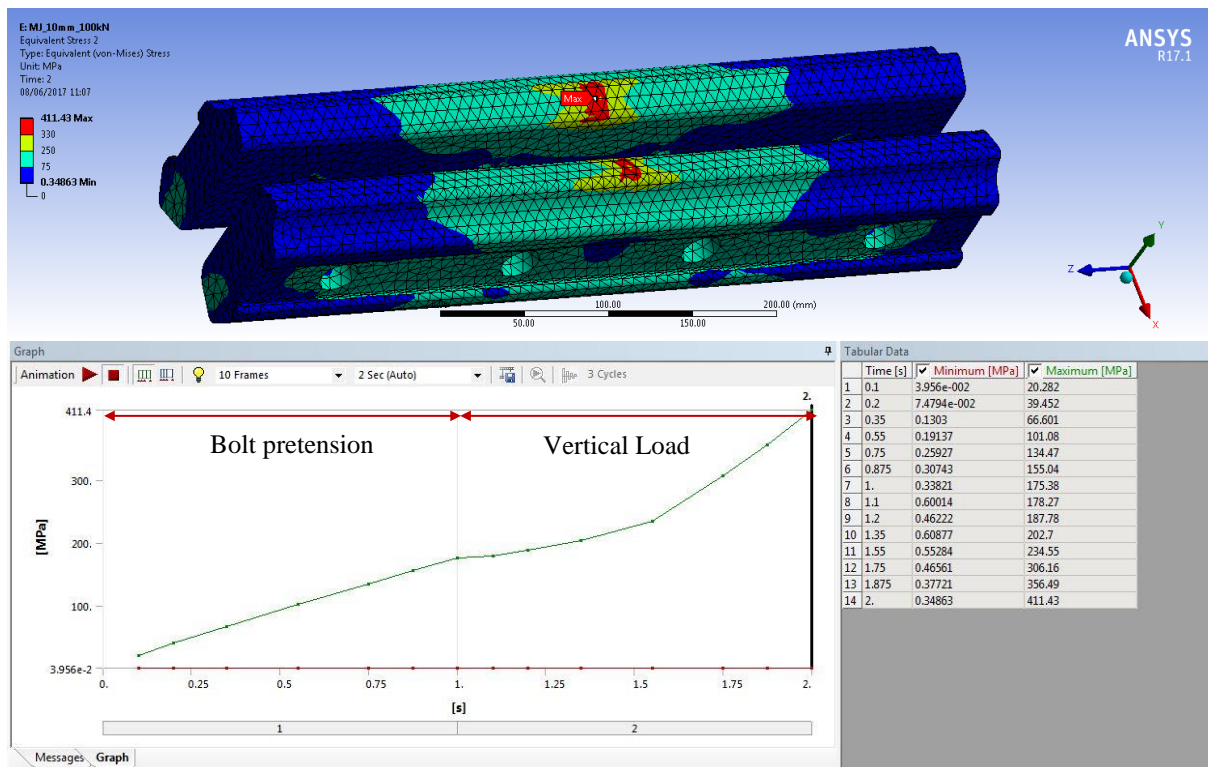
Figure 4.35 Equivalent (Von Mises) stresses σ_e - Mechanical RJ - 100kN preload - Load case 1 (i) stress contour (ii) magnitude during loading steps
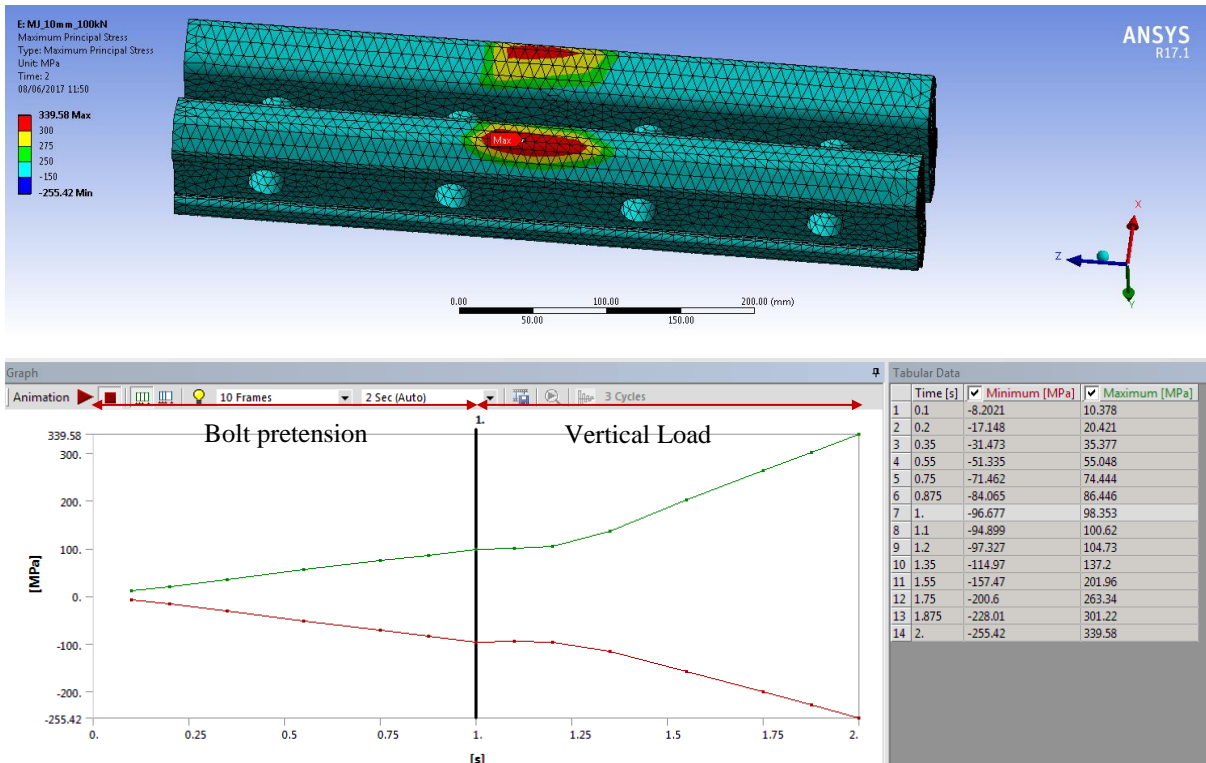
Figure 4.36 Maximum principal stresses σ_1 - Mechanical - 100kN preload - Load case 1 – (i) stress contour (Bottom fishing surface view), (ii) magnitude during loading steps
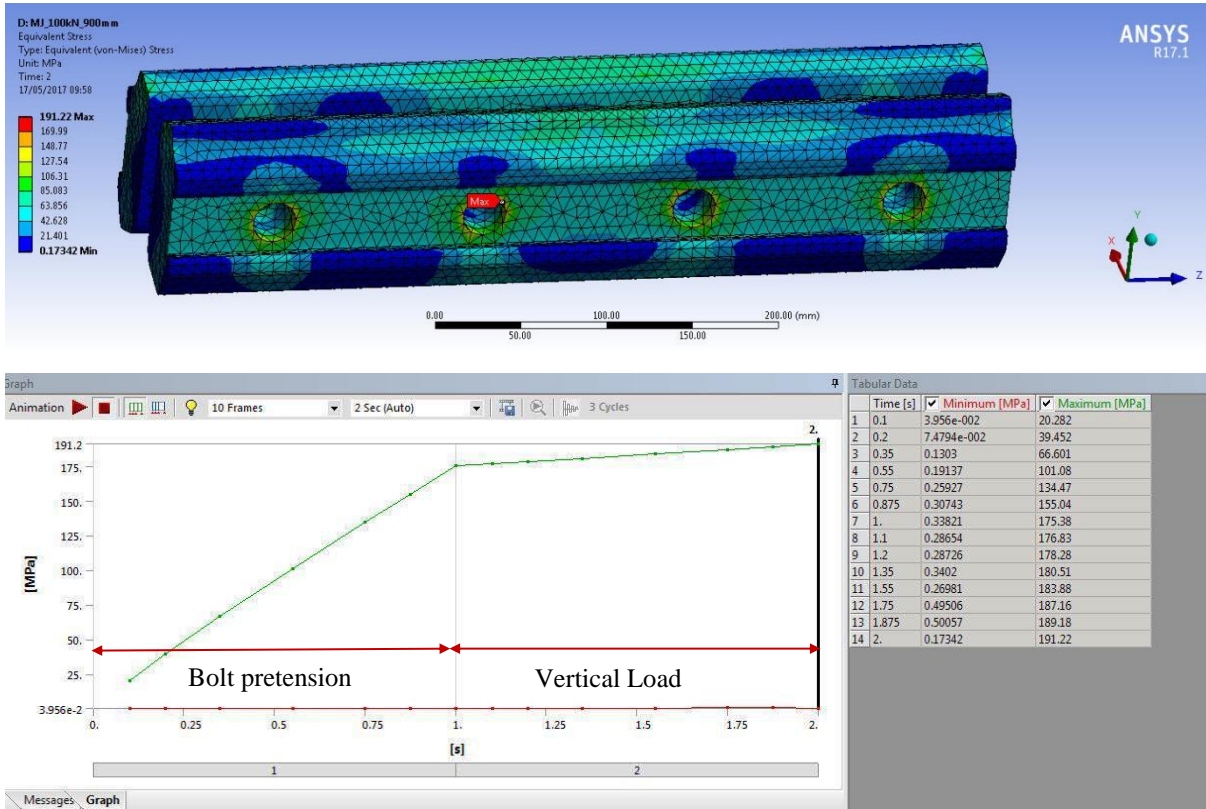
Figure 4.37 Equivalent (Von Mises) stresses-Mecanical-4H-100kN preload-Load case 2

In load case 1 (1A) $\sigma_{emax} = 411MPa$ appears on the top fishing surface (see Figure 4.35). However, stress is below 250MPa in the rest of the fishplate area. By looking at the principal stresses, a compressive $\sigma_{1min} = -255MPa$ was found on the top fishing surface and a tensile $\sigma_{1max} = 340MPa$ was found on the bottom fishing surface (see Figure 4.36), with $\sigma_1 < 300MPa$ in the rest of the fishplate. By assessing the whole fishplate area, load case 1 (sagging deformation) gave three different ranges of von Mises stress $\sigma_{e\ load\ case\ 1}$: 330-411MPa, 250-330MPa, <250MPa. Whereas load case 2 (hogging deformation) gave $\sigma_{e\ load\ case\ 2}$: 191MPa (node), 120MPa (around holes), and <60MPa. In terms of max principal stresses three relative areas can be identified $\sigma_{1\ load\ case\ 1}$: 300-340MPa, 250-300MPa, <250MPa whereas $\sigma_{1\ load\ case\ 2}$: $-100 < \sigma_1 < 104MPa$.

By comparing the results of the previous configurations $\sigma_{1max\ Load\ case\ 1}$ is 3.2 times larger than $\sigma_{1max\ Load\ case\ 2}$. In terms of σ_{emax} the difference reduces to 2.15. By looking at the average stress developed in the whole fishplate body without the individual nodal peaks a max of $\sigma_{e\ Load\ case\ 2} = $ 60-120MPa can be found against $\sigma_{e\ Load\ case\ 1} = 250MPa$. The sagging deformation of the fishplates is more severe in terms of stress singularities found, thus more critical for the fatigue failure. This is expected due to the wheel above the discontinuity where the moment of inertia is decreased ($I=I_{2x\ fishplate} \neq I_{eff\ CEN56\ IRJ} < I_{CEN65}$) as described in Section 4.2.1. The increased peak stress values are correlated to the increased load case used (200kN) that exceeds any other load case found in the literature for FEA of rail joints.

As mentioned above, the fishplates meet the criteria against yielding as the stress values found are below the yield limit S_y (850 MPa) and the calculated safety factors were calculated $S_y/\sigma_{emax} > 1$ for all cases. However, the calculated fatigue factor $S_e/\sigma_{1max} = 1.03 \sim 1$ (Table 4.7) and the comparison of von Mises stresses with the endurance limit (350 MPa, LB Foster, 2016) (see aforementioned discussion of

Figure 4.31) indicates that the top and bottom fishing surfaces of the fishplates may be considered as prone to fatigue failure initiation during the IRJ life that can lead to fishplate crack initiation and ultimately fishplate break. These locations are not detectable with visual inspection and should be considered as critical for fishplate design. The stress singularities found in the rail end upper fillet area coupled with the effects of wheel impacts and dipped joint can also be a precursor of crack initiation towards either the rail head or the rail hole (see Figure

4.38). These conclusions are in agreement with recent rail break findings (RAIB, 2014). However, fatigue failure incudes both load cases and the stress range should be calculated according to an appropriate fatigue failure method, as described below.
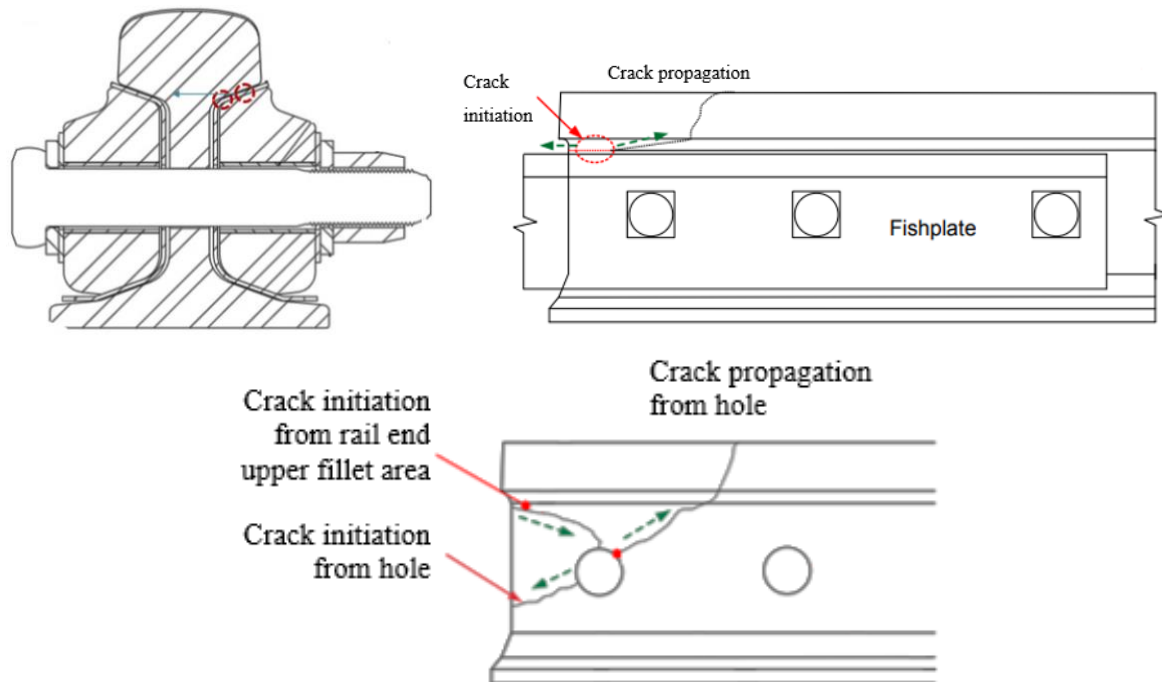
Figure 4.38 Potential fatigue failure modes amended from RAIB (2014)

Fishplate fatigue life estimation

In this section recommendations for the fatigue life estimation of the fishplates is presented. The fatigue assessment procedure involves the determination of the spectrum of the number of cycles of each of the individual stress/strain ranges expected in the life of the rail joint fishplates. The strain life approach addresses Low Cycle Fatigue (LCF) whereas stress life deals with materials which undertake High Cycle Fatigue (HCF), more than 10^5 cycles. Stress life calculates total life without distinguishing between crack initiation or propagation. A stress life can be therefore used to estimate the expected number of loading cycles that a RJ can withstand assuming a maximum stress component which is found from the critical forces on the RJ. The fatigue life can be estimated for the two aforementioned critical cases representing typical operational conditions: (1) the wheel load directly above the joint and (2) two wheel load forces in a span equivalent to a typical UK locomotive wheel base of (minimum wheel base 1.8 m

according to GM/GN2589 (RSSB 2004) and GE/RT8073 (RSSB 2009)), one on each side of the RJ. The stress life approach requires the calculation of alternating and mean stress. When experimental data (material curves) is not available a correction of the mean stress is accounted through empirical criteria that combine the alternating and mean stress with the material properties (yield stress, tensile strength, endurance limit). Budynas and Nisbett (2011) mention different criteria such as modified Goodman, Gerber, and Soderberg for metal failure life estimation due to fluctuating stresses. A detailed analysis of them is presented in Budynas and Nsbett (2011) whereas an example of the application of Gerber criterion is presented in Appendix E. Browell and Hancq (2006), while describing an ANSYS fatigue module, mentioned that most experimental data fall between the Goodman and Gerber theories with the Soderberg usually being overly conservative. They reported that the Gerber theory is usually a good choice for ductile materials; the Gerber theory treats negative and positive mean stresses the same, whereas Goodman and Soderberg are not bounded when using negative mean stresses like the herein case. Goodman and Soderberg are conservation approaches, because although a compressive mean stress can retard fatigue crack growth, ignoring a negative mean is usually more conservative (Browell and Hancq-Ansys, 2006). On the other hand, BS 7608 (BSI 2015b) is also applicable for the fatigue assessment of the fishplates as it covers steel material products with yield strengths in the range 200-960MPa and ultimate tensile strengths in the range 360 to 1200MPa. In both cases the determination of resultant stress range is required after taking into account all stress reversals during the life of a rail joint. According to BS 7608 (BSI 2015b), the directions of principal stresses shall be used to determine which principal stress range is relevant. Then, the number of cycles (N) can be calculated through a theoretical formula.

The fatigue life (in cycles) can be calculated in terms of million gross tons (MGT) of traffic through the equation:

$$MGT = \frac{N\ (in\ cycles)*Q(in\ kN)*2}{9.81\ x\ 10^6} \qquad \text{eq.4.7}$$

Where N is the calculated number of cycles and Q is the wheel load. The fatigue life of rail joints due to fishplate fatigue failure is estimated for various track categories according to equivalent million gross tons per annum (EMGTPA) that constitutes a measure of annual tonnage carried by a section of track. An example of the fatigue life estimation of the fishplates for the four RJ types is presented in Appendix E using signed equivalent stress criterion, which is not a normal technique (different of the BS 7608).

Nevertheless, a comparison of the fatigue life estimation of the RJ fishplates between the different stress life theories and comparison among different decision approaches is recommended for future research.

Validation of optimised numerical model

To validate the performance of the numerical model, two different laboratory tests were modelled using the FE software. Their calculated deflections were compared to measured deflections assessed in laboratory experiments. The maximum magnitudes of deflections of each load case were compared for each laboratory case study. These case studies included: the 4-point bend laboratory configuration described in Section 4.2.1 and a 3-point bend laboratory configuration of a 6-bolt glued IRJ as described below. The validity of the numerical model to assess maximum deflection of IRJs is described below and is detailed in Paper 3 (Appendix C).

Validation Case study 1: Laboratory model 1

The deflections of a 4-bolt glued Class A CEN 60 (3 m length) was measured by using the VG in a 4-point bend test under static and cyclic loading. The laboratory configuration is described in Section 4.2.1. A linear static FE model to simulate the above 4-point bend test was performed including the set-up settings (materials, bolt preload, mesh, type of contacts) described in Section 4.3.2 (and Paper 3) with support conditions representing the laboratory test (see Figure 4.39). The maximum deflection in the railhead position (same position as the VG measurements) was found to be 2.58 mm to 6.23 mm for the various load cases, 160 kN to 404 kN. Quite a good correlation was found between the deflections measured by the camera and that found from the FE model (see Figure 4.40). A difference of 2-11% for the various load cases was found.
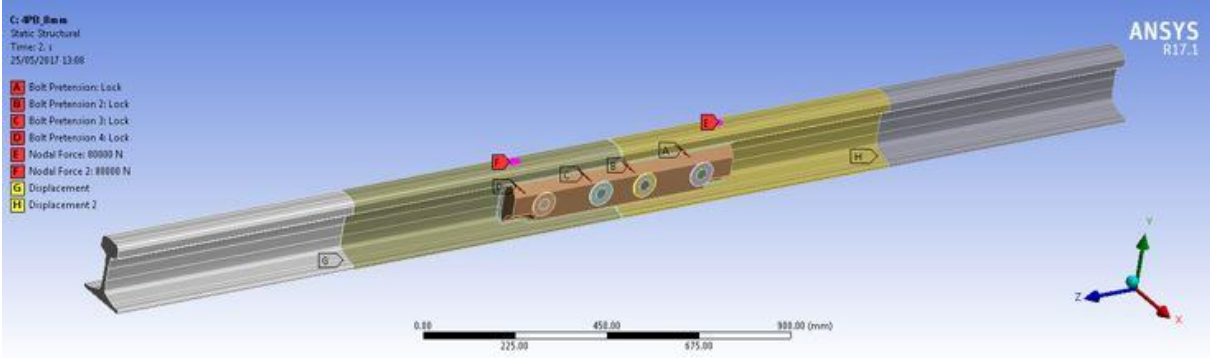
Figure 4.39 FE model of 4-point bend laboratory configuration
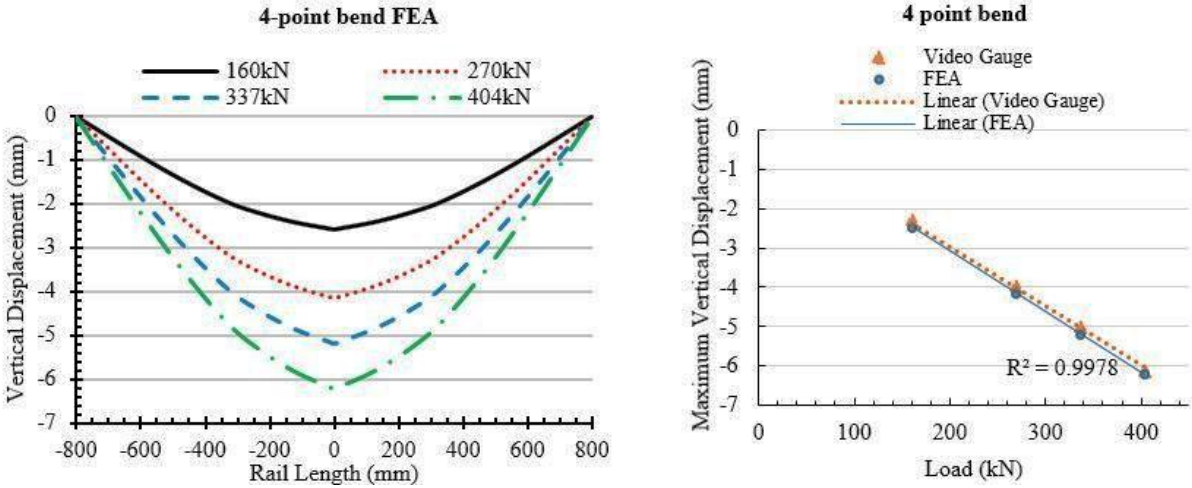
Figure 4.40 Comparison between FEA calculated and VG measured deflection results for the 4-point bend test

Validation Case study 2: Laboratory model 2

The deflections of a 6-bolt glued Class A IRJ of 1.3 m length were measured by dial gauges (placed on top of the railhead in nine positions) under static 3-point bend loading. The load was applied 13 mm away from the centre of the joint in steps from 20 kN to 200 kN. A static FE model was created to simulate the above experiment (see Figure 4.41) with the same settings (mesh, contacts, bolt preload and vertical load) as described in Section 4.3.2 (and Paper 3). Very good correlation was found between experimental and FEA deflections. A comparison is presented in Figure 4.42 for the deflections of the central path along the top surface of railhead. A difference of 2-10% for the various load cases was found showing that the model represents quite accurately the deflection histories of the rail joint.
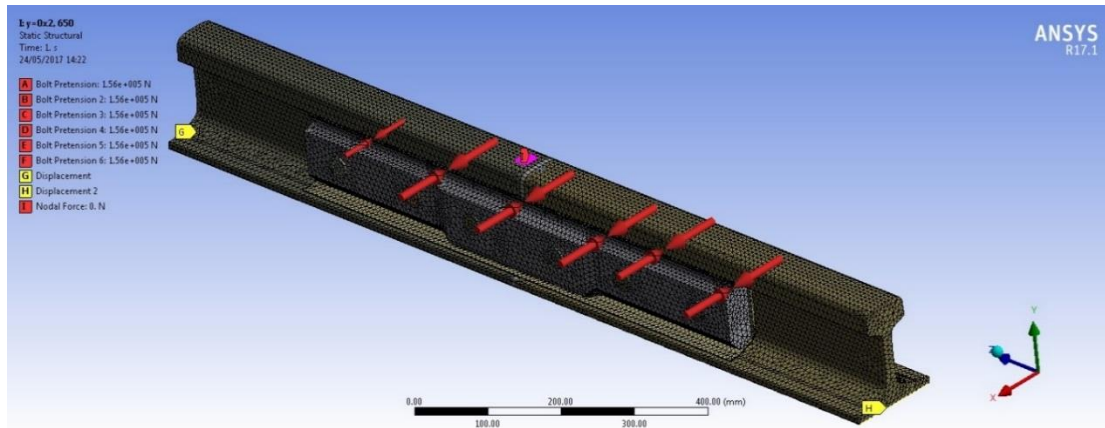
Figure 4.41 FE model (showing mesh, loading and boundary conditions) of the 3-point bend laboratory configuration
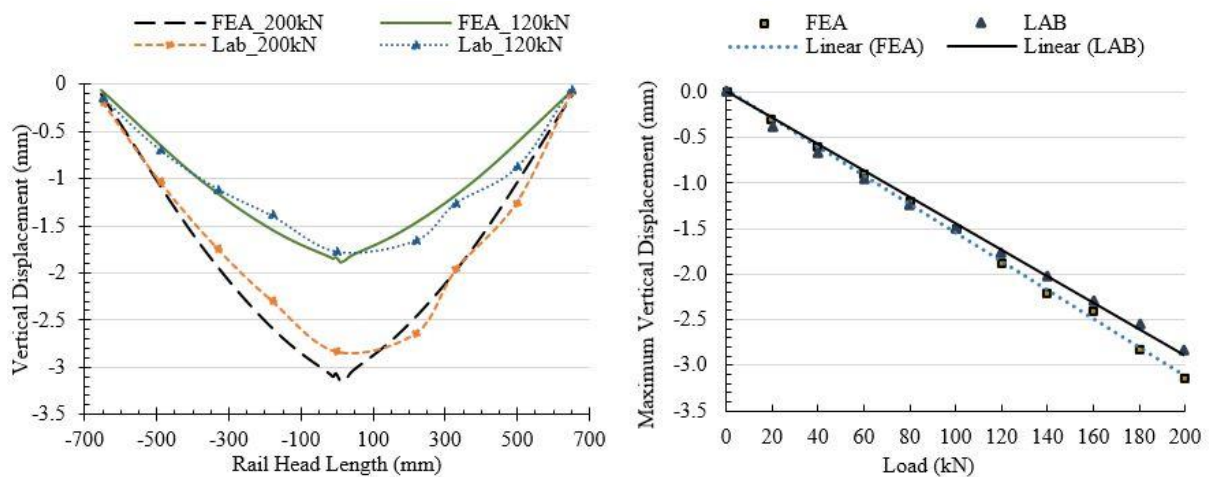
Figure 4.42 Comparison between FEA calculated and measured by dial gauges deflection results of the 3-point bend test

Concluding remarks

This model investigated the deflection and stress distribution for four different types of RJs commonly used in the UK railway network (three insulated and one mechanical). Stress concentrations were found at the rail-fishplate fishing interfaces, areas that are difficult to be observed in the field. Class B and class C fishplates developed peak stresses of lower magnitude than did the mechanical and glued RJs; this was a result of the encapsulation insulating material, and due to the different type of contact that exists in the interface between rail and fishplate. The glued joint developed higher peak stress values due to the increased contact areas between the components of the assembly (higher stiffness), but experienced the least deflection.

The results indicated that the fishplates are experiencing two-axis bending during the vertical wheel load due to the curved contact area between the rail and the fishplate. This causes pressure imparted by the underside of the railhead to the fishplate to have vertical and lateral components. This curved fishing interface induces bending in the fishplates about both their major and minor principal axes. The bolt pretension accounts for a significant percentage of the stresses developed in the fishplate web. The type of FE analysis used here is advantageous over an analytical approach (BOEF for the calculation of bending moment and calculation of normal stress for beams in bending) as it takes into account the multi-axial stress components. Also, it is advantageous over previous studies as it takes into account the effect of sleeper support conditions, the bolt preload and the detailed contacts between the rail-fishplate-bolts-insulation components. The stress evaluation found by this study is used for assessment against fatigue through the endurance limit approach.

4.4 SUMMARY

This chapter has provided a comprehensive examination of the research undertaken to achieve the overall research aim and objectives, as outlined in the map of the research development process. It has explained how the various experimental and numerical modelling primary data have been used to enable the assessment of track deflection, of track stiffness and a deeper understanding of the RJ performance.

The majority of the research undertaken is documented in Papers 1 to 4 (Appendix A to D). Therefore, for a more detailed review of the work, it is recommended that the relevant EngD papers are consulted.

5 FINDINGS & IMPLICATIONS

This chapter summarises and concludes on the findings of the research based on the methodology developed and in the context of field track deflection and rail joint performance procedures assessed (Section 5.1). It then, as is required by the EngD, reviews and explains the implications of the work on both the sponsoring company and the wider industry (Section 5.2). It finishes by presenting a brief critical review of the work undertaken (Section 5.3) and identifies further research required to further develop and refine the work (Section 5.4).

5.1 THE KEY FINDINGS OF THE RESEARCH

The research was broken down into four main objectives that covered a number of research areas and tasks. Each of the objectives provided some key findings that helped to fulfil the aims and needs of the research.

5.1.1 LITERATURE REVIEW

Having specified the general aim, a more thorough investigation of previous work studies was conducted with attention to rail and rail joint deflection assessment, the existing literature was critically evaluated, within the aim to identify gaps and to build on these.

The literature review compared existing measurement techniques of track deflection assessment, modelling techniques for the deflection assessment of rail joints and highlighted deficiencies in current understanding (Objective 1). This revealed deficiencies in previous techniques of direct measurement of the track deflection as a whole system. It was concluded that although there are different procedures for assessing the vertical track stiffness, which to use depends upon the excitation frequency, the spatial resolution, the frame rate (in case of PIV and DIC video techniques) and the model used to codify stiffness. Designers need to consider a range of different analytical or empirical numerical models.

Literature revealed the potential advantages of the VG technique as an efficient way to assess track deflection, such as time saving, reduction of track possession, achieving high accuracy, high resolution, and high sampling frequency (Paper 1 and 4). This enabled the formulation of new assessment procedure (VG) that meets the current needs of industry in an effective way (Objective 2 and 4).

There is very limited field experimental work of RJ deflection and RJ vertical stiffness assessment, with the RJ being a weak component of the railway system. In particular, the magnitude of deflection and the bending behaviour of a RJ under real field conditions is not clearly defined. Current standards define limits of RJ fatigue only through fatigue static and cyclic laboratory tests which neglect the effect of the underlying trackbed deterioration on the deterioration rate of IRJs. This led to research to improve understanding of these parameters in order to facilitate further optimisations in design (Objective 3).

The review came across numerous rail joint performance models proposed by many researchers (Paper 3). It was found that optimisation of IRJs performance had been only investigated either by material optimisation (endpost, insulation, rail steel hardening) or by fishplate geometrical optimisation. The majority of previous research studies have focused on assessing the localised fatigue in the rail discontinuity by looking in micro scale at the rail joint as a component, whereas the rail joint deterioration is progressively increasing because of the increased damage of the underlying structure. The literature review revealed the hypothesis that the deflection level of a RJ can be reduced by structural strengthening of the track structure in its vicinity (Objective 3).

5.1.2 Track deflection assessment using the Video Gauge

In developing Objective 2 of the research, deflection data was collected using the VG methodology through three main techniques: laboratory measurements, field measurements of plain rail and rail joint (conventional ballasted track) and field measurements of ballastless trackforms and transition zones.

Laboratory measurements

Four-point bending tests were conducted to investigate the deflection increment in a glued IRJ (Section 4.2.1) in comparison with a plain rail. In contrast with previous laboratory tests, plain rail and IRJ deflection was measured by the VG while a comparison was made with LVDT. The IRJ deflection range was found to be from 2.76 mm to 7.12 mm for a load range of 160 kN to 404 kN. The IRJ was found to deflect 61% more than the plain rail while a back calculation of the effective moment of inertia of the IRJ showed that the IRJ was 37% less stiff than the plain rail. This methodology validated the VG method as an effective technique for assessing

the IRJ deflection under cyclic loading. Furthermore, the collection of detailed IRJ deflection data were used in the validation of the numerical modelling (Section 4.3.2).

Applicability of the VG to assess track deflection and track stiffness parameters (Obj. 2)

Although rail and IRJ deflection data was obtained from the laboratory tests, these were of limited use as they were not fully representative of the operational conditions. This research project proposed an optimised and adapted experimental methodology using the VG (see Appendix F) to accurately assess real-time track deflection data under high speed traffic loading. This project was the first recorded use of the VG in the rail industry. In addition, this study provides for first time direct deflections of IRJ in high speed real-time operational conditions.

Throughout the project four different sites were monitored (Section 4.2), further meeting Objective 2 to obtain primary deflection data from a range of trackforms and under various operational conditions, including ballasted track under low speed (Site A), ballasted track including IRJs under high speed (Site B), ballastless track (IVES and PORR) and renewed ballasted track under controlled low speed (Site C) and transition zone between ballasted and slab track on the approach of a bridge under high speed (Site D). The procedural development of the VG methodology in the above case studies as well as their detailed findings were presented in the international Stephenson Conference IMechE (Paper 1) and was published in a leading journal ICE Transport (Paper 4).

The key finding for the research is that the VG is capable of providing accurate direct deflection assessment of ballasted and ballastless track remotely. The deflections measured can be used directly for the evaluation of the performance of a trackform when a rail deflection envelope is available or for the evaluation of the global track stiffness under a known wheel load. Furthermore, it can be used for the evaluation of track support stiffness parameters when coupled with an appropriate track model.

Deflection variations due to different train vehicles, bogie spacings and wheel spacings can be measured through the VG for various train speeds (up to 125mph) and in high sampling frequency (200 Hz). The deflection of various track components (rail, sleeper, slab, rail joints) over a long track distance (depending on the camera and working distance, here over a length of 6.5 m) can be measured simultaneously and remotely, without the need for fixing

complicated instrumentation to the track. Thus, the VG enables the performance assessment of critical railway track zones that need to be investigated promptly, during their service life and between maintenance periods, saving time and reducing the time of possession.

The actual rail deflections can be used directly for global stiffness derivation under a known wheel load. Furthermore, a back-calculation method was proposed that enables the track system support stiffness and moduli for various positions to be determined from the deflection data by using the static wheel load data, calculated from the published gross weight of the train vehicles and an analytical model for the track behaviour such as the beam on elastic foundation. Thus, the VG can be used for the assessment of track stiffness variation of critical zones such as track irregularities and transition zones.

The deflection bowl for a long piece of track can be derived directly through the deflection measurements for each sleeper position in the absence of the wheel load data, indicating the load transfer along the measured track length. This allows the assessment of the dynamic response of the track as a holistic system, providing useful information for both the superstructure and substructure's bearing capacity through the analysis of multiple rail and sleeper deflections.

Significant consideration is given to the level of accuracy, resolution, and repeatability of the VG results. The accuracy of the VG is acquired through the calibration of the system by using a known distance within the recorded image while the target brightness controls the effectiveness of the system. Any moving shadows, motion blur, highlights, or overexposed pixels will interfere with tracking a target. Brightness can be controlled through the camera's sensor shutter speed, aperture, together with the level of lighting. The latter depends on constant or not weather conditions, alteration between sunny and cloudy weather during the measurements that may cause shadows of the passing train vehicles/wheels on the rail). The The repeatability of the deflection data was shown though the repeatability of the deflection magnitude for each of the trackforms measured, while the repeatability of the stiffness values relies on the assessment of the deflection of a point under a couple of passages of similar trains. It was found that predictions based on the average of deflections measured for a wide range of similar trains converges to an appropriate result.

The anticipated resolution of each test depends on the combination of the focal length of the camera used and the distance to the object, and is given as $1/100^{th}$ pixel to be 0.01-0.04mm for certain distance and focal length. However, variations of the measurement resolution within

each image are principally down to the quality of the target that the software sees. The resolution obtained has been calculated for each deflection time history as the standard deviation of the deflection points when there is no load being applied. This was calculated for each measured point for each test and was found to be less than 0.05mm, as expected.

5.1.3 POTENTIAL FOR EXTERNAL REINFORCEMENT OF IRJs TO REDUCE DEFLECTION AND IMPACT ON BALLAST (OBJ.3 & 4)

The deflection data obtained from the laboratory and field measurements (Section 4.2.1 and 4.2.2) were used to validate a numerical 3D FE model capable of simulating plain ballasted track and IRJ responses under vertical load (Objective 3). The model was used to investigate if external structural strengthening can reduce the deflection, and hence the deterioration level of an IRJ (Objective 4). Four model configurations were selected, representing the plain ballasted track, a suspended glued insulated rail joint (IRJ) and two methods of externally reinforced IRJ, with strap rails and I-beams (Section 4.3.1). Reinforcement techniques were shown to influence deformation of IRJs, producing IRJs with remarkably different deflections and dip angles tested in a wide range of sleeper support conditions (Figure 4.23). The externally reinforced IRJ was for first time, proposed in the rail industry while the above modelling procedure and parametric analysis was published in the IMechE Part F Journal of Rail and Rapid Transit (Paper 2).

More specifically, the following conclusions were derived:

- An IRJ deflects more than plain rail. The deflection of an IRJ is influenced measurably by the support conditions, in addition to the impact force. The decrease of deflection does not have a linear correlation with the stiffness increase. A sleeper support stiffness decrease from 30 to 5 kN/mm can triple the deflection of an IRJ.

- For support conditions 5-30 kN/mm/ per sleeper end, that match the trackbed stiffness observed in the field through the findings of the VG methodology (Section 4.2), the use of external reinforcement using strap rails reduces the deflection of an IRJ up to 13%. Strap rails are recommended as a cost-effective reinforcement method for maintaining the IRJ deflection over time and thus reducing its impact on ballast.

- Use of I-beam steel sections 39% stiffer than strap rails reduces the deflection of an IRJ by up to 15%. I-beam structural track reinforcement can lower the deflection of IRJ to a level similar to that of plain rails.

- The effect of external reinforcement on the reduction of deflection and dip angle of an IRJ becomes more significant for soft support conditions.

- Structural strengthening reduces the total dip angle of an IRJ for all support conditions by a significant level.

- The total dip angle does not have a linear correlation with stiffness increase.

This analysis suggests IRJ deflection is sensitive to sleeper support stiffness. Although a perfect new glued IRJ was considered, this highlights the need to ensure that the deterioration rate of an IRJ, and consequently the impact on ballast, will be diminished if the global track stiffness is increased in the vicinity of the IRJ. In this case, the use of strap rails is suggested as a simple and cost-effective way to increase the life expectancy of an IRJ.

5.1.4 THE RESPONSE TO BENDING OF MECHANICAL AND INSULATED RAIL JOINTS (OBJ. 3 & 4)

The numerical model was adapted and optimised to investigate deflection and stress distribution for four new rail joint designs (insulated glued, dry, dry encapsulated and one mechanical) as designed by LB Foster for the standard requirements of Network Rail (Network Rail, 1996; Network Rail, 2003; BSI, 2015a and RSSB, 2011), to explore their behaviour under fatigue static vertical load (Objective 3). The 3D FE analyses considered frictional contacts in the interfaces of the rail joint assemblies and typical linear elastic sleeper support conditions (30 kN/mm). An increased load case of 200 kN, based on real operational data, which has not been covered in past literature was investigated, while the bolt preload was also considered in the models.

The fatigue strength of fishplates can be assessed through the evaluation of stresses for the critical load cases. Stress concentrations, stress multi-axiality and loading variability are some of the factors affecting significantly the fatigue integrity of structural components consistent with railway applications. The FE analyses of this study, validated by laboratory measurements, were used as a parametric tool for design validation and optimization of IRJs in UK industrial practise (Objective 4). Section 4.3.2 reported the sensitivity of deflection and stress distribution of the rail and fishplates according to the various rail joint designs and their loading. The modelling technique was validated against laboratory and field measurements. The modelling procedure, analysis and validation were published in the IMechE Part F Journal of Rail and Rapid Transit (Paper 3). The results revealed the following conclusions:

- The fully glued IRJ type decreased the overall joint deflection by 22% in comparison with the mechanical RJ and by 42% in comparison with the dry joints as a result of increased contact in the interfaces of the joint assembly.

- The top and bottom fishing surfaces of the fishplates, that are in contact with the head and foot curved rail area, experience larger stress concentration as a result of the load distribution due to wheel load above the joint inducing compressive pressure on the top fishing surface and tensile pressure on the bottom fishing surface. These areas are difficult to observe in the field.

- The fishplate designs developed stresses below the yield limit. The 200 kN wheel load did not cause material plasticity in the rail—fishplate interface.

- The fishplates of dry joints developed peak stresses of lower magnitude than those of the glued IRJ due to the different type of contact that exists in the interface between the rail and the fishplate. The glued IRJ has increased bonded contact between the components of the IRJ assembly, thus has higher stiffness, it experiences decreased deflection but increased peak stresses. However, away from the peak stress area (whole body of fishplate) the glued IRJ experiences the least deformation (see Figure 4.29).

- The fishplates experience a two-axis bending during the vertical wheel loading. The pressure imparted by the underside of the railhead to the fishplate has a vertical and lateral component, due to the curved interface. This fishing curved interface induces bending in the fishplates on both its major and minor principal axes.

- The type of FEA used in this study is advantageous over previous FEA of IRJs as it takes into account the effect of sleeper support conditions, four types of RJs with increased thickness around the bolt area with increased fillet contact area, detailed frictional contacts among the interfaces of rail-fishplate-insulation-bolts, and bolt pretension.

- The bolt pretension significantly affects the stress level developed in the fishplate web and dominates the stress level experienced around the bolt areas when the wheel is not above the joint. When the wheel is above the joint, the vertical wheel load governs the maximum stress developed.

- Assessment against fatigue can be performed through the endurance limit approach if reverse bending stresses are calculated for the "hogging" deformation of the fishplates.

This analysis suggests that the bending behaviour and the fatigue strength of fishplates is sensitive to sleeper support stiffness, bolt pretension, stiffness and contacts of the joint assembly, joint design, and contact surface between rail and fishplate. Although optimised designs of rail joints with increased railhead end fillet contact area were considered, this study highlights the need to ensure good IRJ design with an appropriate bolt pretension while considering the effect of degraded support conditions on the deterioration rate of IRJs.

5.2 IMPLICATIONS/IMPACT ON THE SPONSOR AND WIDER INDUSTRY

One of the differences between the EngD and a traditional PhD is that the EngD takes place with strong connections with industry. As a result, it is expected to have an immediate impact on the wider industry (Section 5.2.1) and sponsoring company (Section 5.2.2).

5.2.1 IMPLICATIONS FOR THE WIDER INDUSTRY

A published objective of the GB Railway Strategy (published by the Technical Strategy Leadership Group (TSLG)) is to develop innovative track designs that combine the maintainability and initial low cost of traditional ballasted track with the stability of slab track. Better geometry, reduced tamping, and improved longevity can be combined to minimise long-term costs. Network Rail's Technical Strategy in response to the TSLG's document includes ass a key objective a move toward increasing track resilience and improving cost efficiency using a combination of ballasted and slab track (ballastless track forms) to reduce maintenance.

For a step-change to be realised either in component life or whole system performance, a better understanding is needed of superstructure-substructure interaction, and the deformation performance needed of rail components and track support systems to achieve this.

The research reported herein shed light on existing concerns and enhanced the understanding of deformation in various track structures and railway components. During its course, the research innovatively featured tools such as experimental measurements using the VG and numerical modelling (Chapter 4) which can be adopted by industry.

Specifically, the numerical model developed in Paper 3 provides to industry a method of evaluating magnitudes and distributions of deflections and stresses in various rail joint types. This constitutes a practical model to be routinely applied in industry as a supplement to existing

studies (mostly intended for reducing the lipping, localised plastic deformation of the rail head edges). The numerical modelling procedure, established in Paper 3, can be followed to realistically replicate the bending deformation of rail joints, given support stiffness and wheel force data. By investigating the sensitivity of support stiffness, rail joint design, contact interfaces (joint type), bolt preload and wheel force, industry can be reassured that rail joint deflections and fatigue life are predictable. Their effect can also be mitigated by design by external structural reinforcement (Paper 2). Although this investigation was limited to numerical models, this was seen to reduce deflections and dip angles and consequently impact on ballast, particularly for soft or deteriorated trackbed conditions.

Furthermore, the formulation of a new assessment procedure (VG) for the UK railway industry's track forms was introduced through this research project. The field assessment procedures reported in Papers 1 and 4 is an improvement on existing site monitoring. It has proved capable of rapidly collecting high definition deflection data and possible stiffness characteristics for multiple track components for various track structures and loading conditions, saving time and the need for full possession. The deflection behaviour of various track structures in the UK rail network including ballasted track, ballastless track, and transition zones was tested. Table 1.4 in Chapter 1 details the projects undertaken and the technical reports produced that were delivered in the wider UK rail industry, formulating a formal commercial application of the VG in the UK railway industry. The data were used by the wider rail industry for the evaluation of the load distribution of track structures and novel track forms (Asphalt track including PORR, IVES, and V-TRAS transition systems). Furthermore, the field deflection data for the transition zone (Site D) were incorporated, by the UK Cross Industry Track Stiffness Group, in the official document "A Guide to Track Stiffness" (Powrie and Le Pen 2016). Finally, the optimised and adapted VG methodology was presented in the international Conference BCRRA (Bearing Capacity of Roads, Railways and Airfields) as part of the Workshop "Railway Track Settlements: Innovations in Monitoring and Maintenance" introducing the advantages of the VG to a wider international audience.

5.2.2 IMPLICATIONS FOR THE SPONSOR

As part of the rail industry LB Foster is also in line to benefit from the implications raised in Section 5.2.1. This research project has provided LB Foster with access to guidance, data and expertise to assess track deflection and track stiffness characteristics. This allowed LB Foster to benefit by undertaking the following consultancy projects (see also TR 4-7, Table 1.4):

I.   Video Gauge deflection measurements of transition zone –Phase 1: Prior to renewal.

II.   Video Gauge deflection measurements of transition zone –Phase 2: After renewal.

III.   Video Gauge deflection measurements of new installed novel V-TRAS transition module between slab and ballasted track.

IV.   Video Gauge deflection measurements of novel ballastless track forms with asphalt underlayment (PORR, IVES), novel transition module (V-TRAS) and ballasted track.

Furthermore, this research project provides LB Foster with expert knowledge of the implications of optimising an IRJ by external reinforcement and of a mechanical fatigue assessment of their product offering (rail joints). The LB Foster rail joint offering is designed according existing UK specifications and is tested and validated by bending fatigue laboratory tests. This research project provides LB Foster with expertise in FE modelling as a practical tool for routine validation of RJ design optimisation. With the formation of the model, there is a body of deformation data that can be used to assess the load distribution and bending deformation. Finally, these models can be used to predict the behaviour of RJ designs against deflection and fatigue endurance targets. The EngD data has been used to reinforce client confidence in the performance of existing and optimised rail joint design allowing economic and knowledge benefits for LB Foster. In particular this project allowed LB Foster to undertake the Network Rail-Fishplate design Contract that included the re-design of all types of rail joints in the Network Rail network, validating them based on the FE analysis studied in Section 4.3.2. Finally, the fatigue life estimation analysis and relationships studied in Section 4.3.2 and described in Appendix E have helped LB Foster to complete the FMECA (Failure mode, effects and criticality analysis) of dry joints in order to successfully deliver the contract for Dry joints for the State of Railway of Thailand/Mitsubishi.

5.3   CRITICAL EVALUATION OF THE RESEARCH

An important part of academic rigour is to critically evaluate the research carried out. It is necessary to reflect on the work and gain an understanding of the effectiveness of the research and how it may have been improved. With all research, there are limitations such as limited resources to explore all variables with significant depth. In turn, this project had inherent simplifications.

5.3.1 VIDEO GAUGE DATA COLLECTION

In order to investigate deflection of plain rail and IRJ, deflection data was collected under controlled laboratory conditions, field real-time conditions for several case studies.

Although there were sufficient resources to conduct laboratory testing (hydraulic actuators), there was little control over the specimens used (plain rail and IRJ sections). This depended on the availability of spare specimens provided by the sponsoring company. Two different sections of rail and IRJ were tested that complicated the analysis and the conclusions. However, the laboratory results were only used for preliminary investigation, as laboratory testing can only provide an indication of the actual performance, and for the validation of the numerical modelling.

Furthermore, due to the limited availability of laboratory specimens, only one IRJ type was examined, the glued IRJ. This is considered the most robust and stiff IRJ type and most widely used in fast and high traffic lines of the UK rail network.

The field data showed some variability of the maximum deflections due to different train types running at different train speeds over the same rail joints. Additionally, little control existed in the selection of sites and no other site investigation data was available for the sites used, apart from the types of trains running through, as published online. The VG was used to assess the deflection of ballasted track of unknown trackbed characteristics (subgrade modulus, subgrade type, presence of sleeper voids, tamped or not, maintained or not e.g. stone blowing, renewal, time from last renewal). Consequently, an absolute comparison of the FE model and the measured data was not possible as the trackbed conditions were unknown. In addition, the age and condition of the IRJ tested in the field was unknown. This, justifies the parametric analysis for varying sleeper support stiffness conducted in Section 4.3.1. It was concluded that track deflection variance, and consequently track stiffness variance, can be caused by variance of dynamic loading with severe impact in low stiffness systems. However, what was shown here is that when the VG is used in between maintenance periods (Site D), the deflection values could ameliorate maintenance guidance, by assisting in the problem identification and providing information of the bearing capacity of the substructure.

5.3.2 RAIL JOINT MODELLING AND ANALYSIS

The rail joint model was validated through the laboratory and field deflection data and the deflections values measured in the field. Additionally, it was validated against current UK deflection limits (10 mm) according to NR/SP/TRK/064 (Network Rail, 2003).

Further refinement of the mesh density of the model was possible at the cost of slower computing time, but a range of mesh densities < 8 mm was found to have little effect < 9% on the maximum stresses on the top fishing surface of the fishplate and a negligible effect on the deflection. Further discussion of the details of the numerical model can be found in Paper 3, which expands on geometrical details, contact formulation, and force convergence details that relate to the size of the model, the complexity of the load sequence, and the computer capability and licence used.

Linear elastic constitutive law, were used in the model and the equivalent von Mises stresses (yield criterion) were obtained. The von Mises stresses were then compared to the yield limit and the endurance limit. A static analysis was performed that fit with the objectives of the project. The aim of the research was to create a routine model that could be used as an effective tool for the validation of RJ design and optimisation in railway industrial practice. A static analysis does not include the uncertainties of a dynamic analysis relating to validation of damping factors or vehicle suspension modelling factors. A thorough literature review and thorough parametric dynamic analysis would be required to critically select these values for a dynamic analysis or use of multibody dynamics would be required. For this project, each assembly configuration (geometry) was firstly created in Solidworks (CAD software) and then the model was set up in ANSYS Mechanical. The model settings had to be re-set each time geometry modification was required.An additional "Space claim" licence was bought for a limited time during the research period to allow advanced joint connections of beam elements (bolt positions) to be included. A tool that allows geometry modifications was not available (such as ANSYS Design Modeler). A dynamic analysis, and especially the simulation of the train wheels as deformable flexible bodies (using deformable solid elements), would require higher computational effort, additional research time, and mesh optimisation tools (such as geometry partition) to overcome any convergence issues and facilitate the mesh and simulation process. Modelling the vehicle using multibody dynamics, taking into account the primary suspension stiffness and damping properties is recommended for future research, though a

larger length of model is required in order for the track response to not to be affected by the boundary and initial effects.

The modelling of the sleeper support conditions (springs of certain stiffness per sleeper effective length) was used to incorporate stiffness values determined in accordance with current standard practice (30 kN/mm, RSSB, 2011; Network Rail, 2016) (Section 2.2.3). It is considered that modelling the trackbed layers with solid elements in the same linear elastic constitutive law, would increase the computational time but would not affect significantly the results.

5.4 RECOMMENDATIONS FOR INDUSTRY/FURTHER RESEARCH

Although the EngD has illuminated critical aspects of the assessment of track deflection and rail joint bending behaviour, and based upon the aforementioned research findings and conclusions, the following recommendations are proposed herein to extend the knowledge and understanding of IRJs and track stiffness.

Measurements of track stiffness using the VG of particular sites (soft, medium and stiff subgrade) under various train speeds to investigate the effect of speed for a given static wheel load and if possible, for measured/ known trackbed stiffness (modulus of elasticity of subgrade) is recommended. This will test the sensitivity of the VG methodology for the derivation of absolute dynamic track stiffness values and the identification of the dynamic component of the track stiffness value. Further testing of a wide range of trackforms is recommended to establish its applicability for track performance assessment in the rail industry. The prediction of voids below sleepers and their range through the VG data is suggested through comparison of measurements with void meters and VG data analysis.

Further numerical modelling of already deteriorated IRJs is recommended to investigate the effect of wheel load, and bolt pretension in a time dependent analysis including the effect of train speed. This would require field measurements of IRJs of known deterioration rate (dip angle, wheel forces and deflection/stress/ strain) for its validation. In addition, an investigation of the impact of bolt looseness (tensile and shear stresses around the bolt holes) in the deterioration rate of IRJs is recommended. Investigation of the effect of rail joints on the deterioration of trackbed in terms of cumulative plastic strain and settlement on top of subgrade (Li and Selig, 2016) is also suggested. In the latter case, the trackbed (ballast and subgrade

layers) should be included in the model. Careful attention is required in the boundary conditions of the model, the restriction of any reflective stresses from the boundaries, a better representation of the wheel-rail interface using the Hertzian contact stiffness in order to be able to predict dynamic forces (as output), while a software licence able to run an analysis across multiple processors (cores) is required capable of running models of larger size in efficient time. A parametric analysis of speed, dip angle, and subgrade modulus will demonstrate their effect on the IRJ (deflections, stresses, strains) and trackbed behaviour (stresses, strains, settlement). Furthermore, many aspects of the finite element analysis would benefit from further investigation; particularly for rail joints, element types and sizes, dimensional tolerances, and material properties for regions directly affecting the calculated maximum stresses or deflections (foundation assumption, and strap rail connections). Finally, a comparison of the fatigue life estimation of RJ fishplates between the different stress life theories and comparison among different decision approaches is recommended so as the most efficient method to be established.

A field implementation and validation of the enhanced IRJ with strap rails and I-beam sections (Paper 2) in soft trackbed conditions and deflection measurements of the developed product is suggested. This requires precast concrete sleepers that already exist in the rail industry with a fastening system in the required position for the strap rails whereas special design of fastening system is required for the I-beams to be connected to concrete sleepers. Optimisation of the length of strap rails for staggering joints, applicable in US, is also recommended. An economic evaluation of the total cost and long-term monitoring, up to 2-3 years, of an IRJ with and without the reinforcement is required for a cost benefit analysis.

6 REFERENCES

Akhtar, M., O' Connor, T. and Davis, D. (2008). Revenue service evaluation of advanced design insulated joints. *AREMA 2008 Annual Conference*, Salt Lake City, Utah, USA, September 21-24 2008.

Anderson, J.S. and Rose, J.G. (2008). In-situ test measurement techniques within railway track structures. *Proceedings 2008 ASME/AIEE/ASCE Joint Rail Conference*, Wilmington, DE, April 2008, 21 pp.

Andersson, A., Berglund, H., Blomberg, J., & Yman, O. (2013). *The Influence of Stiffness Variations in Railway Tracks*. Chalmers University of Technology.

ANSYS Inc. (2015) An overview of methods for modelling bolts in ANSYS V15, July 17 2015.

ANSYS Inc. (2016) ANSYS Mechanical User's Guide. Release 17.1, April 2016

Askarinejad, H., Dhanasekar, M. and Cole, C. (2012). Assessing the effects of track input on the response of insulated rail joints using field experiments. *Proc IMechE, Part F: J Rail Rapid Transit.* 2012 Sep 13;227(2):176–187.

Askarinejad, H., Dhanasekar, M. Boyd, P. and Taylor, R. (2012). Field measurements of wheel-rail impact force at insulated rail joint. *Experimental Techniques* Sep 18; 39 (5)

Auersch, L. (2005). Dynamics of the railway track and the underlying soil: the boundary-element solution, theoretical results and their experimental verification. *Vehicle System Dynamics*, *43*(9), 671–695

Badinier T. and Maïolino S. (2016) Computation of Ballasted Track Damage: Comparison of Coulomb Criterion, Drucker Prager and Matsuoka Nakai. *Proceedings of the 3rd International Conference on Railways Technology: Research, Development and Maintenance.* J. Pombo. Civil -Comp Press, Stirlingshire, Scotland.

Bandula-Heva, TM., Dhanasekar, M. and Boyd, P. (2012). Experimental investigation of wheel/rail rolling contact at railhead edge. *Exp Mech* ; 53: 943–957.

Bastin R. (2006). Development of German non-ballasted track forms. *Proceedings of the Institution of Civil Engineers-Transport*, Thomas Telford Ltd; 159 (1): 25-39.

Beagles, A.E., Beaty P., Fletcher, D.I., Lewis, R. and Temple, B.P. (2015). Insulated rail joint enhancement: testing and analysis. *IMechE The Stephenson Conference: Research for Railways,* London, UK, 21-23 April 2015.

Beaty, P. (2014). *Experimental Testing Procedures to Investigate and Improve Insulated Rail Joint Design and Life Cycle*. MSc Thesis, University of Sheffield, UK.

Beaty, P., Temple, B., Marshall, M.B. and Lewis, R. (2016). Experimental modelling of lipping in insulated rail joints and investigation of rail head material improvements. *Proceedings of the IMechE, Part F: Journal of Rail and Rapid Transit*, 230 (4). pp. 1375-1387. ISSN 0954-4097

Berggren, E. (2006). Measurements of track stiffness and track irregularities to detect short waved support conditions. *Proceedings of International Conference on Railway Track Foundations. 11th -13th September*, Birmingham, UK.

Biabani, M. M., Indraratna, B., and Ngo, N. T. (2016). Modelling of geocell-reinforced subballast subjected to cyclic loading. *Geotextiles and Geomembranes*, 44(4), 489-503.

Bowness, D., Lock, A., Powrie, W., Priest, J. and Richards, D. (2007). Monitoring the dynamic displacements of railway track. *Proceedings of the IMechE Part F Journal of Rail and Rapid Transit* 221(1):13–22

British Steel (2017) Steel Grade Composition and Properties. British Steel UK.

Browell R., Hancq A. (2006) Calculating and displaying fatigue results, ANSYS fatigue module, March 29, 2006, ANSYS Inc.

BSI (2003) BS EN 1991-2:2003 Actions on structures. Part 2: Traffic Loads on Bridges. British Standards Institute, London UK.

BSI (2013) BS EN 13450 Aggregates for railway ballast. British Standards Institute, London UK.

BSI (2014a) BS EN 13146-4 Railway applications - Track - Test Methods for Fastening Systems - Part 4: Effect of repeated loading. British Standards Institute, London UK.

BSI (2014b) BS EN 13230-6 Railway applications. Track. Concrete sleepers and bearers. Part 6. Design. British Standards Institute, London UK.

BSI (2015a) BS EN 16843:2015 Railway applications – Infrastructure - Mechanical Requirements for Joints in Running Rails. British Standards Institute, London UK.

BSI (2015b) BS EN 7608 Guide to fatigue design and assessment of steel products. British Standards Institute, London UK.

BSI (2017a) BS EN 16432-1:2017 Railway applications. Ballastless track systems. General requirements. British Standards Institute, London UK.

BSI (2017b) BS EN 16432-2:2017 Railway applications. Ballastless track systems. System design, subsystems and components. British Standards Institute, London UK.

Budynas, R.G., Nisbett, J.K. (2011). Shigley's mechanical engineering design. New York: McGraw-Hill. Ninth edition.

Burrow, M. P., Shi, J., Wehbi, M., and Ghataora, G. S. (2017). Assessing the Damaging Effects of Railway Dynamic Wheel Loads on Railway Foundations. *Transportation Research Record: Journal of the Transportation Research Board,* (2607), 62-73.

Carolan, ME., Jeong, DY. and Perlman, AB. (2014) Engineering studies on joint bar integrity, Part II: finite element analyses. *In: Joint rail conference 2014*, Colorado Springs, Colorado, USA, 2–4 April.

Cemex Rail Solutions (2013) Sleepers, Products brochure. Cemex Rail Solutions.

Charlton, ZI. (2007) *Innovative Design Concepts for Insulated Joints*. MSc Thesis, Faculty of Virginia Polytechnic Institute and State University.

Costa, P. A., Lopes, P., & Cardoso, A. S. (2018). Soil shakedown analysis of slab railway tracks: Numerical approach and parametric study. *Transportation Geotechnics*, 16, 85-96.

Dahlberg, T. (2004) Railway track settlements - a literature review. Report for the EU Projet SUPERTRACK.

Dahlberg, T. (2001). Some railroad settlement models - a critical Review. *Proc. IMechE, Part F: J. Rail and Rapid Transit.* 215 (F4), 289–300.

Dhanasekar, M. and Bayissa, W. (2011). Performance of square and inclined insulated rail joints based on field strain measurements. *Proc IMechE, Part F: J Rail Rapid Transit*. pp1-15

Dhanasekar, M. and Bayissa, W. (2009) Review of Insulated Rail Joints. Report, CRC for Rail Innovation, R3.100, Brisbane, Australia.

Feng, H. (2011) *3D-models of railway track for dynamic analysis*. Master Thesis. Royal Institute of Technology, Stockholm.

Fleming, P.R., Frost, M.W. and Lambert, J.P. (2007). Review of lightweight deflectometer for routine in situ assessment of pavement material stiffness. *Transportation Research Record: Journal of the Transportation Research Board*, 2004, pp. 80-87.

Fortunato, E., Paixão, A. and Calçada, R. (2015). Field measurements and numerical modelling of transition zones −A research project in a recent portuguese railway line. *Proceedings of Railway Engineering -2015 Conference, June 30th-July 1st*. Edinburgh, UK.

Gallou, M., Frost, M., El-Hamalawi, A. and Hardwick, C. (2017). Applicability of Video Gauge for the assessment of track displacement. *The Stephenson Conference: Research for Railways, IMechE*, London, UK, 25th-27th April 2017, pp. 141-148

Garcia-Palacios, J., Samartin, A. and Melis, M. (2011). Analysis of the railway track as a spatially periodic structure. *Proceedings of the IMechE Part F: Journal of Rail and Rapid Transit*, 226(2), 113–123.

Govan, C., Sharpe, P. and Brough, M. (2015). The rail trackform stiffness tester-development and early trials to assess stiffness characteristics of novel trackforms. *Proceedings of Railway Engineering -2015 Conference, June 30th-July 1st*. Edinburgh, UK.

Gray, D.E. (2014) *Doing Research in the real world*. 3rd Edition. London: SAGE Publications Ltd.

Grossoni, I., Iwnicki, S., Bezin, Y. and Gong, C. (2014). Dynamics of a vehicle-track coupling system at a rail joint. *Proc IMechE Part F J Rail Rapid Transit.* 229(4):364–74.

Hardwick, C. (2013) *The Effects of Third-Body Materials in the Wheel-Rail Interface*. PhD thesis, University of Sheffield.

Himebaugh, A.K. (2006). *Finite Element Analysis of Insulated Railroad Joints.* Faculty of the Virginia Polytechnic Institute and State University, Blacksburg, Virginia.

Himebaugh, A.K., Plaut, R.H. and Dillard, D.A. (2008). Finite element analysis of bonded insulated rail joints. *International Journal of Adhesion and Adhesives*, 28(3), 142–150.

Hunt G.A (1996) Development of a performance specification for rail pads. Research report No. RR-TCE-6, 2 July 1996, Track and Civil Engineering Group, British Rail Research, Derby, UK.

Hunt, G.A. (1986). *Dynamic analysis of railway vehicle/track interaction forces*. Doctoral dissertation. Loughborough University.

Hunt, M. (2018) Connectivity Challenges from High Speed rail to existing infrastructure, HS2 Ltd, *Permanent Way Institution Journal*, January, Vol 136, Part 1.

Innotrack (2006) Methods of track stiffness measurements. Deliverable D2.1.11 for Innotrack project. TIP5-CT-2006-031415.

Iwnicki, S. (2006) *Handbook of Railway Vehicle Dynamics*, 1st Edition, CRC Press, NY, Taylor & Francis Group, LLC.

Iwnicki, S. D. and Stow, J. M. (1998). Modelling the behaviour of freight vehicles. *Institution of Civil Engineers Railway Seminars - The Interaction of Vehicle and Track Design*; May 20 1998.

Kim, H. (2016) *Trackside Measurement of Critical Zones in Railway Tracks.* PhD Thesis. The Birmingham Centre for Railway Research and Education. The University of Birmingham UK.

Lamas-Lopez, F., Alves-Fernandes, V., Cui, U.J., Costa D'Aguiar, S., Calon, N., Canou, J., Dupla, J.C., Tang, A.M. and Robinet, A. (2014). Assessment of the double integration method using accelerometers data for conventional erailway platforms. *Proceedings of the Second International Conference on Railway Technology: Research, Development and Maintenance*, Civil-Comp Press, UK, Paper 58.

Laryea, S., Safari Baghsorkhi, M., Ferellec, J.-F., McDowell, G.R. and Chen, C. (2014). Comparison of performance of concrete and steel sleepers using experimental and discrete element methods. *Transportation Geotechnics*, 1, 225-240.

Lassoued, R. and Guettiche, A. (2011). Mechanical behaviour of railway track. *Physics Procedia*, *21*, 166–173.

LB Foster (2014) Insulated Rail Joints catalogue 2014.

LB Foster Rail Technologies (2010) Identified failure modes of IRJs (based on Trust output).

LB Foster Rail Technologies (2016) Endurance limit assessment, 12 May 2016 (Based on Trust Output).

Le Pen, L., Watson, G., Powrie. W., Yeo, G., Weston, P. and Roberts, C. (2014). The behaviour of railway level crossings: Insights through field monitoring. Transportation Geotechnics 1: 201-213.

Lechner, B. (2013). General requirements for ballastless rail-trackforms asphalt and concrete pavement design. *In International Journal of Pavements Conference,* São Paulo, Brazil December 9th- 10th 2013.

Li, M.X.D. and Berggren, E.G. (2010). A study of the effect of global track stiffness and its variations on track performance: simulation and measurement. *Proceedings IMechE J Rail and Rapid Transit* 224 (5): 375-382.

Lichtberger, B. (2005). *Track compendium.* Eurailpress Tetzlaff-Hestra GmbH & Co. KG, Hamburg, 634.

Liu, J and Freudenstein, S and (2013) Investigations on ballastless tracks in tunnel without reinforcement. *Electronic Journal of Structural Engineering*. 13(1):35–40.

Lundqvist, A. and Dahlberg, T. (2005). Load impact on railway track due to unsupported sleepers. *Proceedings of the Institution of Mechanical Engineers, Part F: Journal of Rail and Rapid Transit*, *219*(2), 67–77.

Mishra, D., Qian, Y., Huang, H. and Tutumluer, E. (2014). An integrated approach to dynamic analysis of railroad track transitions behaviour. *Transportation Geotechnics* 1, 188-200.

Murray, C. (2013) *Dynamic monitoring of rail and bridge displacements using digital image correlation.* Mater Thesis. Queen's University, Kingston, Ontario, Canada.

Network Rail (1996) NR/SP/TRK/023 (NR-RT/CE/S/023) Insulated Rail Joints Issue 1. London, Network Rail.

Network Rail (2003) NR/SP/TRK/064 (NR-RT/CE/S/064 Issue 2) Assembly of BR MkIII 4- and 6- hole insulated joints, London, Network Rail .

Network Rail (2008) NR/L2/TRK/2102 Design and Construction of Track. Issue 8. London, Network Rail.

Network Rail (2011) NR/L2/CIV/020 Design of Bridges Issue 1 Part 10.2.6 Additional loads for the design of bridges structures supporting directly fastened and embedded rails. London, Network Rail.

Network Rail (2015) NR/L2/TRK/001/mod11 Inspection and Maintenance of Permanent Way. Issue 5. London, Network Rail.

Network Rail (2016) NR/L2/TRK/4239 Issue 1. Trackbed investigation, design and installation. London, Network Rail.

Nogy, L. (2016). Railway Earthworks Instability Diagnosis Using Track Geometry Measurement Data-CCQ and Top 35m. *Permanent Way Institution Journal*.

Oregui, M., De Man, A., Woldekidan, M. F., Li, Z., & Dollevoet, R. (2016). Obtaining railpad properties via dynamic mechanical analysis. *Journal of Sound and Vibration*, 363, 460-472.

Paixão, A.; Fortunato, E. & Calçada, R. (2014). Transition zones to railway bridges: track measurements and numerical modelling. *Engineering Structures*. Vol. 80; p. 435-443; 0141-0296.

PORR (2012) Slab Track Austria System ÖBB-PORR elastically supported slab, Porr Bau GmbH.

Porrill J. (2015) Non-ballasted trackforms. Ballast and Beyond- PWI technical seminar. 20th May 2015, London.

Powrie, W. and Le Pen, L. (2016) A Guide to Track Stiffness. Cross Industry Track Stiffness Working Group UK. August 2016.

RAIB (2014). Class investigation into rail breaks on the East Coast Main Line. Rail Accident Investigation Branch, Department for Transport. Report 24/2014. November 2014, Derby UK.

Recuero, A.M., Escalona, J.L. and Shabana, A.A. (2011). Finite-element analysis of unsupported sleepers using three-dimensional wheel-rail contact formulation. *Proceedings of the IMechE Part K: Journal of Multi-Body Dynamics*, 225(2), 153–165.

Rhomberg Sersa Rail Group (2016a) Slab Track IVES. Rhomberg Rail Consult GmbH.

Rhomberg Sersa Rail Group (2016b) Universal transition module V-TRAS. Rhomberg Sersa UK Ltd.

Ribeiro, C.A. and Calçada, R. (2017). Assessment of the short and long term behaviour of the track on railway transition zones. *The Stephenson Conference: Research for Railways, IMechE*, London, UK, 25th-27th April 2017, pp. 13-23.

RSSB (1993) Permissible Track Forces for Railway Vehicles. Group Standard GM/TT0088.

RSSB (2004). Guidance Note: The design and Construction of Freight Wagons. Group Guidance Note GM/GN2589 Issue 1.

RSSB (2009) Requirements for the Application of Standard Vehicle Gauges. Group Standard GE/RT8073 Issue 2.

RSSB (2011) Track System Requirements. Group Standard GC/RT5021 Issue 5.

RSSB (2015) Rail traffic Loading Requirements for the Design of Railway Structures. Group Standard GC/RT5112.

RSSB (2016) Loading requirements for Track Systems, Phase 1 Summary report, T1073-01 Phase 1, London September 2016.

Selig, E.T. and Waters, J.M. (1994). *Track geotechnology and substructure management*. Thomas Telford.

Sharpe, P. and Collop, A.C. (1998). Trackbed investigation-a modern approach. *Proceedings of the First International Conference of Railway Engineering*. London.1998.

Shih, J. Y., Thompson, D. J., & Zervos, A. (2017). The influence of soil nonlinear properties on the track/ground vibration induced by trains running on soft ground. *Transportation Geotechnics*, 11, 1-16.

Soylemez, E. and Ciloglu, K. (2016) Influence of Track Variables and Product Design on Insulated Rail Joints. *Transp Res Rec J Transp Res Board*. 2016 Jan; 2545:1–10.

Spiryagin, M., Cole, C., Sun, Y. Q., McClanachan, M., Spiryagin, V., and McSweeney, T. (2014). Design and simulation of rail vehicles. CRC Press. 1st edition.

Stark, T. D., Wilk, S.T., Thompson II, H. and Sussmann Jn, T. (2015). Effect of unsupported ties at transition zones. *Railway Engineering 2015 Conference, June 30th-July 1st*. *Edinburgh*.

Stark, T.D., Wilk, S.T., Rose, J.G. and Moorhead, W. (2016). NURail Project; ID: NURail2016-UKY-R11, NURail Center, University of Illinois at Urbana Champaign U.S., University Transportation Center, March 22 2016.

Steffens, D. M. (2005). *Identification and development of a model of raiway track dynamic behaviour*. MEng Thesis. Queensland University of Technology.

Sun, Y.Q., Cole, C., Kerr, M., and Kaewunruen, S. (2009). Use of Simulations in Determination of Wheel Impact Forces P1 and P2 Due to Rail Dip Defects. *In AusRail 2009*.

Telliskivi, T., & Olofsson, U. (2001). Contact mechanics analysis of measured wheel − rail profiles using the finite element method. *IMechE Part F J Rail and Rapid Transit;* 215, 65–72.

Thompson, H.B., Sussmann, T.R., Stark, T.D. and Wilk, S.T. (2015). Non-invasive monitoring of track system gaps. In *Proceedings of Railway Engineering -2015 Conference, June 30th-July 1st*. Edinburgh, UK.

Vale, C., Ribeiro, N., Calcada, R. and Delgado, R. (2011) Dynamics of a precast system for high-speed railways tracks. *In 3rd ECCOMAS Thematic Conference on Computational Methods in Structural Dynamics and Earthquake Engineering*. Corfu, Greece 2011.

Van Dyk, B., Drsch, M., Edwards, R., Ruppert, C. and Barkan, C. (2103). Evaluation of dynamic and impact wheel load factors and their application for design. RAILTEC. TRB14-4714. Transportation Research Board 93rd Annual Meeting.

Vossloh Fastening Systems (2015). Vossloh GmbH, April.

Vossloh Fastening Systems GmbH (2009). Design of Slab Track and Fastening Systems. [Online]. Available: http://railtec.illinois.edu/CEE/pdf/PPT%27s/Spring09/Steidl%202-27-09.pdf. [Accessed 30.11.2014].

Vossloh Rail Services (2017). Glued Insulated Joint IVB 30. [online] Available: http://www.vossloh-cogifer-uk.com/admin/resources/main-content-downloads/vtsivb30.pdf [accessed: 30/06/17]

Waterfall, P., Temple, B., Hardwick, C., Sharam, J. and Plumb, A. (2015) Video Measurement techniques for understanding wheel- induced lateral forces and track component deflections. *The Stephenson Conference-Research for Railways*. London, UK; 21-23 April 2015.

Wehbi, M. and Musgrave, P. (2017) Optimisation of Track Stiffness on the UK Railways. [online] Available: https://www.researchgate.net/publication/318960587 [accessed: 30/08/17]

Wen, Z., Jin, X. and Zhang, W. (2005). Contact-impact stress analysis of rail joint region using the dynamic finite element method. *Wear,* 258, 1301-1309.

Whitney, B. (2013). Examples of rail joint damage mechanisms 24 October 2013.

Whitney, B. (2015). Broken Rail Management Update, Vehicle/Track System Interface Committee Seminar, October 29th 2015, Network Rail UK.

Witt, S. (2008). *The influence of under sleeper pads on railway track dynamics.* Linköping University, Sweden.

Zakeri, J.A. and Abbasi, R. (2012). Field investigation on variation of rail support modulus in ballasted railway tracks. *Latin American Journal of Solids and Structures*, 9, 643–656.

Zarembski A., Euston, T. and Palese J. (2005). Use of track component life prediction models in infrastructure management. *AusRAIL PLUS 2005 Conference and Exhibition* Sydney, 22-24 November 2005.

Zhang, X., Zhao, C., & Zhai, W. (2016) Dynamic Behavior Analysis of High-Speed Railway Ballast under Moving Vehicle Loads Using Discrete Element Method. *International Journal of Geomechanics*, 17(7), 04016157

Zhang, Z. (2015). *Finite element analysis of railway track under vehicle dynamic impact and* longitudinal loads (Doctoral dissertation). University of Illinois at Urbana-Champaign.

Zhu, K., Qian, Y., Edwards, J.R. and Andrawes, B.O. (2017) Finite element analysis of rail end bolt-hole and fillet stress on bolted rail joints. *Transportation Research Record: Journal of the Transportation Research Board*, 2607: 33-42.

Zimmermann H. (1888). Die Berechnung des Eisenbahnoberbaus. Ernst & Korn, Berlin, Germany (in German).

APPENDIX A - PAPER 1

Abstract

Numerous techniques have been used for the measurement of the track displacements and consequently, the assessment of track stiffness. Some of the most commonly employed are linear variable displacement transducers (LVDTs), geophones and older video monitoring techniques based on Particle Image Velocimetry (PIV). In this paper, the application of the Video Gauge, a relatively new technique, is investigated. This technique can be seen as a quick and reliable way to capture data of high quality and resolution, which can be directly employed for the evaluation of track displacement and hence stiffness. The Video Gauge is used at three different track sites measuring different ballasted track components under various train speeds and types.

1   INTRODUCTION

Understanding track stiffness is vital property for the design and maintenance of railway track structures. Its evaluation is important to assess track quality, component performance, localised track faults and to optimise maintenance periods and activities. In addition, its evaluation can help in the investigation of the performance of novel trackforms, as well as the validation of numerical models. Track stiffness may be affected by many factors including track component; condition, ballast condition, by unsupported sleepers, discontinuities of rail bending stiffness (i.e. rail joints), transition zones from a ballasted track to slab systems (bridges and tunnels), as well as condition of the substructure layers. These factors can induce variations in the wheel–rail contact forces and affect the deterioration rate of track geometry and components (1).

Track system stiffness can be estimated by measuring track system displacement and calculating the stiffness from the applied load (a direct approach) or by measuring deflection (via velocity) of a sleeper using a falling weight deflectometer (FWD) and evaluating trackbed stiffness per sleeper end (an indirect approach). Direct displacement methods employ techniques, such as linear variable displacement transducers (LVDTs) (2), laser deflectometers (2, 3) and remote video monitoring using PIV (4,5) and Digital Image Correlation (DIC) (6, 7). Alternatively displacement can be measured indireclty. Geophones (3-5) have been employed for measuring velocity time histories, which can be transformed to displacements through integration. Similarly, accelerometers can be used by integrating the signal twice. The accuracy of all measuring techniques where load is not directly measured but vehicle weight is used depends on the train speed, on the instrument sampling frequency and the amount of the displacement measured.

This paper focuses on the use of Video Gauge (VG) technique (see also section 2) for the measurement of track vertical displacements and the procedure needed for the estimation of track stiffness. The benchmarking of the Video Gauge as a useful system to assess various parameters of the railway system such as dynamic deflection under high speed or in tracks with high train-induced movement, 3d deflection for calculation of lateral effects, strains and forces was previously shown (8). Relevant work conducted with the VG included track behaviour investigation at switches and crossings (9). The current work describes complementary technical results of the VG with an improved methodology (large quantity of data with a larger field of view from shorter distance). The developed strategy of the VG has been deployed on ballasted track components under different train speeds and field conditions.

The Video Gauge was also used to measure the displacement of a rail joint. The rail joint can be considered as a weak point in the railway system, which has been experimentally assessed in the past (10, 11), however for the measurement of rail joint deflections, there is a lack of literature work related to video techniques.

2 METHODOLOGY

The Video Gauge technology is based on digital image correlation (DIC). This compares digital images from frames at different time intervals, by tracking the behaviour of pixel (target) groups between frames. Under external excitation (i.e. dynamic loading), DIC allows the calculation of the displacement of a target with respect to time. Measurements were taken using up to two high speed cameras mounted on surveyor's tripods, in the track cess, at a distance of *2-5.5 m* from the measured line. The sampling frequency (frames per second) used during recording were up to *200 Hz* with a resolution of under *10 microns*. Appropriate lenses were used to provide a field of view up to *6.3m*. A typical video image with a target array (fixed or painted) is illustrated in Figure 1. Measurements were performed for several train passages in each location assessed.

Figure 1. Typical video image from Site C showing target array on rail web and sleeper edges

Three sites were assessed. The deflection of the rails, sleeper and where possible rail joint were measured. Details are given below:

A main line with a speed of *40 mph*. Here, rail and sleeper displacements were measured simultaneously. The measurements were taken at a sampling frequency of *124 Hz*.
A fast line with a speed of *125 mph*. In this case, rail joints displacements were measured and compared with those of adjacent plain rail under the same train passage. The measurements were taken at a sampling frequency of *75 Hz*.
A fast line on a transition zone (approach to a railway bridge) with a speed of *125 mph*. Here, rail and sleeper displacements were measured under high speed train passages. A total track length of *6.3 m* was measured in this case. The measurements were taken at a sampling frequency of *175 Hz*.

While there is some inconsistency in the nature of the sites and trains used, this was down to the availability of sites and safety considerations.
The accuracy of Video Gauge technique depends on the train speed, sampling frequency and the amount of the displacement measured. In particular, the higher the train speed, the higher the displacement frequency for each vehicle. In other words, the possibility to capture the maximum displacements imposed by the wheel passage (load) between two supports depends on the camera's capture rate capability. More information with respect to the train type, speed and wheel loads considered are provided in Table 1.

Table 1. Characteristics of trains monitored

Site	Train type	Speed(mph)	Wheel load (F) (kN)
A	Class 170	40	60
B	Pendolino Class 390	125	75
	Desiro Class 350	72-101	55
C	Intercity 225	125	100
	Intercity 125	125	100

3 THEORETICAL BACKGROUND

The main aim of the paper is to approximate the track stiffness employing the Video Gauge technique. The vertical track stiffness (S_{system}) can be defined as the point load (F) required to produce a unit displacement (δ_{rail}) of the rail measured in *kN/mm*. This can be considered as the global or composite track stiffness depending on rail flexural rigidity (*EI*) and on effective support stiffness.

$$S_{system} = \frac{F}{\delta_{rail}}$$
(Eq. 1)

The term modulus (k) is used to describe the line load required to cause a unit deflection and it is defined as load per unit length (*MN/m*) per unit displacement (δ). The track support system modulus (k_{system}) is related to both the railpad ($k_{railpad}$) and trackbed modulus ($k_{trackbed}$) (*Eq.2* (12)). It should be noted that in *Eq.2*, the rigid sleeper stiffness is omitted as the inertia effects and the ground acceleration have not been considered (a quasi-static analysis) (12). "A quasi-static analysis does not automatically calculate loads that may arise from dynamic effects and assumes that the accelerations of the track structure and the ground are negligible" (12). Dynamic effects due to high P2 forces may have influence the magnitude of the displacements in Site B. P2 forces comprise inertia forces associated with the dynamic response of the unsprung masses to variation of the vertical alignment of the rail.

$$\frac{1}{k_{system}} = \frac{1}{k_{railpad}} + \frac{1}{k_{trackbed}}$$
Eq. 2)

According to Beam on Elastic Foundation theory (12) the rail displacement *w(x)* can be linked with the track support system modulus (k_{system}) (*Eq.3*) where *L* (*Eq.4*) is the characteristic length from the point load along the rail that the displacement bowl extends (12) this, depends on the rail flexural rigidity (*EI)*, while *x* describes the longitudinal distance along the track:

$$w(x) = \frac{F}{2k_{system}L} e^{\frac{-x}{L}} \left(\cos\left(\frac{x}{L}\right) + \sin\left(\frac{x}{L}\right) \right)$$
(Eq. 3)

$$L = \sqrt[4]{\frac{4EI}{k_{system}}} \qquad\qquad (Eq.\ 4)$$

For $x=0$, *Eq.3* provides the rail displacement ($w(0)$) for the position where the load is applied, leading to simplification of *Eq.1* (*Eq.6*):

$$w(0) = \delta_{rail} = \frac{F}{2k_{system}L} \qquad\qquad (Eq.\ 5)$$

$$S_{system} = 2k_{system}L \qquad\qquad (Eq.\ 6)$$

Finally, the spring stiffness of the railpad ($s_{railpad}$) correlates with the railpad modulus through the formula $k_{railpad}=s_{railpad}/sleeper\ spacing$ (12). The effect of the railpad is more severe for high trackbed modulus ($k_{trackbed}$) and the overall system modulus (s_{system}) cannot exceed that of the softest component of the trackform.

4   RESULTS AND DISCUSSION

In this section, the results of the measurements conducted in the three track sites (A, B and C), in UK, are presented and discussed. From the measurements, the track stiffness was approximated using the equations described in section 3.

4.1   Site A

The vertical displacements of both the rail and sleeper of a conventional ballasted track were measured. In this site one camera was used. This captured detailed rail and sleeper displacements, over a distance of *1.4 m* of track length during the passage of two passenger trains (Class 170). A typical time-displacement plot is illustrated in Figure 2. From this plot, the maximum displacement (average of peaks which show the passage of each individual wheel) was obtained correspondingly for the rail and sleeper position. This was used for the estimation of track stiffness (see *Eq.1*, section 3). In particular, the maximum rail displacement obtained was $\delta_{railmax}=3.02\ mm$, while the corresponding track stiffness (S_{system}) was *19.9 kN/mm*.
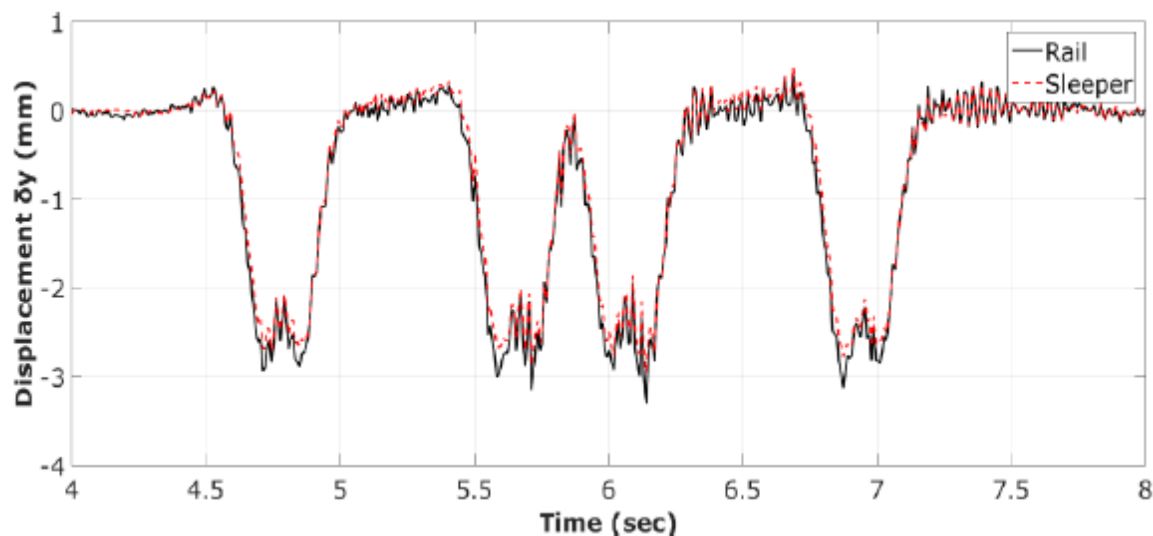
Figure 2. Vertical displacement time history during the passage of a passenger Cross Country Class 170 train (40 mph)

As mentioned in section 3, the track stiffness depends on the railpad and the trackbed stiffness. Therefore, to estimate the railpad stiffness, the relative displacement between the rail and sleeper (δrelative=δrail-δsleeper) was calculated (0.34 mm). Then the railpad stiffness ($s$railpad) can be estimated (94.7 kN/mm). This value can be assumed to be realistic, even if it is higher than typical values (60 kN/mm (12)). In addition, the trackbed stiffness was estimated (5.8 kN/mm), which can be assumed to correspond to soft support conditions, as it is lower than the stiffness of a renewed or well-maintained ballasted track (50 kN/mm, (12)).

4.2 Site B

In site B the displacement of a rail joint was measured by the Video Gauge in comparison to the displacement of adjacent plain rail under the passage of five high speed passenger trains (three Pendolino Class 390 and two Desiro Class 350). In this site two cameras were used measuring a distance of 2m track length. A typical time- displacement plot for the rail joint and the adjacent plain rail is depicted in Figure 3.
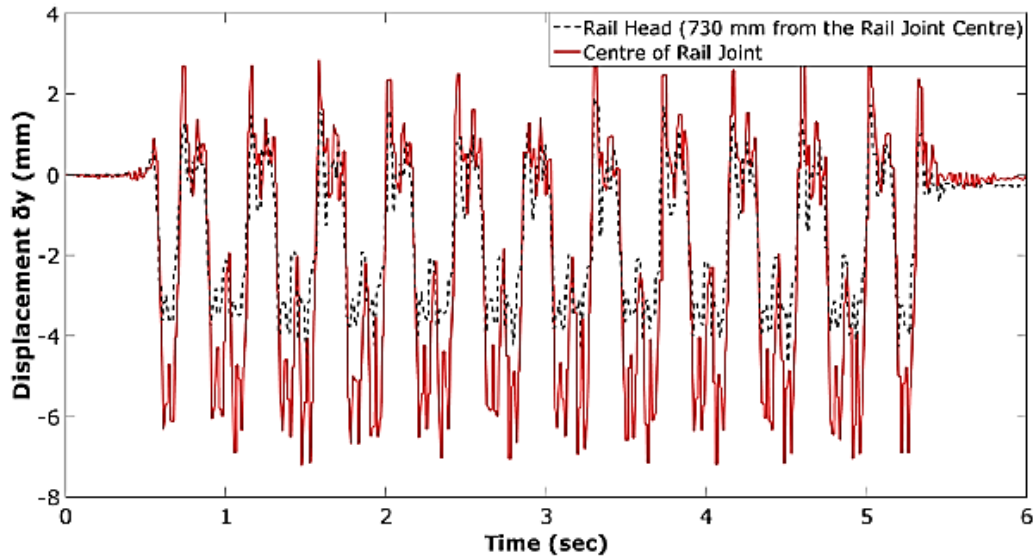
Figure 3. Displacement –time history for rail joint and plain rail during the passage of a Pendolino Class 390 train (125 mph)

Studying the above plot, it can be observed that the rail joint deflects more than the adjacent plain rail (*730 mm* from the centre of the rail joint). This can be explained by the structural discontinuity, due to the lower section modulus of the joint fishplate, interacting with the wheel impact load. The displacement increment that occurs in the rail joint causes amplification of the dynamic forces induced, which can lead to rail joint and track degradation. Additionally, the positive displacements seen on the plot are assumed to correspond to uplift of the rail ahead of, or behind the wheels. Some differences in amplitude of peak values (that correspond to the passage of each wheel) can be observed. Some of the possible reasons can be variation of vehicle weight (i.e. number of passengers), potential wheel flats (affecting the dynamic forces P2 induced in the rail) and others. In order to derive the effect of the train speed and axle load on the plain rail and rail joint displacement, the average of all peak values, for each case, was used. This can be seen in Figure 4.

Figure 4. Comparison of average maximum displacements for varying train speed and axle load.

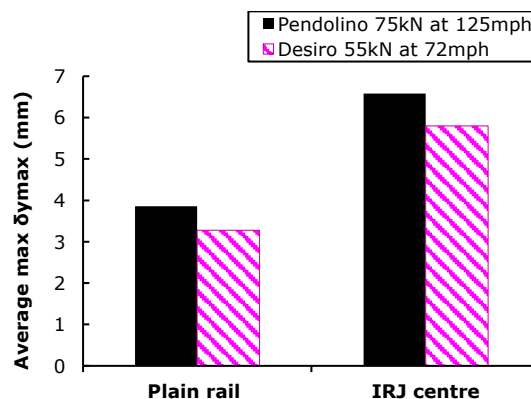The track stiffness of site B is estimated between *16.8-19.4 kN/mm* according the maximum rail displacements found for the two train types, that is close to that estimated for site A. The stiffness at the rail joint is estimated around *10.5 kN/mm*. Peak displacements could be being amplified due to increased P2 at the joint. Additionally, ineffective discrete support conditions, such as voided sleepers underneath the joint could also increase the joint displacement.

4.3   Site C

At Site C, rail and sleeper displacements were measured in a transition zone from an embankment towards a bridge. Here two cameras were used measuring a distance of *6.3 m* of track length under various train passages up to *125 mph*. In this case the impact of ineffective sleepers was investigated. In particular, Figure 5 illustrates a typical time –displacement history of two sleepers (G1, G6). From this the increased displacement of the first sleeper against the sixth sleeper is shown. Furthermore, Figure 6 shows the transition zone and the sleeper displacements (based on maximum of each train passage).
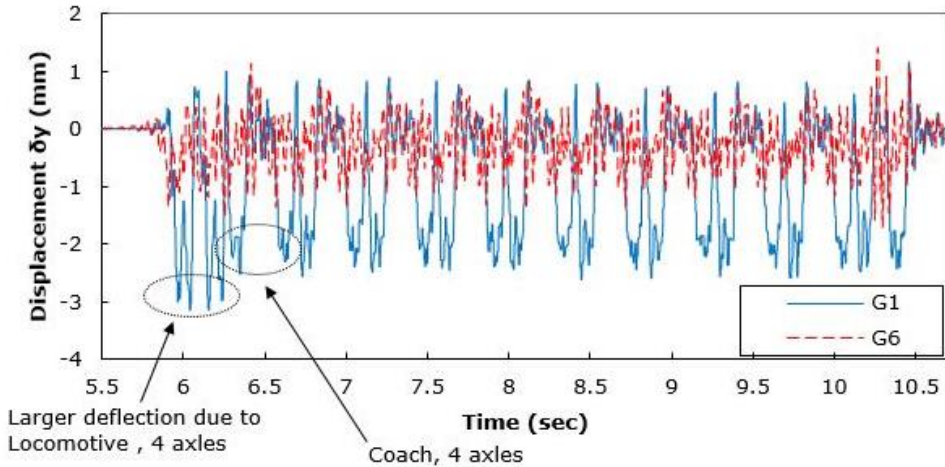

Figure 5. Time- displacement history for the first (G1) and sixth (G6) sleeper in advance of the bridge during Intercity train passage at 125 mph
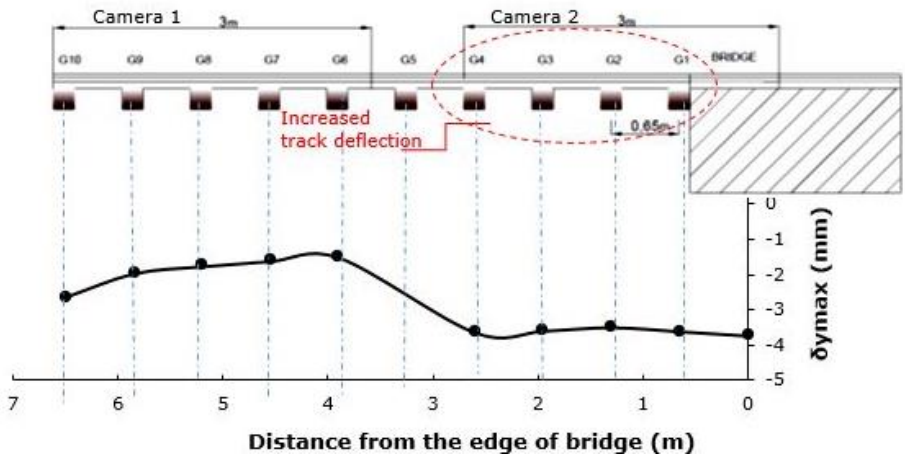

Figure 6. Transition zone general layout and maximum sleeper dynamic displacements at the approach of an overbridge

Increased deflections were observed on the approach of the bridge. This might have occurred due to track degradation caused by unsupported sleepers with gaps in the sleeper-ballast interface. It should be noted that maintenance work (re-packing of ballast) conducted before the measurements might have influenced the results. At this transition zone (site C) stiffness variation can be associated with drainage problems detected in the embankment, which caused wet beds and sleeper voids. Finally, the stiffness per sleeper end was estimated varying from *27.6* to *61.4 kN/mm* which agrees with typical values of trackbeds (12).

5   CONCLUSIONS

In this paper, the Video Gauge, a high definition optical technique for measuring real-time operational dynamic rail-track displacements has been described. A number of field measurements were conducted in the attempt to verify the applicability and reliability of the Video Gauge. In particular, the dynamic displacement histories of different track components were measured, subjected to various train speeds (40-125 mph) and sampling frequencies varying from 75 to 200 Hz (capture rate in frames per second). From the aforementioned investigation it can be concluded that the Video Gauge helped to:

- Acquire displacement data of rail and sleepers for the conventional ballasted track examined.
- Evaluation of track stiffness based on rail and sleeper displacements.
- Acquire displacement data of rail joints and estimation of track stiffness at rail joints
- Investigation of the degradation rate of transition zones through the measurements of rail and sleeper displacements as well as an estimation of track stiffness on transition zones.

These show that the Video Gauge can serve as a valuable tool for the assessment of track displacements and provide information about potential deterioration rate of track irregularities and transition zones. Investigation of the impact of the ratio of the noise after the wheel passage to the signal amplitude on measurement accuracy is recommended for future studies. Further testing of various innovative trackforms is planned in order to be used for life prediction and behaviour assessment.

REFERENCE LIST

1. Dahlberg T. Railway Track Stiffness Variations – Consequences and Countermeasures. *Int J Civ Eng.* 2010;8(1):1–12.
2. Farritor S, Fateh M. Measurement of Vertical Track Deflection from a Moving Rail Car. TRID. Report, University of Nebraska, USA, 2013.
3. Innotrack. Methods of track stiffness measurements. Report, Deliverable D2.1.11 for Innotrack project, Project no. TIP5-CT-2006-031415; 2006.
4. Burrow M, Priest M, Ghataora G.S, et al. Track subgrade performance and monitoring. In: *Railway Engineering -9th International Conference and Exhibition*. London, UK, 20-21 June 2007.
5. Bowness D, Lock A, Powrie W, et al. Monitoring the dynamic displacements of railway track. *Proc Inst Mech Eng Part F J Rail Rapid Transit.* 2007;221(1):13–22.
6. Murray C. *Dynamic monitoring of rail and bridge displacement using digital image correlation.* Master Thesis, Queen's University, Canada, 2013.
7. Thompson II H., Sussmann TR Jr, Stark TD, et al. Non-invasive monitoring of track system gaps. *Railway Engineering - 13th International Conference & Exhibition*. Edinburgh, UK, 30 June-1 July 2015.
8. Waterfall P, Temple B, Hardwick C, et al. Video Measurement techniques for understanding wheel- induced lateral forces and track component deflections. In: *The Stephenson Conference-Research for Railways*. London, UK; 21-23 April 2015.
9. Liu, X., Markine, V. L., & Shevtsov, I. Dynamic experimental tools for condition monitoring of railway turnout crossing. In: *The Second International Conference on Railway Technology: Research, Development and Maintenance*. Ajaccio, Corsica, France, 8-11 April 2014.
10. Askarinejad H, Dhanasekar M, Cole C. Assessing the effects of track input on the response of insulated rail joints using field experiments. *Proc Inst Mech Eng Part F J Rail Rapid Transit.* 2012 Sep 13;227(2):176–87.
11. Soylemez E, Ciloglu K. Influence of Track Variables and Product Design on Insulated Rail Joints. *Transp Res Rec J Transp Res Board*. 2016 Jan; 2545:1–10. 1.
12. Powrie W, Le Pen L. A Guide to Track Stiffness. Cross Industry Track Stiffness Working Group; UK; August 2016.

APPENDIX B - PAPER 2

Abstract

This paper aims to investigate alternative ways of reducing the deterioration and failure of railway track insulated rail joints (IRJs). Joints deteriorate faster than rail initially due to the structural discontinuity present. This weakness results in both extra displacement as a consequence of applied load and the dynamic force that results as a consequence. Over time this situation worsens as the impacts and applied stresses both damage and soften the ballast and supporting subgrade under the joint. This study initially presents a static finite element model designed to simulate the mechanics of IRJs and a comparison between plain rail and a suspended insulated rail joint under various support stiffnesses. Product design options of reinforced IRJs are then chosen as input variables of the model. Results of the model are compared with field and laboratory data acquired via the Video Gauge, which is a new high-resolution optical measurement technique. Results show that the use of strap rails or more robust I-beam sections in the vicinity of the IRJ to stiffen the support structure can significantly reduce the displacement and the subsequent dip angle seen at an IRJ. This potentially presents a means of improving the IRJ behaviour. Their impact becomes more significant for soft support conditions. Although these results are indicative for new IRJ conditions, field measurements indicate that the magnitude of deflection of IRJs is a result of the structural discontinuity of the rail, the dynamic P2 force, the wheel condition, the degraded ballast and it significantly increases with time under repeated load. Thus, it is recommended that careful field implementation and testing will indicate the effect of an external enhancement on the timely degradation of insulated rail joints.

Keywords
Rail joint, Insulated rail joint, dipped joint, modelling, reinforcement, track

1 INTRODUCTION

The railway system's dependability is based on the rail components' structural integrity. The failure of insulated rail joints (IRJs) is a worldwide problem in railway networks and a major component of the maintenance cost. The mechanical failure of an IRJ can increase ballast degradation and can also impede the electrical integrity of an IRJ thereby causing train detection issues (signalling). IRJs are considered a weak point because of the discontinuity in the stiffness of rail. The main aim of this study was to investigate the effect of external enhancement in the performance of IRJs as a strategy of improved performance of the jointed track. IRJs deflect more than regular plain track because of the lower cross section area, lower section moment of inertia of the fishplate and the elasticity of the insulation layer. This structural discontinuity interacting with the wheel impact load causes a vicious cycle of joint and track degradation. With the passage of a single wheel over the joint, joint anomalies such as bolt looseness and rail height mismatches are caused and with repeated wheel passage rail end wear occurs. The degraded joint provokes large deflections and amplifies the dynamic force induced at the joint. This leads to the acceleration of the track degradation, which in turn provokes a progressive increase on the joint deflection. It was hypothesised by the authors that structural reinforcement of the track structure in the vicinity of the joint could reduce the initial deflection increment to less than or equal to that of the plain rail. Thus, the damage cycle can be reduced. This was shown in this paper by finite element (FE) modelling validated by field measurements using high-precision optical equipment. This paper starts with a literature review describing the mechanics of an insulated rail joint, current track deflection field measurement techniques and previous modelling of IRJs. The accuracy of Video Gauge for measuring the performance of IRJ is evaluated using laboratory testing, then field measurements of plain rail and IRJ are presented. The methodology includes an implicit static finite element model to investigate the effect of structural changes and stiffness on the deflection of standard plain track and of IRJs. The parameters used include the selection of sleeper type, sleeper spacing, stiffness per sleeper end, material properties of rail, fishplate, railpad and endpost, and type of external structural strengthening for a suspended IRJ. As model outputs, rail deflection and dip angle of the IRJ were evaluated. A comparison was conducted between the FE model and the field data, followed by a discussion of the results.

1.1 Mechanics of IRJ

The main purpose of a rail joint is to separate electrical circuits in rails and turnouts whilst joining two pieces of rail where continuously welded rail is not possible. This is achieved through the use of joint bars (fishplates), fastened through the web of the rail with bolts. Insulated rail joints (IRJs) are critical components of railway signalling infrastructure where sections of track are separated into separate blocks so track circuits to be used for train detection. While a purely mechanical bolted joint just comprises fishplates and bolts, an IRJ includes material fitted between the rail ends made of a non-conductive material (endpost) as well as an insulated lining to separate the fishplates from the rails all to maintain electrical separation of the adjoining rails (see Figure 1). Sometimes IRJs are also glued to increase joint robustness.

Although the fishplates are designed to offer a similar shear capacity to the parent rail section they support, a bolted joint arrangement remains weaker in resistance to bending. As a consequence, rail joints deflect more than adjacent continuous rails on nominally the same support conditions. This also means that an increased dynamic force is generated as a wheel passes over the joint and over time, a ballasted support structure will accrue more damage and the deflection at a joint is usually found to progressively increase until maintenance limits are reached or failure occurs.
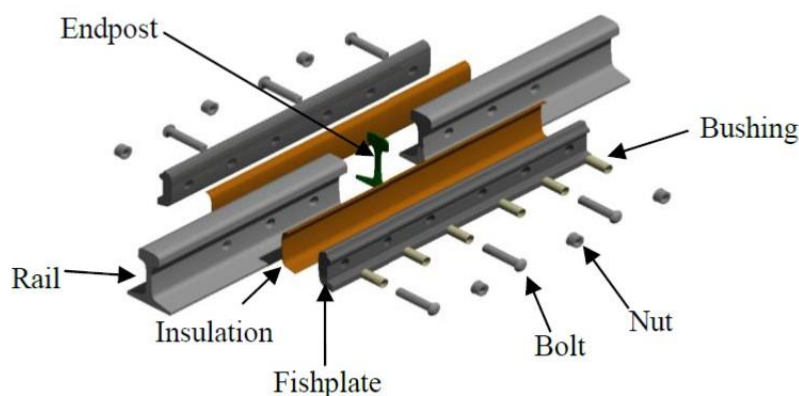

Figure 1. View of IRJ assembly (amended from [1])

In a standard UK fishplated joint, the moment of inertia of the joint fishplates is only 29% of that of the parent rail [2]. This stiffness discontinuity results in around 90% of the bending moment being transferred across the joint [3]. This can be improved by modifying the design of the joint or the support conditions; however, the weakness in bending is still present. In addition, it has been found that the dynamic impact from wheel in a rail joint is three times larger than the static wheel load [4]. The service of the rail joints varies depending on the traffic loading and frequency; Australian research has claimed that it can be only 50 MGT of freight traffic [5]; American research has claimed 200 MGT with replacement requirements in a period of 12-18 months with costs of $10,000 per mile per year [4], which is significantly less than the service life of other rail components that withstand up to 1000 MGT [6], whereas failures of IRJ cost Network Rail (UK) £10 millions in a two year period [7].

An IRJ can fail mechanically, electrically or both. Mechanical (structural) failure occur either in the fishplates, rail, bolts or epoxy [8] due to high static, dynamic and fatigue loads that weaken or cause the total failure of rail joint components. Electrical failure is caused when the electrical isolation between the two adjoining rails is lost and can be caused either by a mechanical failure or by other factors such as lipping or contamination.

Additional to the vertical, longitudinal and lateral forces applied in the track system [9, 10], the P2 force represents the total vertical force from the combined static gravity load on the wheel

and dynamic force from the unsprung masses due to any variations in the alignment of the rail including vertical track irregularities such as a rail joint.

P2 forces can cause rapid deterioration of track quality. Key parameters for its calculation are the train speed, the size of the defect, the track stiffness, the bending stiffness of the rail and the mass of the rail and the wheelset. A maximum permissible value of P2 has been defined at 322 kN (static load + dynamic increment) for a defined defect angle of 20 mrad [11].

1.2   Previous experimental testing of IRJ

The evaluation of IRJ performance in the laboratory and in the field has been assessed in the past by strain gauges and impact load detectors [1, 4, 12-15]. Results included time histories of bending, shear, lateral shear strains and wheel-rail forces. The literature shows that no work has been conducted in measuring the displacements of rail joints and interpretation of the IRJ displacement in relation to the plain rail and underlying support stiffness or structure. For this reason, measurement techniques exploited for track deflection will be applied to identify IRJ deflection.

1.3   Review of current track deflection field measurement techniques

A wide range of techniques have been used in the past decade to measure the deflection performance of railway track during the passage of a train. The following methods have been identified [16]:

- Linear variable displacement transducers (LVDT) [17]
- Geophones [18]
- Laser deflectometer [19]
- Remote video monitoring using PIV and DIC [20]

1.4   The Video Gauge

In this paper the Video Gauge (VG), previously used only once [21], is used for real-time in-situ high resolution measurements. It is based on Digital Image Correlation (DIC) principles and Video Extensometry (VE). DIC is based on pattern recognition techniques and image pixel tracking. VG exploits sub-pixel pattern recognition algorithms that enable ultra-high resolution measurements of displacement, strain and rotation to be made. It supports the use of multiple cameras for 2D or 3D measurements. Frame by frame comparison allows for measurement of deflections. The VG system enables data of high quality and quantity and offers substantial time and cost saving when compared with traditional instrumentation sampling [16]. Frequencies, higher than any other technique (up to 300 Hz) can be reached whereas sampling frequencies more than 300 Hz can be achieved by using expensive higher frame rate cameras.

The suitability of the VG for measuring sleeper and rail modules has been shown in the past [22], but never for measuring rail joints. For the purposes of this research the efficacy and accuracy of the VG for measuring rail joints in the field was evaluated first by laboratory measurements (see section 2.1).

1.5   Modelling of IRJs

Most Finite Element Modelling (FEM) of IRJs [23-25] comprises FEM of the ratchetting (plastic strain accumulation) in the rail head edges at the discontinuity between the rail ends in the case of a mechanical or an insulated rail joint. Recommendations have been restricted to fishplate and endpost material/size optimisation for improved rail joint performance. Rail deflections and stresses in the epoxy layer with different sleeper and fishplate dimensions with centred and off-centred loading have been investigated [26]. Maximum rail displacements were found in a range of 1.7-3.1 mm. Few authors have looked at the problem from a holistic point of view by looking at the impact of the track support structure on a rail joint. The range of maximum rail deflection for continuous rail was presented at 1-3.3 mm (0.13 in) and 1.1-4.3 mm (0.17 in) for a suspended IRJ for various support conditions [27]. Finally, it was recently shown by a 2D vehicle-track model that the impact force P1 that is mostly causing the track degradation due to the accordance of frequencies with those of the track, is greatly influenced by the joint angle, the mass of the rail and the mass of the wheelsets, whereas the peak force P2 is mainly affected by the support stiffness at the joint angle apart from the mass of the wheelset and the railpad stiffness [28].In the past the track deflection for various wheel loads and track conditions have been measured. The range of rail displacements measured varies for different measurement techniques, different types of track and trains. For example, 1-7 mm of rail deflection has been measured with PIV video cameras, LVDTs and geophones [18, 29]. Filtered rail displacements of post-processed geophones output data have been found lower than absolute values from video techniques. A range of 2 -10 mm of rail displacement has been identified for gap sizes 0 -30 mm between the sleeper and the ballast (for singular or multiple unsupported sleepers). Perfect track has been found to deflect in a range of 1.5 - 3 mm whereas degraded ballasted track has been measured to deflect up to 10 mm [29]. Nevertheless, little work has been conducted into the effect of the support structure on the displacement of IRJs. The majority of previous studies have been focused in experimentally measuring the impact wheel forces and strains in IRJs for validating FE models aiming to reduce the localised rail fatigue (plastic strain) by looking at micro scale at the rail joint, whereas the IRJ degradation is progressively increasing due to the increased damage to the underlying structure. IRJs displacements have been evaluated only by numerical models (1 - 4.5 mm for various track conditions) [26, 27]. There is no current literature showing the effect of structural enhancement of the performance of rail joints by using numerical modelling of joints compared to plain track validated with accurately assessed field displacements.

2 EVALUATION OF PLAIN RAIL AND RAIL JOINT DISPLACEMENTS

The applicability of Video Gauge (VG) for measuring IRJs was validated in the laboratory. The deflection increment of IRJs was evaluated in both laboratory and field conditions in order to validate the numerical model.

2.1 Laboratory validation

A 4-bolt standard (wedge fit) glued IRJ, rail joint (CEN 60) of 3 m length was tested in a four-point bend under cyclic loading at a frequency of 1 Hz. The joint endpost was centrally positioned between two vertical hydraulic actuators, (separation distance 600 mm) and applied a synchronised vertical cyclic force onto the rail. The displacement was recorded by the VG at a frequency 66.36 Hz from a distance of 800 mm using a lens of 16 mm focal length. This resulted in a horizontal field of view 550 mm giving a resolution of 3.7 pixels/mm. A LVDT was also positioned on top of the endpost for comparison with the VG values in order to check the accuracy of the VG. The loading used (120 – 404 kN) exceeds the maximum static wheel load on UK infrastructure (25 tonne axle load) and approximates the vertical dynamic force generated by the static wheel load and low frequency dynamic [P2] forces based on recent research [2]. Figure 2 shows a comparison between the LVDT and the VG data. The excellent correlation of the results indicated that the Video Gauge was successful in measuring accurately the complex dynamic deflection histories of plain rail and rail joint.
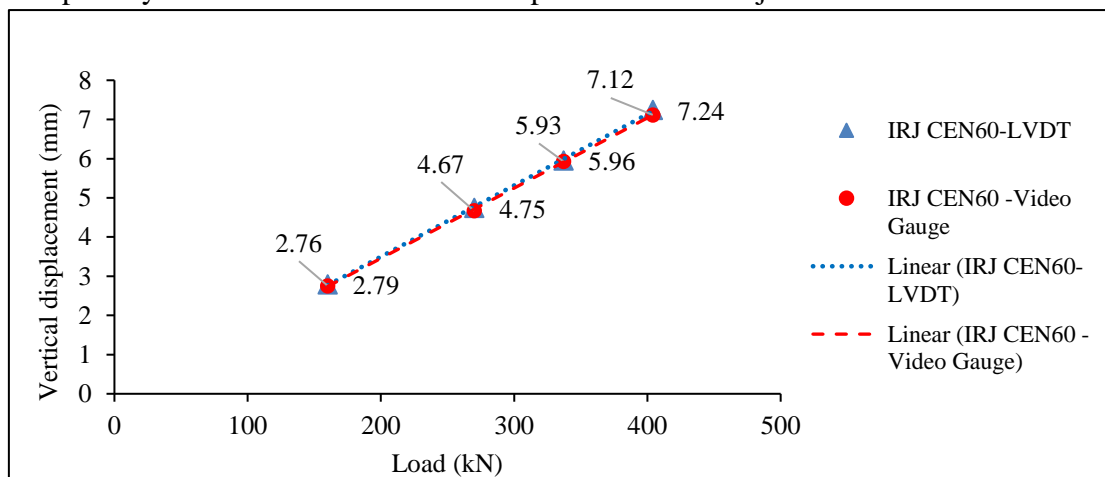
Figure 2. Comparison between Video Gauge and LVDT displacement values for IRJ CEN 60 at varying load cases

2.2 Field measurements

The deflection of a 6-bolt rail joint and the adjacent plain rail were measured on a live railway line at Winsford (UK). Two high speed cameras were used recording at 75 fps from a distance 5.5 m. Lenses of focal length 75 mm and 50 mm were used in order to provide a field of view of 2 m. Five different passenger trains were measured, (two Desiro and three Pendolino type trains). From the time history, the speed of each train was calculated. The Desiro trains are

lighter (11 tonnes axle load, observed speed 57 - 115.5 mph) than Pendolino trains (15 tonnes axle load, observed speed 125 mph). Figure 3 shows a typical time-displacement plot during the passage of an 11-car Pendolino at 125 mph. Each vehicle consists of 4 axles. The positive displacement is uplift of the rail, ahead of or behind the wheels. By taking into account the maximum displacement value captured for each train, a displacement trace of each measurement point was plotted (see Figure 4). Distance is measured horizontally (x=0 m) from the centre of the IRJ along the parent rail.
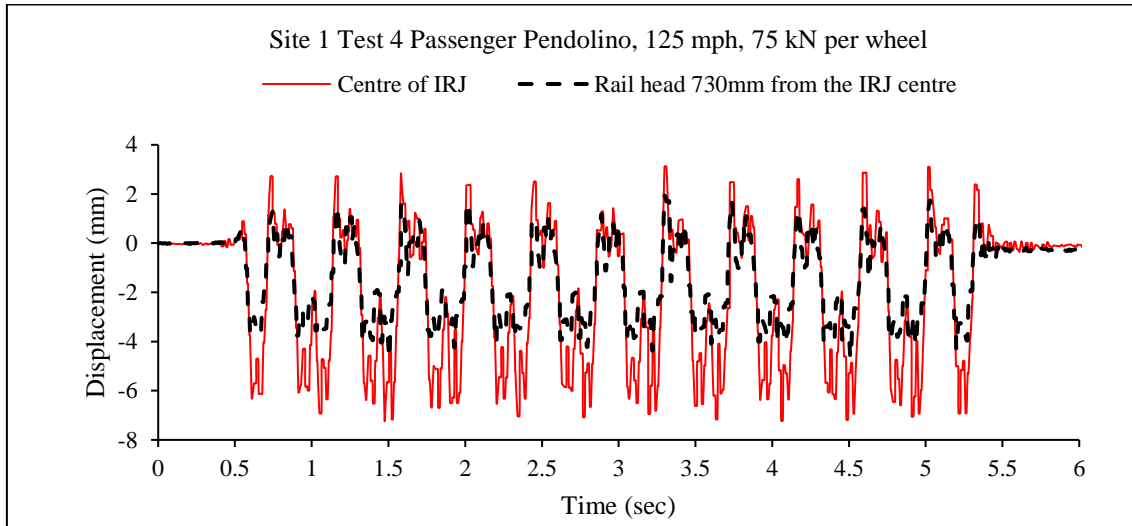

Figure 3. Time-displacement plot. Comparison between IRJ and rail due to passage of passenger train at 125mph.
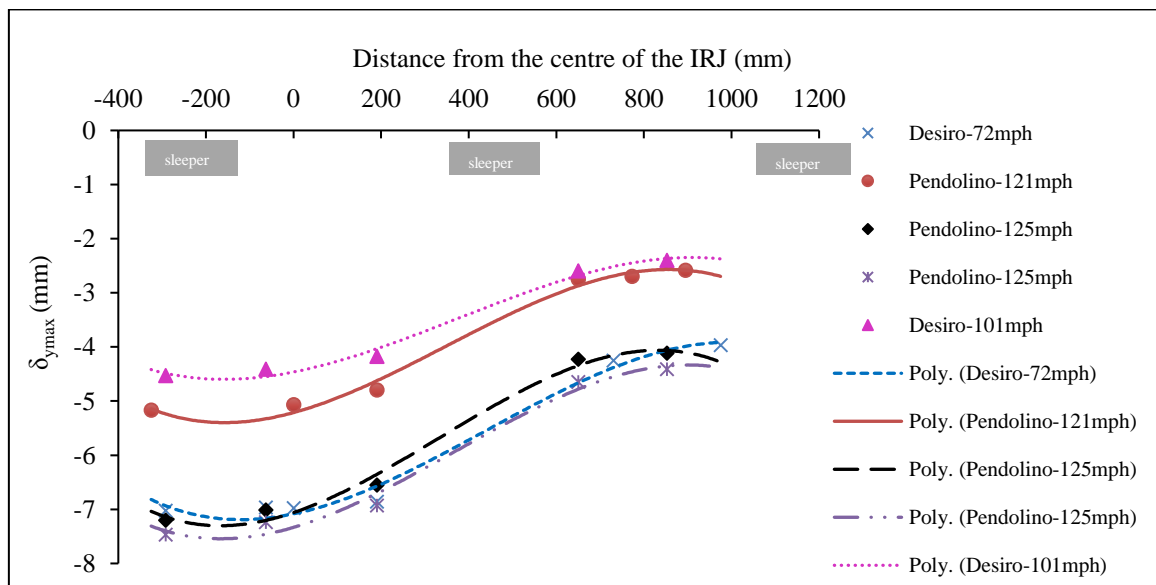

Figure 4 Maximum displacements of rail head at various distances from the centre of the IRJ.

By looking at the results, it can be seen that there are local differences in the field measured displacements. This can be attributed to three main causes; firstly, the fact that absolute maximum displacement values have been plotted rather than an average or RMS value of all peak values around a wheel passage; secondly the fact that the sampling frequency (75 Hz) may not be adequate to capture the maximum deflection at the train speed; thirdly the wheel impact and the existence of potential wheel flats in some trains may have caused an increase in the P2 force, increasing the resulting displacement. For this reason, the comparison between the averages of peak displacements for each wheel between three different train types and speeds for the two track positions is presented in Table 1. The results presented are typical of other tests of IRJs undertaken at other site locations under similar train speeds. Differences between trains of similar axle load are attributed to wheel impact factors.

Table 1. Comparison of average of peak displacements between centre of IRJ and plain track 730mm away from the IRJ for various trains and speeds.

Position	Plain rail	IRJ centre
Distance from the centre of IRJ	730 mm	0 mm
Average of peak vertical displacements (mm)		
Pendolino at 125 mph	3.86	6.58
Desiro at 101 mph	2.36	4.23
Desiro at 72 mph	3.28	5.8

The table shows typical plane rail displacements between 2.36 and 3.86 mm and larger joint deflections of 4.23 to 6.58 mm as would be expected. The values agree with the literature.

3   FINITE ELEMENT ANALYSIS (FEA) MODEL

A numerical model was created that represent the plain track and the rail joint deformations. A basic plain rail model was first constructed for the appropriate track geometry. An investigation of the appropriate track length to be simulated was conducted and a ten-sleeper long track was selected as optimal after looking at the load distribution pattern. The sleeper deformation was investigated in an initial phase with different types of underlying support stiffness. The plain track model was compared with a model that included a rail joint in the middle of the track length. Reinforcement with strap rails was investigated in plain track before being applied to the same model with an IRJ added. By varying the underlying support stiffness, the model was used to show the effect of structural changes in the track deflection.

ANSYS Mechanical was used to perform 3-dimensional linear static structural analysis. All components of the track assembly were modelled as solid bodies. Table 2 describes the material properties assigned to the different components. The FE model included two CEN 56 rails of moment of inertia 2320.0 cm^4 (length 6500 mm) in a length of ten sleepers (see Figure 5). The

sleeper spacing was 650 mm and track gauge was 1435 mm. The rails are sitting on rail pads of 10 mm thickness of medium stiffness 150 kN/mm. An endpost of thickness 6 mm made of polyurethane was used as insulation layer between the rails with a joint. Fishplate of length 914 mm and sectional area A=3967.77 mm^2, used in 6-bolt IRJs, was used. Bonded contact was applied between all components except the rail-endpost interface where frictional contact with a coefficient 0.2 was applied. Concrete G44 sleepers were used with the appropriate geometry [30]. "*Monoblock sleepers are always packed over an area on either side of the centre of the rail and ideally there should be no pressure between the sleeper soffit and the ballast in the concrete section*" [3]. For this reason the effective length of 500.1 mm at each side of the bottom surface of the sleeper was used for the ballast pressure that is equal to Lp=(L-c)/2, where L is the sleeper length and c the rail seat spacing. The support stiffness caseswas applied through spring elements in the effective length in both sides of the load position. Three support stiffness cases of 30, 115 and 200 kN/mm were investigated in an initial modelling phase assessed from recent literature [31, 32]; further cases with degraded support stiffness or sand 15 kN/mm were subsequently added. A minimum dynamic sleeper support stiffness of 30 kN/mm per sleeper end has been defined for a renewed trackbed and of 60 kN/mm for a new trackbed [9]. A single static 125 kN force was applied in the vertical direction on the centre of each rail (see Figure 5). The load represents the maximum UK static load in UK track infrastructure. The load was applied in all cases as a pressure in the centre of the railhead. The load application area was selected by taking into account the ellipsoidal area of a wheel –rail contact patch according to the Hertz theory and after mesh optimisation. The plain rail was modelled for single load in the mid-span between two sleepers allowing comparison with the suspended IRJ. Body meshing with 5 mm element size was applied in the endpost and in the rail section adjacent to the joint (622 mm on both sides of the endpost). A refined meshing (see Figure 5) with maximum element size 30 mm was applied in the four supporting sleepers around the joint. (Note, in this study the elastic linear behaviour of the railpad controls partially the rail uplift whereas the spring behaviour of the rest of the fastening system was not considered as critical for the structural evaluation of the IRJs.) The bolt/bonded interface was not of direct interest as the IRJ was not tested to destruction. Bolt connections can trigger failure in degraded joints but the aim in the model was to simulate joints in a non - degraded state. Elastic constitutive law was used as the induced stresses due to the static load are not in excess of yield limits. Thus, material behaviours beyond yield were not of interest and an elasto-plastic failure criterion was not needed.

3.1 Model variables

Table 3 presents the cases modelled: a) plain track, b) suspended IRJ (SUS-IRJ), suspended IRJ enhanced with strap rails (SR SUS-IRJ), d) suspended IRJ strengthened with beams (BS SUS-IRJ). The reinforcing strap rails are rail sections with second moment of area I=2320 cm^4 positioned on top of the four central sleepers surrounding the IRJ. The reinforcing effect of a larger steel beam section with second moment of area I=3227 cm^4, (39% stiffer of that of the strap rail) and of a size that can fit in the track geometry was also evaluated (see Figure 6 and Figure 7). Outputs of deflection rail dip angle and strain were produced.

Table 2. Material properties in the FEA model

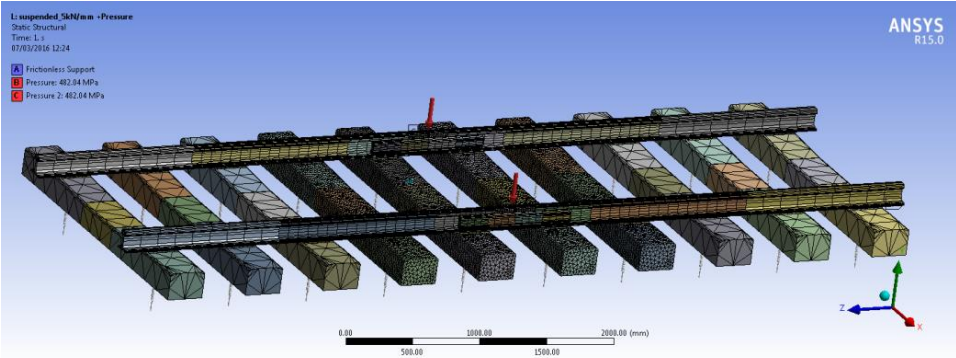| Material properties						
Component	Material	Stiffness	Modulus of Elasticity	Poisson's ratio	Density	
		k	E	v		ρ
Rail/Fishplate	Structural steel		200 GPa	0.3	7850 kg/m³	
Railpad		150 MN/m	38.265 MPa	0.3	300 kg/m³	
Sleeper	Concrete		30 GPa	0.18	2300 kg/m³	
Endpost	Polyurethane		20.7 MPa	0.3	1200 kg/m³	

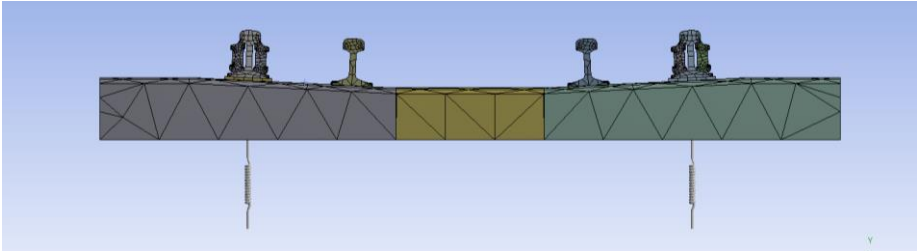Figure 5. Geometry and meshing of the FEA model

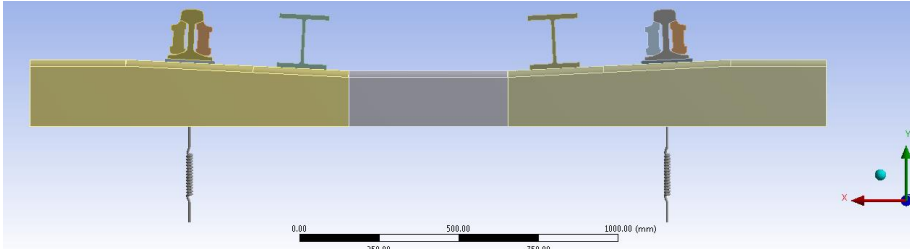Figure 6. IRJ strengthened with strap rails FEA model

Figure 7. IRJ strengthened with I beams FEA model

Table 3. Parametric study cases

Configuration	Sleeper type	Second moment of area of enhancement	Stiffness per sleeper end (kN/mm)
Plain track	Concrete		5, 15, 30, 115, 200
Suspended IRJ (SUS-IRJ)	Concrete		5, 15, 30, 115, 200
Suspended IRJ enhanced with strap rails (SR SUS-IRJ)	Concrete	I_{xx}=2320 cm^4	5, 15, 30, 115, 200
Suspended IRJ strengthened with I beams (BS SUS-IRJ)	Concrete	I_{xx} =3227 cm^4	5, 15, 30, 115, 200

3.2 Verification of compressive stress on the rail head

The maximum Von-Mises stress on the rail head for the SUS-IRJ for the case of support-stiffness 30 kN/mm per sleeper end was measured to 1157.7 MPa. This value correlates with the values (1000-1250 MPa) found in the literature [23-25].

3.3 Model correlation with experimental data

From the FEA model of plain rail for the stiffness case of 30 kN/mm per sleeper end the maximum deflection in the rail head was measured at 2.13 mm (see Table 4). This correlates with the plain rail deflection measured by the VG in the laboratory at 120 kN (2.32 mm). Field measurements for plain rail gave a range of values 2.36 mm-3.86 mm for load cases 55-75 kN (see Table 1). The soft (degrading) support conditions reducing from 30 kN/mm until 5 kN/mm per sleeper end gave a range of rail vertical deflections between 2.13 mm and 6.78 mm respectively. (Note, the supporting stiffness can vary on site depending on the trackbed quality underneath each measuring point. In addition, the existence of voids in the interface of sleepers and ballast can cause non-uniformity in the rail deflection under same type of soil.) VG measurements gave a range of 4.23 mm to 6.58 mm for IRJ deflections in the field for varying speeds and train types. The FE model showed that a suspended IRJ deflects from 2.67 mm until 8.03 mm for support stiffnesses 30 kN/mm until 5 kN/mm. The agreement between the experimental and numerical data shows the validity and robustness of the FE model to validate its suitability for further investigation on IRJs effects under various wheel loads.

The verified FE model was then developed further to identify the effect of track structural changes on the IRJ deflection.

4   FEA RESULTS

A typical deformation plot of the suspended IRJ with reinforcing strap rails is illustrated in Figure 8. Figure 9 illustrates the typical displacement plot for the suspended IRJ for various support stiffnesses. Table 4 shows the maximum deflection and the calculated dip angle for

each case. The effect of strap rails and I beam strengthening on the displacement and dip angle of the suspended IRJ under varying stiffness is shown in Figure 10 and Figure 11 respectively.

The dipped rail joint is taken into account in numerical models as a form of wheel–rail irregularity. An effective length of 500 mm on either side of dip is projected as the effective length of the irregularity of a dipped rail joint [33] . This is different to what industry considers; the effective length for the angle of the dipped RJ measurement is 125 mm on each side [3].
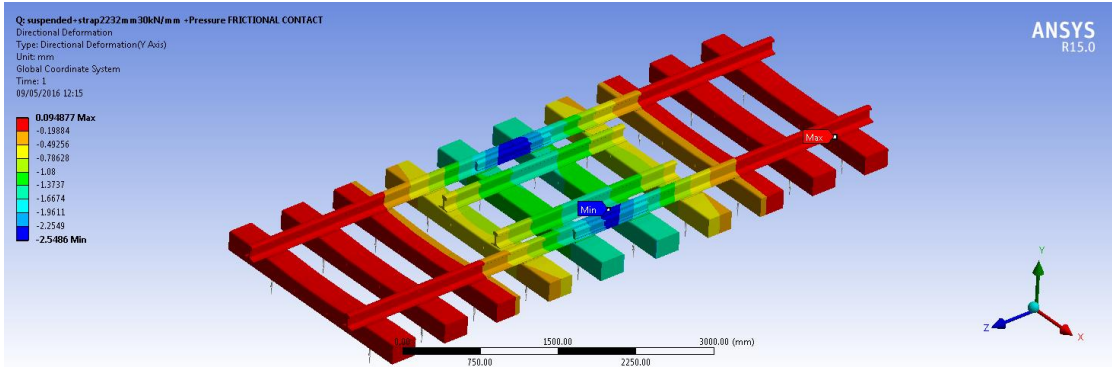
Figure 8. Deformation of suspended IRJ enhanced with strap rails (SR SUS-IRJ) with 30 kN/mm support stiffness per sleeper end.
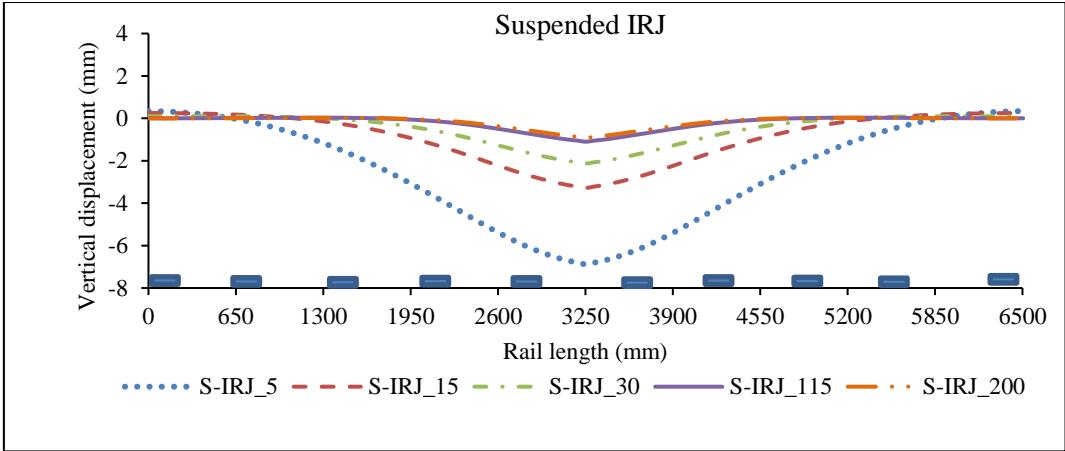
Figure 9. Deformation of suspended IRJ with stiffness variation.

Table 4. Deformation results for plain rail and IRJs modelled for varying support stiffness.

Stiffness per sleeper end (kN/mm)	200	115	30	15	5
	Maximum vertical displacement (mm)				
Plain rail	0.93	1.11	2.13	3.26	6.78
SUS-IRJ	1.28	1.49	2.67	3.97	8.03
SR SUS-IRJ	1.22	1.42	2.45	3.57	7.01
BS SUS-IRJ	1.19	1.38	2.37	3.45	6.8
	Total dip angle (mrad)				
SUS-IRJ	3.57	3.72	4.31	4.79	5.88
SR SUS-IRJ	3.5	3.61	4.04	4.35	5.04
BS SUS-IRJ	3.37	3.47	3.84	4.11	4.7

Figure 10. Effect of reinforcement on displacement of suspended IRJ for varying support stiffness

Figure 11. Effect of enhancement on total dip angle of suspended IRJs

5   DISCUSSION OF RESULTS

Both laboratory and field measurements verify that the rail joint deflects more than plain rail. The order of magnitude of the VG measured plain rail deflections are in agreement with literature review findings [18, 20, 29]. A comparison between the FEA results of plain rail and SUS-IRJ with the field measurements is depicted in Figure 12. The FE model was run with a wide range of support stiffness to capture the li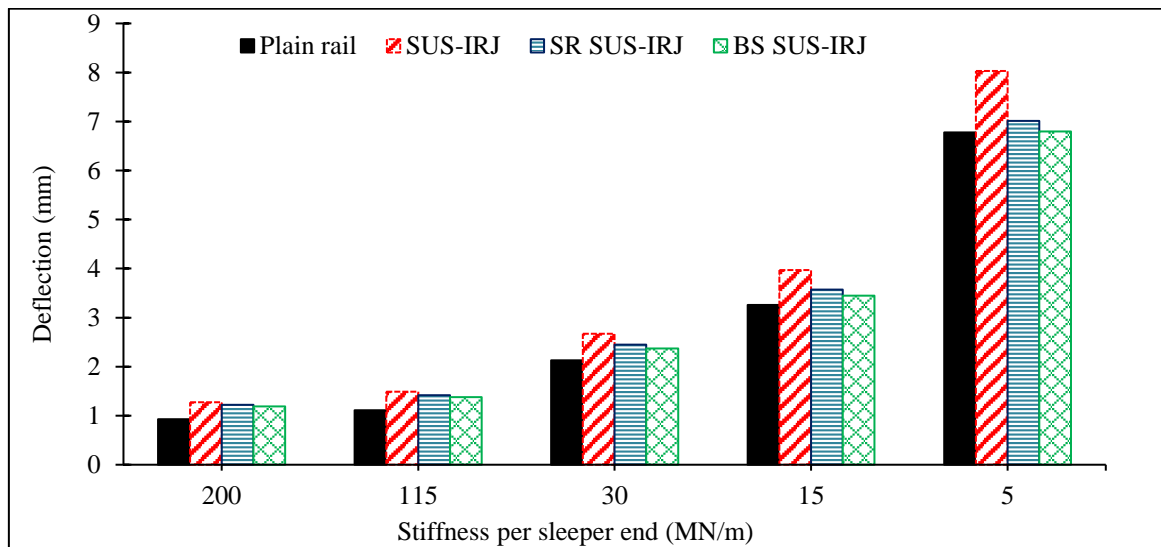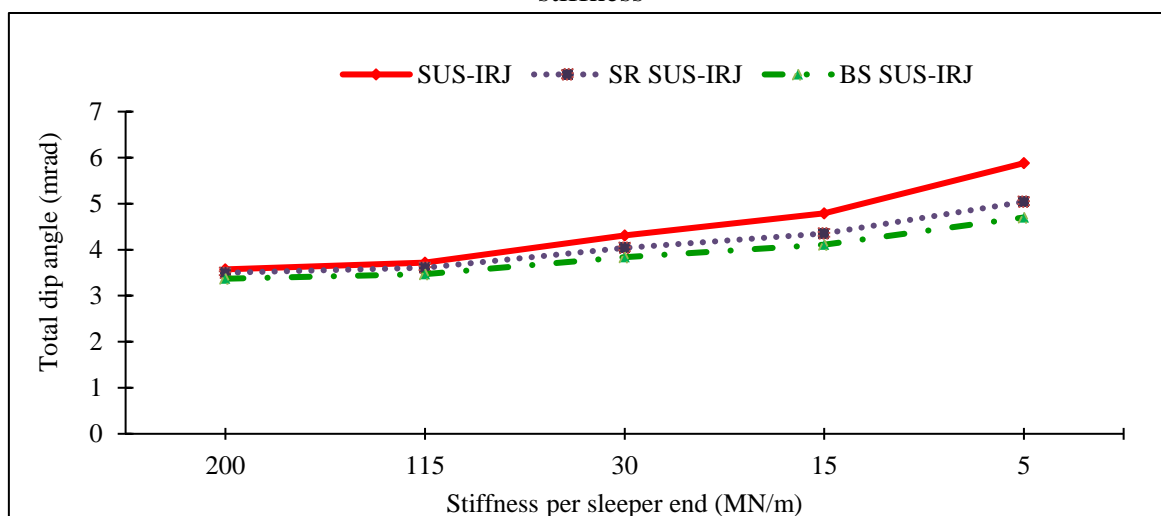kely range of support conditions seen in the field. The soft support conditions from 30 kN/mm until 5 kN/mm per sleeper end gave a range of rail vertical deflections between 2.13 mm and 6.78 mm respectively showing comparability. The actual stiffness of the track substructure layers in the field is not known so a comparison of the absolute values cannot be made.
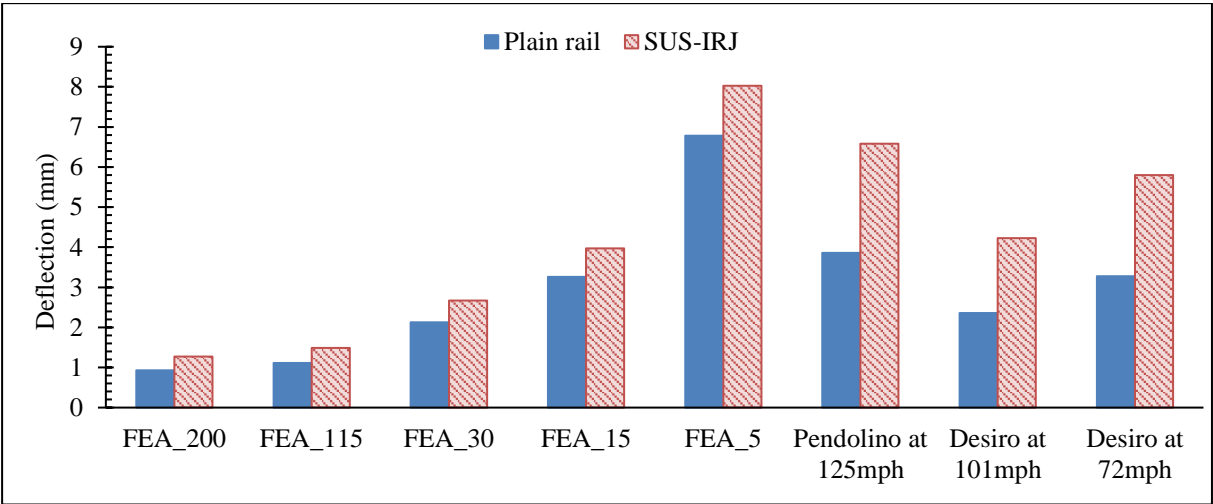
Figure 12. Comparison between FEA models and field deflection data for plain rail and SUS-IRJ.

The magnitude of FEA IRJ deflections are in agreement with previous research [26, 27]. All FE models showed that the deflection of a SUS-IRJ varies depending on the support stiffness. They proved that the additional deflection in a IRJ compared to that of a reference rail is lower when the model includes uniform support stiffness along the rail length whereas this increases with the degradation of the track underneath the joint. The current study investigated the effect of uniform degraded track support whereas the stiffness of a discrete number of sleepers underneath the joint was altered in other research [27].

An interpretation of the FE study indicated that the softer the support conditions, the higher the additional deflection an IRJ accumulates compared to that of a reference rail. However, the relationship between the deflection increase and the stiffness decrease is not linear. For the case of 30 kN/mm per sleeper end, the SUS-IRJ deflects 25% more than the plain rail with a difference of 0.54 mm. For softer support conditions (15 kN/mm) the additional deflection is 0.71 mm whereas the difference decreases for stiff support conditions. The FE model gave a

range from 2.67 to 8.03 mm for the deflection of a suspended IRJ for a support stiffness decreasing from 30 to 5 kN/mm that is in good agreement with the VG field data 4.23-6.58 mm. By taking into account the higher degradation rate of the ballast beneath an IRJ due to the cycle of deterioration of an IRJ and track conditions (due to the dynamic amplification of the wheel load at the joint) increased dynamic deflections can be found in the field. It should be noted that discrete ineffective support conditions in FEA (gaps in sleeper–ballast) interface in discrete sleepers underneath the IRJ) could increase the IRJ deflection.

In addition to the displacement, the dip angle of the suspended IRJ was calculated from the FE model for an effective length of 125 mm from each side of the centre of the IRJ [3]. This ranged from 3.57 mrad to 5.88 mrad for stiffness 200 kN/mm to 5 kN/mm per sleeper end (see Figure 11). The total dip angle was calculated from the VG field data for a number of cases. The values 1.26 - 4 mrad were found for speeds 57 – 125 mph. The dynamic P2 forces were calculated as 58.5 - 108.4 kN and the load factors P2/F wheel were calculated to the range of 1.1 - 1.45. The numerical data are close to the field data that further validates the FE model.

The numerical model indicates that the dip angle for the SUS-IRJ increases at a lower rate than that of the displacement under independent support in a non –linear relationship. For 50% decrease in the support stiffness (from 30 kN/mm to 15 kN/mm per sleeper end) the maximum displacement of a SUS-IRJ increases 49% (from 2.67 mm to 3.87 mm) whereas the dip angle 11% (from 4.31 mrad to 4.79 mrad). For more degraded support conditions by altering the support stiffness from 15 kN/mm to 5 kN/mm the maximum displacement is doubled from 3.97 mm to 8.03 mm whereas the dip angle increases 23%. The magnitude of total dip angle of non -degraded IRJs that was used as input in previous research ranges from 1 to 14 mrad, and it has been assessed experimentally using various dip lengths from 0.1 m to 1.4 m [34]. By using the P2 force equation [11], the P2 force changes linearly with the static load, the speed and the dip angle and non- linearly with the track stiffness [34]. This means that by using the same equation the dip angle correlates non- linearly with the track stiffness as the current study indicates.

The effect of strap rail is greatest for the softer support conditions and less for stiffer support conditions. The strap rails decrease the deflection of the SUS-IRJ by 8% in the case of 30 kN/mm support. The SR SUS-IRJ deflects 15% more than the plain rail at 30 kN/mm, 9.5% more than the plain rail at 15 kN/mm, and 3% more than the plain rail at 5 kN/mm. However, the SR SUS-IRJ deflections are still higher than the deflections of plain rail for all support cases (Figure 10).

The strap rail reinforcement has a significant impact on the total dip angle. The rails decrease the total dip angle of the SUS-IRJ by 6% for the standard support-stiffness case (30 kN/mm), 9% for medium support conditions 15 kN/mm and 14% for softer support conditions (5 kN/mm) as shown in Table 4. This range follows the rate of displacement decrease due to strap rail enhancement.

The use of two standardised steel I beams has a higher effect on the improvement of the SUS-IRJ performance due to the 39% higher second moment of area. The BS-SUS IRJ deflects 11% less than the SUS-IRJ and 11% more than the plain rail for of 30 kN/mm support. For the softer support stiffness (15 kN/mm) the BS SUS-IRJ deflects 13% less than the SUS-IRJ and 6% more than the plain rail. The use of specific steel beams (that can easily be found in the steel industry) can improve the IRJ performance but could constitute a more expensive solution. The beam strengthening decrease the total dip angle 11% for 30 kN/mm/sleeper end, 20% for very soft conditions (5 kN/mm) whereas its effect is less significant for the stiff support. These relationships are depicted in Figure 11. These results clearly show the deflection can be reduced and life expectancy of joints can be increased by use of an external reinforcement.

Further investigation of the fastening system is required in order for such a beam to be connected to timber or concrete sleepers. In contrast, strap rails can be easily connected to timber sleepers through specific spikes. Precast concrete sleepers already exist in the rail industry with a fastening system in the required position for adding strap rails. The fact that the strap rails are already simply used in the rail industry in several cases such as transition zones, switches and in expansion joints facilitates the simple field implementation of a reinforced IRJ into the rail industry's specifications, as the additional load they transfer into the sleepers has been previously approved.

6   CONCLUSIONS

A validated static numerical model capable of simulating plain rail and IRJ responses such as displacements, and total dip angle was created. The model was used to evaluate if external structural strengthening can reduce the deflection, and hence the deterioration level of an IRJ, so that the progressive deterioration in time of the ballast beneath the joint can be avoided.

The conclusions are summarised as follows:

- IRJs deflect more than plane rail and lead to increased local rates of trackbed degradation.
- The deflection of an IRJ is influenced measurably by the support conditions and by the dynamic increment of the generated P2 force regarding the speed and vehicle characteristics. The train type and the axle load affect the deflection.
- The decrease of deflection does not have a linear correlation with the stiffness increase.
- Use of strap rails reduces the deflection of a suspended IRJ. This improvement still makes the suspended IRJ deflect more than the plain rail. However, the strap rails are recommended as a cost-effective external reinforcement for maintaining the IRJ performance over time.

- Use of 39% stiffer I-beam sections reduces the deflection of a suspended IRJ to a greater level than that achieved by strap rails. More robust beams can lower the deflection of IRJ to a level similar to that of plain rails.
- The effect of external reinforcement on the reduction of displacement and dip angle of an IRJ is more critical for soft support conditions.
- The structural strengthening reduces the total dip angle of a suspended IRJ for all support conditions by a significant level.
- The total dip angle has not a linear correlation with the stiffness increase.

ACKNOWLEDGEMENTS

REFERENCES

1. Soylemez E, Ciloglu K. Influence of Track Variables and Product Design on Insulated Rail Joints. *Transp Res Rec J Transp Res Board*. 2016 Jan; 2545:1–10. 1.
2. Beaty P. *Experimental Testing Procedures to Investigate and Improve Insulated Rail Joint Design and Life Cycle*. MSc Thesis, University of Sheffield, UK; 2014.
3. Cope GH. *British Railway Track: Design, construction and maintenance*. 6th ed. Cope GH, England: Permanent Way Institution; 2001.
4. Akhtar M, O' Connor T, Davis D. Revenue service evaluation of advanced design insulated joints. In: *AREMA 2008 Annual Conference*, Salt Lake City, Utah, USA, September 21-24 2008.
5. Dhansekar M, Bayissa W. Review of Insulated Rail Joints. Report, CRC for Rail Innovation, R3.100; 2009.
6. Zarembski AM, Euston TL, Palese JW et al. Use of track component life prediction models in infrastructure management. In: *AusRAIL PLUS 2005*, Sydney, Australia, 22-24 November 2005.
7. Beagles AE, Beaty P, Fletcher DI et al. Insulated rail joint enhancement: testing and analysis. In: *Institution of Mechanical Engineers. The Stephenson Conference: Research for Railways,* London, UK, 21-23 April 2015.
8. Charlton ZI. *Innovative Design Concepts for Insulated Joints*. MSc Thesis, Faculty of Virginia Polytechnic Institute and State University; 2007.
9. GC/RT5021:2011. Railway Group Standard. Track System Requirements.
10. BS EN 1991-2:2011. Traffic loads on bridges.
11. GM/TT0088:1993. Permissible Track Forces for Railway Vehicles.

12. Askarinejad H, Dhanasekar M. Minimising the failure of rail joints through managing the localised condition of track. In: *Railway Engineering Conference 2015*, Edinburgh, UK, 30 June-1 July 2015.

13. Askarinejad H, Boyd P, Dhanasekar M. On-Track Testing of Insulated Rail Joints. Report No R3.100 (Previous BT17), CRC for Rail Innovation, Queensland University of Technology, Australia; 4 May 2011.

14. Askarinejad H, Dhanasekar M, Cole C. Assessing the effects of track input on the response of insulated rail joints using field experiments. *Proc Inst Mech Eng Part F J Rail Rapid Transit*. 2012 Sep 13;227 (2):176–87.

15. Bandula-Heva TM, Dhanasekar M, Boyd P. Experimental Investigation of Wheel/Rail Rolling Contact at Railhead Edge. *Exp Mech*. 2012 Dec 11;53 (6):943–57.

16. Gallou M, Temple B, Hardwick C, Frost M, El-Hamalawi A. Applicability of Video Gauge for the assessment of the track displacement. In: *The Stephenson Conference: Research for Railways*, London, UK, 25-27 April 2017.

17. Zakeri JA, Abbasi R. Field investigation on variation of rail support modulus in ballasted railway tracks. *Lat Am J Solid Struct*. 2012;9:643–56.

18. Bowness D, Lock A, Powrie W, Priest J, Richards D. Monitoring the dynamic displacements of railway track. *Proc Inst Mech Eng Part F J Rail Rapid Transit*. 2007 Jan 1;221 (1):13–22.

19. Innotrack. *Methods of track stiffness measurements*. Report, RSSB, Report no.TIP5-CT-2006-031415; 2006.

20. Murray C. *Dynamic monitoring of rail and bridge displacement using digital image correlation*. Master Thesis, Department of Civil Engineering, Queen's University, Kingston, Ontario, Canada; 2013.

21. Liu X, Markine V, Shevtsov I. Dynamic experimental tools for condition monitoring of railway turnout crosisng. *The Second International Conference on Railway Technology: Research, Development and Maintenance*, Ajaccio, Corsica, France; 8-11 April 2014.

22. Waterfall P, Temple B, Hardwick C, Sharam J, Plumb A. Video Measurement techniques for understanding wheel- induced lateral forces and track component deflections. *The Stephenson Conference-Research for Railways*. London, UK; 21-23 April 2015.

23. Mandal NK, Peach B. An Engineering Analysis of Insulated Rail Joints : A General Perspective. *Int J Eng Sci Technol*. 2010;2(8):3964–88.

24. Sandström J, Ekberg A. Numerical study of the mechanical deterioration of insulated rail joints. *Proc Inst Mech Eng Part F J Rail Rapid Transit*. 2009 May 1;223(3):265–73.

25. Zong N, Wexler D, Dhanasekar M. Structural and Material Characterisation of Insulated Rail Joints. *Electron Jourrnal Struct Eng*. 2013;13(1):75–87.

26. Himebaugh AK. *Finite Element Analysis of Insulated Railroad Joints*. MSc Thesis, Virginia Polytechnic Institute and State University; 2006.

27. Carolan ME, Jeong DY, Perlman AB. Engineering studies on Joint bar integrity, Part II: Finite element analyses. *Joint Rail Conference 2014*, Colorado Springs, Colorado, USA, 2-4 April 2014.

28. Grossoni I, Iwnicki S, Bezin Y et al. Dynamics of a vehicle-track coupling system at a rail joint. *Proc Inst Mech Eng Part F J Rail Rapid Transit.* 2014 Oct 12;229(4):364–74.
29. García AO. *Numerical and experimental analysis of the vertical dynamic behaviour of a railway track.* MSc Thesis, Delft University of Technology; 2014.
30. NR/L2/TRK/030 ISSUE 4:2016. Concrete sleepers and bearers.
31. Andersson A, Berglund H, Blomberg J et al. *The Influence of Stiffness Variations in Railway Tracks.* Bachelor Thesis, Chalmers University of Technology; 2013.
32. Grossoni I, Andrade AR, Bezin Y. Assessing the role of longitudinal variability of vertical track stiffness in the long-term deterioration. *IAVSD 24th International Symposium on Dynamics of Vehicles on Roads and Tracks*, Graz, Austria, 17-21 August 2015.
33. Steffens DM. *Identification and development of a model of railway track dynamic behaviour.* MEng Thesis, Queensland University of Technology; 2005.
34. Sun YQ, Cole C, Kerr M et al. Use of Simulations in Determination of Wheel Impact Forces P1 and P2 Due to Rail Dip Defects. In: *AusRAIL PLUS 2009*, Adelaide, Australia, 17-19 November 2009.

APPENDIX C - PAPER 3

Gallou M. Frost M., El-Hamalawi A., Hardwick C. Assessing the deflection behaviour of mechanical and insulated rail joints through finite element analysis. Proceedings of the Institution of Mechanical Engineers, Transport. Epub ahead of print, 8 April 2018.

Abstract

Rail joints constitute a weak component in the railway system. In this paper three- dimensional (3D) finite element analyses (FEA) are carried out to study the structural deflection performance of rail joints under a fatigue static test through vertical stiffness assessment. Four different types of 4-bolted joints are investigated under a dynamically enhanced static load including a glued insulated rail joint (IRJ), a dry encapsulated IRJ, a dry non-glued IRJ and a mechanical RJ. The analysis focused on the accurate simulation of the contact types between the interfaces of rail joint components, namely among the rail, fishplate faces, bolts, insulating materials and on the effect of the elastic supporting structure of the joint on the overall joint deflection. The effect of bolt pretension is included in the model. The vertical displacement of IRJs is measured experimentally both by dial gauges and Video technique both in laboratory and in field. The numerical modelling investigated the effect of different contact types on the interfaces of the rail joint components during the performance of fishplates, and of the rail in the vicinity of the RJ under a given support condition. The vertical displacements of the rail joints were presented and assessed against specified endurance tests' limits and field measured deflection values that validate the model. Stress distribution in the fishplates was presented that could allow the calculation, through a stress-life approach, the fatigue life of the fishplates and consequently of the joints due to repeated wheel passage. A comparison of the performance of the aforementioned RJ types is included. The results indicate this FE model to be practical to be routinely applied to industry, as it was used in UK Rail industry study to allow designers to optimise life expectancy of IRJs.

Keywords: rail joint, track structure, insulated rail joint, fishplate, 3D finite element modelling

1   INTRODUCTION

The main purpose of a rail joint is to join two pieces of rail where continuous rail is not possible or electrical separation is required. The structural objective of a joint is to transmit the bending moment and shear force developed from the external loads from the rail to the fishplate across the joint to the adjacent rail and subsequently to the support structure.

The rail joint is a location of weakness that deteriorates faster than surrounding track and can give rise to serious maintenance problems. Failure mechanisms of IRJs can be either electrical, mechanical or both. The dominant failure modes of rail joints in the UK are insulation (29%) and fishplate failures (23%) [1]. Fishplate failures include cracked or broken fishplates, bent fishplates, fishplates with a visible nib at the expansion gap; signs of wheel flanges striking fishplates can also be the reason for damage [2]. Additionally, lipping, contamination (failed insulation) and rail defects often occur whereas fewer RJs failures are attributed to bolt failure (and/or broken bolts) and broken rails [1]. The problem of fatigue cracking in fishplates is driven by the changes in shear stresses which occur as the wheel passes across the joint. Fatigue is particularly severe in bolted joints due to the stress concentration effect on the bolt holes and the dynamic enhancement of the static wheel load due to the structural discontinuity (lower bending stiffness at the joint) [3, 4].

Studies of the field measurement of deformation in terms of stresses or displacements in traffic or loaded fishplate joints are limited. Literature indicates measured tension stresses in the fishplate of 110 MPa or in 48in (1.2 m) fishplates under live train loading at 62 mph of wheel-rail load 160 kN [5] but the location of the stress measurements in the IRJ is not explained. A vertical strain value of 492 μs (that correspond to 103 MPa) was measured by strain gauges in the rail head 15 mm from the rail gap for a wheel load of 130.7 kN during a live train passage of a velocity 46.3 mph [6]. Recorded strain time series from glued IRJs giving a ratio of the measured strain (ε) to the yield strain (ε_y) with a peak value of 0.124 (that correspond to a stress value of 105.4 MPa) under measured wheel-rail forces up to 200 kN have also been stated in the literature for strain values related to the outer web face of the fishplate [7].

Given the behaviour at rail joints it is vital to have a good understanding of their performance under load. The aim of this research was to create FE models to serve as a template for a family of rail joint designs. The structural performance of four different types of 4- hole rail joints is examined in this paper: glued IRJ (Class A), dry encapsulated IRJ (Class B), dry non-glued IRJ (Class C) and mechanical RJ.

While much modelling of fishplated joints has been performed, fewer modelling papers have appropriately included support conditions. This paper seeks to address this issue (to produce a model that can be used to assess a series of joint designs) firstly describes the joints assessed then reports on literature on previous FE models of joints. From this, the FE model developed is presented and the results of each model are shown. Next, laboratory tests to validate the model are presented and finally the results are discussed. The support conditions in combination with the loading environment govern the rail joint deformation behaviour. The magnitude of deflection depends on the magnitude of vertical load and the stiffness per sleeper

end used. The support environment used in the model of this paper is aligned with field recommended conditions. Softer support conditions could produce different deflection results. Additionally, the bolt pretension plays an important role in the stress distribution around the fishplate holes and accounts for a significant percentage of the stresses generated in the fishplate.

Finite element analysis is an essential tool to quantify the maximum bending stress in the assembled fishplate under operational loading conditions and define the potential areas of failure. Stress results found from previous FEA studies are considered subjective to the assumptions of each FEA model and are discussed in Table 1 whereas vertical displacement of IRJs is rarely investigated in the literature [6].

1.1 Joint types according to insulation

Insulated rail joints are designed to insulate track sections and are classified in the UK rail network according to the insulation type and the type of track they are used for [8].

- Class A: glued joints suitable for CWR (continuous welded rail)
- Class B: dry (non-glued) encapsulated joints suitable for CWR
- Class C: dry (non-glued) joints for jointed track.

In all IRJs an insulating endpost is used to insulate the rail ends from each other that is commonly manufactured from nylon, epoxy fibre-glass laminated sheet or polyurethane. The glued IRJ consists of an insulating liner with an adhesive which is placed between the rail web and the fishplate. In addition the liner, ferrules and washers are fully filled with adhesive to prevent voids in the completed joint. This type of joint adds further structural integrity in the discontinuity, tend to last longer in terms of structural and electrical reliability and are used as a more permanent solution. A typical glued IRJ used in UK rail network is illustrated in Figure 1. The dry encapsulated IRJ includes steel fishplates encapsulated and bonded to an insulating elastomer material whereas the dry IRJ includes an insulating liner between the rail and the fishplate without any adhesive. The liner includes insulating ferrules of the same material that enter the fishplate holes (see Figure 2). Class A and Class B joints are used where high electrical and mechanical durability are required. Class B joints are commonly installed in switches and crossings. Class C are economically advantageous over the other two IRJ grades and are used in jointed and light trafficed track.

Mechanical joints are used in jointed track to join track sections when no insulation is required. A mechanical rail joint consists of the rail, the steel fishplates and 4 or 6 bolts. The two pieces of rail can be tight-fastened without gaps (see Figure 3) or fastened with a gap typically at 6mm.
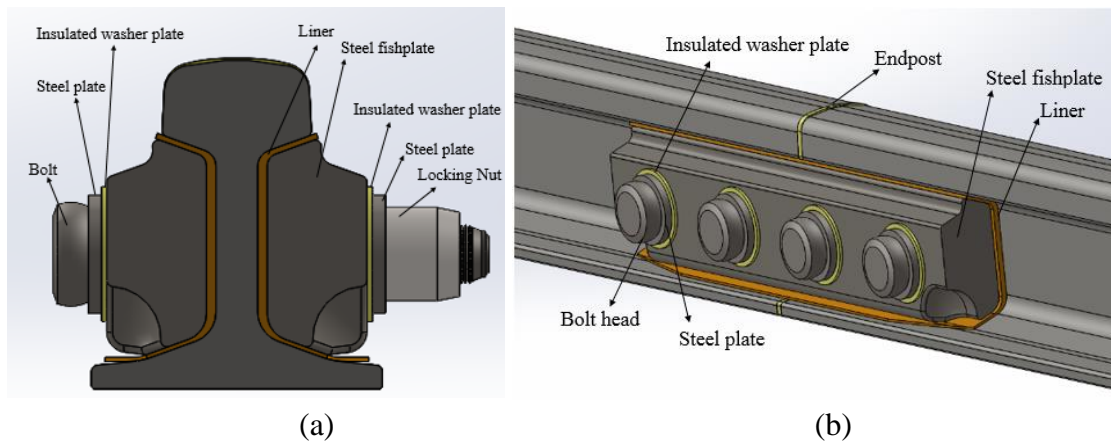
(a)   (b)

Figure 1. (a) cross and (b) front section of a glued Class A IRJ

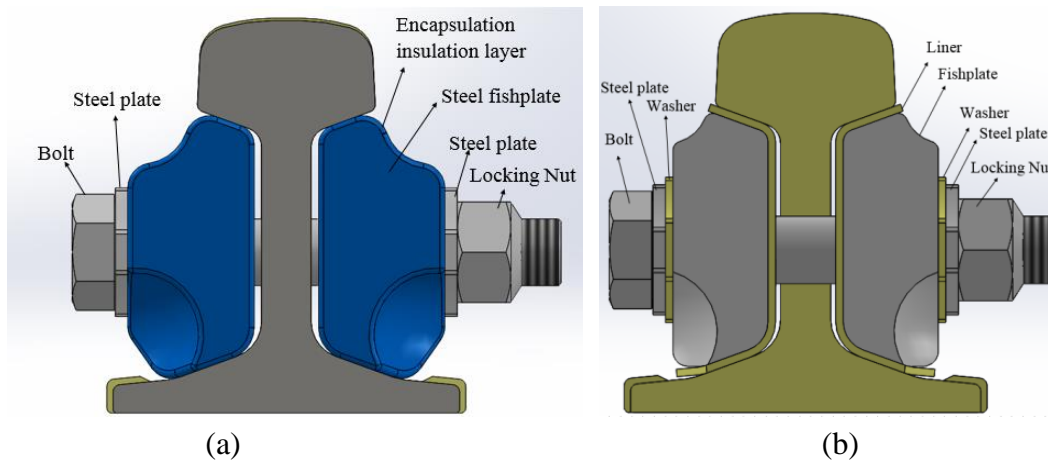(a)   (b)

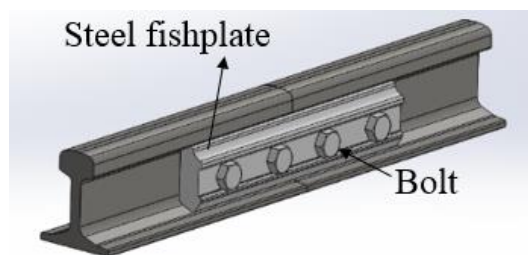Figure 2. Cross section of (a) dry encapsulated Class B IRJ, (b) dry Class C IRJ

Figure 3. Tight mechanical rail joint

1.2   Joints according to support type and number of bolt holes

Support for joints are split into two types. A suspended joint that is an unsupported joint situated between two supports (sleepers) with regular spacing. A supported joint is situated on top of one support, one sleeper or a double sleeper. Rail joints can be 4-hole or 6-hole. 4-bolted joints are positioned in straight track or more often in turnouts or tight radius sections and near switches and crossings mainly due to space restrictions, whereas 6-hole fishplates are used

when the joint is needed to be as strong as possible so that the stiffness discontinuity can be reduced and are more common in tangent track.

2   REVIEW OF MODELLING OF IRJS

Extensive modelling of joints has been conducted over many years. This section briefly reviews these models which are summarised in Table 1. The majority have focused on the wheel- rail contact and the plastic deformation of railhead edges at the discontinuity [3, 9, 10]. The scope of the analysis of these models that is lipping ("localised ratchetting"), although requires a very detailed study and advanced modelling techniques, may not require a detailed study of the track condition supporting the rail joint (stiffness per rail bottom area or stiffness per sleeper end). However, these studies focus only on the railhead material damage. In IRJ modelling, in some instances, it is acceptable to have non-continuous (fee or fixed) rail ends-for example, if only the "lipping" (localised ratchetting) is of concern. In such cases, the effect of the far edges is negligible particularly if thermal effects are disregarded [16, 17]. In field conditions, a vicious cycle of mechanical deterioration of the rail joint and its support conditions (trackbed) occurs due to the increased dynamic loading caused by the structural discontinuity. (Hence the aim of this study is to look at wider joint deflection not just localised performance). Investigation of the structural performance of rail joints that would allow investigation of the fatigue life estimation of rail joints has been restricted to recommendations on fishplate thickness [3, 5, 11] and endpost material [5]. Some of these models include elastic support of the rail joint [5, 11, 12, 13, 14, 15] but they ignore either the non-welded contact interfaces between rail, fishplate, bolts and insulating layers or the bolt pretension. Major failure modes of IRJs comprise bond failure (delamination of endpost), loosening of bolts and broken fishplates. These failure modes are attributed to the increased vertical deflection at a joint and the increased stress values experienced in the fishplates, while they are connected to the effective stiffness of a rail joint.

Another way of improving the joint life that has been investigated in the past is the inclined-cut joints, termed as "angle scarfed" joints whose rail ends are cut diagonally to the rail direction. The performance of inclined-cut joints has been investigated in the past [20] concluding lower vertical impact strains in the inclined IRJ but higher shear strains against square –cut joints, but without generalising whether they are more beneficial than square-cut joints. The inclined-cut glued IRJ has been developed in the past [21], the advantages of which were reduction lipping in the rail head, reduction of noise and improvement of wheel transfer but there was no demonstration of fatigue life improvement for this type of joints. While investigation of inclined –cut joints has been conducted before, is beyond the scope of this paper.

Table 1. Review of previous research studies of rail joints

Author	Research topic	Modelling technique	Comments
Solymez E. and Ciloglu K., 2016[5]	Effect of track variables in IRJ	Bonded IRJ, wheel – rail dynamic analysis, 3D FEA, ANSYS	Examines only glued (bonded) IRJs under 60 mph, parametric analysis for fishplate stiffness, endpost material, supported vs suspended IRJs, wood vs concrete ties, 222 kN bolt preload. Max normal stresses on fishplates on concrete ties (spacing 609 mm, I_{Rail}= 3931 cm^4, 1220 mm fishplate length) up to 200 MPa for a wheel load 160 kN. It was concluded that contact pressure resulting from impact load is not affected by various track support conditions. Stiffer fishplate with stiffer I_{Rail} under a lower wheel load in comparison with the authors' model. Results are not comparable to the authors' model. Contact pressure, contact force and rail max shear stress are also examined except normal stresses in fishplates. Model length 1.5m in 3D, 11m in 1D.
(Mandal NK, 2016) [9], Mandal NK & Dhanasekar M., 2013) [10]	Plastic deformation of railhead in IRJ	3D FEA, ABAQUS, plastic deformation of railhead, non-linear isotropic and kinematic material hardening model for 2000 cycles	Six-bolt suspended IRJ, account for bolt pre-tension 200 kN. 700mm spacing, 3D part 2.4 m, 9.6m in 1D. 174 kN wheel load. Too low vertical displacement (0.2 mm). Sleepers fixed with zero degrees-of-freedom not representative of field conditions in contrast with the authors' model. Model representative of a laboratory experiment of rail joint. The plastic zone of the top surface of rail head material is investigated.
(Grossoni I. et al., 2014) [12]	Dynamic response at a RJ	2D FEA vehicle –track coupling model, track system: rail as beam on a double-layer discrete viscous -elastic foundation, idealised form of rail irregularity (IRJ) through quadratic function (second order polynomial)	2D Model includes three parameters of IRJs (joint max deflection, joint angle and joint length) by using a mathematical idealisation of dipped beam in 2D. It shows that the joint shape plays a role in the magnitude of P2 force that actually affects the track degradation. The dip angle is used in the 2D model as input for wheel-rail impact forces calculation. A 3D model can provide ground for a more thorough investigation of stress development on the interfaces between the RJ components.
(Bandula-Heva TM, Dhanasekar M. & Boyd P., 2012) [16]	Wheel/rail rolling contact at railhead edge	3D FEA validated by PIV and strain gauges in laboratory	FE model of wheel-railhead-rail body (without full IRJ assembly) to simulate laboratory conditions of half of IRJ under loaded wheel passage to determine railhead vertical, lateral and shear strain components. Used to investigate railhead edge behaviour due to accumulation of plastic deformation.
Bandula-Heva TM & Dhanasekar M., 2014) [17]	Localised plastic strain accumulation in railhead edge	3D FEA of railhead edge using Caboche kinematic hardening law using experimental uniaxial monotonic tension tests of railhead coupons.	FE model validated as abovementioned in Ref 16 used to predict localised plastic strain in railhead edge..

(Zong N. et al., 2013) [13]	Wheel –rail contact impact loading of IRJ	Wheel rail contact impact model, 3D FEA	Account for wheel-rail frictional contact, 200 kN bolt preload, elastic support per rail end. The model examines the contact and impact force, contact pressure, validated against vertical strain in rail web with field test. It doesn't present structural performance of the joint in terms of deflection, stresses on fishplate, does not comment on how the rail-fishplate interfaces were modelled. A modal analysis was carried out indicated the frequency of the impact force has been dominated on its seventh mode. Railhead damage was indicated in the model in form of reduced gap, vertical dip and residual stress of rail end sample was analysed using Neutron diffraction technique.
Patel Q., Kumar V. and Nareliya R., 2013) [14]	Fatigue life estimation of RJ using FEA	Wheel-rail dynamic 3D FEA, standard RJ.	The model included a mechanical non-inuslated RJ on a two sleeper configuration on elastic support. Lack of symmetry and short length of model may affect the results. Mesh is not presented. Contact type in between rail-fishplates that is usually frictional for the standard RJ is not commented. Bolts were modelled with solid elements. A max Von Mises stress of 214 MPa was found in rail joint.
(Mandal NK & Peach B., 2010) [3]	FEA of IRJ	Static 3D FEA of a 6-bolt IRJ, objective to investigate the effect of fishplate width on stresses in railhead.	Fixed support on rail bottom, the rail was tied to the sleepers, no interaction between rail and fishplate, welded joint. The effect of fishplate width in stresses on railhead and in deflection was investigated. Too stiff conditions indicated very low deflection results.
(Sandström J. & Ekberg A, 2009) [18]	Fatigue impact and plastic deformation of IRJ	3D FEA of IRJ, wheel rail contact, non-linear kinematic hardening constitutive model	The model indicates that the main failure mechanism of IRJs is ratcheting and not the low cycle fatigue. Model included only part of wheel, railhead edges and endpost. Effect of increase of frictional coefficient between rail and wheel, increase of endpost thickness and effect of rail edge bevelling under multiaxial loading conditions on the total accumulated plastic strain in rail are investigated.
(Himebaugh AK et al, 2007) [11]	FEA of bonded IRJ	Static 3D FEA of supported IRJ in ABAQUS	One type of supported bonded IRJ. The model included a fishplate of length 1.2 m, no rigid bolts modelled, wooden sleepers and elastic foundation. A model length of 7.6m was considered sufficient to model on each side of the wheel after parametric analysis. The effect of thickness and length of joint bar, load position and size of sleepers on rail deflection and epoxy stresses are investigated under vertical 145 kN and tensile 1330 kN load in the rail.
(Ding K. & Dhanasekar M., 2007) [19]	Flexural behaviour of bonded-bolted butt joints due to bolt looseness	ABAQUS 3D FEA, pre-stressing of bolts, inplane bending in bolted IRJ.	Elasto-plastic material law for fishplates only, elastic law for the rest. Bonded connections among rail-fishplates-bolts, bolt preload are accounted. Effect of looseness of bolts under biaxial stress on the RJ.
(Talamini B. et al, 2007)[15]	Fatigue estimation of fishplates	Static 3D FEA in ABAQUS, wheel rail contact, 6-bolted RJ.	A 3D static model of a mechanical RJ including elastic support conditions under a vertical wheel load increased by a dynamic load factor is used to estimate the bending and reverse bending stresses on fishplates. A fatigue life estimation of the fishplates is proposed using Miners's Law. A comparison is made between FEA results and theoretical stress calculations using the beam theory and thermal stresses. The study suggests the 3D FEA can provide a better understanding of a biaxial bending behaviour of fishplates that is critical for fatigue calculations which cannot be predicted by beam theory.

Most previous FEA studies of rail joints consider a joint as a bonded assembly. No modelling was found describing the structural performance of various types of less stiff, four bolted rail joints under a critical dynamic load case looking at the frictional contact in rail/fishplate/insulating layer interfaces within the aim of assessing the fatigue life of joints due to mechanical failure of fishplates and thus assessing their resistance to bending and their vertical stiffness/deflection. Previous modelling by the authors has shown that the elastic support conditions produce displacement values that are in a good agreement with field data measured with a high accuracy video technique under high speed traffic [22].

3   FEA MODEL

3.1   Material properties, contacts and boundary conditions

A model was therefore developed to address some of the issued identified above from past work, to produce a practical and routine validated model that could be used by industry to assess the overall deflection and likely implication on joint life including an estimation of underlying trackbed support.   This section reports the model developed to include support stiffness. ANSYS Mechanical was used to perform 3D static structural analysis of the joints identified in Section 1. The basic model included four CEN 56 rails of moment of inertia 2320.0 cm^4 of 2 m each covering a length of six sleepers. The sleeper spacing was set as 700 mm and the track gauge as 1435 mm. A railpad of thickness 10 mm and of medium stiffness (150 kN/mm) was used between the rail and the sleeper that acts as a resilient spring to vertical movement of the rail (that includes uplift). Bonded contact was applied between the rail and the railpad (it is considered that the use of fastening clips would add value to the model in case of rail subjected to longitudinal and lateral forces but is not included in this paper). A non-linear contact type between rail and railpad was ignored, as it is considered that the toe load of a fastening clip would provide some vertical resilience to uplift. Two loading cases were initially studied in order to assess the fishplate "sagging" and "hogging" deformation. The load case presented here (see Figure 4) includes a wheel load of 200 kN applied as a nodal force on top of the centre of railhead at a distance of 10mm from the rail gap.   This will give maximum compressive stress at the top of the fishplate (sagging deformation). This load case is prescribed by the national UK rail operator and accords with the maximum static load in UK rail infrastructure (25tonne axle load), increased by a dynamic factor of 1.6 [23]. The purpose of this research was to create models that would serve as template for a family of rail joint designs for design studies. A further study of hogging performance will be the subject of a further publication. Nodal force was used over an area that corresponds to the wheel-rail contact patch according to Hertzian contact.

The steel of rail and fishplates has a yield strength (S_y) 850 MPa [24]. The tensile strength of the steel used was set at 1150 MPa. Bonded contact was applied between the rail pads and the sleepers. Concrete G44 sleepers were used with a cant 1/20. All components are modelled with solid elements.

For the accurate simulation of the elastic behaviour of soil-track interaction, the principle of Winkler (1867) was followed, according to which the use of springs is suggested with spring stiffnesses selected according to the support flexibility underneath the sleepers. The springs were connected in an effective length in both the sides of the sleeper bottom. The length is considered effective at both sides of the load position that is equal to $Lp = (L-c)/2 = 500.1$ mm, where L is the sleeper length and c the rail seat spacing. This assumption better simulates the fact that monoblock sleepers are packed over an area on either side of the centre of the rail [25]. A minimum dynamic sleeper support stiffness of 30 kN/mm per sleeper end has been used as defined for a renewed track bed [26].

The rational selection of the boundary conditions plays an important role in the creation of a functional FE model. For this reason, the following constraints were applied:

- In the position of the springs, stiffness was applied in the Y direction.
- As far as the rail ending faces of the model are concerned, displacement constraints were applied in the X and Z direction to prevent rigid-body motions, allowing free movement in Y direction. The sum of the reaction forces at the constraint points are zero. No part of the rail ending faces can move, rotate or deform in the X and Z direction. The deflection in all model configurations in this study at the rail ends was shown to be almost zero (see Figure 19). Boundary conditions were applied to at least three sleepers from the position of the load. The authors tested in a preliminary study the length of the model and this was shown to be suitable as not to affect the deflection bowl of the joint.

Table 2 describes the material properties assigned to the different components. Figure 5 shows the geometry and meshing of the model. A refined mesh of maximum size 8mm was applied in the rail joint vicinity and in the load application areas. The majority of elements used in all IRJ models in this study is higher order 3-D, 10-node tetrahedral quadratic element SOLID187 that has a quadratic displacement behaviour (shape function) and do not suffer from shear locking. This type of element is well suited to modelling irregular meshes such as those produced from complex CAD geometries with curved outlines and complex contact surfaces. A smaller part of the mesh was hexahedral 20-node of quadratic shape elements (in railpads and washers). The authors carefully tested the 10-node against 20-node quadratic elements under same element size in a four-point bend test and no difference in the deflection and stress results was observed. Only linear shape function suffers from shear locking and poor bending deformation characteristics, so shear locking is not considered an issue.
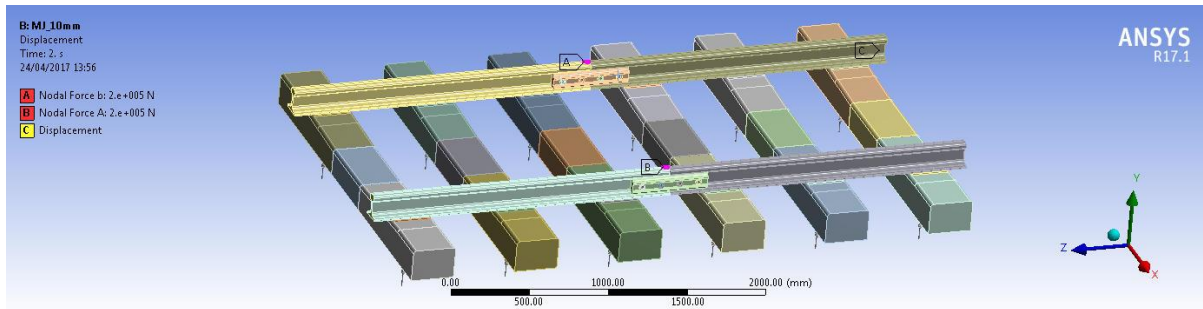
Figure 4. View of the model showing the loading positions at 10mm from the rail end.

Table 2. Elastic Material Properties

Component	Material	Stiffness	Modulus of Elasticity	Poisson's ratio	Density
		k	E	v	ρ
Rail, Fishplate	Steel		210 GPa	0.3	7850 kg/m^3
Railpad	Elastomer	150 MN/m	38.265 MPa	0.3	300 kg/m^3
Sleeper	Concrete		30 GPa	0.18	2300 kg/m^3
Endpost	Polyurethane		20.7 MPa	0.3	1265 kg/m^3

3.2 Bolt pretension

The effects of bolt pre-tension are accounted for in the model. Beam elements were used to provide shear resistance to vertical load [27]. These elements were then given a pre-load value equivalent to the expected pre-load generated from the tightening torque permissible on a Grade 8.8, M24 (or M27 dependent on joint design) bolt. The pre-load was calculated from the equation:

$$F = \frac{T}{K*d}$$

(Eq.1)

where T is the permissible tightening torque, d the bolt diameter and K a bolting coefficient with a value of 0.2 (156 kN for M24 and 184 kN for M27).

This load was applied as part of a multi-step analysis in the model, with a total duration of 2 seconds. The bolt pre-load was applied as a ramped load over the course of 1 second – to mimic the effects of assembling the joint and tightening fasteners. The vertical load, of 200 kN, was then subsequently applied as a load for a duration of 1 second. The second load step applies the load gradually over 5 to 10 substeps, each substep uses up to 50 equilibrium iterations for an accurate solution to be obtained.
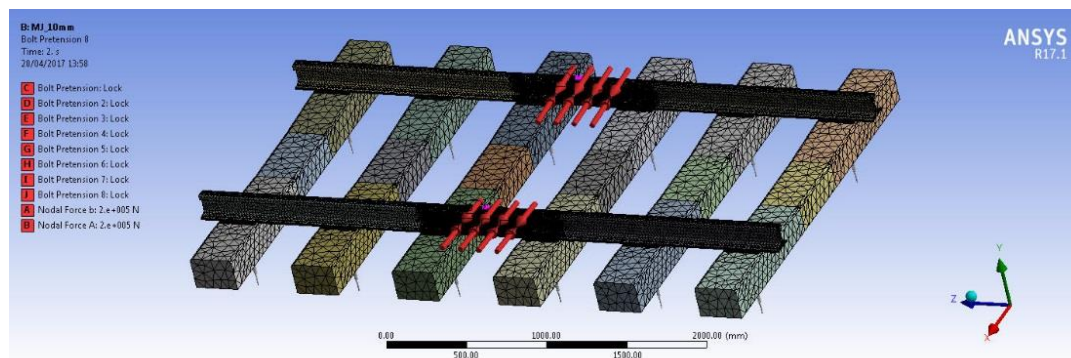
Figure 5. Model layout showing bolt preload and mesh

3.3 Numerical model configurations

Table 3 presents the different configurations modelled: (a) glued IRJ- Class A, (b) mechanical RJ, (c) dry (encapsulated) IRJ- Class B and (d) dry (non-glued) IRJ- Class C. All joints were 4-bolted. Insulating liners are of 3 mm thickness and the encapsulation layer is a resin coating of thickness 3 mm. The fishplate properties of the configurations studied are described in Table 4. The material properties of the insulating layers that varied along the RJ types are presented in Table 5.

Table 3. Model configurations

Joint type	Rail combination at joint		No Holes	Fishplate type
	Rail section 1	Rail section 2		
Glued	CEN56	CEN56	4-hole	Insulated Class A
Mechanical	CEN56	CEN56	4-hole	Standard
Dry	CEN56	CEN56	4-hole	Insulated (encapsulated) Class B
Dry	CEN56	CEN56	4-hole	Insulated (non-glued) Class C

Table 4. General fishplate properties

	Property	Length	Fishplate hole diameter	Mass	Moment of inertia I_{xx}	Cross sectional area
	Units	mm	mm	kg	cm^4	mm^2
Fishplate type	Insulated Class A-CEN 54E1-6H (3pb)	800	32	22.707	242.554	3613.22
	Insulated Class A-CEN60-4H (4pb)	650	35.5	21.65	264.768	3966.91
	Standard Mechanical CEN 56- 4H	507	25.5	14.69	298.08	3871.03
	Insulated Class A CEN 56-4H	508	35.5	15.47	210.20	3684.12
	Insulated encapsulated Class B CEN 56-4H	508	36	16.40	237.85	3703.47
	Insulated non-glued Class C CEN 56-4H	508	36	12.65	252.12	3499.79

Table 5. Material properties of insulation materials

Material properties				
Component	Material	Modulus of Elasticity	Poisson's ratio	Density
Insulation layer_ Class A & C (Pultruded liner)	Glass Fibre Reinforced Polyester Resin	8000 MPa	0.38	1850 kg/m^3
Insulated washer	Epoxy Glass Sheet G10	2400 MPa	0.35	1920 kg/m^3
Encapsulation layer- Class B	Altech	2100 MPa	0.39	1090 kg/m^3
Ferrule Class A	Epoxy Glass Sheet G10	2400 MPa	0.35	1920 kg/m^3
Ferrule Class C	Glass Fibre Reinforced Polyester Resin	8000 MPa	0.38	1850 kg/m^3

The varying FE assumptions among the varying RJ types are described below. The meshing, loading, bolt pretension and boundary conditions were applied in the same manner as described above.

3.3.1 Glued Insulated Rail Joint-Class A

The Classification A joint configuration includes an insulating liner that electrically separates the steel and is glued to both the fishplate and the rail. Pultruded Glass Fibre Reinforced Polyester Resin is used in this study as a liner. Bonded contact was applied between the fishplate and the insulated washers and ferrules. Bonded contact was also applied between the rail/liner /fishplate interfaces to simulate the glued faces (see Figure 6).
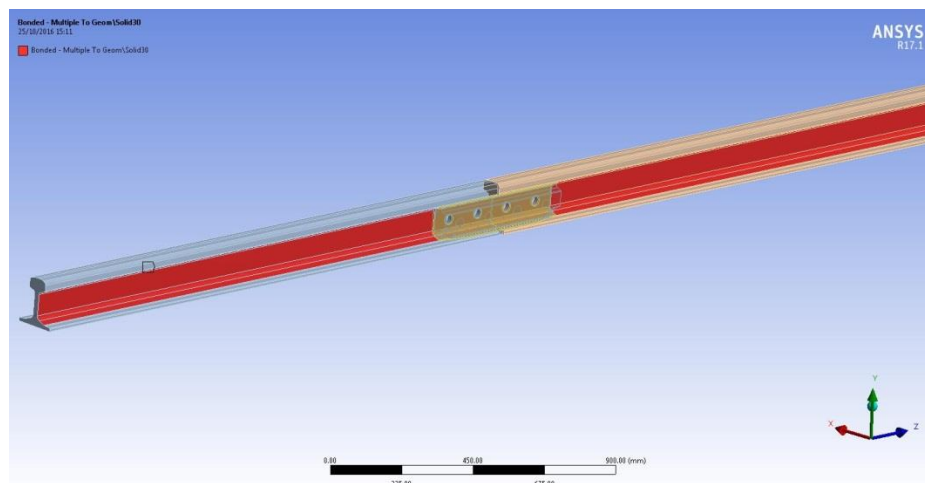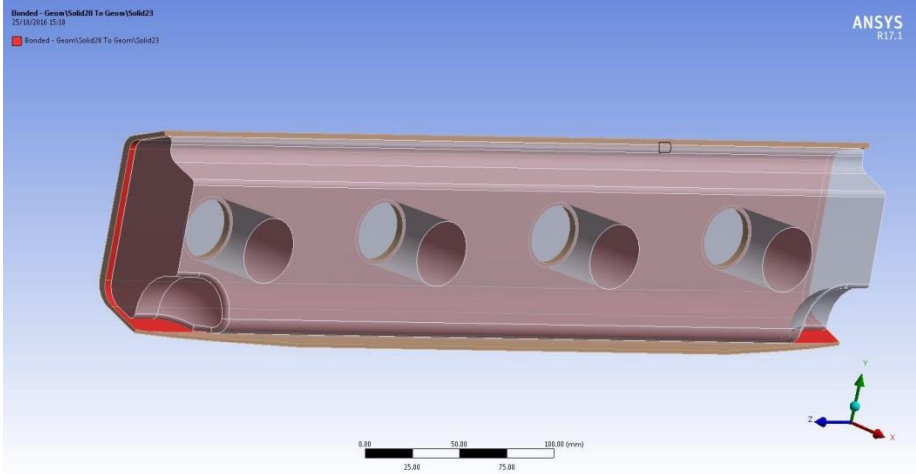
Figure 6. Bonded contact between (a) the rail and liner and (b) the fishplate and the liner to simulate glue.

3.3.2 Mechanical Rail Joint

Only the upper and lower "fishing "surfaces of the rail were given frictional contact with the fishplates(s) with a coefficient of friction 0.2 (see Figure 7) with a gap existing between the rail web and fishplate.
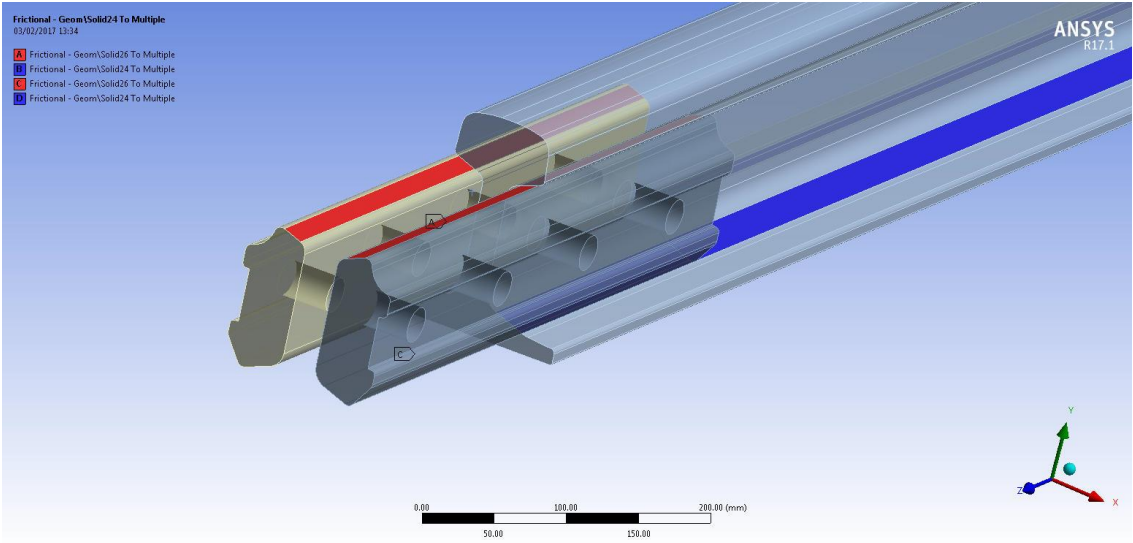

Figure 7. Frictional contact between rail and standard fishplate.

3.3.3 Dry encapsulated Insulated Rail Joint-Class B

The fishplate is fully encapsulated in an elastomer material. The material used is ALTECH PA6 A 1000/310 IM. Frictional contact was applied between the upper and lower "fishing" faces of the rail and the fully encapsulated plates with a coefficient of friction 0.2 in the same way as in the mechanical RJ (see Figure 7). Bonded contact was applied between the encapsulation layer and the steel fishplate.
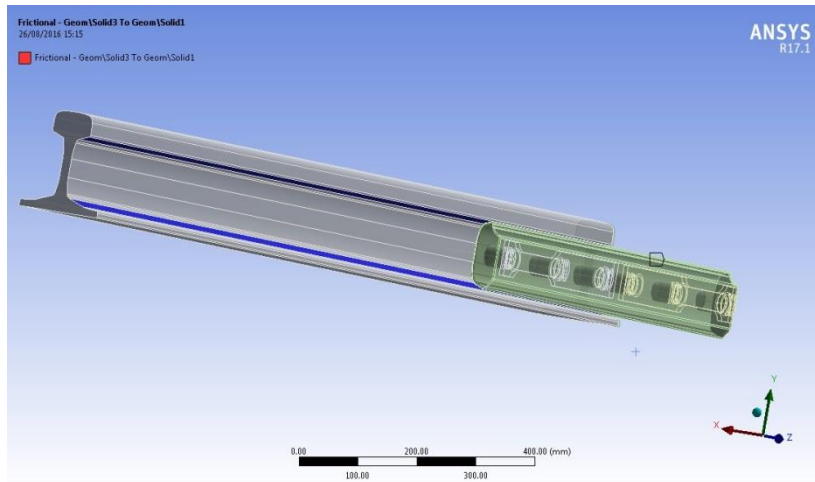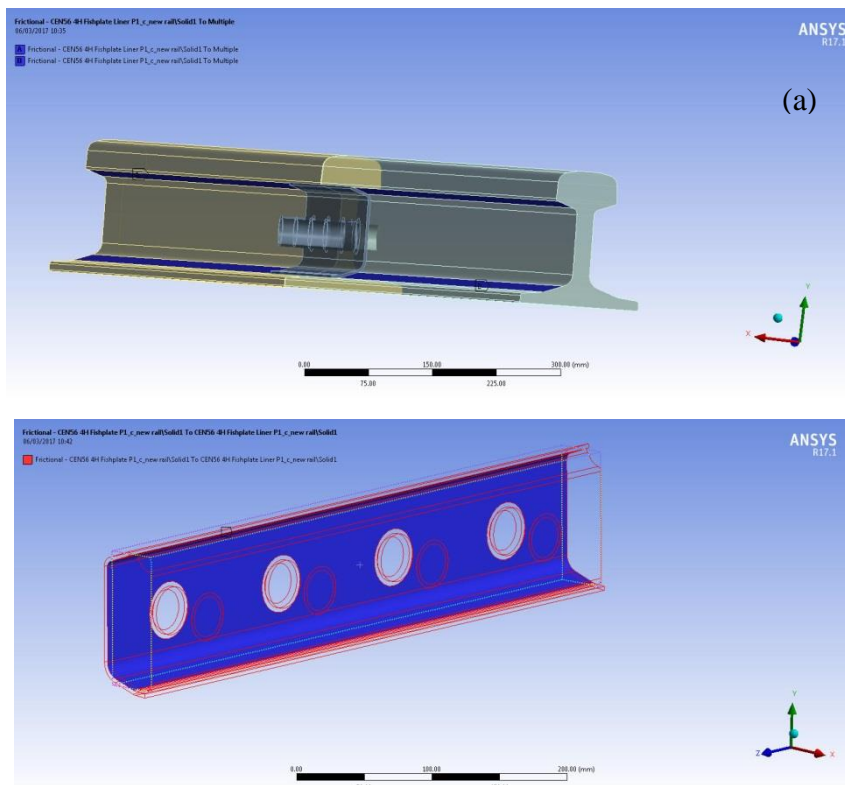
Figure 8. Frictional contact between rail and fully encapsulated fishplate

3.3.4   Dry non-glued Insulated Rail Joint-Class C

A Pultruded Glass Fibre Reinforced Polyester Resin was used in this study as a liner between the rail and the fishplates. Contacts between the upper and lower fishing faces of the rail with the liner were given frictional contact of 0.2. Frictional contact was given between all inside faces of the liner with the fishplates and between the fishplate hole faces and the insulated ferrules (see Figure 9).
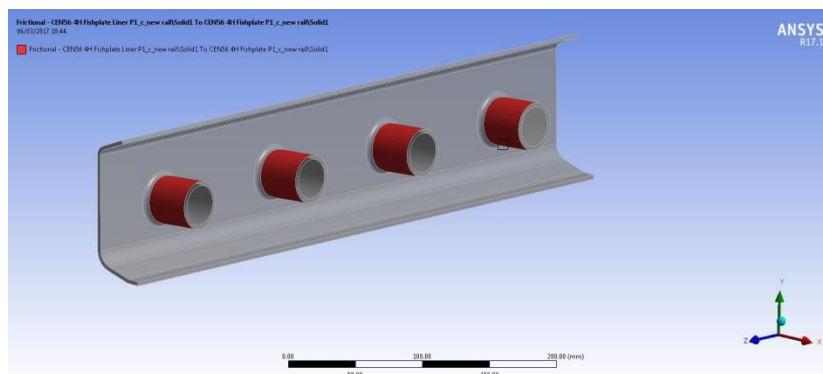
Figure 9. Frictional contact between (a) rail and liner top and bottom fishing surfaces, (b) liner and fishplate and (c) faces of insulated ferrules (incorporated with the liner) to that of the fishplate.

This model had an increased number of frictional contacts inserting non-linearities in the model that are in combination with: a) the large size of the model, b) the existence of multiple bolt loads and c) the complexity of the load sequence aggravated the solution to converge. Thus, both load steps applied the load gradually over 25 sub steps, each sub step uses up to 25 equilibrium iterations (see Figure 10). An advanced contact formulation was used to enforce compatibility at the non-linear frictional contact interfaces. Augmented Lagrange formulation with a normal stiffness factor 0.01 updated on the end of each equilibrium iteration was used for the non-linear solid body contact of faces adding additional controls to automatically reduce contact penetration allowing contact detection at integration points [28]. These analysis settings allowed the establishment of a relationship between two faces of frictional contact region to prevent them from passing through each other. The software for such a contact formulation based on a pure penalty method assumes that the contact force along the normal direction is written as follows:

$$F_{normal} = k_{normal} * x_{penetration} \qquad (Eq.2)$$

Where k_{normal} is the contact stiffness, $x_{penetration}$ is the distance between two existing nodes on separate contact bodies, F_{normal} the contact force [28].

In addition, an interface treatment was used adjusting the initial position of the reference and target contact surfaces to eliminate any gaps or penetrations formatted during loading for the non-linear contact types. This setting automatically calculates an offset based on the minimum gap between two non-parallel faces to close the contact region allowing localised contact [28].
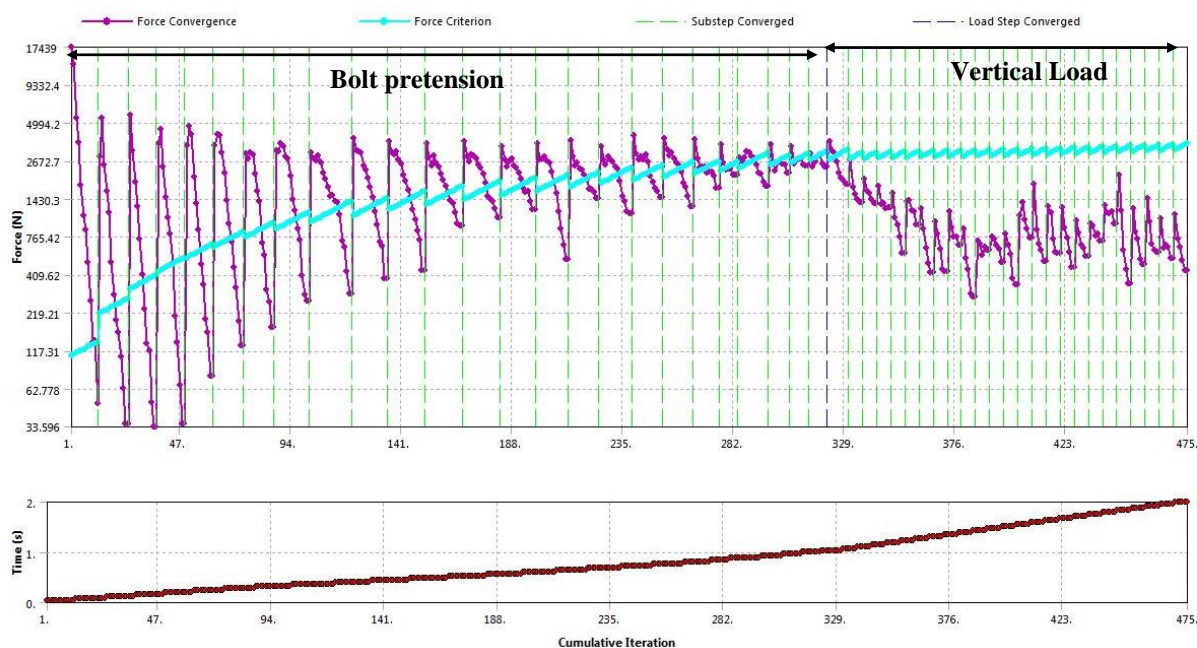
Figure 10. Force convergence along the solution of IRJ Class C.

4   EXPERIMENTATION AND LABORATORY VALIDATION

Validation of the FE model was conducted in terms of quantifying the accuracy of the model by comparing numerical solutions to experimental data. Initially joint deflections were compared between a laboratory 3-point bend test and the corresponding FE model. FE model was also validated in terms of joint deflections measured by the high definition Video Gauge technique in a 4-point bend test. A strain comparison among FEA and experimental data while useful was not part of this study. This would require a more complex laboratory set up with strain gauges. The assessment of strain from the Video Gauge in rail joints may be possible it has not been validated yet and both elements were outside the scope of this work. In addition, in IRJ worldwide specifications [8, 29, 30, 31, 32] the mechanical performance of rail joints is approved by bending fatigue endurance tests where deflection limits are used as the acceptance criterion for the assessment of their structural stiffness and response to vertical load, hence why deflection was assessed in this study as a primary routine validator.

4.1 3-point bend testing

A 6-bolt glued IRJ Class A of 1.3 m length with rail section CEN54E1 with an endpost of 8 mm thickness was tested in a three-point bend under static loading. The geometrical characteristics of the fishplate are presented in Table 4 of section 3.3. The load was applied 13 mm away from the centre of the joint to avoid the joint gap. The vertical displacement was recorded through dial gauges placed on top of the railhead in several positions on each rail section (see Figure 11) giving in total 9 readings for each load case. The loading occurred in steps from 20 kN to 200 kN. A static FE model was created to simulate the three-point bend

test based on the above (Secion 3). The vertical displacement in Y axis was set to zero in the two end edges of rail foot in the position of supports as shown in Figure 12. Bonded contact was applied among all interfaces of the glued IRJ components. The model had a minimum mesh size of 8mm and the model included 476929 nodes and 295687 elements running in a computational time of 2 h 37 min. A parametric analysis was performed to assess the magnitude of deflection with a mesh that would reduce the computational time and it was concluded that a coarser mesh with minimum element size of 16mm provided the same deflection results. Thus, the basic loading case of 200 kN was performed in an 8mm maximum element mesh and the parametric analysis of 20 kN to 180 kN was performed in the model with a coarser mesh. An exaggerated deflection shape of the FE model is shown in Figure 13.

Very good correlation was found between experimental and FEA deflection data. A comparison is presented in Figure 14 for the vertical displacement at the central path along the top surface of railhead. A difference of 2-10% for the various load cases was found showing that the model represents quite accurately the complex deflection histories of the rail joint.
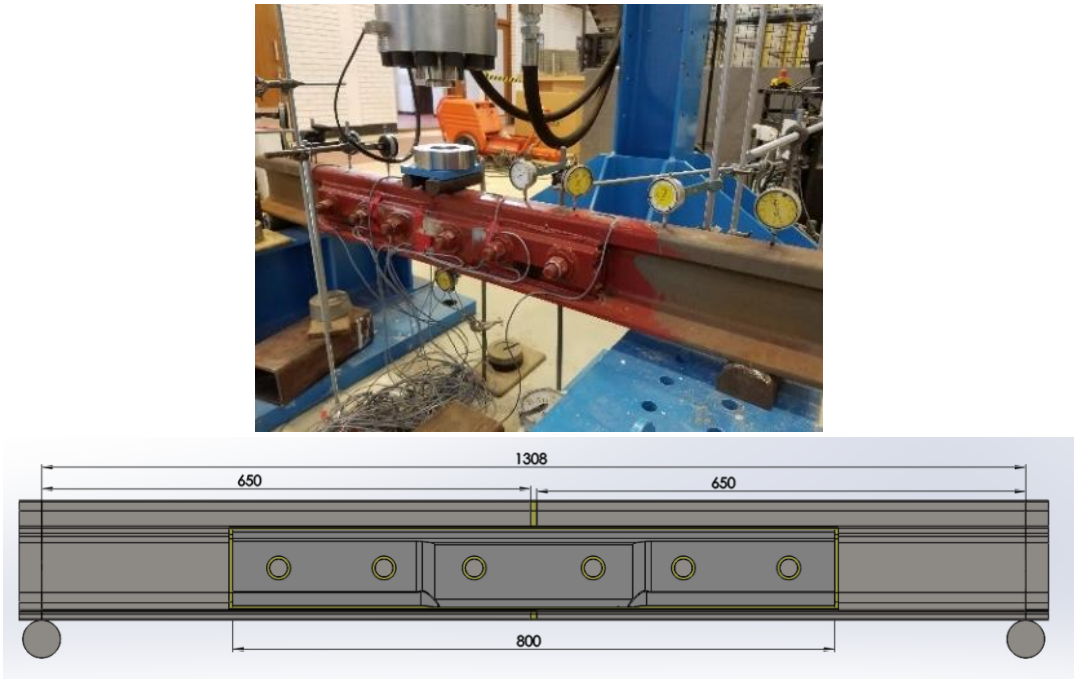
`

Figure 11. (a) Laboratory 3-point bend test showing set-up and position of dial gauges (b) Geometry of the 3-point bend configuration
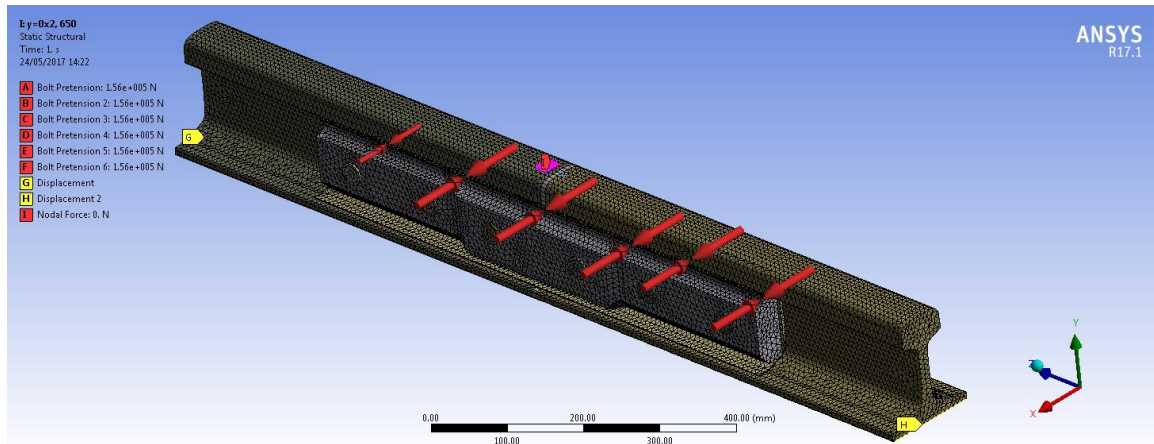
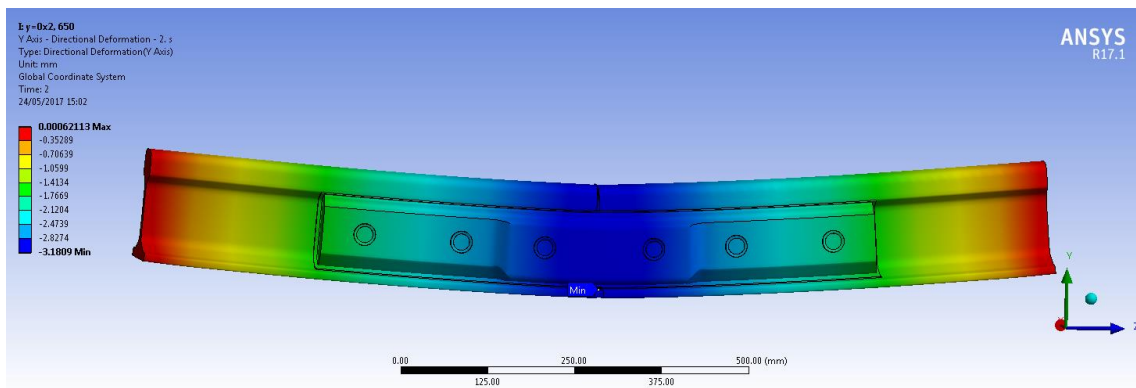Figure 12. Mesh and boundary conditions of the 3-point bend FE model

Figure 13. Exaggerated deformed deflection shape of the 3-point bend FE model
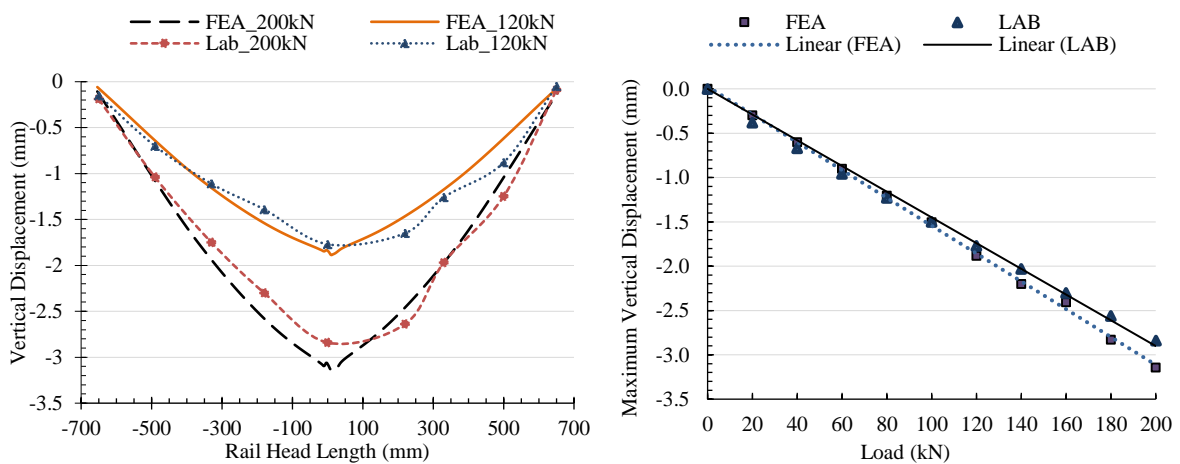

Figure 14. Comparison between Lab and FEA results of the 3-point bend test

4.2 4-point bend testing

Laboratory measurements of a 4-bolt glued Class A CEN 60 (1.5 m each rail section) IRJ using high accuracy video technique (Video Gauge) were conducted in a 4-point bend test under cyclic loading (see Figure 15). The geometrical characteristics of the fishplate are presented in Table 4. The endpost was of 6 mm thickness and it was in bonded contact with the rail faces.

The two forces were applied at 300 mm from the gap on the centre of the top of railhead whereas the IRJ was supported at a distance of 800 mm on each side of the gap. Four load cases were performed from 160 kN to 404 kN. It is noted that the extreme load cases selected for this laboratory test were chosen according to the specification [8] to reach mechanical failure of the rail joint, which is out of the scope of this paper. The measured vertical displacement in the centre of the rail joint (rail head edges) was found in a range of 2.29 mm to 6.11 mm.

Linear static FE modelling to simulate the above 4-point bend test was performed. The model set up (see Figure 16) was performed in the same way as described in section 0. The maximum deflection in the railhead (same position with the position of Video Gauge measurements) was found 2.58 mm to 6.23 mm for the various load cases. A deflection deformation plot is presented in Figure 17.

Quite a good correlation was found between the deflections measured by the camera and that found from the FE model. A difference of 2-11% for the various load cases was found. A comparison between FEA and experimental data is presented in Figure 18.
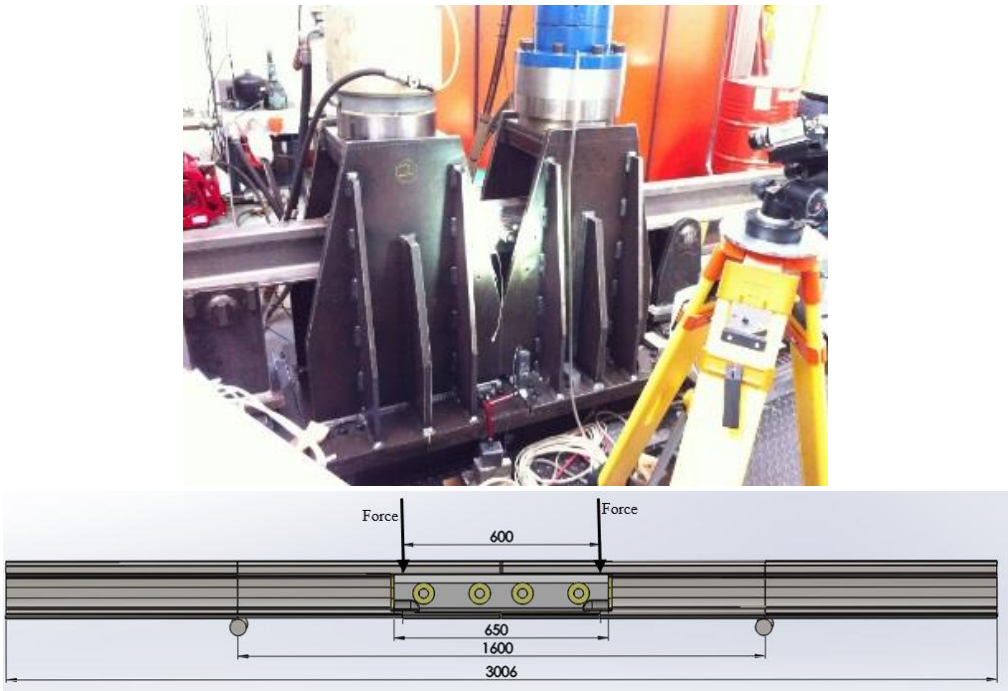

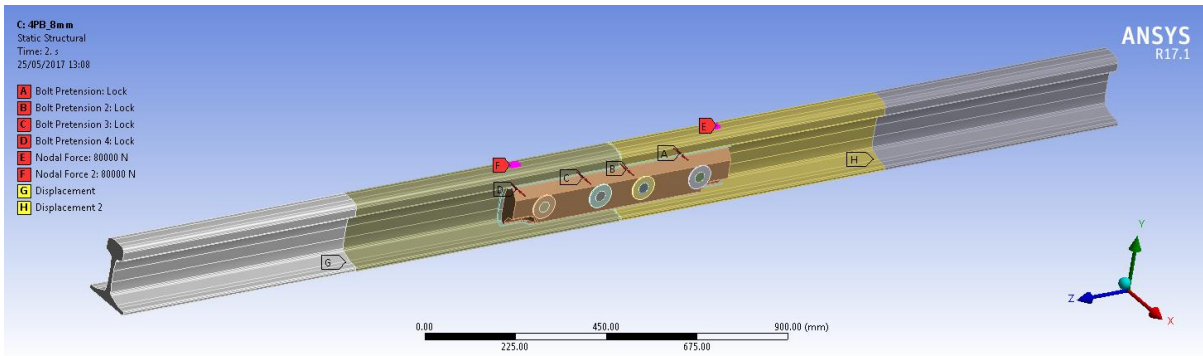Figure 15. 4-point bend configuration

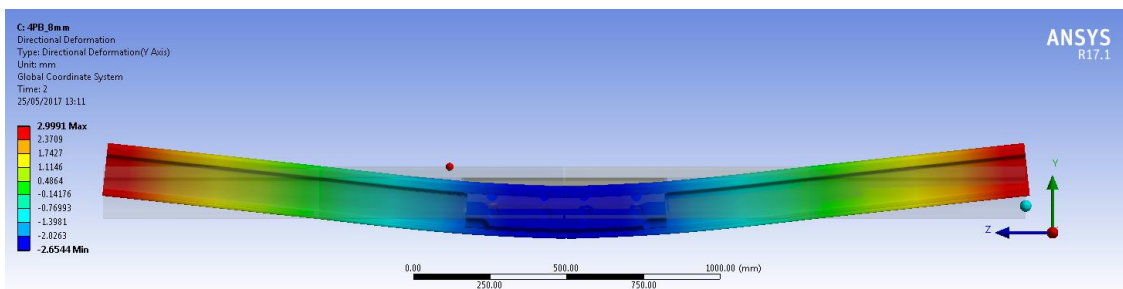Figure 16. FEA model of 4- point bend configuration

Figure 17. Vertical displacement of glued IRJ in a four-point bend FEA-load case 160 kN.
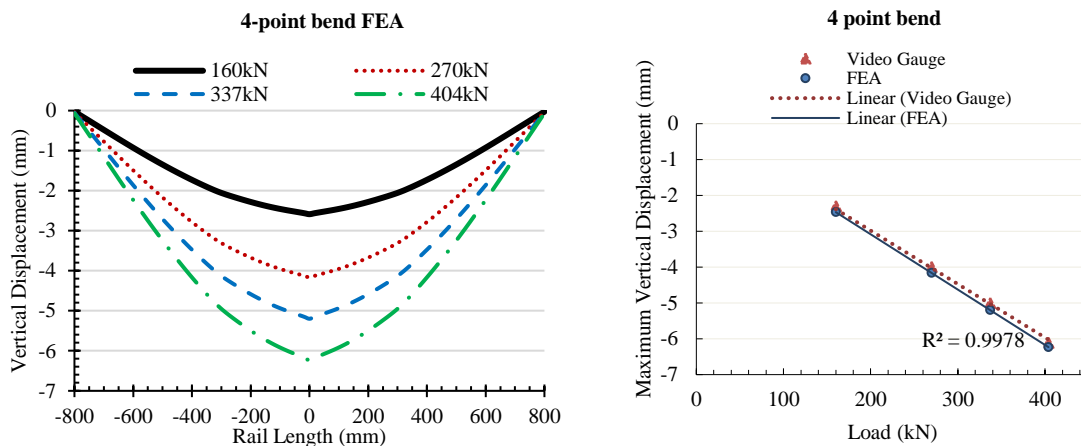

Figure 18. Comparison between FEA data and lab results for the 4-point bend test.

5   RESULTS FROM FE ANALYSIS

Results in terms of vertical displacement and equivalent von Mises stresses from the models were displayed for all case studies. Although a strain demonstration at some key points of the model could indicate local weaknesses, this could not be validated against experimental data. In addition, the ultimate scope of this paper's model is to assess IRJs' vertical strength through deflection and to allow through stress-life approach the fatigue life calculation of fishplates and consequently of rail joints due to repeated wheel passage. Equivalent stress allows any arbitrary three-dimensional stress rate to be represented as a single positive stress value and is related to the principal stresses by the equation:

$$\sigma_e = \sqrt{\frac{(\sigma_1-\sigma_2)^2+(\sigma_2-\sigma_3)^2+(\sigma_3-\sigma_1)^2}{2}}$$ (Eq.3)

This stress is part of the maximum equivalent stress failure theory used to predict yielding in a ductile material such as steel. According to this theory, the maximum equivalent stress values are compared to material yield limits (850 MPa) to generate the safety factor

$$F_s = \frac{S_y}{\sigma_e}$$ (Eq.4)

The maximum vertical displacement found in the centre of rail foot is presented in Figure 19.
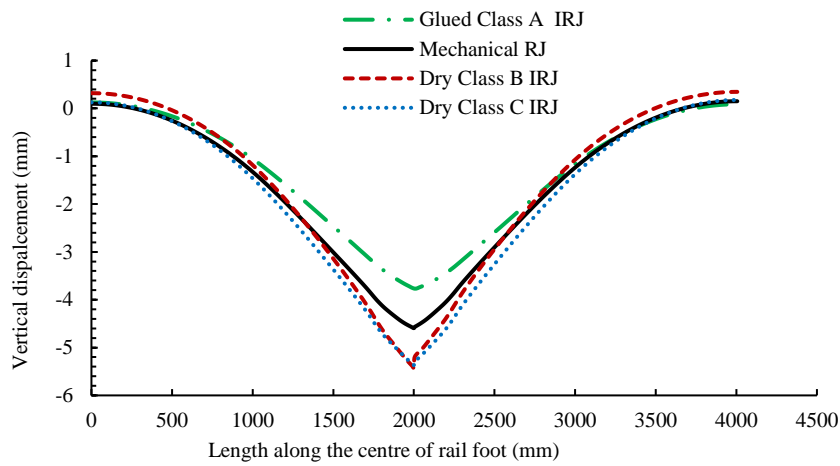
Figure 19. Vertical displacement of the centre of rail foot surface for various rail joint types.

Figures 20-23 illustrate the stress distribution of the pair of fishplates for the configurations studied. Figure 24 describes the equivalent stress distribution along the central path at the top and bottom fishing surface of the fishplate for the varying RJ configurations whereas Figure 25 describes the equivalent stress distribution along the central path at the top and bottom fishing surface of the rail.

Figure 20. Equivalent (von Mises) stresses – Glued Class A IRJ

Figure 21. Equivalent (von Mises) stresses – Mechanical RJ

Figure 22. Equivalent (von Mises) stresses – Dry Class B IRJ

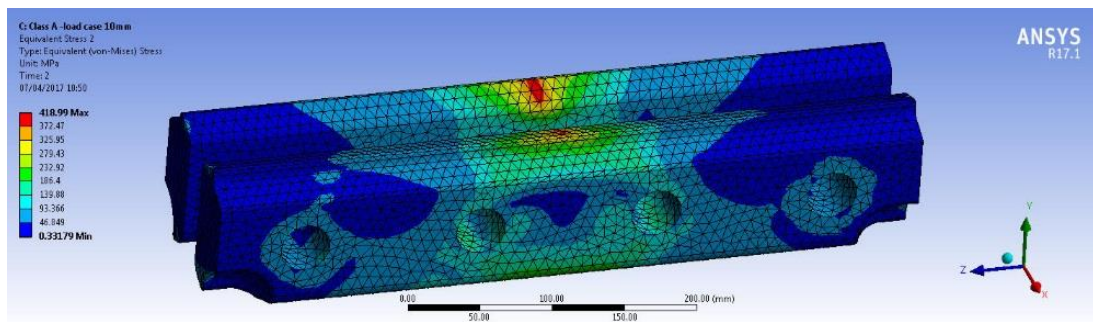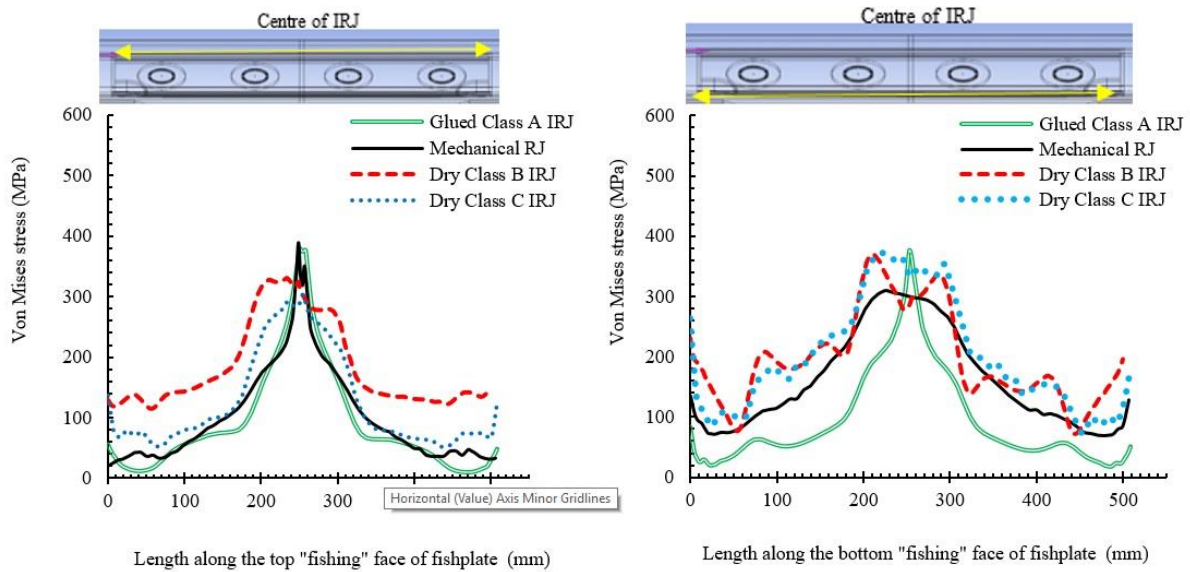Figure 23. Equivalent (von- Mises) stresses – Dry Class C IRJ

Figure 24. Equivalent (von-Mises) stress plots of the centre of top and bottom fishing surface of the fishplate for various rail joint types
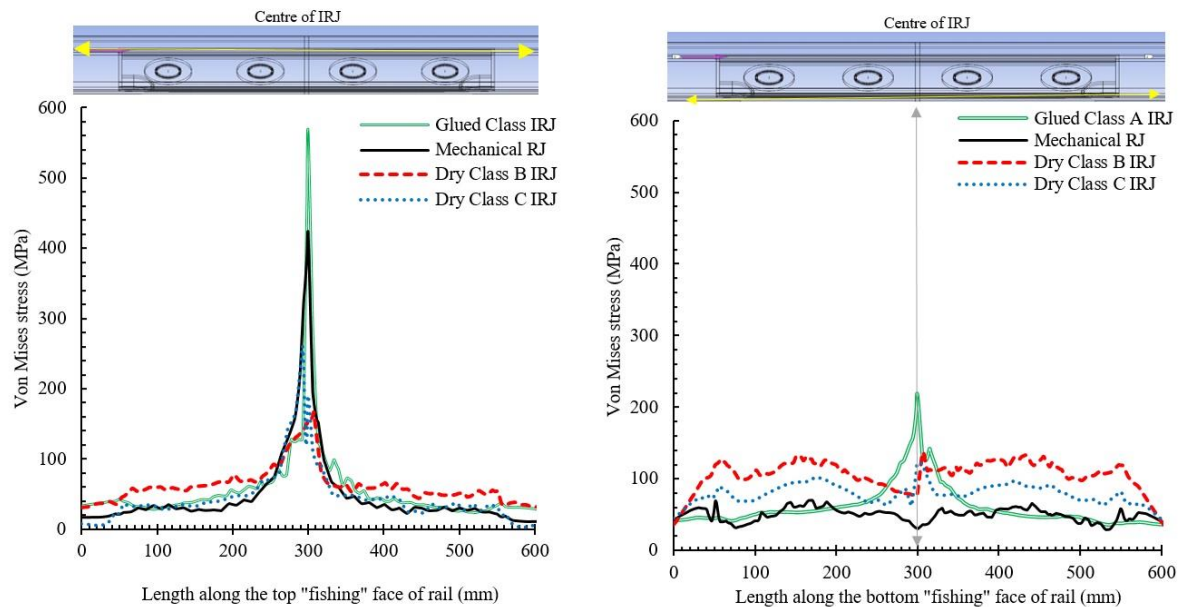
Figure 25. Equivalent (von-Mises) stress plots of the rail head and foot fishing surfaces for various rail joint types

6   DISCUSSION OF THE RESULTS

The displacements found here (3.8-5.4mm using a dynamic wheel load of 200kN and elastic support conditions) accord with real-time dynamic field data measured by the authors (4.2-6.6mm) [22] and are in the same order of magnitude (2.5-6mm) with those found in literature (2.4mm for a 150kN wheel load) [6]. Vertical displacement generally was smaller in the glued IRJ than in the other cases, probably because of the increased contact interfaces.   The stresses found in the web face of the fishplates are in agreement with experimental data [5, 7]. The

deflections measured experimentally are within the acceptance criterion of mechanical testing of glued IRJs which is 10mm for an applied force of 410kN [33]. The fishplates, under the input conditions assumed, meet the criteria against yielding for the four cases studied, as the maximum von Mises stresses found in the fishplates are below the yield strength and within the elastic region (absence of plastic deformation). Taken into account the maximum value of the von Mises stresses found in the fishplates, the safety factor was calculated in a range of 1.92-2 >1 for the four cases. Consistent stress plots were observed except peak values of stress that appeared in small areas of the top and bottom fishing surfaces which are due to the location of the wheel directly above the joint leading to high stress concentration in the rail end head –web fillet area and tensile bending stress on the bottom of the fishplate. A stress singularity is noticed in the rail edge in the head-web fillet area in the top fishing surface (this peak is of lower magnitude in the bottom fishing surface) shown in Figure 25. This constitutes a sharp internal corner with a strong change of direction that represent stress concentration with an infinitely small radius. Increasing mesh refinement only serves to increase the stress without limit. Only replacing with a larger fillet would eliminate the singularity. The stress peak is greater in the glued joint because it is a result of the stiffness of the entire model. These results match with recent studies [34] showing that stress in the rail fishing area reaches its maximum when the wheel is above the joint and that even in joints with well adopted easement, high contact pressure is found in the area adjacent to the easement (top and bottom fishing surfaces). It is also considered [34] that the design of the joint (type of rail section, fishplate design) may affect significantly the stress concentration and consequently the fatigue failure initiation on top and bottom fishing surfaces.

Additionally, peak stresses were developed around holes of the fishplates in two of the four cases. These peaks are considered amplified due to localised discontinuities within the model. Peak stresses can occur at local discontinuities (e.g., sharp corners, notches, holes, fillets). Such points are considered as stress singularities [28]. In this study they are attributed to the interaction of the linear beam elements with the fishplate body. The beams were used in place of modelling physical bolts to reduce the model size significantly. Yielding of ductile materials is important when yielding is widespread whereas failure is most often declared when yielding occurs across a complete section. In all instances, no values were recorded in excess of the material yield strength. However, bolt holes can be considered as potential areas of fatigue failure initiation when generated by high positive shear stress concentration around the bolt hole due to the high repeated impact wheel-rail loads and deflections [34]. Both bolt hole and top and bottom rail –fishplate interfaces are not detectable with visual inspection in the field.

The highest equivalent stress was found on the dry IRJ Class B (443 MPa). Immediately adjacent to this peak, circa 8 mm from the hole edge, the equivalent stress values were decreased to 250 MPa. Top (circa 332 MPa) and bottom (370 MPa) fishing faces of the plate also exhibited increased stress values. This distribution is consistent with the expected "sagging" deformation as a result of the wheel above the joint with compression on the upper and tension in the bottom surface of the fishplate. The corresponding stress values found in the central path of rail fishing surfaces are 166 MPa (top) and 137 MPa (bottom) with higher stress values to appear in the

lower curved area of the rail head (240 MPa on top, 300 MPa on bottom). Figure 21 shows a similar pattern on the mechanical RJ. A peak equivalent stress value of 421 MPa was found on the top fishing surface of the fishplate, however this only occurred around three nodes. Essentially the stresses were found below 250 MPa in the majority of the top fishing area and below 300 MPa in the bottom surface. Peak stresses were also observed in the top fishing surface of the rail.

Parametric analysis of bolt preload for a study when the wheel is not above the joint showed that a 43% preload decrease, lead to a 37% decrease of the von Mises stresses developed in the fishplate. However, when the wheel is above the joint, although the effect of bolt preload did exist the effect of vertical load is dominant in the magnitude of von Mises stresses developed.

Class B and class C fishplates developed peak stresses of lower magnitude than that of the mechanical and glued RJs as a result of the encapsulation insulating material and due to the different type of contact that exists in the interface between rail and fishplate. The glued joint developed higher peak stress values due to the increased contact areas among the components of the assembly but experienced less deflection.

The results indicated that the fishplates are experiencing a two-axis bending due to vertical wheel load. The pressure imparted by the underside of the railhead to the fishplate has a vertical and lateral component, due to the curved geometrical area. This fishing curved area induce bending in the fishplates about both its major and minor principal axes. The bolt pretension accounts for a significant percentage of the stresses developed mainly in the fishplate web. The type of FE analysis used here is advantageous over the theoretical approach that cannot take into account the multi-axial stress components.

This paper investigated the deflection and stress distribution around the rail joint area specifically at the rail-fishplate fishing interfaces, areas that are difficult to be observed in the field for four different types of rail joints commonly used in the UK railway network. This study differentiates from previous studies in terms of the rail joint types studied, the modelling techniques used for each type, the stiffness of the rail joints used (four-hole joints that are less stiff than the six hole), the support stiffness of the joints (stiffness per sleeper end) as well as the increased static wheel load (200kN-arising from an increased static load of 125kN increased by a dynamic factor of 1.6). The findings of this paper, showing defective areas of stress concentrations in both fishplates and rail fishing areas, can help the track design engineers to improve the efficiency and accuracy of rail joint failure detection and establish new strategies for redesign and maintenance of rail joints. The stress evaluation found by this study is planned to be further used for assessment against fatigue through the endurance limit approach that is mainly used for the analysis of fatigue static tests. This will require stress evaluation of the reverse bending stresses due to hogging deformation of the fishplates, an investigation that is planned to be carried out in the future.

7   CONCLUSIONS AND RECOMMENDATIONS

3D finite element analyses were carried out for different rail joint designs to investigate their behaviour under combined biaxial loading in a fatigue static test. Contact non-linearities in the rail joint interfaces and elastic support conditions were taken into account. An increased load case of 200 kN, based on real operational data, which has not been covered in past literature was presented. The mechanical response of four rail joint types under vertical load and bolt preload was investigated showing maximum rail joint deflections and areas of stress concentration for both rail and fishplates. The evaluation of stresses for the load case studied here can contribute to the fatigue strength assessment of fishplates as the stress concentrations, the stress multi-axiality and the variable amplitude loading are some of the factors affecting significantly the fatigue integrity of structural components consistent with railway applications. Furthermore, the current research has used FE analysis for proposed RJs that allow designers to use it as a parametric design script template that will enable commercial studies and optimization to improve the life expectancy of IRJs.   The model was validated against laboratory testing and correlates well with field measurements.

The results revealed the following conclusions:

- The top fishing interface between the rail and the fishplate experiences the larger deformation as a result of the wheel load as expected due to the compressive pressure induced.
- The fishplate designs under the increased load case used here developed stresses below the yield limit. The 200 kN wheel load did not cause material plasticity in the rail—fishplate interface.
- The bolt pretension affects significantly the stress level found in fishplate web and dominates for load cases where the wheel is not above the joint. When the wheel is above the joint, the vertical wheel load governs the maximum stress developed.
- The fully glued IRJ type decrease the overall joint displacement by 22% in comparison with the mechanical RJ and by 42% in comparison with the dry joints as a result of increased contact in the interfaces of the joint assembly.
- Assessment against fatigue can be performed if reverse bending stresses are calculated for the "hogging" deformation of the fishplates.

Acknowledgements

References

[1]   Beaty P. *Experimental testing procedures to investigate and improve insulated rail joint design and life cycle.* MSc Thesis, University of Sheffield, UK, 2014.

[2]   PWI, Guidance for Heritage Railways on the Inspection and Maintenance of Permanent Way and the Inspection and Assessment of other infrastructure that is necessary for the safety of the line. Document 4-Visual inspection.
https://www.thepwi.org/technical_hub/guides (2012, accessing 13 June 2017)

[3]   Mandal NK, Peach B. An Engineering Analysis of Insulated Rail Joints : A General Perspective. Int J Eng Sci Technol. 2010;2(8):3964–3988.

[4]   British Rail Research, Track Unit. Modelling 4-hole fishplated rail joint using the finite element method Report No RR MF 046. Derby, UK, June 1993.

[5]   Soylemez E and Ciloglu K. Influence of Track Variables and Product Design on Insulated Rail Joints. *Transp Res Rec J Transp Res Board.* 2016 Jan;2545:1–10.

[6]   Pang T. *Studies on Wheel/Rail Contact – Impact Forces at Insulated Rail Joints*. MEng Thesis, Central Queensland University, Australia; 2007.

[7]   Askarinejad H, Dhanasekar M and Cole C. Assessing the effects of track input on the response of insulated rail joints using field experiments. *Proc IMechE, Part F: J Rail Rapid Transit*. 2012 Sep 13;227(2):176–187.

[8]   NR/SP/TRK/023 Insulated Rail Joints, March 1996

[9]   Mandal NK. FEA to assess plastic deformation of railhead material damage of insulated rail joints with fibreglass and nylon endposts. *Wear*. 2016;366–367:3–12.

[10]   Mandal NK and Dhanasekar M. Sub-modelling for the ratchetting failure of insulated rail joints. *Int J Mech Sci.* 2013;75:110–122.

[11]   Himebaugh AK, Plaut RH and Dillard D. Finite element analysis of bonded insulated rail joints. *Int J Adhes Adhes.* 2008; 28: 142–150.

[12]   Grossoni I, Iwnicki S, Bezin Y, et al. Dynamics of a vehicle-track coupling system at a rail joint. *Proc IMechE, Part F*: J Rail Rapid Transit. 2014; 229:364–374.

[13]   Zong N, Wexler D and Dhanasekar M. Structural and material characterisation of insulated rail joints. *Electron J Struct Eng*. 2013; 13: 75–87.

[14]   Patel S, Kumar V and Nareliya R. Fatigue analysis of rail joint by using finite element analysis. *Int J Res Eng Technol.* 2013; 2: 80–84.

[15]   Talamini B, Jeong DY and Gordon J. Estimation of the fatigue life of railroad joint bars. In: *ASME/IEEE 2007 Joint Rail Conference and Internal Combustion Engine Division Spring Technical Conference. ASME*, 2007, Pueblo, Colorado, USA, 13–16 March 2007.

[16]   Bandula-Heva TM, Dhanasekar M and Boyd P. Experimental Investigation of wheel/rail rolling contact at railhead edge. *Exp Mech*. 2012; 53: 943–957.

[17] Bandula-Heva T. and Dhanasekar M. Failure of discontinuous railhead edges due to plastic strain accumulation. *Eng Fail Anal.* 2014; 44:110–124

[18] Sandström J and Ekberg A. Numerical study of the mechanical deterioration of insulated rail joints. Proc IMechE, Part F: J Rail Rapid Transit. 2009; 223: 265–273.

[19] Ding K and Dhanasekar M. Flexural behaviour of bonded-bolted butt joints due to bolt looseness. *Adv Eng Softw*. 2007; 38: 598–606.

[20] Dhanasekar M and Bayissa W.Performance of square and inclined insulated rail joints based on field strain measurements. Proc IMechE, Part F: J Rail Rapid Transit. 2011. pp1-15

[21] Vossloh Rail Services. Glued Insulated Joint IVB 30. http://www.vossloh-cogifer-uk.com/admin/resources/main-content-downloads/vtsivb30.pdf [accessed on 30 June 2017]

[22] Gallou M, Temple B, Hardwick C, Frost M, El-Hamalawi A. Potential for external reinforcement of insulated rail joints. *Proc IMechE, Part F: J Rail Rapid Transit*. Epub ahead of print 22 Dec 2016.

[23] Van Dyk BJ Van, Dersch MS, Edwards JR, et al. Evaluation of dynamic and impact wheel load factors and their application for design. *Transportation Research Board 93rd Annual Meeting.* Washington, USA, 12-16 January 2014

[24] British Steel: Steel Grade Composition and Properties, 2017

[25] Cope GH. *British railway track: Design, construction and maintenance*. 6th ed. Cope GH, England: Permanent Way Institution; 2001.

[26] GC/RT5021:2011. Railway Group Standard. Track System Requirements.

[27] ANSYS Inc. An overview of methods for modelling bolts in ANSYS V15, July 17 2015.

[28] ANSYS Inc. ANSYS Mechanical User's Guide. Release 17.1, April 2016

[29] prEN 16843:2015 European Standard Railway applications-Infrastructure-mechanical requirements for joints in running rails, March 2015

[30] AREMA- American railway engineering and maintenance of way association, Part 3, Joining of rail. 2007

[31] AS 1085.12-2002 Australian Standard. Reconfirmed 2013 Part 12: Insulated joint assemblies.

[32] TB/T 2975-2000 People's Republic of China Standard

[33] NR/SP/TRK/064 Assembly of BR MkIII 4- and 6- hole insulated joints, December 2003

[34] Zhu, K., Y. Qian, J.R. Edwards and B.O. Andrawes. Finite element analysis of rail end bolt-hole and fillet stress on bolted rail joints. Transportation Research Record: Journal of the Transportation Research Board, 2017. 2607: 33-42.

APPENDIX D - PAPER 4

Gallou M. Frost M., El-Hamalawi A., Hardwick C. The application of Track Deflection Measurements Made by the Video Gauge. Proceedings of the Institution of Civil Engineers, Transport. Epub ahead of print, 21 May 2018.

Abstract

This paper presents direct track deflection data measured by the Video Gauge (VG), (a Digital Image Correlation method) to determine track stiffness characteristics remotely. Two cases are discussed. First, the deflection performance of two novel ballastless trackforms are coupled with an analytical model to assess their stiffness properties for known train loads. Second, the performance of a bridge transition is evaluated under live train passages by the VG; the traffic loads are assumed based on train type to allow track stiffness interpretation from a number of train passes. A track deflection bowl is assessed to show the performance of the transition. The paper initially discusses the DIC technique and the importance and assessment of track stiffness. It then presents the VG deflection data, the global support stiffnesses and deflection bowls. These novel methods are shown to be consistent with other approaches of track stiffness evaluation. The paper concludes with a discussion on how this methodology can be utilised in the railway industry for assessing the trackbed performance of critical zones without the need for track possessions.

Keywords

Railway systems; Rail track design; Field testing & monitoring

Notation

S_{system} is the global track system stiffness
Q is the applied wheel force exerted on top of rail
δ is the rail deflection
k_{system} is the track support system modulus
x is the distance from the force application point
L is the characteristic length of track
EI is the flexural rigidity of the rail
$k_{railpad}$ is the railpad modulus
$k_{trackbed}$ is the trackbed modulus
c is the sleeper spacing
$s_{trackbed}$ is the trackbed stiffness
$s_{railpad}$ is the railpad stiffness

1 Introduction

In recent years Digital Image Correlation (DIC) techniques have allowed direct measurement of deflections of elements subject to dynamic loading using devices such as the Video Gauge. This technique has been used to evaluate track performance by assessing deflection under load (Gallou et al., 2017). Understanding of the railway track deflection is important to permanent way engineers as it gives an indication of the performance of the track system and identifies areas where there are potential issues, related to the performance of the track components and track quality. One parameter that can be assessed from dynamic deflection of the track under known load is the track stiffness.

The global track stiffness of the whole track structure is assessed as the force applied to the rail divided by the rail deflection. It varies with frequency, dynamic amplitude and position along the track. Acceptable levels of vertical track stiffness are not defined in European guidance, but current UK Standards (Network Rail , 2008, 2016; RSSB, 2011) provide values for

- target formation moduli for new track construction (45 MN/m^2) and for post renewal, (15-45 MN/m^2 according to track category)
- the optimum dynamic sleeper support stiffness, for existing track for different speeds (30 MN/m for line speeds <50 mph (≈80 km/h) and 60 MN/m for line speeds 50-125 mph (≈80-200 km/h).

An optimum global track stiffness value of 45 MN/m and an optimum rail deflection of 2 mm was recently proposed (Wehbi and Musgrave, 2017).

There are various techniques available to measure track load and deflection performance to assess stiffness but many require access to the track to install extensive instrumentation and monitoring equipment. Such access can be difficult to obtain through possessions and has consequent effects on train services. The DIC technique can be undertaken remotely from the track and, at worse, only requires brief access to the track to install targets on the rails and sleepers to improve the target quality; in some cases, targets may not be required. Such remote techniques offer potential advantages over current techniques, such as measurement of multiple points and track components at the same time, at higher capture rates and high resolution leading to a large deflection database of high accuracy offering substantial time and cost saving. The higher the train speed, the higher the deflection frequency of each axle. The video capture rate must be high enough to capture the actual maximum deflection.

This paper presents data from a DIC method of direct track deflection measurement under traffic loading using the Video Gauge and then uses the deflections measured to derive track stiffness characteristics. This is undertaken for situations where the load is known (for tests on novel track forms). Data from a live track are also presented, for particular types of train, where the loads are assumed (based on train type) to allow assessment of a track deflection bowl and the performance of a bridge transition. In the latter case the assumption is that if sufficient train passes are recorded, the deflection and load data will consolidate to a mean that will give sufficiently accurate data to allow track performance and stiffness to be appropriately assessed without the need for measured loading and track access.

Track stiffness, its measurement and the tools currently used are initially discussed. A model used for track stiffness calculation is then presented, followed by the data described. These data and the model are then used to show how stiffness can be assessed from the VG.

1.1 Track stiffness and its assessment

To assess track stiffness, both load and deflection data are typically required. These data are then coupled with a track behaviour model, such as the beam on elastic foundation (Boef), to allow track stiffness to be calculated. Over a number of years, global track stiffness has been assessed from data collected from various techniques, summarised and referenced in Table 1. Deflection measurements have been taken using vehicles with a vibrating (known) wheel axle load, rolling stiffness measurement vehicles, the Portancemètre and direct track instrumentation, including direct methods of measuring track deflection such as linear variable displacement transducers (LVDTs), laser reflectometers, remote video monitoring (RMV) using Particle Image Velocimetry (PIV) and DIC, along with indirect methods such as the use of geophones and accelerometers.

The detection of wheel loads to couple with deflection has been assessed from shear forces by means of strain gauges on the rail. However, such devices require calibration against known applied loads, which is difficult to achieve in the field.

Other devices for measuring local stiffness directly include track loading vehicles and falling weight deflectometers, recently developed into the rail trackform stiffness tester to facilitate use on railways. The advantages and disadvantages of various track stiffness assessment methods are presented in Table 1. The issue with many of the techniques presented in Table 1 is that instrumentation needs to be directly fixed to the track or track possession is required.

Table 1. Advantages and disadvantages of track stiffness measurement techniques

Measurement technique	Advantages	Disadvantages
LVDT (Fortunato et al., 2015)	High accuracy for high speed Direct deflection High capture rate (e.g. 500Hz)	Single axis (non- accurate results if movement in 2 axis) Less safe Need steel rods-additional non-movable reference zero deflection frame
Laser deflectometer (Innotrack,2006; Fortunato et al., 2015)	High resolution to 0.001mm Direct deflection	High cost Ground borne vibration of the tripod may affect the accuracy Single point measurement
Multi-depth deflectometer (Mishra et al., 2014)	Direct deflection Measures permanent deformation	Requires fixed datum at depth Can be problematic to install

Geophones (Innotrack, 2006; Bowness et al., 2007; Le Pen et al., 2014)	Ground and subsurface layers motion (velocity) measured Resolution to 0.07mm	Initial noisy data need correction of signal, filtering and post processing to give accurate deflection values (need Inverse Fourier Transform and integration of velocity time history to absolute deflections) Single point measurement where each geophone is positioned High capture rate of raw voltages (e.g.500Hz) but not of actual deflection
Remote video monitoring (RVM) using PIV (Bowness et al., 2007)	Direct deflection Software comprising with multiple cameras Noise reduction Post process 2D OR 3D Remote monitoring apart from target positioning-Safe Easy set up	High resolution only when long sight e.g.15m Small capture rate e.g. 30Hz Affected by ground borne vibration Only 1 sleeper or location can be monitored at a time
RVM using DIC (Murray, 2013; Thompson et al., 2015) and Video Gauge (Gallou et al., 2017)	All advantages of RVM using PIV High capture rate (e.g. 200Hz) High resolution to 0.001mm Multiple points at a time, enables measuring structures from <0.01mm wide to >1km long. Applicable in frequencies more than 200Hz by using expensive higher frame rate cameras Deflection bowl can be measured	Prone to alternating lighting conditions during outdoors recording.
Vehicle systems RMSV/ Portancemètre /TLV (Innotrack, 2006; Li and Berggren, 2010)	Dynamic track stiffness up to 50Hz and stiffness phase (deflection delay by comparison to force) Continuous measurements over long track length	Additional cost of transport to site and locomotive during measurements. Difficulty for widespread use.
FWD (Sharpe and Collop, 1998; Govan, Sharpe, Brough, 2015)	Indirect deflection of unclipped sleeper under a known falling mass Static support system stiffness without a live train wheel load	Assumptions of linear load distribution in depth to provide deflection of nearby track, uncertainty due to model dependency Neglects the uneven stress distribution below sleepers e.g due to voiding

1.2 The Video Gauge

The VG is based on DIC principles and video extensometry and uses robust industry-grade cameras that enable high resolution measurements of deflection by means of sub-pixel pattern recognition algorithms. Its practical advantages and high precision have been shown in the past and it has been widely used in material testing and infrastructure applications (Waterfall *et al*.2012). The VG was first introduced as a promising tool for rail application by Waterfall *et al*. (2015). The precision of VG for rail deflection measurements was tested by Gallou *et al*. (2016), who measured the dynamic deflections of a rail and rail joint using a VG and the results were compared with LVDT readings in the laboratory. An excellent correlation between the two techniques was found, thus validating its use for subsequent rail application in the field. Its applicability for the accurate assessment of rail deflection and rail joints under high-speed traffic loading was published by Gallou *et al*. (2017).

The VG method has advantages over previous image-based measurement techniques in terms of the capture rate, accuracy, resolution and the quality and quantity of data produced. It enables the measurement of multiple points (over 100) at a time at various perspective planes at sampling frequencies up to 300 Hz and in resolutions of the scale of 0.001mm, comprising multiple cameras and allowing (post) data processing. Hence, high-quality deflection data for a relatively long section of track, from a close distance, can be collected quickly in a safe and cost-effective way. The resolution depends on the quality of the image target (depending on size and varying brightness) and the field of view (depending on lens choice compared with distance to the object). For the VG method, when natural object features are not sufficient for pattern recognition) limited access is required to the track for marking of the rail web or mounting targets on sleepers to improve object target quality. The measurements themselves are made remotely.

It is therefore proposed that if VG can be used to assess deflection accurately, these data could be used to calculate track stiffness. This could be under a known load or by approximation of load from typical train types based on large data sets converging on a mean. Rail deflection depends on trackform condition, train speed and wheel spacing. As a VG is able to evaluate deflections for each individual axle during a vehicle pass, the VG offers greater understanding of track performance assessment, including any dynamic effects. Although an increase in train speed can affect track deflection non-linearly, this effect is limited as long as the speed is not approaching the critical speed (velocity of the wave propagation of the supporting track ground system); however, train speed can be assessed from the video where this may cause issues/variability.

2 Track stiffness: definition and an example of BOEF approach

Various models of track stiffness assessment have been proposed but the global vertical track stiffness can be defined as

$$S_{system} = \frac{applied\ force\ exerted\ on\ top\ of\ rail}{rail\ vertical\ displacement} = \frac{Q(t)}{\delta(t)} \text{ or } S_{system} = \frac{Q(f)}{\delta(f)} \qquad \text{eq.1}$$

where S is the track stiffness as a function of time *(t)* or a function of the excitation frequency *(f)* when assessed in the frequency domain, Q is the applied wheel force exerted on top of the rail and δ is the rail deflection.

There are two approaches to the determination of track stiffness: a static one, which is represented by its magnitude as direct relation of applied load and deflection, and a dynamic one represented by its magnitude and phase, where phase is measured as deflection delay by comparison with force that is mostly related to ground vibration and damping properties (Li and Berggren 2010). Conventional calculations of track stiffness are based on the static approach of the Boef developed by Zimmermann in the 1888. This combines the rail flexural rigidity (EI), the rail-pad stiffness, the trackbed stiffness (ballast, subballast and subgrade) in a spring in series system. The governing differential equation that yields the solution for the rail deflection is (Powrie and Le Pen, 2016):

$$\delta(x) = \frac{Q}{2k_{system}L} e^{-\left(\frac{x}{L}\right)} \left(\cos\frac{x}{L} + \sin\frac{x}{L}\right) \qquad \text{eq.2}$$

where L is the characteristic length of the track, a parameter that defines how far from the point load the deflection bowl extends along the rail, taking into account the flexural rigidity of the rail and the elasticity of the system. This is determined using

$$L = \sqrt[4]{\frac{4EI}{k_{system}}} \qquad \text{eq.3}$$

k_{system} is the series support system modulus, a combination of the railpad modulus *($k_{railpad}$)* and the trackbed modulus *($k_{trackbed}$)* given by:

$$\frac{1}{k_{system}} = \frac{1}{k_{railpad}} + \frac{1}{k_{trackbed}} \qquad \text{eq.4}$$

The term modulus k (measured in MN/m^2) refers to the distributed support stiffness calculated from the sleeper spacing (c) and the discrete stiffness of the railpad, ballast, and subgrade defined as $k_{trackbed}=s_{trackbed}/c$ and $k_{railpad}=s_{railpad}/c$.

Therefore, for the point of application (x=0) of a wheel load and rail deflection measurement by combining the Equations 1 and 2 the global static-stiffness is obtained from

$$S_{system} \left(in \ \frac{MN}{m}\right) = \frac{Q}{\delta(0)} = 2k_{system}L \left(in \ \frac{MN}{m^2}m\right) \qquad \text{eq.5}$$

Figure 1(a) shows the calculated results using this Boef approach for five typical track structures (of assumed trackbed stiffness in a range 10-100 MN/m) for a CEN 56 rail, Q=100 kN, a standard railpad stiffness of 150 MN/m and a typical axle load of 20 ton. The global track stiffness and the track moduli are calculated for each case. Figure 1(b) shows the calculated rail deflections for various trackbed moduli *($k_{trackbed}$)* from 10 to 80 MN/m^2. These figures show that the rail deflection bowl is highly affected by the trackbed support system conditions rather than the rail system properties.
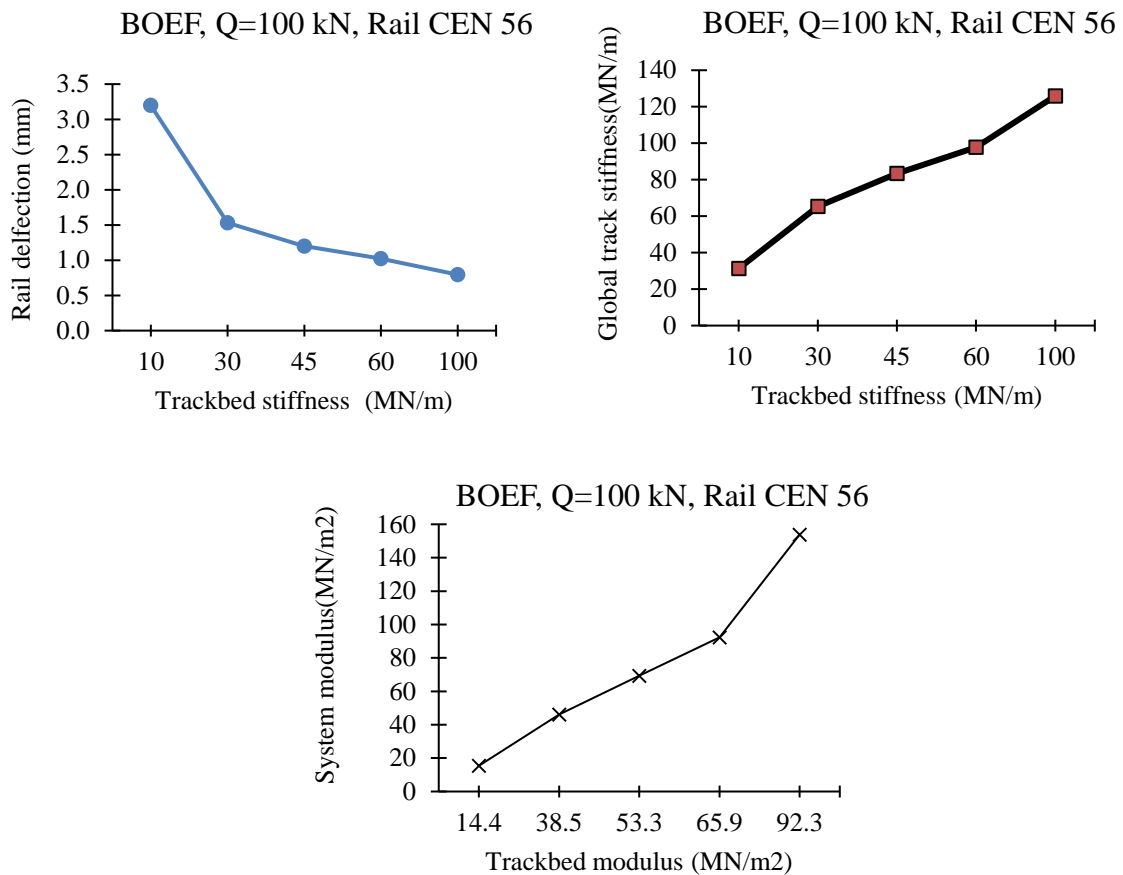
(a)
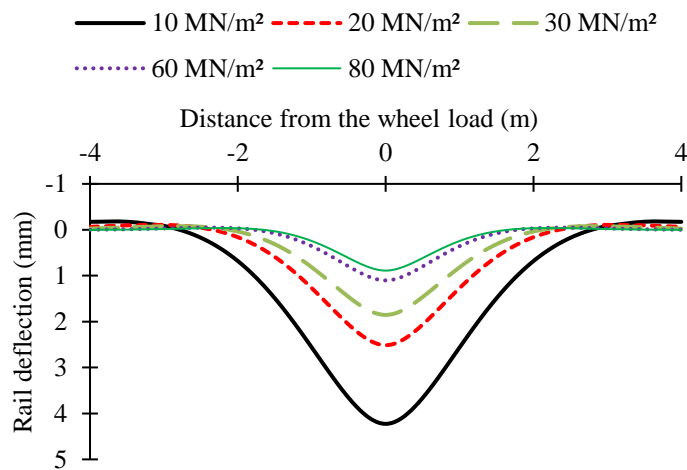
(b)

Figure 1. Results from BOEF for (a) various trackbed stiffness and (b) various support system moduli

3 Measurement of track stiffness

Field results and subsequent calculation of track stiffness from field trial data where deflections were measured with the VG are presented in this section. These trials can be split into two sets: (a) where the load was known and (b) where the load was assumed for a number of vehicle passes. The characteristics of each set of data are summarised in Tables 2 and 3. Train speed was determined in the time domain by determining the time between deflections under individual wheel loading separated by a known vehicle or trainset length from the VG data.

Table 2. Site characteristics

Site	Type of line	Type of track form	Fastening system
1	Test track (Rail Innovation and Development Centre)	PORR IVES Ballasted renewed	Vossloh DFF300 Vossloh DFF304 Pandrol Fastclip FC clip
2	High speed (East Coast Main Line)	Transition zone prior and after renewal	Pandrol Fastclip FC clip

Table 3. Train characteristics

Site	Type of loading	Speed	Set car	Car length	Static wheel load magnitude
1	Locomotive + 2 Sea Urchin wagons	2 to 20 mph	Locomotive		81.5 kN
			Wagon	6.3 m	66.25 kN
2	Intercity 125 (11 cars)	Up to 125 mph	Locomotive Class 43 Bogie spacing Wheel spacing	17.8 m 10.3 m 2.6 m	87.8 kN
			Coach Mark 3 Bogie spacing Wheel spacing	23 m 16 m 2.6 m	52.1 kN
	Class 222 (5 cars)	Up to 125 mph	Carriage	22.8 m	56-68 kN

3.1 Site 1

3.1.1 Experimental technique

The data included measurements of the deflection of three track structures under controlled low-speed train passage of known loading on conventional ballasted and two novel trackforms. The track structures considered were

- Ballasted renewed track, reballasted with new track components
- Ives (Intelligent, versatile, efficient and solid) (Rhomberg Sersa Rail Group, Austria) concrete ballastless modules with asphalt underlayment

- Porr slab system (PORR, Austria) with asphalt underlayment.

The Ives system constitutes individual prestressed concrete units of 250 mm depth and 1 t weight, separated by small gaps (to allow drainage), laid on 250 mm of asphalt. The Porr slab system consists of 5.16 m x 2.4 m x 0.16 m pre-cast concrete slab panels laid on a 100 mm asphalt layer. Deflections were measured at the extremity of the slab modules and in the rail above. A five-sleeper length comprising 3.25 m of renewed ballasted track was also assessed. Measurements of both rail and sleepers/slab modules were undertaken simultaneously. The deflection of the asphalt layer below the Ives system was measured using a steel rod fixed in the gap between the Ives modules. The train set consisted of a locomotive with three axles (16.3 t per axle) and two wagons with two axles each (13.25 t per axle) and was running at a range of velocities from 2 up to 20 mph. At least six train passes were recorded for each trackform and multiple positions were measured for each trackform. The measurements were undertaken at a capture rate of 105 Hz, using two cameras, 2m away from the line, each providing a horizontal x vertical field of view of 1.4 m x 0.74 m. Figure 2 shows views of the Ives track and the ballasted track along with the measurement locations.


(a)

(b)

Figure 2. (a) IVES track, (b) ballasted track

3.1.2 Deflection results

Examples of time-deflection plots of typical monitoring points for each trackform are presented in Figure 3(a). The deflections due to the two-axle wagon passage prior to and after the three-axle locomotive can be clearly seen. The resolution of the measurements was in a range 0.005-0.02 mm. Consistency of the results was found for each monitoring point under the passage of the six trains, indicating the repeatability of the results (24 wheel passages at each point for a known load). The maximum deflections for each position were averaged for all wheel passages from all tests. Figure 3(b) provides a comparison of maximum deflections found for all track components due to the wagon's wheel load. The rail deflections in the ballasted track and Ives and Porr slab tracks were 1.26 mm, 1.85 mm and 1.26 mm respectively, whereas the deflections for the sleepers and the Ives and Porr slab modules were 0.85 mm, 0.32mm and 0.31 mm.
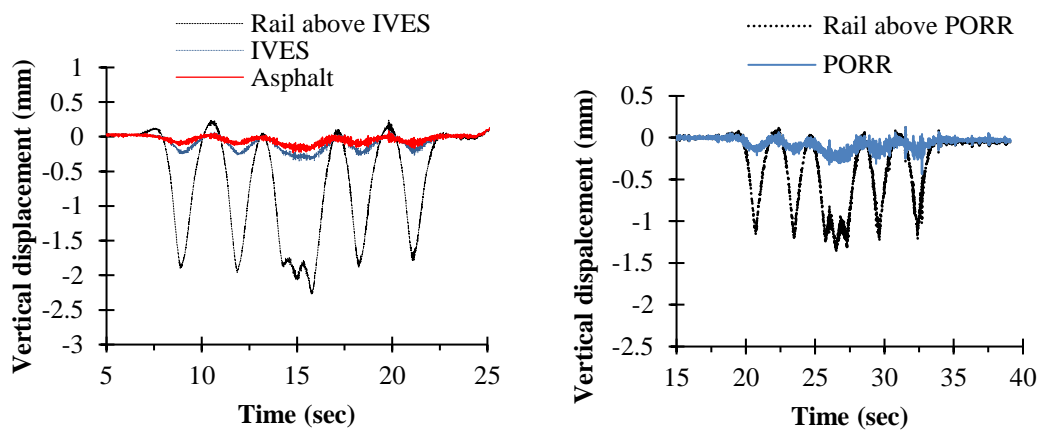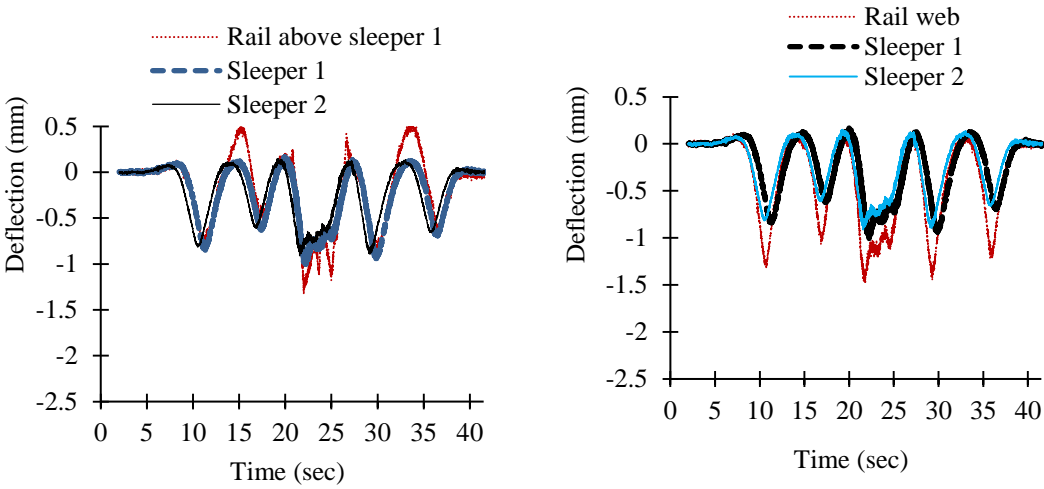
(a)
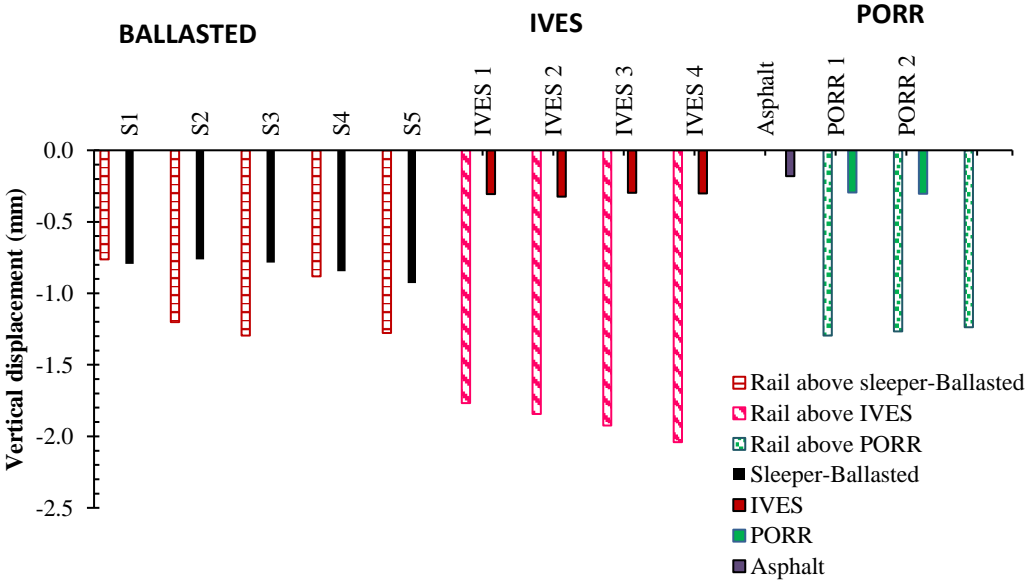
(b)

Figure 3. (a) Time-deflection plots of IVES, PORR and ballasted track under low speed train passage (b) comparison among maximum deflections.

3.1.3 Stiffness evaluation for a known load

The rail deflection includes the effect of rail bending and the effect of the elastic layers (railpad and trackbed). The railpad and the asphalt layer below a slab track (Ives and Porr) provide the elasticity that the ballast and railpad provide in the ballasted track. The static stiffness of the railpad usually used with the Porr and Ives systems is ≥ 22.5 MN/m (Vossloh, 2015).

For the Ives trackform, the global stiffness was calculated to be 36 MN/m. Using the deflections found and the known wheel load, the rail pad stiffness was back-calculated. Then, using the rail bending stiffness (for CEN 56 rail), 0.65 m spacing of the fastening system and the Boef equations as described in section 2, the effective rail pad stiffness was calculated as 14.5

MN/m. This value is lower than the specification. Using the 14.5 MN/m stiffness of the railpad, the support stiffness of the asphalt layer below the Ives slab module was calculated to be 51 MN/m. Table 4 summarises the back-calculated track stiffness parameters back calculated for three trackforms.

The global stiffness of the Porr trackform was directly calculated to be 53 MN/m. The stiffness of the Porr railpad was back-calculated to be 27.1 MN/m, which is within the specification (Vossloh, 2015). The support stiffness of the Porr trackform, which actually represents the stiffness of the asphalt layer, was estimated to 62.3 MN/m according to the rail deflection (1.25 mm) and the calculated stiffness of its railpad (27.1 MN/m). Also the measured asphalt deflection 0.18mm corresponds to 14% of the overall deflection (1.26 mm) for the Porr slab track. (It should be noted that the thickness of the asphalt layer is different for the two trackforms).

The global stiffness of the renewed ballasted track was calculated to be 53 MN/m. The railpad stiffness was estimated to be 84.2 MN/m whereas the trackbed stiffness was determined as 24.3 MN/m (trackbed modulus 37.4 MN/m2); these are within expected values from the standards (Network Rail, 2008, 2006; Powrie and Le Pen, 2016; RSSB, 2011).

Table 4. Stiffness characteristics evaluated from VG data and known load using Boef, for site 1.

Track form			IVES	PORR	Ballasted renewed
Symbol	Description	Units			
EI CEN 56	Rail flexural rigidity	MN.m^2	4.987	4.987	4.987
Q		kN	66.25	66.25	66.25
$s_{trackbed}$	Trackbed stiffness	MN/m	51.0	62.3	24.3
$s_{railpad}$	Railpad stiffness	MN/m	14.5	27.1	84.2
$k_{railpad}$	Railpad modulus	MN/m^2	22.3	41.7	129.5
$k_{trackbed}$	Trackbed modulus	MN/m^2	78.5	95.8	37.4
k_{system}	System modulus	MN/m^2	17.4	29.1	29.0
L	Characteristic length	m	1.04	0.91	0.91
S_{system}	Global system stiffness	MN/m	36.0	53.0	53.0
δ	Rail deflection	mm	1.84	1.25	1.25

3.2 Site 2

3.2.1 Measurement of deflections and stiffness in service

The second site was an assessment of the deflection performance of a transition zone on the approach to a bridge in live track, prior to and after major maintenance. The transition needed regular maintenance due to uneven settlement of the substructure caused by variations in

vertical track stiffness through the transition onto the bridge. Settlement variations can result in increased dynamic loads on the components and increased rail deflections during a train pass.

The field measurements included deflection measurements undertaken prior and after renewal. The maintenance activity included installation of a geocell web (to stiffen the transition track bed) and a sand blanket to provide drainage below the ballast. Initial measurements were conducted directly after manual tamping of the ballast, which temporarily improved performance prior to the main renewal.

3.2.2 Experimental technique

Rail and sleeper deflections through the transition were measured under high-speed train passages (eight Intercity 125 and three class 222 prior to renewal and two Intercity 125 after renewal) in live traffic with the VG (see train characteristics in Table 3). The measurements were undertaken at a sampling frequency 175 Hz using two cameras positioned 5 m from the track. A track length of 6.3 m, covering ten sleepers and the edge of the bridge was assessed. Each camera recorded both rail and sleeper deflections covering a horizontal x vertical field of view 3.5 m x 0.8 m. The anticipated resolution for the specific set-up of the VG system is given as 1/100 pixel to 0.035 mm. Variations of the measurement resolution within a single image are principally down to the quality of the target seen by the software. The resolution obtained was calculated as the standard deviation of the measurements points when there was no load applied. This was found to be in the range 0.016-0.042 mm for the various deflection points. At this site, the applied load was assumed on the basis of the train type observed. The estimated static wheel load was calculated according to the published weight and the number of axles of the vehicles. Although this may not accurately reflect the actual weight of the train (by not taking into account the weight of passengers, fuel and the vehicle dynamic effects), it was assumed that, over a number of passes, train weights will converge to a mean that will offer a way of using these deflection data (this hypothesis will be subject to further work).

3.2.3 Deflection results

Typical plot of the recorded deflection over time for two rail web positions is presented in Figure 4. Each deflection peak corresponds to an axle of an 11-carriage Intercity 125. Four peaks are distinct for each carriage (four axles per car, 44 wheels over each point in total). Consistency was observed among the magnitude of peak deflections due to the wheel passages along each train passage and among the total number of trains. In most tests, maximum values were found due to the wheel load of the locomotive passage, whereas some differences in the intermediate carriages were observed that can be attributed to differences in the actual static passenger load or to wheel defects and dynamic forces. It is observed that the rail did not return to its original level between adjacent wheel spacings on adjacent coaches, whereas between each bogie for each coach, the rail deflection fully recovered with small undulations due to the uplift of the rail ahead or behind the wheel passage. The maximum rail deflections for each

position (averaged for all train passages) along the total measured track length of the transition zone are presented in Figure 5 for the two maintenance phases (i.e. prior to and after renewal).

As noted earlier in the paper, the prior-to-renewal phase occurred after manual tamping and the deteriorated condition of the original transition was temporarily improved. The track deflection was found to be less than 2 mm for a 3 m length on the approach to the bridge. The fact that the rail still deflected by more than 2 mm adjacent to the bridge slab after renewal is attributed firstly due to the nature of the bridge substructure (where timber longitudinal beams support the sleepers off the end of the steel bridge beam) and secondly because dynamic deflections are influenced by the effects of a high train velocity (125 mph).

Studies in the literature often present track stiffness values or frequency values calculated from filtered deflection data after integration of velocity data measured by geophones to assess track quality. Since it is difficult to measure the dynamic load at a specific point of interest, it would be practical to target the deflection envelope (as recommended by Wehbi and Musgrave (2017)) rather than to use a back-calculated track stiffness envelope or integrated frequency envelope to characterise the track quality for different train velocities. The measurements presented here include any potential sleeper voiding and dynamic effects that will influence the results of the Boef model, as discussed later in the paper. The methodology of real deflection measurements presented above could help track designers (Powrie and Le Pen 2016; Sharpe *et al*., 2002) design for an optimum deflection by selecting the appropriate combination of trackbed layers and railpad types that will correspond to an optimum stiffness of the track, as a system.
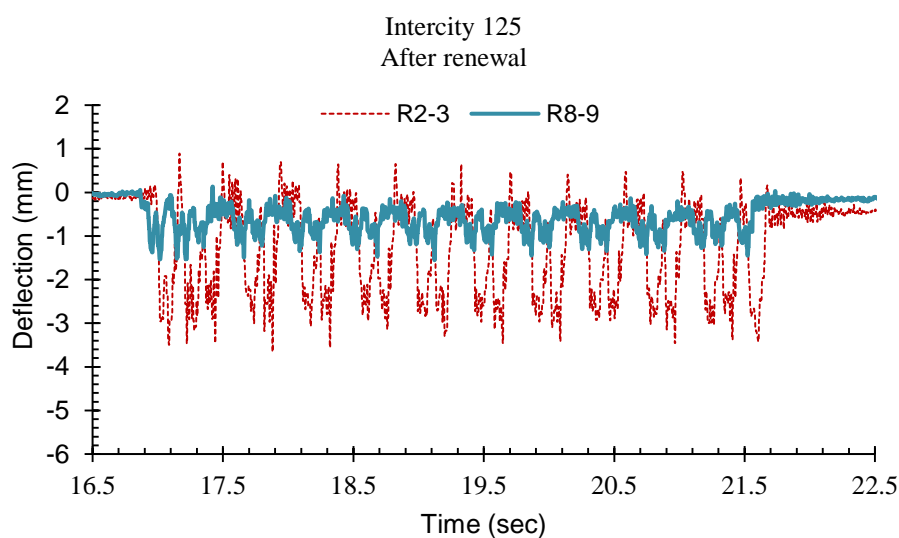

Figure 4. Examples of time –deflection plots of rail web positions in the transition zone under the same passage of Intercity 125.
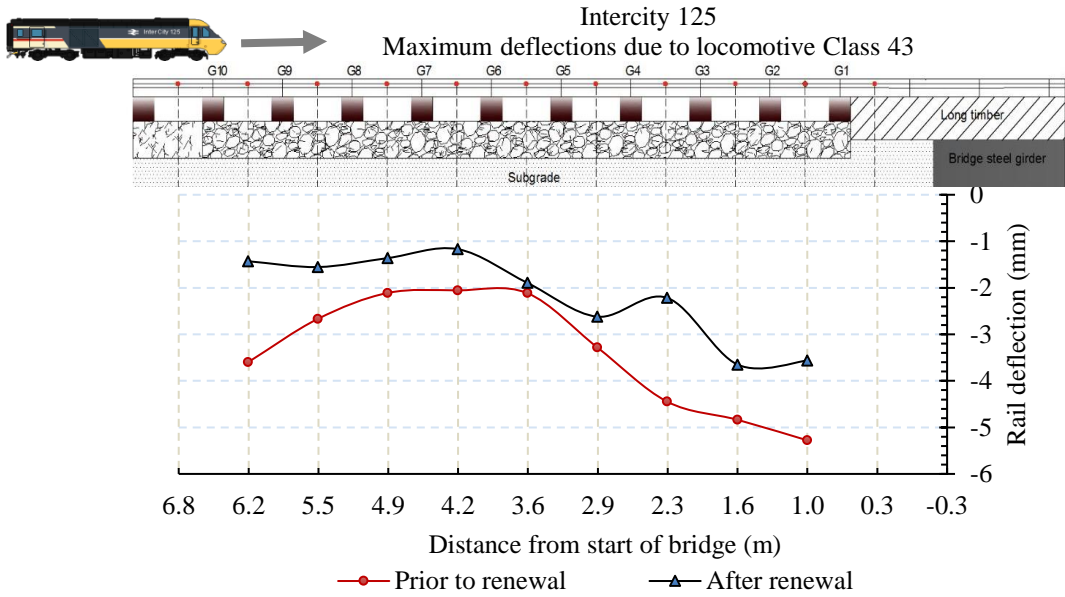
Figure 5. Comparison of rail deflections prior and after renewal

### 3.2.4 Stiffness evaluation for an assumed load

From deflection measurements over a track length of ten sleepers, the variance of the inferred track stiffness characteristics from one point to another, is shown in Figure 6. The global stiffness found by simply dividing the static locomotive wheel load by the rail deflections is shown in Figure 6(a). The variability of the support system stiffness (Figure 6(b)), the track system modulus (Figure 6(c)) and trackbed modulus (Figure 6(d)) were evaluated by taking into account the effect of railpad and rail bending stiffness by using the analytical model described in section 2. In the calculations, a railpad of medium stiffness 200 MN/m was used with a rail section CEN 56 rail section. An increase in track stiffness after the maintenance activity was observed after the third sleeper whereas the stiffness values of the first three sleepers near the bridge remained low and were considered to vary with various dynamic loads, at various speeds.
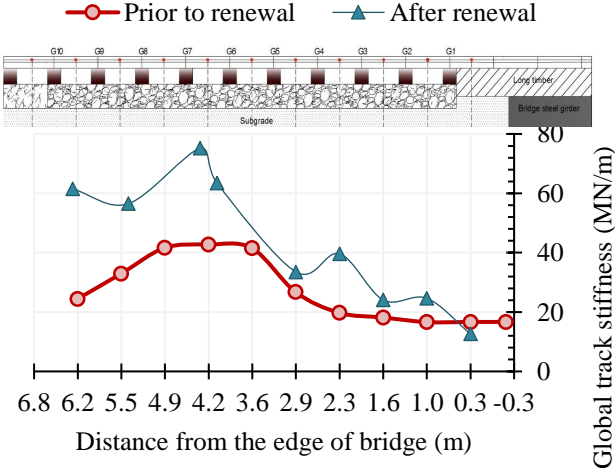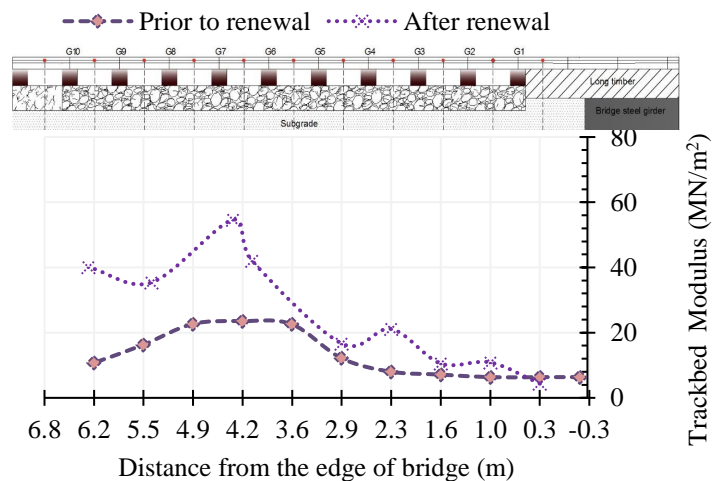
(a)
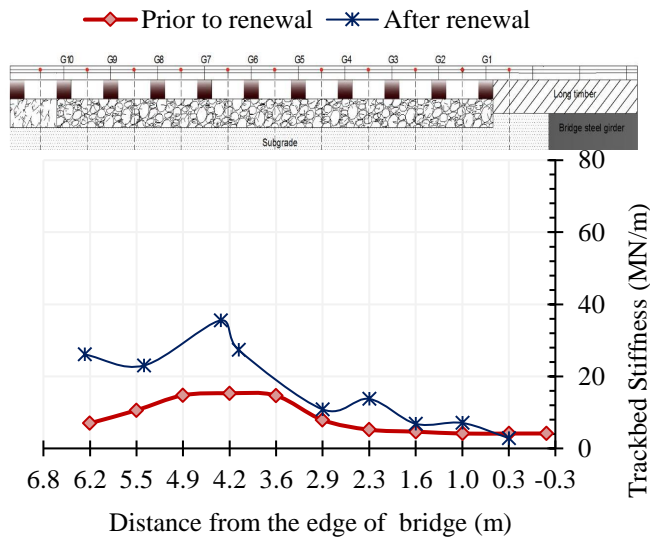
(b)
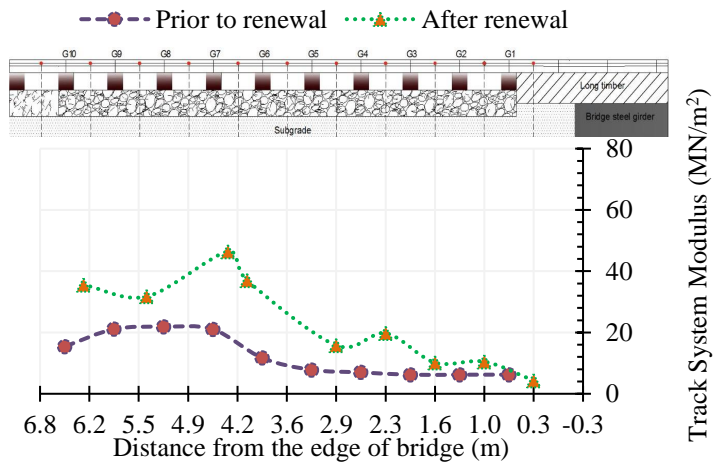
(c)

(d)

Figure 6. Comparison between renewal phases of (a) global track stiffness, (b) support system stiffness, (c) track system moduli and (d) support system moduli

This track stiffness calculation method is based on an assumption of linear elastic behaviour of the railpad and substructure (ballast and subgrade) and consequently may not realistically represent a site's performance where significant voided sleepers may be present prior to renewal, where less consistent behaviour is expected due to a sudden change in track stiffness when passing from ballasted track to a bridge and where non-linear stress-dependent responses and permanent settlements under dynamic loading may affect the track behaviour. To investigate this further, a measured deflection basin from the data (as an indicator of the load transfer under a moving wheel load in the transition zone) for both renewal phases was investigated. The results showed that the VG method could be suitable for visualisation of a change in track stiffness over a short distance of a critical zone and can be used to assess subgrade deflection conditions in an area that needs to be assessed promptly. Additionally, with more cameras, a longer length could easily be assessed.

3.2.5 Deflection bowl as an indication of load transfer and track system behaviour

The deflection bowl due to the passage of the first wheel of a class 222 above each sleeper for the prior-to-renewal phase is presented in Figure 7(a) whereas that due to class 43 wheel passage in Figure 7(b). Each curve represents the deflection measured on every sleeper at a specific time for a specific position of the wheel load. Looking the area where the bowl extends, it can be seen that the behaviour of track was consistent between sleepers G10 and G6 as the deflection over a sleeper extended over an area of two to three adjacent sleepers (giving a 2 m deflection bowl). This compares well to the data in Figure 1(b). From this data, the trackbed modulus was evaluated to be around 20 MN/m^2, based on the assumed train load, and this is typical of that expected for ballasted track. However, the load transfer along the transition zone was different when the wheel was above the area G4 to G1, with this situation improved after renewal (Figure 7(c)).

These findings indicate the requirements for a transition zone to have a gradual increase in overall track stiffness over the length of the transition, where railpad stiffness variations or other structural elements could be used to compensate for a variability in stiffness magnitude. The deflection bowl diagrams can be produced directly from the VG-recorded data without any other input parameters and give realistic values (see Section 2). This shows the potential of the VG system, but further validation is still required.
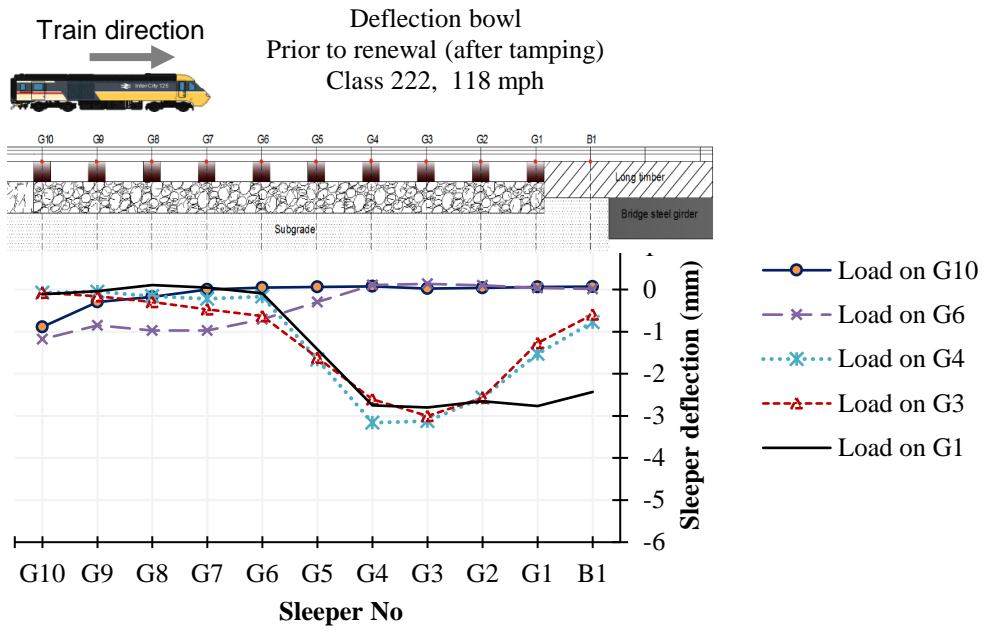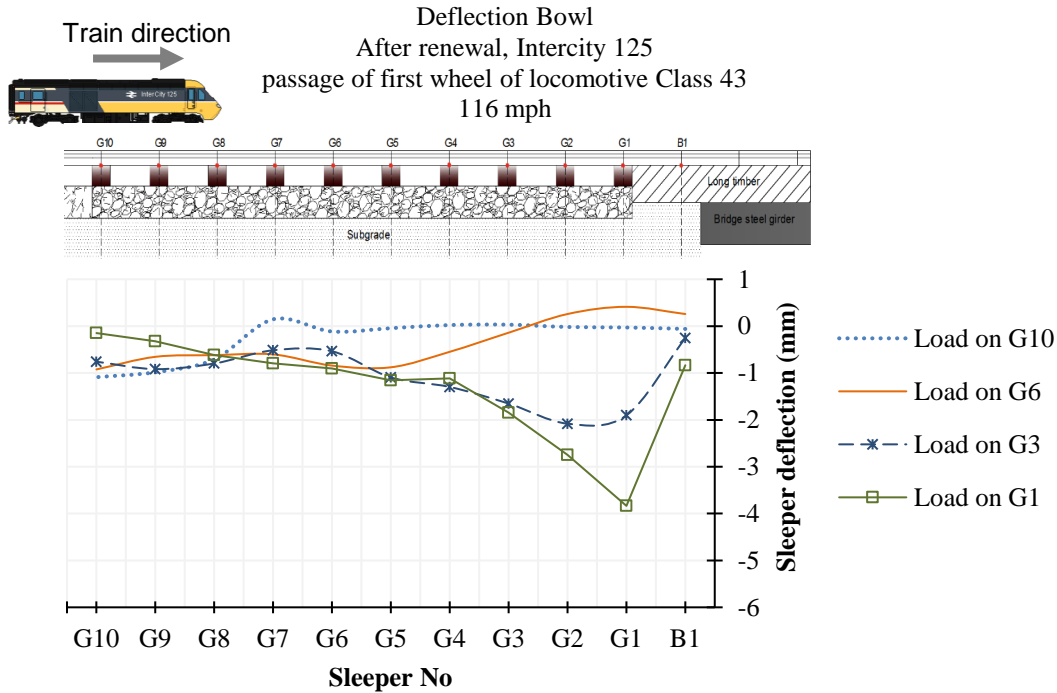
(a)
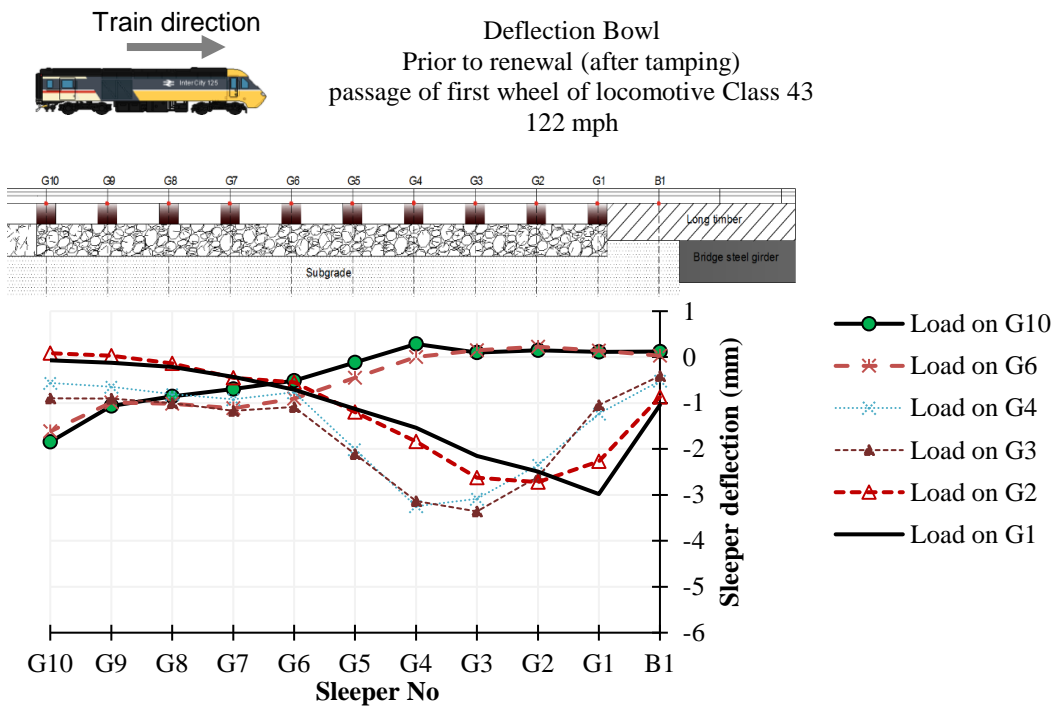
(b)

Figure 7. Deflection bowl of the transition zone (a) prior to renewal due to Class 222 first wheel passage and (b) prior to renewal due to Class 43 and (c) after renewal due to Class 43.

4 Conclusions

The applicability of using VGs for the remote assessment of ballasted and ballastless track deflections and support stiffness characteristics has been shown. Deflections below 2 mm were measured in ballastless and well maintained trackforms, whereas deflections of up to 5.5 mm were found in a transition zone adjacent to a bridge, leading to global track stiffnesses in the range of 18-75 MN/m with an average value of 44-53 MN/m for well maintained and newly repaired track.

A variation in trackbed stiffness in the range of 4-36 MN/m was found between maintenance periods for the transition zone; the trackbed stiffness was determined to be 24.3 MN/m for the renewed ballasted track, whereas the support stiffness of slab modules with underlying asphalt was estimated to be 50-60 MN/m.

The following conclusions were drawn from the results of this study:

- Rail deflections, accurately assessed remotely by VGs, can be used directly for global stiffness derivation under a known wheel load.
- For estimated traffic loads, the VG method can be used to give reasonable estimated track stiffness properties without the need to fix complicated instrumentation to the track. By providing visualisation of the performance of critical zones during service life

and between maintenance periods, the method saves time and cost and avoids the need for a full possession.

- Track system support stiffnesses and moduli for various positions can be determined by using estimated wheel load data and an appropriate model for the track behaviour such as the Boef.

- The deflection bowl for each point of wheel application can be derived directly through the real-time deflection measurements in the absence of the wheel load data, indicating the load transfer in a critical zone. This allows the assessment of the dynamic response of the track as a holistic system, providing useful information for both the superstructure and substructure through the analysis of multiple rail and sleeper deflections.

- The VG system can be used directly for track performance assessment where a rail deflection envelope is available; for critical zones that need to be investigated promptly, this can be combined with an estimated track stiffness envelope.

- Variability of the maximum rail deflections and consequent track stiffness variance can be caused by the variance of dynamic loading; further research is required to investigate and test the sensitivity of the proposed methodology for the derivation of absolute track stiffness values. An evaluation of deflections under various speeds over the same site for various trackbed conditions to determine the effect of the dynamic component to the stiffness range is recommended.

- The use of assumed train loads (averaged over many similar vehicle passes) coupled with remotely measured VG deflections seems to lead to the calculation of reasonable approximations to track stiffness. Although further validation is required, it may offer a cheaper method of evaluating track stiffness in service, especially in cases where modern trains can monitor their own axle weight to complement the VG deflection data.

Acknowledgements

References

Bowness D, Lock A, Powrie W, Priest J and Richards D (2007) Monitoring the dynamic displacements of railway track. P*roceedings of the Institution of Mechanical Engineers Part F Journal of Rail and Rapid Transit* 221(1):13–22

Fortunato E, Paixão A, Calçada R (2015) Field measurements and numerical modelling of transition zones –A research project in a recent portuguese railway line. In *Proceedings of Railway Engineering -2015 Conference, June 30th-July 1st*. Edinburgh, UK.

Gallou M, Frost M, El-Hamalawi A and Hardwick C (2017) Applicability of video gauge for the assessment of track displacement. In *The Stephenson Conference: Research for Railways* (Iwnicki S (ed.)). Railway Division, Institution of Mechanical Engineers, London, UK, pp. 141-148.

Gallou M, Temple B, Hardwick C, Frost M, El-Hamalawi A. (2016). Potential for external reinforcement of insulated rail joints. *Proc IMechE, Part F: J Rail Rapid Transit*. 233(3): 697–708.

Govan C, Sharpe P, Brough M (2015). The rail trackform stiffness tester-development and early trials to assess stiffness characteristics of novel trackforms. *In Proceedings of Railway Engineering -2015 Conference*, (Forde M (ed.)) ECS Publications, Edinburgh, UK, paper no. 1452.

Innotrack (2006) *Methods of track stiffness measurements*. Innotrack, Gothenburg, Sweden, Deliverable D2.1.11 for Innotrack project, Project no.TIP5-CT-2006-031415; 2006.

Le Pen L, Watson G, Powrie W, Yeo G, Weston P and Roberts C (2014). The behaviour of railway level crossings: Insights through field monitoring. *Transportation Geotechnics*, 1(4), 201-213.

Li M.X.D and Berggren E.G (2010). A study of the effect of global track stiffness and its variations on track performance: simulation and measurement. *Proceedings IMechE J Rail and Rapid Transit* 224 (5): 375-382

Mishra D, Qian Y, Huang H & Tutumluer E (2014) An integrated approach to dynamic analysis of railroad track transitions behavior. *Transportation Geotechnics* 1(4), 188-200.

Murray C (2013). *Dynamic monitoring of rail and bridge displacements using digital image correlation*. Mater Thesis. Queen's University, Kingston, Ontario, Canada.

Network Rail (2008) NR/L2/TRK/2102 Issue 8: Design and construction of track. Network Rail, London, UK.

Network Rail (2016) NR/L2/TRK/4239 Issue 1: Trackbed investigation, design and installation. Network Rail,London, UK.

Powrie W and Le Pen L (2016). *A Guide to Track Stiffness.* The Permanent Way Institution. Milton Keynes:

RSSB (Rail Safety and Standards Board) (2011) GC/RT5021 Track system requirements. Issue 5. RSSB, London, UK.

Sharpe, P and Collop AC (1998). Trackbed investigation-a modern approach. In *Railway Engineering 1998: 1st International Conference on Maintenance and Renewal of Permanent Way and Structures*. Brunel University (Engineering Technics Press), pp. 37–44.

Sharpe P, Armitage R J, Heggie W G, Rogers A (2002). Innovative design of transition zones. In *Proceedings of the 2002 Railway Engineering Conference, London, UK* (Forde M (ed.)). Engineering Technics Press, Edinburgh, p. 12.

Thompson H.B, Sussmann T.R, Stark T.D and Wilk S.T (2015). Non-invasive monitoring of track system gaps. In *Proceedings of Railway Engineering -2015 Conference* (Forde M (ed.)) Engineering Technics Press,Edinburgh, p.12.

Vossloh (2015) https://www.vossloh.com/en/products-andsolutions/products-at-a-glance/schienenbefestigungssysteme/ (accessed 03/06/2018).

 Waterfall P., Temple B., Hardwick C., Sharam J. and Plumb A. (2015) Video Measurement techniques for understanding wheel- induced lateral forces and track component deflections. In *Proceedings of the Stephenson Conference: Research for Railways, London, UK* (Iwnicki S (ed.)) Institution of Mechanical Engineers, London, UK, paper no. C1408/089, p. 11.

Waterfall PW, Macdonald JHG, McCormick NJ (2012) Targetless Precision Monitoring of Road and Rail Bridges using Video Cameras. In *Proceedings of the 6th International Conference on Bridge Maintenance, Safety and Management, Lake Como, Italy* (Biondini F and Frangopol DM (eds)) CRC Press, London, UK, pp. 3976–3983.

Wehbi, M & Musgrave P (2017) Optimisation of Track Stiffness on the UK Railways. *The Journal of the Permanent Way Institution* 135(3): 24–31.

Zimmermann H (1888). Die Berechnung des Eisenbahnoberbaus. Ernst & Korn, Berlin, Germany (in German).

APPENDIX E - TECHNICAL REPORT 1

Fishplate Fatigue Failure Estimation

Author: Maria Gallou

Date: 17th January 2018

Revision: 0

Revision	Comment	Approved	Date
0	Issue	Mathew Holland	17/01/2018

Executive summary

The fatigue strength of fishplates of four rail joint types insulated rail joints has been assessed through finite element analysis and theoretical calculations. The selected criteria are making use of the combination of the operational load cases for the rail joints due to the passing wheel load. Typical wheel load and track parameters were considered in the models. Results of number of cycles and years of rail joint life are presented for typical wheel load and rail vehicle speeds.

1. Introduction

Insulated rail joints (IRJs) constitute a weak component of the railway system. Major failure modes of IRJs comprise bond failure (delamination of endpost), loosening of bolts and broken fishplates. These failure modes are attributed to the increased vertical deflection at a joint, the vibration on track and the increased stress values experienced in the fishplates, while they are connected to the effective stiffness of the joint. Mechanical failure of an IRJ can be caused due to cracked or broken fishplates. The design life expectancy of the IRJs can vary significantly according to the P2 wheel-rail forces generated on each joint during its life. Depending the joint design a significant stress concentration can occur and fatigue crack can be initiated. A crack can typically initiate at a discontinuity in the material where the cyclic stress reach exceeds the endurance limit. At a rail joint the discontinuity exist because of rapid change of the cross section, thus the centre of the IRJ is a critical area.

The fatigue limit is a threshold value of the stress amplitude. Stress amplitudes below this level do not lead to failure, while stress amplitudes above the fatigue limit lead to crack initiation and crack growth to failure. Rail joint fishplates are subjected to multiaxial loading considering the bolt pretension and the vertical wheel load.

2. Methodology

For the fatigue calculation process, a structural analysis is required. This includes the determination of critical forces that occur in the rail joint. For this reason two critical load cases representing operational conditions are examined (see Figure 1):

  A. wheel load at 10mm from the rail gap/ IRJ centre
  B. two wheel load forces in a span equivalent to a typical UK wheel base (1.9m), one on each side of the RJ.

In the first case the joint is sagging due to the wheel passage whereas in the second case it is hogging due to the passing of two wheels. A static finite element analysis is conducted to define the maximum and minimum stress values caused by the application of every load case. A dynamic component is accounted to the model to replicate the effect of the P2 force acting above the rail joint (200 kN). The shear forces generated by the bolt pretensional load applied in the bolts, the elastic support conditions of the trackbed and contact non-linearities in the IRJ assembly are also accounted in the model. The model has been created by LB Foster as a

template Finite Element tool to assess fishplate design against fatigue and has been validated by laboratory and field measurements.
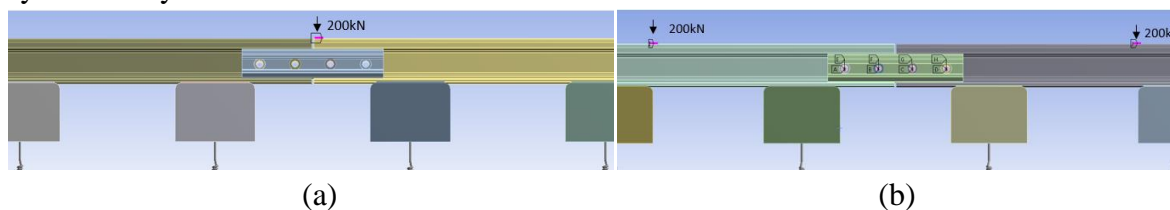

(a)   (b)

Figure 1. Loading cases (a) wheel load at 10mm from the rail end (b) wheel load at 900 mm from the rail end

3. FEA results

Consistent stress plots were observed except peak values of stress that appeared in small areas of the top and bottom fishing surfaces which are due to the location of the wheel directly above the joint leading to high stress concentration in the rail end head –web fillet area and tensile bending stress on the bottom of the fishplate. Figures 2 and 3 show the stress distribution along the central path at the top and bottom fishing surfaces of the fishplate for the various rail joint types for both load cases.
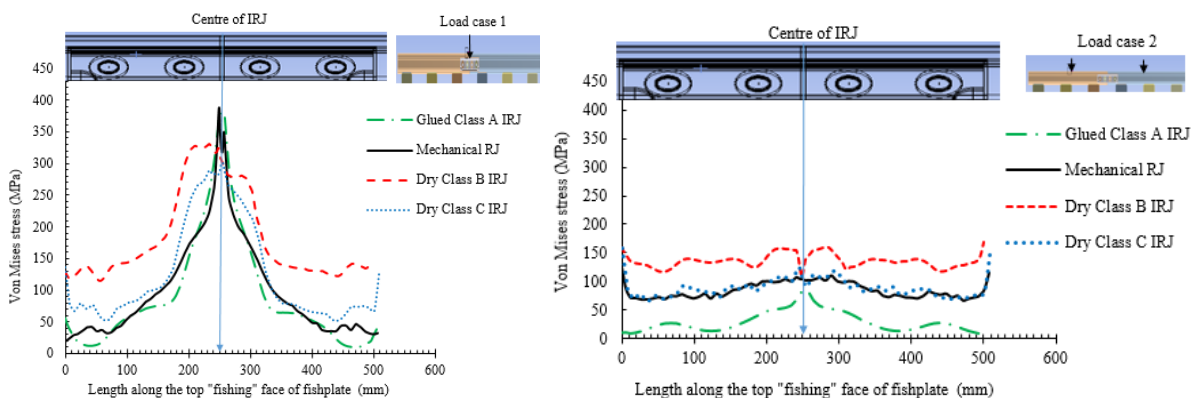

Figure 2. Equivalent (von-Mises) stress plots of the centre of top fishing surface of the fishplate for four rail joint types and two load cases.
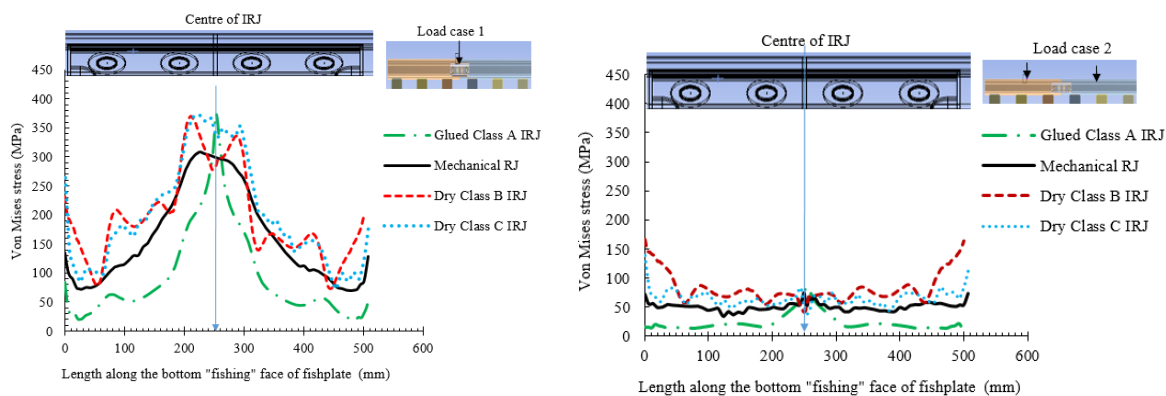

Figure 3. Equivalent (von-Mises) stress plots of the centre of bottom fishing surface of the fishplate for four rail joint types and two load cases.

4. Fishplate fatigue failure estimation

For estimating the stress range, maximum stress values found by the FEA for the two load cases ($\sigma_{sagging}$ and $\sigma_{hogging}$) are used to determine the loading cycle of the rail joint. The fatigue strength of the rail joint is also affected by the stresses imposed by rail tension. The rail is subjected to a tensile stress equivalent to the thermal stress for the maximum temperature differential ΔT of 40°C (-17°C to +23°C). The thermal load in rail is equal to:

$$P_{th} = a * \Delta T * E * A_R \qquad\qquad (eq.1)$$

and the stress imposed to rail during to installation:

$$S_{th} = \frac{P_{th}}{A_{2J}} \qquad\qquad (eq.2)$$

Where E is the steel elasticity modulus 210GPa, A_R is the rail cross sectional area, a is the expansion coefficient of the rail steel (1.15 $*10^{-5}$ per °C (NR/L2/TRK/3011)), A_{2J} the cross sectional area of two fishplates. Table 1 describes the calculation of P_{th} for the various joints.

Table 1. Calculation of tensile stress due to temperature difference

		Mechanical	Glued Class A	Dry Class B	Dry Class C
Temperature difference	ΔT	40	40	40	40
Coefficient of thermal expansion	a_{th}	0.0000115	0.0000115	0.0000115	0.0000115
Modulus of elasticity	E (kN/m^2)	210000000	210000000	210000000	210000000
Rail CEN 56 cross sectional area	A_R(m^2)	0.007169	0.007169	0.007169	0.007169
Joint bar cross sectional area	$\mathbf{A_J}$	0.003871	0.0036841	0.0037035	0.0034998
2 Joint bars cross sectional area	A_{2J}	0.007742	0.0073682	0.0074069	0.0069996
Thermal load in rail CEN 56	$P_{th} = A_R*E*a_{th}*\Delta T$ (kN)	692.5254	692.5254	692.5254	692.5254
Stress due to tension of rail during installation for max ΔT	S_{th} (MPa)	89.45	93.99	93.50	98.94

The Stress-life theory is used for fluctuating stresses. For estimating the stress components, maximum and minimum stress values found by the FEA for the two load cases ($\sigma_e^{sagging}$ and $\sigma_e^{hogging}$) are used to determine the loading cycle of the rail joint. The fatigue life estimation of the fishplates was carried out using the following formulae:

$$\sigma_m = \frac{\sigma_{max} + \sigma_{min}}{2} \quad \text{mean stress} \tag{eq.3}$$

where σ_{max} = the maximum tensional stress and σ_{min} = the maximum compressive stress.

$$\sigma_\alpha = \frac{|\sigma_{max} - \sigma_{min}|}{2} \quad \text{amplitude stress component} \tag{eq.4}$$

For fluctuating loading situations, it is necessary to obtain a completely reversed stress that may be considered equivalent in fatigue damage as the actual fluctuating stress:

$$\sigma_{rev} = \frac{\sigma_a}{1 - (\frac{\sigma_m}{S_{ut}})^2} \quad \text{(Gerber criterion)} \tag{eq.5}$$

S_e = endurance limit = 350MPa [1]

S_{ut} = ultimate strength 1000MPa

$$S_f = \frac{\sigma_\alpha}{1 - (\frac{\sigma_m}{S_{ut}})^2} \tag{eq.6}$$

where S_f the fatigue strength associated with a completely reversed stress σ_{rev} equivalent to the fluctuating stresses.

Number of cycles to failure: $\qquad N = (\frac{\sigma_{rev}}{a})^{\frac{1}{b}} \tag{eq.7}$

Where:

$$a = \frac{(f * S_{ut})^2}{S_e} \tag{eq.8}$$

$$b = -\frac{1}{3} * \log\left(f * \frac{S_{ut}}{S_e}\right) \tag{eq.9}$$

f=0.8 for S_{ut}=1000MPa [2]

The fatigue life (in cycles) can be calculated in terms of million gross tons (MGT) of traffic through the equation:

$$MGT = \frac{N\ (in\ cycles) * 106 * Q\ (in\ kN) * 2}{9.81 * 10^6} \tag{eq.10}$$

The fatigue life of fishplates for the rail joint configuration is estimated for various track categories according to equivalent gross million tons per annum (EMGTPA), that constitutes a

measure of annual tonnage carried by a section of track. The fatigue life for the four joint types is calculated and presented in Table 2 and in Figures 4 and 5.

Noted that in Table 2 a "signed" von Mises stress is chosen where the von Mises stress takes the sign of the largest absolute principal stress. This is used to identify any compressive mean stresses since several of the mean stress theories treat positive and negative mean stresses differently.

In general, most experimental data fall between the Goodman and Gerber theories with the Soderberg usually being overly conservative. The Goodman theory can be a good choice for brittle materials with the Gerber theory usually a good choice for ductile materials. The Gerber theory treats negative and positive mean stresses the same whereas Goodman and Soderberg are not bounded when using negative mean stresses. Goodman and Soderberg are conservative approached because although a compressive means stress can retard fatigue crack growth, ignoring a negative mean is usually more conservative [3].

Table 2. Fishplate fatigue life estimation

| Type of rail joint	Unit	Mechanical	Glued Class A	Dry Class B	Dry Class C
Wheel load	kN	200	200	200	200
S_{J-}	MPa	-388	-380	-332	-302
S_{J+}	MPa	125	85	170	157
S_{th}	MPa	93.99	103.04	93.5	98.94
$S_{min}=S_{J-}+S_{th}$	MPa	-294.01	-276.96	-238.5	-203.06
$S_{max}=S_{J+}+S_{th}$	MPa	218.99	188.04	263.5	255.94
$\sigma_m=(S_{max}+S_{min})/2$	MPa	-37.51	-44.46	12.5	26.44
$\sigma_a=(S_{max}-S_{min})/2$	MPa	256.5	232.5	251	229.5
S_e	MPa	350.0	350.0	350.0	350.0
S_{ut}	MPa	1000	1000	1000	1000
σ_{rev}	MPa	257	233	251	230
f		0.8	0.8	0.8	0.8
a		1828.571	1828.571	1828.571	1828.571
b		-0.120	-0.120	-0.120	-0.120
N	cycles	13267640.76	30007383.77	16069300.64	33806566.71
N	Millions of cycles	13.268	30.007	16.069	33.807
MGT	Million gross tonnes	540.999	1223.527	655.209	1378.471
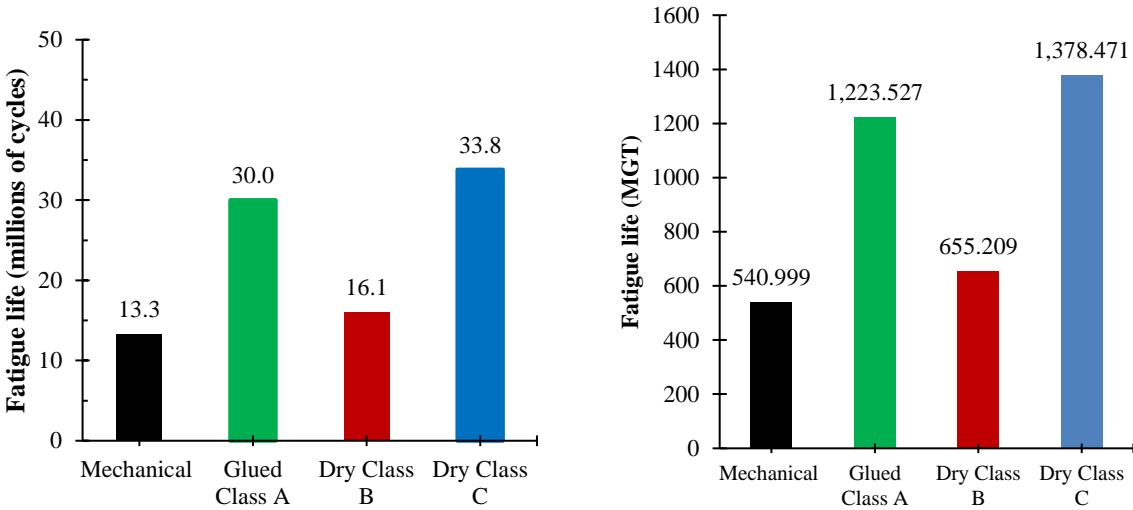
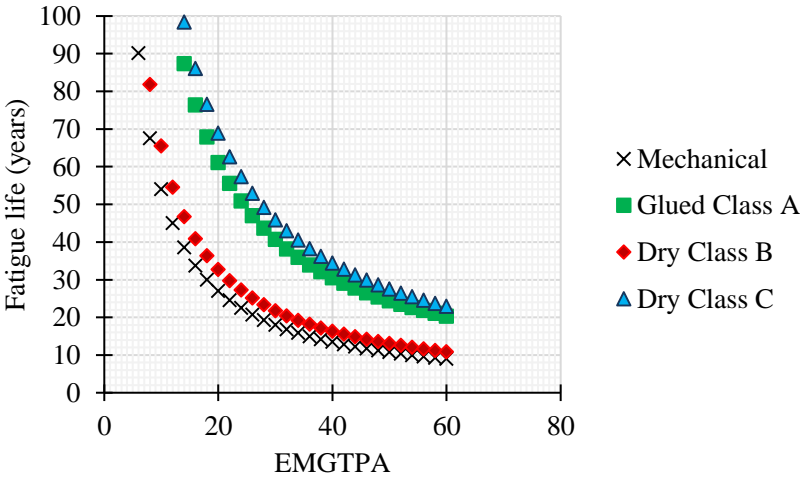Figure 4. Calculated fatigue life of joints expressed in millions of cycles and in MGT.

Figure 5. Calculated fatigue life of joints in years according EMGTPA

5. Conclusions

3D Finite element analysis was carried out for dry Class B rail joint design to investigate their behaviour under combined biaxial loading in a fatigue static test. Assessment against fatigue was performed through accounting sagging and hogging deformation of the fishplates. The fatigue life for the four different joint types were evaluated in terms of cycles, MGT and in years depending on track annual tonnage.

References

1. Endurance limit assessment, LBF-SHF-67404-DOC-04, 12 May 2016
2. Shigley's mechanical engineering design, Ninth edition McGraw-Hill
3. Browell R., Hancq A. Calculating and displaying fatigue results, ANSYS fatigue module, March 29, 2006, ANSYS Inc.

APPENDIX F

Video Gauge calibration and adaptation

The experimental methodology included the calibration and adaptation of the Video Gauge (VG) in the railway in-situ conditions. The following issues needed to be investigated before using the VG in-situ in order accurate deflection measurement to be obtained under the various operational traffic conditions.

- Using appropriate lenses to fit the vertical and horizontal field of view required at the given distance from the track. This defined the allowable target size that influences deflection resolution.

- Testing and employing a range of different targets fixed to rails to improve quality, system accuracy and sensitivity. This included magnetic, charcoal and ultimately spray paint on the rail to create black and white non movable temporary speckle pattern to allow measurements under high speed train passage by tracking target movement.

- Determining the minimum video capture rate required to capture the maximum deflection between supports and maintaining high capture rate though calibration of the camera settings.

The procedure of the resource management and the set-up planning procedure are illustrated in Figure 1 showing factors affecting the capture rate and resolution. The flowchart in Figure 2 shows the set-up and measurement procedure affecting the accuracy. The interrelationship of the effective planning according to site restrictions (train speed, working distance, and brightness of targets) and successful setup on site led to high accuracy in the collected data. In addition, multiple track components (rail, sleepers, clips, slab modules) and multiple positions in the rail were measured simultaneously allowing a robust track performance evaluation and checking of consistency of the results.
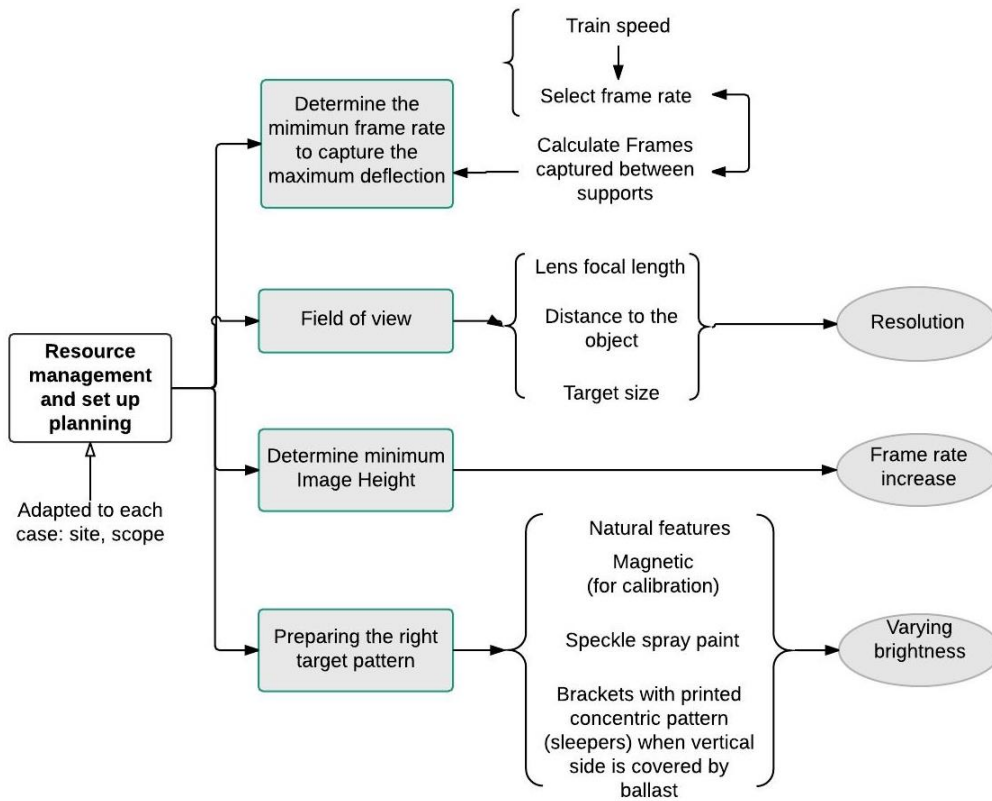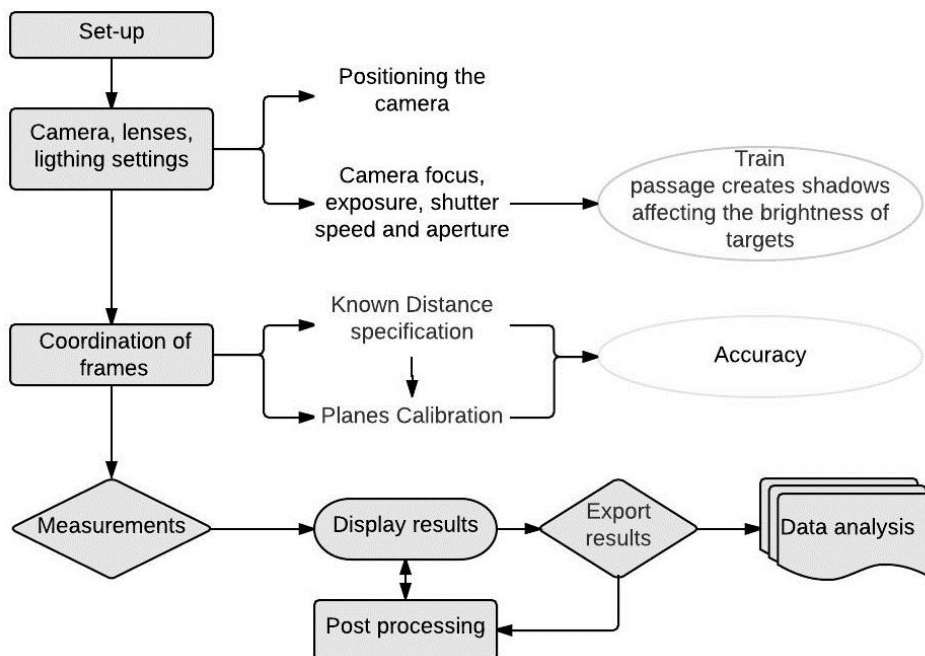
Figure 1 Resource management and set up planning procedure

Figure 2 Set-up and measurement procedure